HELWAN UNIVERSITY
FACULTY OF ENGINEERING MATARIA
CIVIL ENGINEERING DEPARTMENT

Behavior of Deep Beams with Strengthened Openings using Basalt Fiber Sheets

ATHESIS

Submitted in partial fulfillment of the requirement for

P.hD OF SCIENCE DEGREE

Department Civil Engineering

Faculty of engineering in Mataria-Helwan-Egypt

By

HODA AWAD ABD EL ZAHER
M.Sc. in Civil Engineering,
Helwan University, November 2016

Supervisors

Prof. Mostafa Abd EL Magid
Professor of Reinforced Concrete
Faculty of Engineering at Mataria
Helwan University

Assco. Prof. Hala Mamdoh Esmael
Associate Professor of Civil Engineering
Faculty of Engineering at Mataria
Helwan University

Cairo
2024

HELWAN UNIVERSITY
FACULTY OF ENGINEERING MATARIA
CIVIL ENGINEERING DEPARTMENT

Behavior of Deep Beams with Strengthened Openings using Basalt Fiber Sheets

A THESIS Submitted in partial fulfillment of the requirement for Ph.D. of

SCIENCE DEGREE, Department of Civil Engineering

By

HODA AWAD ABD EL ZAHER

M.Sc. in Civil Engineering, Helwan University, November 2016

Approved by the examining committee:

Prof.Mohamed Abdel Razik Ibrahim

Professor of Reinforced Concrete -Faculty of Engineering El Azhar University

Assco. Prof. Nasr Zeinhom Hassan

Associate Professor of Civil Engineering - Faculty of Engineering Mataria- Helwan University

Prof. Mostafa Abd EL Magid

Professor of Reinforced Concrete - Faculty of Engineering Mataria - Helwan University

Assco. Prof. Hala Mamdoh Esmael

Associate Professor of Civil Engineering - Faculty of Engineering Mataria- Helwan University

Supervisors:

Prof. Mostafa Abd EL Magid

Professor of Reinforced Concrete - Faculty of Engineering Mataria - Helwan University

Assco. Prof. Hala Mamdoh Esmael

Associate professor of Civil Engineering - Faculty of Engineering Mataria- Helwan University

ACKNOWLEDGEMENT

Firstly, all thanks are due to Allah who gives me the power to introduce this little treatise in final form. I wish to express my gratitude to all those who helped me during my research and gave me the possibility to complete it.

I'm highly appreciating the role of A Prof .Dr/ Mostafa Abd EL Magid, for his guidance during the work of thesis. His view points are helpful. I'm also grateful for his assistance and helpful remarks during the course of this research. He was of immense help in difficult times and always encouraged me to grow and expand my thinking he is adding greatly to the value of this work. I wish him all happiness and joy.

I would also like to express my thanks and appreciation to Dr. / Hala Mamdoh for her Continuous guidance and helpful advice during the work in this research.

I want to express my deepest appreciation for their encouragement and continuous supervision throughout my studies. Their remarks are helpful as well as instructive. They spent numerous hours to craft me into a better thesis.

Last but not least,

I want to thank my Parents, Husband, sisters, brothers, and my friends.

Eng. /Hoda Awad Abdel Zaher

ABSTRACT

The presence of openings in deep beams is necessary for various purposes, such as ventilation and energy supply, but these openings negatively affect the behavior of those beams. Therefore, many researchers have studied the strengthening of the openings using fibers such as carbon, glass, and steel fibers. Carbon fiber has the greatest impact, but it affects the environment. Negatively, as it causes pollution and great harm to human health, wish to replace it with a non-polluting material that preserves human health, which is basalt fiber, which is an environmentally friendly material that can be recycled, which saves energy. Therefore, this research studies the effect of this material on strengthening different shapes of openings with the same area and perimeter with different orientations and the effect of the shape of the opening on the behavior of deep beams. A study was conducted on the results of 52 deep beams with and without openings analyzed experimentally and by using finite element analysis. The effect of increasing the concrete compressive strength on the behavior of these deep beams was also studied using finite element analysis using the Ansys program, also a study of the effect of increasing the number of layers of basalt fiber has been conducted. It was found that the best shape for openings is the horizontal rectangular opening with horizontal reinforcement, as it restored to the beam what was lost due to the presence of the opening and reached 101% of the total energy of the solid beam that does not have openings. It was also found that increasing concrete strength has a greater influence on the behavior of deep beams with openings than increasing the number of basalt layers .

CONTENTES

Content **page**

LIST OF FIGURES

LIST OF TABLES

CHAPTER ONE
INTRODUCTION

1.1 General Background

Deep beams represent an important structural element, being loaded as beams but having smaller shear-span-to-depth ratios **de Paiva, H. R., & Siess, C. P.,[1]**. A deep beam, in general, has a depth much greater than normal, while the thickness in the perpendicular direction is much smaller than either its span or depth. **ACI-code 318R-19, [2]** defines deep beams as those that have a clear span to overall depth ratio of less than four, or a shear span to effective depth ratio less than two the beam should also be loaded on one face and supported on the opposite face, such as compression struts that develop along the lines of loads and supports. Reinforced concrete deep beams are widely used in many structural engineering applications, such as transfer girders, pile caps, offshore structures (caissons), shear walls, wall footings, floor diaphragms, and complex foundation systems. In deep beams, a significant proportion of the loads are transmitted to the supports directly by arch action. The arch-action phenomenon not only permits the transfer of the concentrated load directly to the support but also reduces the contribution of the other types of shear transfer. The major factors influencing this phenomenon are the ratio of shear span to effective depth (a/d) and the compressive strength of the strut. The compressive strength of the strut is closely dependent on the compressive strength of the concrete and the tensile strength provided by the reinforcement at the top level.

1.2 Problem Definition

Openings are provided for the passage of ducts and pipes. These ducts and pipes are accommodated underneath the soffit of the beam and for aesthetic

appearance, are covered by a suspended ceiling, thus creating a dead space. The height of this dead space adds to the overall height of the building depending on the number and depth of ducts. Hence the provision of the transverse openings enables to reduction of the height of the structure, especially regarding tall building construction, thus leading to a highly economical design. The transverse openings in beams are a source of potential weakness **Campione, G., & Minafò, G., [3]**. An opening creates a discontinuity in the normal flow of stresses, leading to stress concentration at the edges of the opening and early cracking of concrete. To avoid this special reinforcement enclosing the opening should be provided in the form of external or internal reinforcement. Internal reinforcements are steel bars provided along with the main reinforcements during casting. External reinforcements are applied externally around the opening in the form of jacketing of composite materials like glass fiber, carbon fiber, and basalt fiber.

1.3 Research Significance

This research was conducted to try to solve the problems caused by the existence of openings in deep beams by strengthening these openings using a new material such as basalt fibers which have better properties than other fibers, basalt fiber has mechanical properties better than glass fiber and its cost is lower than the cost of carbon fiber **Ramakrishnan, V., & Panchalan, R. K.,[4]**. Also, basalt fiber is environmentally friendly unlike carbon fibers which pollute the environment, basalt fibers easy to handle and process, so there is no need for special processing equipment, It can be recycled unlike carbon and glass fibers and it is convenient with a lot of resins like epoxy, it has excellent shock resistance as it is good for ballistic applications. In this study, the basalt fibers from basalt rocks are used to strengthen openings in deep beams trying to use as an alternative to carbon fibers to strengthen openings in deep beams as it doesn’t produce any toxic reactions with air or with water, and its surface is

anti-explosion. Also, it doesn't produce chemical reactions that may damage the environment or human health. When it contacts other chemicals, it is safe for use in industry and has no pollution **Shetty, M. S., & Jain, A. K., [5]**, so it is better than carbon fiber which pollutes the environment. The basalt fibers do not contain any other additives in a single production process, which gives an additional advantage in cost. Basalt fiber is a high-performance non-metallic fiber made from basalt rock melted at high temperatures. Chopped basalt fiber can be made also from basalt rock, basalt fabrics, and continuous filament wire. Basalt fiber originates from volcanic magma and volcanoes, a very hot fluid or semi-fluid material under the earth's crust, solidified in the open air. Basalt is a common term used for a variety of volcanic rocks, which are gray and dark in color. The molten rock is then extruded through small nozzles to produce continuous filaments of basalt fiber.

1.4 Objectives of Thesis

The objective of this thesis is to study the behavior of deep beams containing openings loaded up to failure and to study the effects and enhancement of strength in deep beams containing openings when strengthened externally by basalt fiber sheets. Experimental and theoretical studies have been done on deep beams with opening strengthened using basalt fiber sheets to study the following:

- Effect of strengthening the deep beams without opening using basalt fiber sheets
- Effect of strengthening different types of openings in the deep beams using basalt fiber sheets.
- Effect of strengthened orientation of basalt fiber sheets on the behavior of the deep beams.

1.5 Outline of Thesis

Chapter (1): INTRODUCTION

This chapter presents remarks on deep beams, openings, and basalt fiber sheets. It also presents the objectives of the thesis and the main contents of it.

Chapter (2): LITERATURE REVIEW

This chapter presents a historical review of the composite materials, their different types, shapes, and methods of production, and a review of some selected previous work, concerning the applications of different types of FRP sheets to strengthen concrete structure elements especially deep beams with opening.

Chapter (3): EXPERIMENTAL PROGRAM

This chapter describes the experimental program for the concrete deep beams strengthened with basalt fiber sheets, the properties of used materials, test setup, specimen preparation, and number are also stated in this chapter.

Chapter (4): EXPERIMENTAL RESULTS

This chapter describes the results of the experimental tests for the reinforced deep beams.

Chapter (5): ANALYSIS AND DISCUSSION OF EXPERIMENTAL RESULTS

This chapter describes the discussion for the analysis of the obtained results for the reinforced deep beams.

Chapter (6): FINITE ELEMENT ANALYSIS

This chapter represents a simulation of the tested deep beams by the finite element program used in the study (Ansys 19 R2). And comparison of results obtained from experimental samples with the same samples in a finite element program also, parameters from finite element analysis are added in this chapter.

Chapter (7): CONCLUSIONS AND RECOMMENDATIONS FOR FUTURE WORK

This chapter contains the main conclusions and recommendations based on the experimental outcome and analytical results obtained and suggestions for future work.

REFERENCES

CHAPTER TWO
LITERATURE REVIEW

2.1 Introduction

In recent days, various fibers have been developed and used in construction, industrial, and highway engineering. Steel is mainly used in various applications. Also, fiberglass polythene fibers, carbon fibers, and polyamide fibers are now developed and used in construction, industrial, and infrastructure development. In that list, new fiber is added, called basalt rock fibers. Basalt originates from volcanic magma shown in Figure (2-1) and flood volcanoes, a very hot fluid or semi-fluid material under the earth's crust, solidified in the open air. Basalt is the name given to a wide variety of volcanic rock, which is gray. Brown or dark in color, formed from volcanic lava after solidification. The heavily thickened lava contains olivine, clinopyroxene (salite), plagioclase, and opaque metal oxides. Plageocene and pyroxene make up 80% of many types of basalt. Table (2-1) shows the results of the chemical analysis of the basalt rock **Czigány, T.et al., [6]** shown in Figure (2-2)

Figure (2-1): Volcanic magma

Table (2.1): Chemical composition of basalt rock

Chemical	SiO2	Al2O3	Fe2O3	MgO	CaO	Na2O	K2O	TiO2	P2O5	MnO	Cr2O3
W%	52.8	17.5	10.3	4.63	8.59	3.34	1.46	1.38	0.28	0.16	0.06

Figure (2-2): Basalt rock

2.2 The Origin of Basalt Fibers

Basalt is the most common rock type in the earth's crust (the outer 10 to 50 km). Basaltic magma is commonly produced by direct melting of the earth's mantle, the region of the earth below the outer crust. The ocean floor is mostly made of basalt. Huge outpourings of lava called "flood basalts" are found on many continents. Basalt is composed mainly of silica and alumina with lime, magnesium oxide, and ferric oxide found in lesser percentages **Branston, J. S., [7].** Basalt rock can be used to make basalt bars, basalt fabrics, chopped basalt fiber strands, continuous basalt filament wires and basalt mesh. Some of the potential applications of these basalt composites are plastic polymer reinforcement, soil strengthening, bridges and highways, industrial floors, heat and sound insulation for residential and industrial buildings, bulletproof vests, and retrofitting and rehabilitation of structures **Ralph, C.et al., [8].** A French scientist in the United States filed the first patent revealing the technique of producing basalt fiber in the year 1923 and subsequently, the research was started in the United States of Soviet Russia (USSR). The development of basalt

continuous fibers (BCF) technology was conducted in the USSR; it had the status of a closed scientific programs. Therefore, there was no contact with scientists and engineers from abroad. The main development efforts were given by USSR for defense and aerospace applications. The first samples of BCF were received at a scientific research institute in Ukraine of USSR in 1956-61: but the initial industrial equipment was very expensive and large energy consuming. After the dismantling of USSR in 1990's this research or technique was made available to others. Recent efforts are taken for this technology to lower the cost and commercial use. **Jamshaid H. and Mishra R. A, [9].**

2.3 Basalt Fiber Production

In many ways, basalt fiber technology is like glass fiber technology, except for only one material, basalt rock. Basalt continuous filaments are made from the basalt rocks in a single-step process melting and extrusion process. The technological process of manufacturing basalt filament consists of melt preparation, fiber drawing (extrusion), fiber formation, application of lubricants and finally winding. Basalt fibers are currently manufactured by heating the basalt and extruding molten liquid through a die in the shape of fibers **Singha K. A, [10] and, Fiore V.et al., [11]**, as shown in plant layout Figure (2-3). Crushed rock materials are charged into bath type melting furnace by a dozing charger, which is heated using air gas mixture or electrically. Crushed rocks are converted into melt under temperature of 1285^0C to 1450^0C in the furnace bath. Molten basalt flows from the furnace to feeder through feeder channel and feeder window communicate to recuperate. The feeder has a window with a flange connected to a type bushing and is heated by furnace waste gases or electrically. The melt flows through platinum-rhodium bushing with 200 holes which is heated electrically. The fibers are drawn from melting under hydrostatic pressure and subsequently cooled to get hardened filaments. A sizing liquid with components to impart strand integrity, lubricity, and resin compatibility is applied, and then filaments are collected to form 'strand' and

forwarded to take up devices to wound on forming tube. By varying the drawing speed of the fiber and temperature of the melt, fibers of a wide size range could be produced. For example, with a drawing speed of 12m/s and nozzle temperature of 1325^0C a fiber of 7 micron were produced while at 4m/s and 1285^0C a fiber of 17 micron was produced. Basalt fibers are also produced with the Junkers technology by melting the basalt rock and then forming fibers out of it as shown in Figure (2-4). The essence of the method is that the melt of 1580 ºC coming from the gas-heated furnace is transmitted to a horizontal shaft fibrising machine that has three centrifugal heads. The lava adhered to the heads flies off due to the centrifugal force and as a result of blowing 60-100 mm long fibers of 6-10 μm diameter are formed from the viscous liquid **.**Basalt is an igneous rock found in abundance throughout the world. Basalt rock is crushed, loaded into a furnace and liquefied. Next, basalt filaments are drawn through platinum-rhodium bushings. As the filaments cool, they are coated with a sizing agent. The sizing agent is necessary to prevent abrasion during transportation; however, it also provides manufacturers with a way to differentiate their fiber from their competitors. For example, the performance of E-glass fiber depends on parameters such as fiber volume and aspect ratio, but the fiber itself differs little from manufacturer to manufacturer. In regard to interfacial properties (e.g. bond strength and alkaline resistance), sizing is the primary variable **Kamenny Vek., [12] and Lee JJ.et al.,[13]**. In general, the manufacturing process and chemical composition of basalt fiber is similar to that of glass fiber **Lee JJ.et al., [13**].

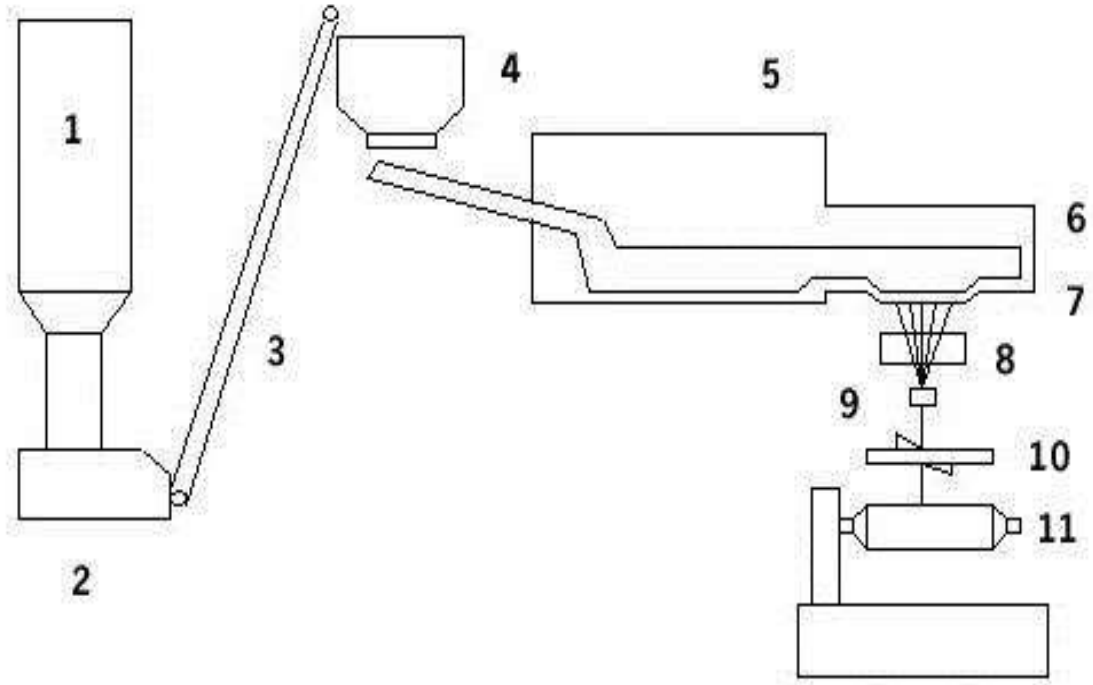

1. Batch silos: raw material supply,
2. Weighing, dosing, and mixing,
3. Pneumatic transport,
4. Batch box: charging,
5. Melting Furnace,
6. Feeder,
7. Bushings, (continuous filament formation),
8. Sizing application,
9. Draw plate feeder; Strand formation,
10. Lubricator,
11. Automated winder.

Figure (2-3): Plant layout of basalt fiber formation, [12]

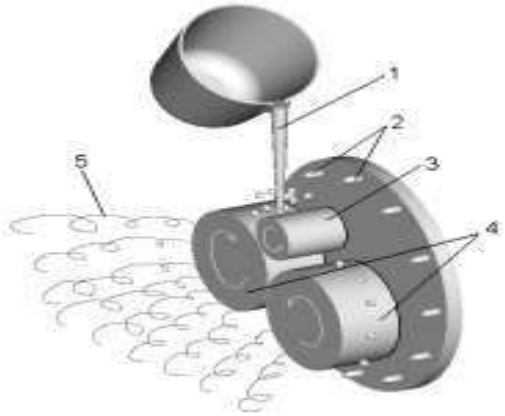

1 – Basalt lava, 2 – Blowing valves

3 – Accelerating cylinder, 4 –Fiberization cylinder

5 – Basalt fibers

Figure (2-4): Junkers type basalt production **[9]**

2.3.1 Cost of Fiber Production

The raw material required for the basalt fibers production, viz., basalt rock, single material, is inexpensive and readily available in the world (mainly in India). The energy required to melting basalt rock in fiber formation higher than E-glass fiber and similar to S2-glass fiber (E-glass fiber and S2-glass fiber are types of glass fiber). The bushing of platinum-alloy used in process is very costly. And productivity of fiber is low during learning. Thus, basalt fiber cost somewhere between E-glass and S-glass fiber but should come down **Fiore V.et al., [11].**

2.3.2 Beneficial Aspects of Basalt Fiber

Basalt fibers can be manufactured directly from a single raw material (basalt rock) without the need for additives, making the process simpler than that of glass fiber **Rabinovich F.et al., [14].** As a result, the fibers can be manufactured with conventional processes and equipment, and less energy, which offers an economic advantage**.** Moreover, the fibers are considered 100% natural, have no toxic reaction with air or water, and the fiberization process is said to be

more environmentally friendly than that of glass fiber **Composites World, [15]**. In terms of mechanical and physical properties, basalt fiber has gathered attention due to its high elastic modulus, high strength, corrosion resistance, high-temperature resistance, and lightweight **Kumbhar, V. P., [16]**. Table (2-2) compares some physical and mechanical properties of basalt and E-glass fibers. In general, research into using basalt fiber as a concrete reinforcing material has grown in popularity because of its potential to replace glass fiber. Basalt fiber is often reported to offer better mechanical properties and a more economical, environmentally friendly manufacturing process. With such good characteristics, and its manufacturing process dating back to 1923 **Kumbhar, V. P., [16]**, it seems to be quite a mystery as to why its use has been so limited in the FRC industry; the following sub-section will discuss some possible reasons for this shortcoming.A key concern with basalt fiber is its chemical durability. Its alkaline resistance is often said to be good, on the basis that it may be better than that of E-glass. For example, one basalt fiber manufacturer states the fibre is very durable based on a weight loss of only 0.35% after immersion in a cement solution, in comparison to E-glass fiber that lost 4.5% of weight **Kumbhar, V. P., [16]** However, this is very indirect justification, since focus should be on the stability of the mechanical properties and matrix-fiber bond strength over time, when considering their application in concrete reinforcing. **Lee et al., [13] and Rabinovich et al, [14]**. Have shown basalt fiber loses tensile strength over time in a calcium hydroxide solution intended to replicate hydrating cement. In these cases, basalt fiber generally retained more strength than E-glass fiber. However, the improvement may be considered trivial when after 90 days, the basalt fibers still lost more than 50% of its tensile strength. There is a lack of research into the fiber-matrix bond strength, and how it changes with time. The issue of chemical durability may be further complicated by differences in basalt fiber produced by different manufacturers. Although production from a single raw material can be considered beneficial, it also

means that manufacturers have less control over the consistency of the final product. The chemical composition and crystalline structure of basalt rock varies greatly by geographical location. Therefore, only select basalt rock can produce filaments with desirable properties. As a result, the market share of basalt fiber has been reduced due to variability in the material properties of fibers manufactured with raw material from different locations Furthermore, manufacturers use proprietary sizing to give their fibers a competitive advantage in the market. Thus, it may be difficult to quantify interfacial properties, since they may differ significantly when using fibers purchased from different manufacturers.

2.4 Properties of Basalt Fibers

Basalt fibers have different properties as follows:

2.4.1 Thermal Resistance

Basalt fiber has excellent thermal properties to that of glass fibers. It can easily withstand the temperature of 1200^0C to1300^0C for hours continuously, without any physical change, which is like S2 glass fibers and carbon fibers. Unstressed basalt fibers and fabrics can maintain their integrity even up to 1250^0C, which makes them superior compared to glass and carbon fiber.

2.4.2 Mechanical Strength

Basalt fiber has tensile strength 3000-4840 MPa, which is higher than E-glass fiber. It has higher stiffness and strength than E-glass fiber. Basalt fiber has slightly higher specific gravity, 2.65– 2.8 g/cc, than other fibers.

2.4.3 Chemical Resistance

Basalt fibers have very good resistance against alkaline environment, with the capability to withstand pH up to 13-14. It also has good acid and salt resistance.

2.4.4 Corrosion and Fatigue Resistance

Basalt fiber has better corrosion resistance. It does not undergo any toxic reaction with water and air or gases also. Moisture regain and moisture content

of basalt fibers exist in the range of less than 1%. Basalt materials have strong resistance against the action of fungi and micro-organisms.

2.4.5 Abrasion Property

Basalt material is extremely hard and has hardness values between 5 to 9 on Mohr's scale, which results in better abrasion property. Even continuous abrasion of the basalt fiber-woven fabrics over the propeller type abraders do not result in the splitting of fiber by fracture and results only in breaking of individual fibers from woven structure which eliminates possibility of causing hazards.

2.4.6 Ecological Friendliness

Basalt fibers have a natural raw material, which is basalt rock it does not cause any damage to health. Basalt fiber has no biological hazards and solves waste disposal problems. It does not clog the incinerator as glass. Hence, it is incinerator friendly.

2.5 Comparisons of Characteristics Between Continuous Rock Fibers And Other Fibers

A comparison of Basalt fibers and other fibers is listed in Table (2-2)

2.6 Continuous Basalt Fibers Products and Its Application.

2.6.1 Products

Figure (2-5) shows various products of basalt fibers. Continuous basalt filaments have the following primary products as Continuous basalt (CBF) fibers, chopped fibers, CBF roving, and CBF yarns **Branston, J. S., [7] and Ólafsson, H., & Þórhallsson, E., [18].** By using these primary products, the secondary products are produced such as basalt rebar, basalt geo-textile, basalt mesh, basalt fiber pipes, and basalt laminates.

Table 2-2: Comparison of mechanical and thermal characteristics **[17]**

Capability	Basalt fiber	E-glass fiber	S-glass fiber	Polyamide fiber	Carbon fiber
Tensile strength, (M Pa)	3000~4840	3100~3800	4020~4650	2900~3450	3500~6000
Elastic modulus, (G Pa)	79.3~93.1	72.5~75.5	83~86	70~140	230~600
Elongation at break, %	3.1~6	4.7	5.3	2.8~3.6	1.5~2.0
Specific gravity(g/cc)	2.65-2.8	2.5~2.62	2.46	1.44	1.75~1.95
Diameter of filament, mμ	6~21	6~21	6~21	-	5~15
Temperature of application, °C	-260~+500	-50~+380	-50 +300	-50~+290	-50~+700
Melting Temperature,°C	1450	1120	1550	-	-

(a) CBF Filaments **(b)** Copped fibers **(c)** CBF roving

(d) CBF yarns **(e)** Basalt rebar **(f)** Basalt geotextile

Figure (2-5): Products of basalt fiber sheets. **Branston, J. S., [7]**

2.6.2 Applications

Continuous basalt fiber[s] products are used in various applications. They are as follows.

2.6.2.1 Nuclear Power Plant

Basalt materials do not absorb radioactive radiation, which makes them consider the potential in the production and transportation of radioactive materials, in nuclear power plants. Protective caps using geo-composites in the waste disposal sites, incorporating the basalt materials, can offer the best protection for human health and environment against the radioactive wastes.

2.6.2.2 Concrete Reinforcement

Requirement of the moderate strengthening in civil structures and high fire resistance can be met with basalt fibers. Basalt filaments incorporated unidirectional rods are used as the reinforcement of concrete slabs in hydraulic engineering and construction in seismically hazardous regions. It is also used in reinforcement for bridges, tunnels, railway sleepers etc. The basalt rebar consisting of 80% of basalt fiber with an epoxy binder offer better mechanical property to the reinforced concrete and are less expensive. Basalt rebar have same coefficient of thermal expansion (8 ppm/0C) as that of concrete, which increases the compatibility and performance in adverse conditions. In the accelerated weathering tests, basalt fiber shows better results as compared to glass fibers. Exposed to 600^0C for 2 hours also results in almost retention of 90% of normal strength while carbon fiber and glass fibers loss their volumetric integrity. Chopped fibers are used in cement concrete which increases crack resistance and fracture toughness of concrete. It does not have any adverse effect in concrete mixing.

2.6.2.3 Building Material

Basalt fibers can also be used in the interiors, partitioning of buildings, fireproof doors, and sound insulations for the building. They have better sound insulation property. It can act as a barrier in the frequency range up to 1800Hz to the extent

of 80% to 95%. It is also used as and warmed panels for construction of prefabricated houses such as roofing. Basalt fibers have better thermal insulating properties, almost three times than the asbestos. Basalt fabrics are used as fire blocking material in the public transport systems. Both woven as well as knitted fabrics are used for these applications. It is used in port construction and sea platforms because of better chemical and salt resistance property and for environment safety.

2.6.2.4 Road Construction

Basalt geo-mesh offers a number of advantages over glass and metal mesh for the pavement reinforcement. They are ecological safe and can withstand very high temperature of molten asphalt. The basalt geo-meshes are chemically inert and lighter than metallic meshes. They are also safe in tunnel lining work. Basalt geo-textile is suitable for soil and embankment stabilization and environmental and ecological safety.

2.6.2.5 Abrasion Resistance Basalt Fiber Pipes and Casting

High pressure pipes can be manufactured through filament winding, using fabrics and prepegs impregnate with a binder. These pipes are useful as components for transporting corrosive liquid and gases. Also, basalt plastic pipes can be used for a longer service life, i.e., 60 to 80 years, which is 2 to 3 times longer than the metallic pipes. These are used in cement industries, chemical, oil and petrochemical industries. Basalt fibers are also used in conveyor system for reinforcing the belts and coating for rollers to increase the life span.

2.6.2.6 Agriculture

Basalt fibers can be used in various agricultural applications like land drainage pipes, pies for irrigation, and hosing. Also, it is used in agricultural machine construction.

2.7 Deep Beam

A reinforced concrete deep beam may be defined as one whose depth is comparable to its span and the main factor affecting the definition of reinforced concrete deep beam is span-depth ratio (*Ln/d* or *L/H)* which should not be greater than 5.0. where L and Ln are span and clear span of reinforced concrete deep beam &H and d are overall depth and effective depth of a deep beam respectively as shown in Figure (2-6). The ***ACI* code [2],** defines a deep beam as a structural member whose span depth ratio *(L/H)* is *5* or less. But the **Euro- International Concrete Committee [19]** , decided that a beam could be considered deep if *L/H <2* or *2.5* for simply supported and continuous beams respectively. Some investigators have decided that the shear - depth ratio (*a/d)* is more meaningful to define deep beam, and that a beam could be considered deep if (*a/d) <0 .5* The behavior of deep beams is governed by shear. Since large portion of compressive forces are directly transferred to supports by arch action, their shear strength is much greater than that predicted by usual equations. Comparison between deep beams and ordinary beams is shown on Table (2-3). **Mohamed, E. I. A [20]**

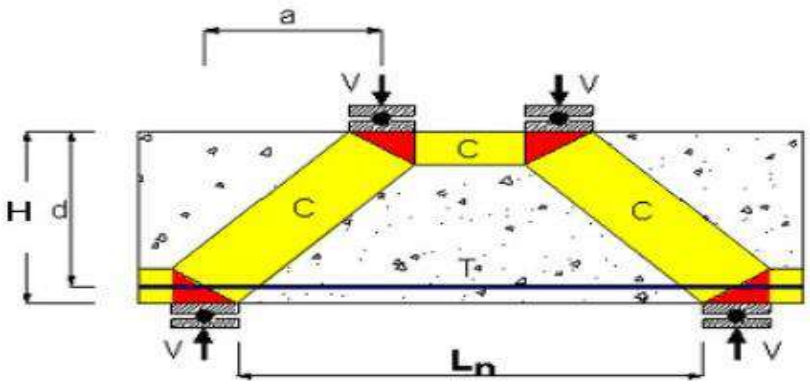

Figure (2-6): Reinforced concrete deep beams, **Mohamed, E. I. A [20]**

2.7.1 Applications of Deep Beams in Buildings

Reinforced concrete deep beams have many useful applications in building structures such as transfer girder as shown in Figure (2-7), wall footings,

foundation pile caps, floor diaphragms, and shear wall. Particularly the use of a deep beam at the lower level in tall buildings for both residential and commercial purpose has increased rapidly.

Table (2-3): Comparison between deep beams and ordinary beams

No.	Deep beam	Ordinary beam
1	Plane section before bending does not remain plane after bending.	Plane section before bending remains plane after bending.
2	The resulting strain is nonlinear.	The strain is linear.
3	Shear deformations become significant compared to pure flexure..	Shear deformation is neglected.
4	The stress block is non linear even at the elastic stage.	The stress block is considered linear at the elastic stage.
5	It is subjected to two-dimensional state of stress.	It is subjected to one dimensional state of stress

Figure (2-7): Applications of deep beams

2.7.2 Design Recommendations of Reinforced Concrete Deep Beams

2.7.2.1 Portland Cement Association (1946) [Erlin, B ,21]:

This document proposed a design procedure applicable to reinforced concrete deep beams with H/L > 2/5 for continuous deep beams and H/L > 4/5. There are two essential ratios when using this procedure, the *height/span* ratio, H/L, denoted as *B*, and the width of support span ratio, W/L, denoted as E. The design method is as follows: The stress coefficients can be selected from the charts. A coefficient is obtained to calculate the resultant of all concrete tensile stresses, *T*. The area of reinforcement (*Asl*) given by:

$$Asl = \frac{T}{fs} \tag{2.1}$$

where:

fs, is the allowable working stress of the steel.

Suggestions were given for verification of shear strength. The shear stress v is computed as:

$$\nu = \frac{8V}{7bd} \tag{2.2}$$

And the permissible shear stress of the concrete deep beams could be considered equal to: $\nu_c (1+ \frac{5H}{L}) /3$ (2.3)

Where ***vc*** is the permissible shear stress for shallow beams.

The tensile steel, As1, equation (1) was modified as calculated by equation (*4*) given below:

$$Asl = \frac{1.5T}{fs} \tag{2.4}$$

They also advised to distribute the area of steel within the whole of the tension zone, by spreading half of the area of steel uniformly throughout the tension zone and the other half should have a progressively linear distribution with increasing distance from the neutral axis.

2.7.2.2 Uhlman (1952) [22]

Uhlman provided some recommendations for the design of reinforcement in deep beams. The minimum width of the section of simply supported beam and loaded in its own plane is:

$$b = \frac{0.06L}{\sqrt{K}} \quad (2.5)$$

Where:

L = span of beam.

K = a coefficient in tabular form in Uhlman's report which is a function of HL

H =overall depth of the beam section.

The area of the main reinforcement given by:

$$A_S1 = \frac{M}{fs\,Z} \quad (2.6)$$

where:

M = Bending moment at mid-span.

fs = Permissible steel stress.

z = Lever arm.

The lever arm value obtained from graphs for different loading conditions is a function of the overall length and the height of the deep beam. In the case of deep beam with loading along the lower edge, The required area of hanging steel is provided by:

$$A_{hs} = \frac{W}{fs} \quad (2.7)$$

where:

W = applied load between the supports.

In the case of a combination of loading, the superposition of the reinforcement calculated for each case is advised.

2.7.2.3 Strut-and-Tie Model Method (STM)

The second analysis method allowed by ACI 318 **[2]** for the design of deep beams is STM. STMs comprise compression struts and tension ties that transfer

the forces through the member through the joints referred to as nodes then to the supports; as opposed to deep beam method (DBM) which transfers the force through shear reinforcement and an internal moment couple with flexural reinforcement. Before cracking has occurred in a reinforced concrete beam, an elastic stress field exists. Cracking disturbs the stress field causing the internal forces to alter their path. The STM analysis evaluates stresses as either compression (struts) or tension members (steel ties) and joins After inclined cracks have formed in deep beams, the beam takes on a "tied arch" behavior allowing the forces to transfer directly to the supports, not vertically through the member until being transferred by the web and flexural reinforcement. This behavior provides some reserve shear capacity in deep beams but not in shallower members. Shallow beams generally fail shortly after inclined cracks form unless flexural reinforcement is provided, the forces in strut and tie must remain in equilibrium for the applied external loads.

Define of Strut

The strut is the compression field in the deep beam. It is necessary to check that crushing of the compressive struts does not occur. The cross-sectional area of the compressive struts is highly dependent on the details at their ends.

Idealization of the Strut

The most common types of struts utilized in design are:

1-Prismatic Strut

Struts could be idealized as prismatic compression members (prismatic struts) as shown by the straight line outlines of Figure (2-8)

2-Tapered Strut

If the effective compression strength at the two ends of the strut differs due to different bearing lengths, the strut is idealized.

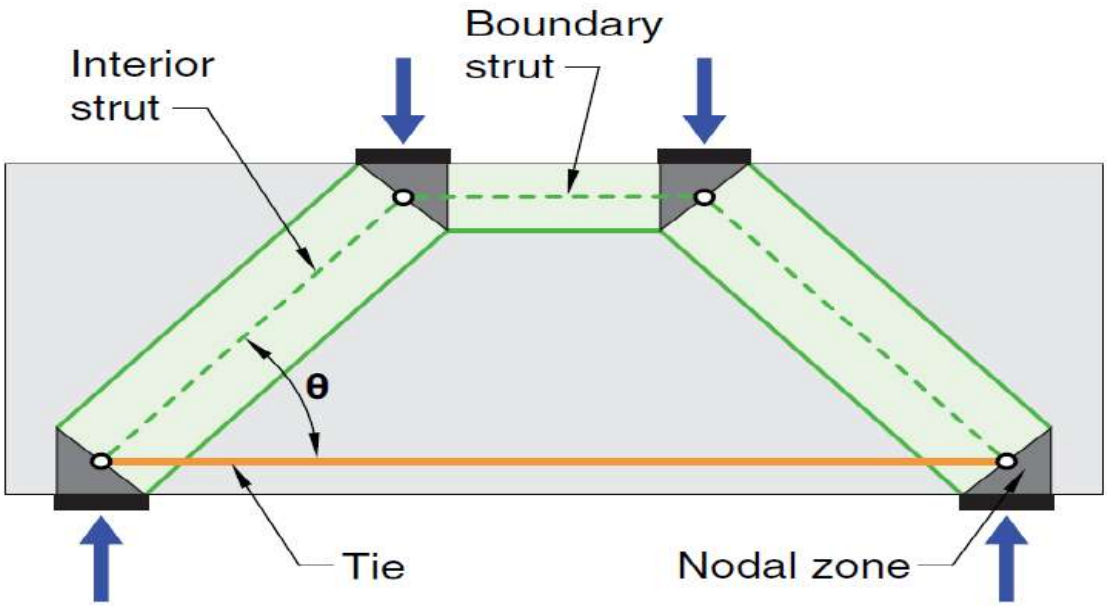

Figure (2-8): Strut and tie model for deep beam

3-Bottle Shaped Strut

As the stresses transfer through the bottle shaped strut. As arise that can produce provided to Transfer the stresses after cracking has occurred or to keep cracking from occurring, the member or structure may fail after cracking. Once cracking has occurred, the internal stresses transfer to the supports.Without reinforcement to over the cracks, the stresses could redistribute and consolidate causing concrete crushing member. With adequate reinforcement, the relates to the crushing strength of the concrete strength becomes an issue during design, compression reinforcement can be added to the struts to inc regions as well as struts. they spread out forming the stresses, transverse tension forces longitudinal cracking as shown in Figure (2-9).

Definition of Tie

A tie consists of the non-prestressed or prestressed reinforcement along with the portion of the surrounding concrete that is concentric with the axis of the tie. For design purposes, the concrete in a tie is not considered to resist tensile axial force developed in the tie

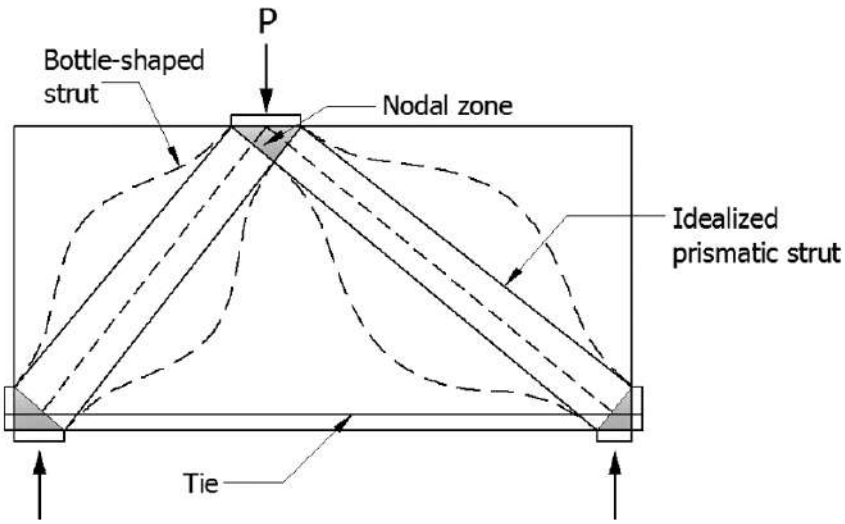

Figure (2-9): The bottle-shaped strut

Definition of Nodes

Nodes are the intersection points on the beam in a strut-and-tie model between the axes of the struts, ties, and concentrated forces acting on the beam. At least three forces should act on a node in a strut and tie model to maintain equilibrium. The nodes are classified. According to whether the forces applied on them are in compression (C) or in tension (T) Figure (2-10). If a node connects only compressive forces it is called a CCC node. A CCT node is a node that connects one tension force and two (or more) compression forces. Similarly, a CTT node connects one compression force and two (or more) tension forces. The fourth type of nodes, TTT, connects only tension forces.

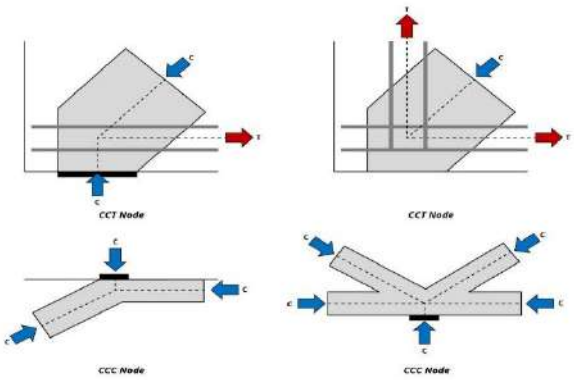

Figure (2-10): Illustration of nodes in deep beams

Definition of Nodal Zone

The nodal zones are the volume of concrete around a node that is assumed to transfer strut and tie forces through the node . The nodal zones are classified as hydrostatic or non-hydrostatic nodal zones. In a hydrostatic nodal zone, the stresses on all the loaded faces of the node are equal and the axis of the struts and/or ties are perpendicular to the loaded faces. For a non-hydrostatic nodal zone, the stresses taken on a surface perpendicular to the strut axis must be determined. **ACI 318-19[2]** defines the nodal zone as which is bounded by the intersection of the effective strut width, sw, and the effective tie width, tw.

ACI 318-19[2] Strut-and-Tie Model Provisions

The ACI 318 **[2]** specifies the limiting compressive stress in a strut, fce, as a function of the concrete compressive strength, f'c, and a reduction factor, βs. The limiting strut compressive stress equation

is given as follows:

$$f_{ce} = 0.85\beta_s f'_c \quad (2.8)$$

The reduction factor is a constant value determined based on the type of strut, the type of concrete, and the type of crack control crossing the section. The reduction factor values are stated as follows:

$\beta_s = 1.0$ For prismatic struts

$\beta_s = 0.75$ For bottle-shaped struts with crack control satisfying Section A.3.

$\beta_s = 0.60\lambda$ For struts in tension members or the tension For bottle- shaped struts without crack control satisfying Section A.3.3

$\beta_s = 0.40$ flange member of member

$\beta_s = 0.40$ flange of member

$\beta_s = 0.60$ For all other cases

In the above expressions, λ is a modification factor for to account for lightweight and sand-lightweight concrete. Values for λ are given in Table 1. It should also be noted that a bottle-shaped strut can be designed without sufficient crack

control if the lower reduction factor is used (ACI Section A.3.2.2 (b)). In order for a strut to satisfy the crack control requirements of Section A.3.3, the concrete strength must not be greater than 6000 psi, and it must have a ratio of crack control reinforcement area perpendicular to the strut to gross concrete area of at least 0.003 (ACI Section A.3.3.1). To determine the ratio of crack control reinforcement area perpendicular to the strut to gross concrete area, the following equation can be used:

$$\sum = \frac{Asi}{bsi} \sin(\alpha i) \geq 0.003$$

where: *Asi* = Area of surface reinforcement at spacing *si bs* Width of strut

αi = Angle at which layer of reinforcement crosses strut

For concrete strengths greater than 6000 psi (41.38 N/mm2), the minimum ratio of crack control reinforcement area perpendicular to the strut to gross concrete area must be calculated knowing the force in the strut, Pstrut, and an assumed 2 to 1 ratio of longitudinal forces to transverse forces in a bottle-shaped strut (ACI Section A.3.3). An equation that can be used to determine the minimum amount of crack control across a bottle-shaped strut for an assumed 2 to 1 ratio of longitudinal forces to transverse forces is given as follows:

$$\sum = \frac{Asi}{bsi} \sin(\alpha i) \geq \frac{pstrut}{4fy * bs * si}$$

The ACI 318 [5] specifies the limiting compressive stress in a node, fce, as a function of the concrete compressive strength, f'c, and a reduction factor, βn. The limiting node compressive stress equation is given as follows:

$$fce = 0.85\beta n f'c \qquad (2.9)$$

The reduction factor is a constant value given as a function of the node type. The reduction factor is 1.0, 0.80, and 0.60 for CCC nodes, CCT nodes, and CTT nodes, respectively.

2.7.3 Deep Beams with Openings

In various forms of constructions, openings in the web region of deep beams are sometimes provided for essential services and accessibility. Figure (2-11) shows

a deep beam with web opening in a building. In such situations, it is highly important to know the behavior and ultimate strength of these beams. It is well known that the so-called classical elastic theory of bending is not applicable to problems involving deep beams. As such, the stress pattern is non-linear and deviates considerably from those derived by Bernaulli and Navier. Based on ultimate load theory a number of investigators studied the problem of deep beams with solid webs and put forward certain empirical and semi-empirical equations for predicting their ultimate load capacity. Some national codes (CEB-FIP, 1970; BSCP 110, 1972; ACI318, 1971; 1978) eventually incorporated some provisions regarding design of such beams. However, studies on deep beams with web openings are very limited and no national code even provides any guidance for design of deep beams with web openings.

In the recent past Kong and his associates (1973) at the Universities of Nottingham Cambridge and Newcastle upon Tyne studied at length the problems of deep beams and presented semi-empirical formulae for predicting the ultimate strengths of both solid beams and beams with web openings. The CIRIA deep-beam design guide (Ove Arup and Partners, 1984) dealing with the design and detailing of web openings was mainly based on published literature, an intuitive feel for the forces, and constructional experiences. These approaches tended to be cautious in the absence of adequate test data. Therefore, there is a definite need for understanding of in particular the behavior and strength of deep beams with openings in the web.

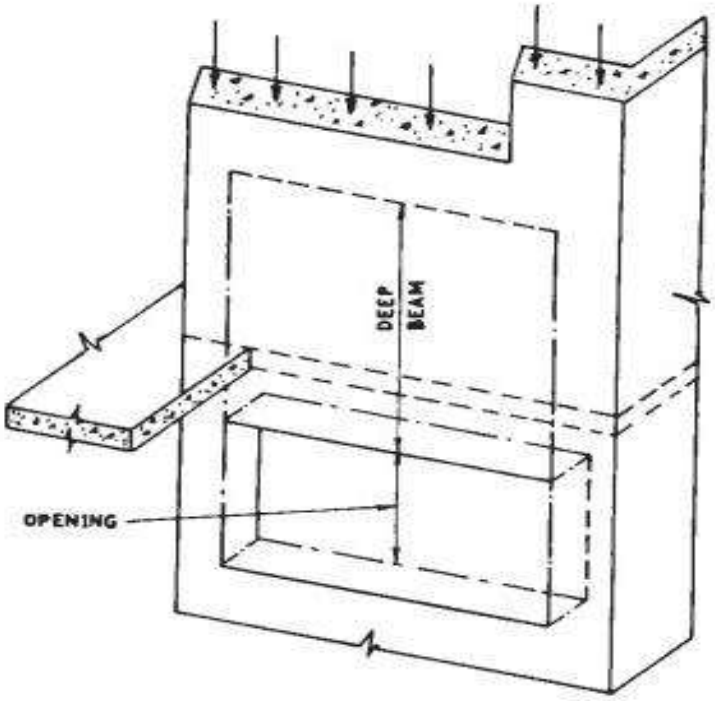

Figure (2-11); Deep beam with openings. **Kong, F. K., [23]**

2.7.3.1 Factors Influencing The Behavior of Deep Beams With Opening

The main factors affecting the behavior and performance of deep beams with web openings are:

i) span to depth ratio.
ii) cross-sectional properties (i.e., rectangular section, Tee-section, etc.).
iii) amount and location of main longitudinal reinforcement; amount, type and location of web reinforcement.
iv) properties of concrete and reinforcements.
v) type and position of loading.
vi) size, shape and location of web opening etc.

2.7.3.2 General Behavior in Shear Failure (Under Two-Point Loading)

Concrete strain variation at mid-span section indicates that before first cracking, the beam behaves elastically, shows a non-linear distribution of strain and more than one neutral axes (Figure 2-12). The number of neutral axes decreases with incremental loads and at ultimate stage only one neutral axis is present. Concrete

strain variation at the plane of rupture shows the deep beam behavior also before cracking and persistence of diagonal tension till failure. However, the extent of crack width and the deflection pose no problem at the service loads. If, however, the crack width is limited to 0.3 mm, the corresponding load will be in the range of 60–70% of the ultimate load **Ray.S.P,[24].**

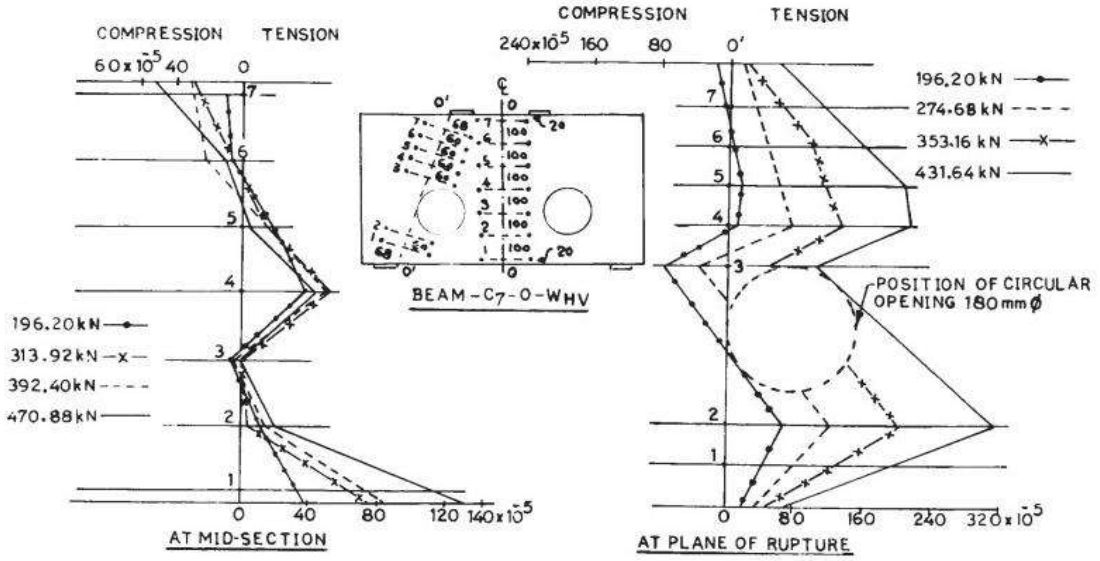

Figure (2-12); Concrete strain variation at the mid-section and plane of rupture of a typical deep beam with web openings. **Ray.S.P, [24].**

2.7.3.3 Criterion of Failure and Strength Theory

From the mode of failure for beams with web openings and a beam without web opening, it is clear that the failure along the critical diagonal path is by sliding. This particular mode of failure can be interpreted in terms of Coulomb's internal friction theory and Mohr's generalised failure criterion with straight line envelopes, combined as used by Guralnick (1959) in the case of an ordinary reinforced concrete beam, Figure (2-13). By this, two independent physical properties of concrete, namely cylinder compressive strength *f'C* and cylinder splitting tensile strength *f't* are accounted for the ratio *f't/f'C* varies widely (from about 1/8 to 1/16) with the quality of concrete. In absence of any practical test data, adoption of a suitable ratio for *f't/f'C* may be erratic. Therefore, the

parameters f'C and f't to be used for deep beams should be determined by independent tests**.**

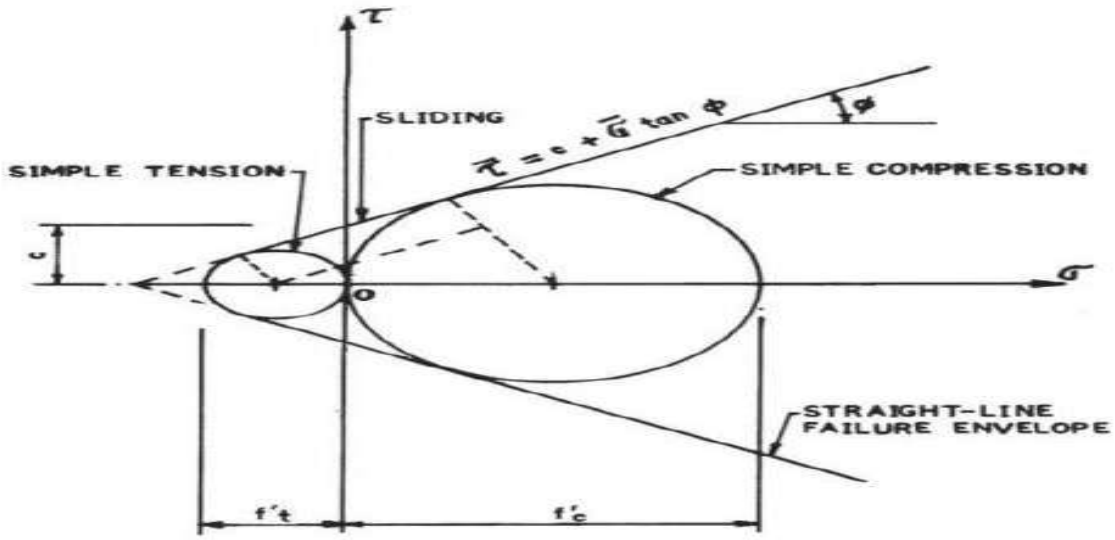

Figure (2-13): Proposed simplified morh-coulomb failure criterion **(Ray and Reddy,).[24]**

2.7.3.4 Ultimate Shear Strength Kong and Sharp ,Kong Fk.et al., [23]

Based on experimental investigations in which the opening interrupts the main load path joining the loading and supporting points**, Kong FK., [23]** proposed an empirical equation to predict the ultimate shear strength (Vn) of deep beams with web openings as follows (SI units):

$$Vn = C_1 \left[1 - 0.35\frac{K1\,X}{K2\,h}\right] f_t'\, b_w\, m_2\, h + C_2\, A_s \frac{y}{h} \sin^2 \theta_3 \qquad (2.10)$$

where C1 = 1.40 for normal weight concrete and 1.35 for lightweight concrete, C2 = 300 N/mm^2 for deformed bars and 130 N/mm^2 for plain round bars, y is the depth of longitudinal reinforcements, x is clear shear span. bw and h are the width and overall depth of beam, respectively. k1, k2, and m2 are coefficients defining the location of opening shown in Figure (2-14). ft' is the tensile strength of concrete and can be assumed is equal to 0.5√fc', and as is the total areas of longitudinal reinforcement.

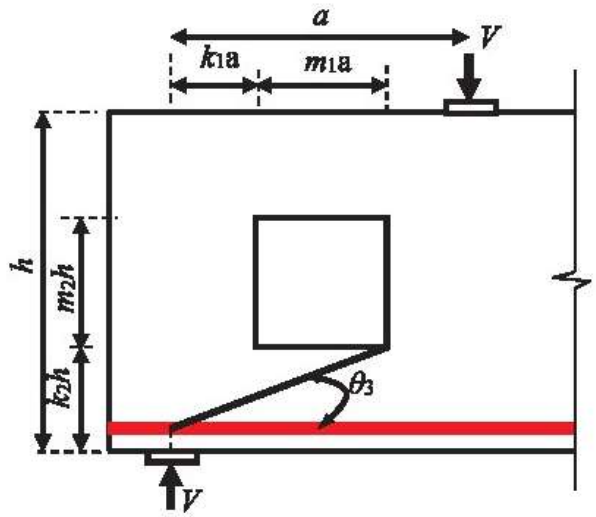

Figure (2-14): Identification of the symbols. **Kong and Sharp**, **[23]**

2.7.3.5 Ultimate Shear Strength,Tan et al. [25]

Tan et al. [25] proposed an analytical method by modifying Mohr–Coulomb's failure criterion. Starting from the principal stress at bottom nodal zone, the ultimate shear strength of deep beams with web opening can be calculated as follows (SI units):

$$V_n = \frac{1}{\frac{\sin 2\theta_3}{ft_3 Ac_3} + \frac{1}{fc' Astr_3 \sin\theta_3}} \quad (2.11)$$

where Ac_3, $Astr_3$, and ft_3 correspond to concrete struts at the lower part of the opening only and they can be calculated as follows:

$$f_{t3} = \frac{2As\, fy \sin\theta_3}{Ac_3/\sin\theta_3} + f_t' \;,\; Ac_3 = b_w k_2 h \;,\; A_{str3} = b_w (w_t \cos\theta_3 + l_p \sin\theta_3) \quad (2.12)$$

l_p is the width of the support bearing plate. The other symbols have their usual meaning.

2.7.3.6 Ultimate Shear Strength,Tseng et al. [26]

Tseng et al. [26] proposed an analytical model based on the strutand-tie concept that can satisfy the requirements of equilibrium, the constitutive laws of the materials, and displacement compatibility. Based on this study; the following equations can be used in ultimate shear strength prediction (SI units):

V_{cal} = min of (V_{1c},V_{2c}, V_{3y}, V_{4y}) (2.13)

$$V_{1c} = \frac{\sin\hat{\theta}_{12}\, k_{134}\, k_{13} A_{sh13}\zeta.\, f'_c}{\sin\hat{\theta}_{12}\, k_{134} + \sin\hat{\theta}_{13}\, k_{124}\cos(\hat{\theta}_{12} - \hat{\theta}_{13})} \sin\hat{\theta}_{13}\left(1 + \frac{k_{124}}{k_{134}}\right)$$

$$V_{2c} = Cd_{24} \sin\hat{\theta}_{24}\left(1 + \frac{k_{134}}{k_{124}}\right)$$

$$V_{3y} = \frac{Tn_3}{\cot\hat{\theta}_{13} - \cot_{34}} + \min\left((K_{24} A_{sh24}\zeta.\, f'_c \sin\hat{\theta}_{24}),\left(T_{n4} - T_{n3}\frac{\cot\hat{\theta}_{34}}{\cot_{\theta_{13}} - \cot\hat{\theta}_{34}}\right)\tan\hat{\theta}_{24}\right)$$

$$V_{4y} = \frac{Tn_4}{\cot\hat{\theta}_{24}\cot_{34}\frac{k_{134}}{k_{124}}} + \frac{Tn_4}{\cot\hat{\theta}_{34} + \cot\hat{\theta}_{24}\frac{k_{124}}{k_{134}}}$$

θ is the angle of the diagonal shear element with respect to the horizontal axis as shown in Figure (2-15). Vic, V2c, V3y, and V4y are the shear forces in the shear elements as shown in Fig. 21b. k is the shear stiffness; refer to **Tseng et al. [26]** for more details about calculations procedure.

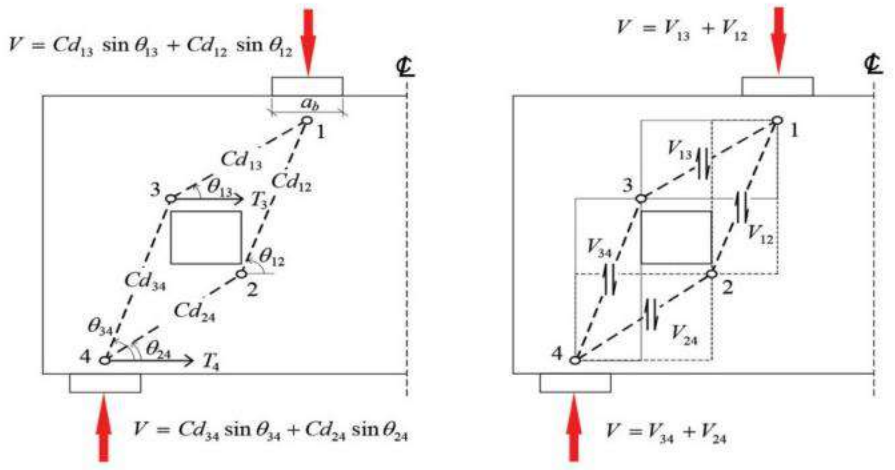

(a) Diagonal compressions of struts (b) Shear forces within shear elements

Figure (2-15): Shear distribution among loading paths **[Tseng et al., 26].**

2.7.3.7 Ultimate Shear Strength, Liu and Mihaylov [27]

Liu et al., [27] proposed a new model for deep beams with rectangular openings based on the two-parameter kinematic theory (2PKT) for solid beams **Mihaylov et al., [28].** In the new model, a deep shear span with an opening was represented by two solid shear spans: one above and one below the opening. By linking the two sub-models, the proposed kinematics-based approach can describe the complete deformed shape of the shear span with four degrees of freedom (DOFs). These DOFs can be solved by combining the kinematic conditions with equilibrium conditions and constitutive relationships for the mechanisms of shear resistance across the critical shear cracks. The model explicitly considered both the main beam reinforcement and the upper reinforcement in the slab. The transverse displacements in the critical shear cracks above and below the opening were also considered. In calculation either the top or the bottom shear span, the two-parameter kinematic theory (2PKT) for solid beams is used as follows:

$$V = V_{CLZ} + V_s + V_{ci} + V_d \quad (2.14)$$

where V_{CLZ}, V_s, V_{ci}, V_d are the shear carried by the critical loading zone, stirrups, aggregate interlock, and dowel action of the flexural reinforcement, respectively. More details about of V_{CLZ}, V_s, V_{ci}, and V_d calculations can be found in **[27]**

2.7.3.8 Ultimate Shear Strength of Modified Compression Field Theory, Vecchio and Collins, [29]

The modified compression field theory (MCFT) is an analytical model proposed by **Vecchio and Collins [29].** The theory is based on a smeared-crack approach in which the cracked concrete is treated as a new material with unique stress-strain characteristics. The cracks are

assumed parallel to the principal compressive stress directions in the concrete, while the principal strain directions deviate from the stress directions due to slip displacements in the cracks. The slip displacements and crack widths are used to calculate the aggregate interlock stresses transferred across the cracks. In addition to the aggregate interlock, the MCFT also accounts for the tension stiffening and softening of the concrete, compression softening, and confinement of the concrete, as well as the yielding of the reinforcement. Equilibrium, compatibility, and material stress–strain relationships are considered in terms of average stresses and average strains, in addition to local stresses at crack positions. For ease of application, the theory was incorporated in an analytical program (Vector2) **Wong PS, Vecchio FJ, [30].** In prediction for the current study, default constitutive relationships implemented in program VecTor2 were used. The only exception is the compression behavior of the concrete for which the Popovics model **Wong PS, Vecchio FJ , [30]** for normal strength concrete was used.

2.7.3.9 Ultimate Shear Strength of The ACI 318 [2] and CSA A23.3 [31]

Both the **ACI 318 [2] and the CSA A23.3 [31]** permit for using the strut and tie model to predict ultimate shear strength of deep beams with web openings. However, some differences can be noted in term of the nominal force carried by the strut and nodes that can be summarized as follows:

The ACI 318 [2] specifies that force carried by the strut is calculated as $F_{ns} = f_{ce} A_{cs}$; where Acs is the smaller cross-sectional area at either end of the strut, and f_{ce} is calculated as follows (SI units):

$$F_{ce} = 0.85 \beta_s f_c' \quad (2.15)$$

where fc′ is the concrete compressive strength. βs is the strut efficiency factor that depends on strut geometry, the reinforcement provided, and stress

conditions in the member. For a strut of uniform crosssectional area over its length, βs = 1.0, while for a bottle-shaped strut, βs = 0.6 when no web reinforcement is provided and βs = 0.75 when the minimum web reinforcement is provided (0.3%). On the other side, the **CSA A23.3 [31]** considered the influence of cracking that results from coexisting transverse tensile strains on the force carried by the strut as follows (SI units):

$$f_{ce} = \frac{f c'}{0.8+170\varepsilon 1} \quad (2.16)$$

$$\varepsilon_1 = \varepsilon_{frp} + (\varepsilon_{frp} + 0.002) \cot^2 \theta \quad (2.17)$$

where ε_{frp} is the tensile strain in the tie bar located closest to the tension face in the deep beam and inclined at an angle θ to the strut axis. At nodes, according to the **ACI 318 [2]**, the nominal force carried by the nodal zone is calculated as $F_{nn} = f_{ce} A_{nz}$; where A_{nz} is the area of the nodal face; and fce is calculated as follows:

$$F_{ce} = 0.85 \beta_n f_c' \quad (2.18)$$

The value of the nodal efficiency factor βn in the **ACI 318 [2]** depends on the node boundary condition and is equal to 1.0 for node subjected to compression in all direction and 0.80 for node subjected to compression and tension. Considering the **CSA A23.3 [31]** provisions, the stress limits in nodal zones shall not exceed 0.65αfc′, where α depends on the nodal boundary conditions and is equal to 0.85 for node subjected to compression in all direction and 0.75 for node subjected to compression and tension. An iterative design process was required to predict ultimate capacity without exceeding the stress limit of any of the truss elements. This places great demand on computational time. To overcome this problem, **CAST software [32]** was utilized to calculate the strut and tie forces according to the applied load. The following step was to verify that the stress limits in the nodes, ties, and struts were in accordance with the design codes. The iterative process was terminated as soon as

one of the struts and ties element reached its stress limit, and the applied load was considered the maximum load predicted by the STM.

2.8 Previous Work

High, C. et al., [33] investigated the use of basalt fiber bars as flexural reinforcement for concrete members and the use of chopped basalt fibers as an additive to enhance the mechanical properties of concrete. The research program presented in this paper comprises two studies. The first study evaluated the flexural behavior of concrete members reinforced with BFRP bars. As part of the first study, the mechanical properties and bond strengths of two BFRP bars were investigated. The second study investigated the effect of using two different types of chopped basalt fibers to enhance the characteristics of concrete. This research concluded that the use of basalt fibers resulted in an increase of the modulus of rupture of the concrete. However, the increase in the flexural strength was more pronounced for a concrete mix containing fly ash, and admixtures, and with a low w/c ratio, Slippage of the BFRP bars could occur for a low reinforcement ratio in the range of the balanced ratio. Slippage of the bars can be avoided by using a high reinforcement ratio of at least double the balanced reinforcement ratio. This behavior can be attributed to the high-stress demand on the bars of specimens with low reinforcement ratios. This behavior also highlights the necessity for designing BFRP-reinforced flexural members to fail in compression. Also, using basalt fibers slightly increased the 28-day compressive strength of concrete containing fly ash and admixtures with a low w/c ratio. also, the early compressive strength of concrete containing fly ash and admixtures may significantly increase due to the use of basalt fibers. Figures (2-16) and (2-17) show some of the results of the research.

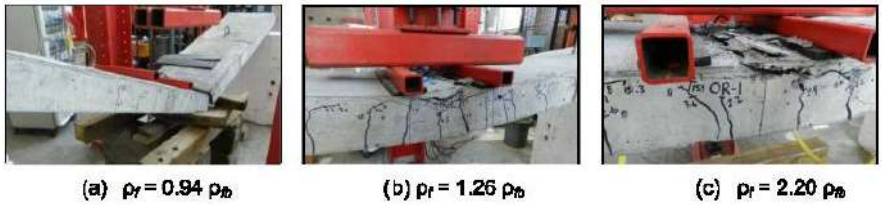

Figure (2-16): Flexure specimens at the conclusion of the test, **High, C. et al., [33]**

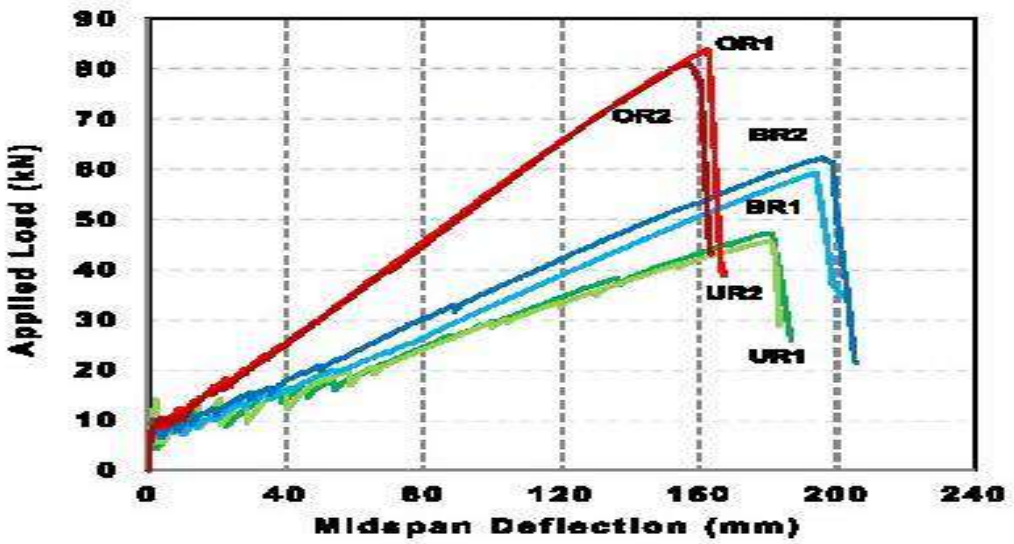

Figure (2-17): Load-deflection behavior of flexure specimens, **High, C. et al., [33]**

Ahmed, M. M. et al., [34] investigate the flexural behavior of concrete beams reinforced with Basalt fiber reinforced polymer (BFRP) bars when they subjected to repeated loadings and to improve their stiffness. For this purpose, an experimental program was set up on eight specimens consisting of pure Basalt FRPRC beams and hybrid BFRPRC beams with 2050 mm length and a cross-section of 150 x 200mm were carried out and tested under static or repeated loading followed by static loading up to failure. The results were discussed and analyzed. The test results indicated the contribution of adding steel reinforcement to concrete beams reinforced with BFRP bars. Finally the research concluded that The repeated loading has a slight effect on the ultimate load carrying capacity of the tested beams; however the deflection and cracks

propagation increase significantly, Type of loading (static or repeated) has no effect on the mode of failure of beams but the cracking pattern due to static loadings was somewhat more segment and extensive than that due to repeated loading, The cracks width and their extent in hybrid beams is mainly controlled by steel rebars. Where, the maximum crack width and their extent increases as the Af /(Af +As) ratio increases., Adding low modulus BFRP rods with steel reinforcement decreases the obtained mid span deflection at any load level and increased the ultimate deflection, The cracking load was increased considerably with decreasing the Af /(Af +As) ratio, due to the fact that the existing of steel bars as tensile reinforcement to form hybrid beam delayed the appearance of cracks and increased the elastic stiffness of the cross section.

El-Kom, S., [35] tested five series of plates under four different loading conditions. The dynamic responses such as: frequency, mode shape and damping factor were extensively investigated using FFT analyzer. Experimental modal analysis was carried out using B & K data acquisition type (3160-A-042) analyzer equipped with B & K Pulse 17.1 software. The experimental analysis and finite element technique were utilized to study the effect of open steel mesh configuration, basalt fiber ratio and boundary fixations on dynamic characteristics of concrete. In addition, the investigated basalt fiber plates were tested in the high frequency range (up to 140 kHz) through ultrasonic attenuation technique. For this purpose, an experimental setup was designed and constructed to measure dynamic elastic modulus, phase velocity and damping attenuation. The effect of mesh-layer de-bonding on the dynamic characteristics (natural frequency and damping ratio) was investigated. Damage was detected using vibration measurements and identified by comparing signals in higher frequency ranges before and after damage. Good agreement between analytical and experimental modal analysis. This result opens the way to carry out several scenarios to achieve the best analysis of the dynamic performance of concrete structures reinforced with basalt fibers. The following conclusions were arrived

at the dynamic characteristics of basalt fiber plates differ depending on mesh and configuration boundary conditions. Therefore, basalt fiber structures may be tailored for specified modal parameters and nodes positions to satisfy certain operations conditions. The numerical results from finite element method indicate good agreement with those obtained from modal analysis. However, it is recommended to use finer mesh for the numerical finite element method considering more nodes of vibration.Figure (2-18), The mutual influences of basalt fiber volume, open mesh area, boundary conditions and vibration mode are significant on the damping capacity. The use of basalt fibers resulted in an increase in the modulus of rupture of the concrete. However, the increase in the flexural strength was more pronounced for a concrete mix containing fly ash, and admixtures, and with low water-cement ratio. Finally, this study is useful for the designer in order to select the basalt fiber volume fraction, open mesh area, and boundary conditions, to shift the natural frequencies as desired or to control the dynamic nature.

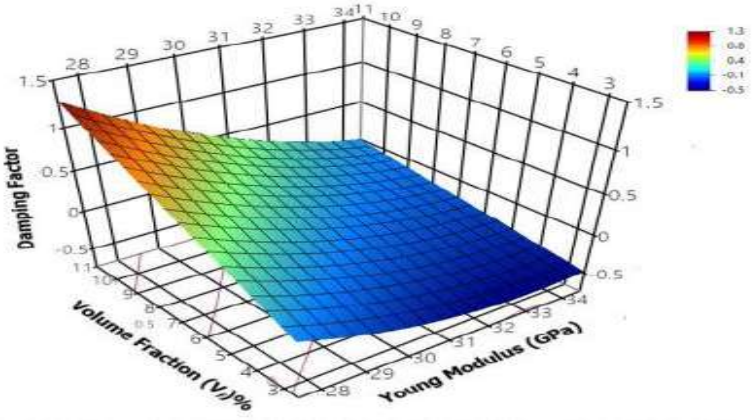

Figure (2-18): Frequency response surface of volume fraction and young modulus for five specimens' concrete basalt fiber, **El-Kom, S., [35]**

Ólafsson, H., & Þórhallsson, E., [18] made a review of the state of art of knowledge of basalt fiber, the production methods and a review of tests on basalt fiber as a strengthening material for concrete structures. There are several types of basalt fiber strengthening methods used to strengthen concrete. In this

paper three types are mentioned: External strengthening, fiber matrixes, and rod type material. Basalt composite bars are made by utilizing basalt fibers and a resin epoxy binder. They are non-corrosive, consist of 80% fibers and have a tensile strength three times that of the steel bar normally used in building construction. it is concluded that basalt bars are of great interest for the building industry. This is still quite new and needs to be researched further. There are several masters and doctor's thesis available on the usage of basalt fiber, but few with research and testing of basalt fiber bars. Pros: The benefit of using basalt fiber or other FRP material is that it is non-corrosive; this means it is a good choice for reinforcing concrete structure located close to the sea such as bridges and houses. The strength is very good, about three times the strength of the common steel rebar. The heat resistance is very good which is extremely important for buildings. Basalt is the most common rock on earth so there is no lack of sources, which means this material is much cheaper than other rock material, like for example carbon fiber.

Thorhallsson, E. R., & Snaebjornsson, J. T., [36] presented Two research projects**,** a test of prestressed concrete with internal basalt rods instead of steel and a test of columns strengthened by wrapping fiber-reinforced composite sheets around the columns to increase their strength and ductility. These experimental tests show increasing strength and ductility for both the beams and the columns. All the prestressed beam specimens failed in bending-shear, both for (a/d) ratio of 2,63 and for a shear span to depth (a/d) ratio of 10,67. In general the shear strength of FRP beams is less than that of steel-reinforced beams as the dowel actions are much lower for the FRP beams. Two extra beams were reinforced with external steel stirrups to test the bending capacity. Those beams failed in flexure due to compression failure of the concrete and tendon rupture. BFRP prestressed beams without shear reinforcement are vulnerable to transverse loading even if the (a/d) ratio is high. Comparison of these experimental results and relevant shear equations showed, that the shear force

and bending moment distribution along the span or the slenderness of the beams needs to be considered to determine the shear capacity with accuracy to ensure safety. The experimental results from the confined reinforced concrete columns clearly demonstrated that BFRP wrapping can enhance the structural performance of concrete columns under axial loading. The confinement effect is directly related to the shape of the cross-section. The number of BFRP layers and the corner radius are the major parameters controlling the behavior of the wrapped concrete columns. To enhance the confined behavior, the stiffness of the BFRP jacket can be increased by applying additional layers as well as by increasing the corner radius of square columns.

Branston, J. S., [7] presented a better understand potential applications of three different types of basalt fiber construction: filament and bundle dispersion fibers, and basalt fiber reinforced polymer bars (minibars). Mechanical performance was evaluated by measuring the effect of the fibers on the pre- and post-cracking behavior of concrete, and by investigating how the fiber-concrete interfacial properties influenced that behavior. Durability was evaluated by measuring the effect of the fibers on unrestrained plastic shrinkage, and their ability to prevent shrinkage cracking when restraint is present. Results suggest that filament dispersion fibers can be used for early-age crack control, minibars can replace rebar in applications for which it is not vital, and further research is required on bundle dispersion fibers to enhance their effect on post-cracking behavior. The results presented in this paper suggest basalt fibers are effective in mitigating plastic shrinkage cracking by reducing the magnitude of the shrinkage strain and by restricting crack propagation if they do occur. In the case of low w/c ratio mixes, it is the latter mechanism which is most prominent. Thus, it could be stated that the fibers are more efficient when w/c ratio is greater (e.g., regular strength concrete), but are still beneficial when the w/c ratio is low (e.g., high strength concrete). The filament dispersion fibers were most beneficial, likely due to two reasons: an increased surface area resulting in

higher frictional restraint, and a greater probability of bridging cracks because of the increased number of uniformly spaced filaments. Moreover, filament dispersion fibers 25 mm in length were more effective than fibers 12 mm in length, although, the difference was minor and may be a result of the inherent variability in both test methods used. From a manufacturing point of view, the fibred Osage required to eliminate cracking could likely be decreased by reducing the diameter of the filaments. This would increase the number of individual filaments and the surface area of the fibers as a whole, with respect to the quantity of material. Filament dispersion fibers were able to completely prevent shrinkage cracking at a dosage of 0.1% by volume in all cases in this study. However, in practical applications, shrinkage cracking could likely be eliminated at even lower fiber dosages, since the environmental conditions and mix proportions used in this study were designed to exaggerate the effects of shrinkage. It has been well established that the workability decreases with increasing fiber dosages. Eliminating shrinkage cracking with the lowest possible fiber dosage could provide maximum benefit with minimal interference to the workability. Related literature suggests the effect on workability is more detrimental with higher modulus fibers like basalt. Therefore, it could be concluded that basalt fibers are likely best suited for use in regular strength concrete (e.g., higher w/c ratio, higher slump mixes), since they can eliminate cracking by restricting crack growth in addition to reducing strain, without requiring measures to restore workability. In low w/c ratio concrete mixes, basalt fibers are still effective, but it may be preferential to use low modulus fibers to reduce the impact to workability (e.g., polypropylene). Although this study has concluded that bundle dispersion fibers and minibars are not optimal for plastic shrinkage cracking, they still clearly provided some benefit. Therefore, it may be of interest to pursue future research into the use of these fibers as secondary reinforcement with the intent of minor enhancements

to both mechanical behavior and reducing plastic shrinkage strains and cracking.Figure (2-19) shows some of the results of the research.

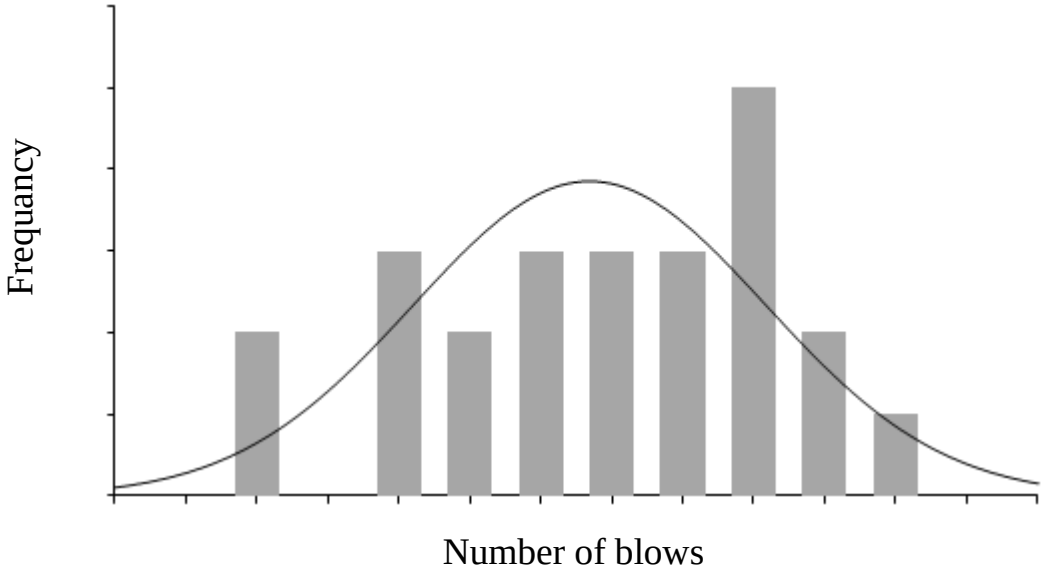

Figure(2-19): Histogram with normal distribution curve overlayed (N2 of MB-43-20) **, Branston, J. S., [7]**

Irine, F., [37] investigate and compare the compressive, flexural, and splitting tensile strength of basalt fiber reinforced concrete with plain M30 grade concrete. In this research, the effect of inclusion of basalt fibers on the compressive, flexural and splitting tensile strength of fiber reinforced concrete was studied. Based on the laboratory experiment on basalt fiber reinforced concrete, cube, beam and cylindrical specimens have been designed with basalt fiber reinforced concrete containing 1kg/m3, 2kg/m3 and 4kg/m3 basalt fibers. The experimental test results demonstrated a considerable increase in compression, flexural, and splitting of specimen at 3, 7 and 28 days with addition of basalt fibers**.** It has been observed that the workability of concrete decreases with the addition of Basalt Fibers. However, this difficulty can be overcome by using plasticizers or super-plasticizers. The percentage increase of compressive strength of basalt fiber concrete mix compared with 28 days compressive strength of Plain Concrete is observed as 14%. The percentage increase of split tensile strength of basalt fiber concrete mix compared with 28 days compressive strength of Plain Concrete is observed as 62% .The flexural

strength of basalt fiber concrete is also found to have a maximum increase of 54% at 4kg/m3 of fiber content. It was observed that the percentage increase in the strength of basalt reinforced concrete increases with the age of concrete. Also, it was found from the failure pattern of the specimens, that the formation of cracks is more in the case of concrete without fibers than the basalt fiber reinforced concrete. It shows that the presence of fibers in the concrete acts as crack arrestors. The ductility characteristics have improved with the addition of basalt fibers. The failure of fiber concrete is gradual as compared to that of brittle failure of plain concrete.

Surya Sunder, S.et al., [38] studies experimentally the incorporation of external strengthening of circular openings with singular and double openings at shear zone using BFRP (Basalt fiber reinforced polymer) wrapping system inside and around openings. The effect of BFRP sheets with different openings has been studied in terms of initial crack load, ultimate failure load, cracking pattern, and deflection. Effect of single and double circular openings having same area is studied. And it was found that beams with double circular opening is better than beams with singular circular opening. Hence circular openings can be used for passage of ducts, pipes etc. than rectangular openings. The experimental study consists of casting of eighteen rectangular reinforced concrete beams including beams with and without opening. Circular openings are provided at the shear zone. All the beams casted are tested to failure. The beams are indicated by the label BC1, BCO1, BCO2BFCO1, BFCO2. Each having same longitudinal and transverse steel reinforcement. All beams had the same geometrical dimensions. The behavior of beams with circular and rectangular opening (keeping area constant) under strengthening using BFRP is carried out. Four beams with circular opening are provided using the technique of form work extrusion. Four beams are strengthened with BFRP sheets and the other one without opening is unstrengthen. These beams are tested under three-point loading in the loading frame, the ultimate failure. load of the beam and

deflection have been recorded and results were compared with the control beam without opening and control beam with rectangular and circular opening. B00:Control specimen without opening, BCO1: Beam with one circular opening without strengthening, BCO2: Beam with two circular opening without strengthening, BFCO1: Beam with one circular opening with strengthening, BFCO2: Beam with two circular opening with strengthening. Beams of length 1m, width 0.15m, depth 0.25m having single and double circular opening. High-Yield Strength Deformed bars of 10 mm diameter are used for the longitudinal reinforcement and 6 mm diameter bars are used as stirrups. The tension as well as compression reinforcement consists of 2 no's 10 mm diameter's bars. All the specimens were tested for flexural strength under three point loading control beams, beams with circular and rectangular opening, beams strengthened with BFRP were tested in universal testing machine having capacity 1000kN.The specimens were arranged with simply supported conditions, centered over bearing blocks adjusted over an effective span of 760mm. Figure (2-20) and (2-21) show the crack pattern of strengthened and unstrengthen beam respectively.

Figure (2-20): Crack pattern of strengthened beam with one circular opening. **[38]**

Figure (2-21): Unstrengthen beam with one circular opening. **[38]**

From the overall study, it can be concluded that the strengthening with BFRP around and inside circular openings having two openings having same area is more efficient than single circular opening and openings having same area.

Chin, S. C.et al., [39] presents the review of studies performed to investigate the behavior of Reinforced Concrete (RC) beams containing different types of openings. For the last 4 decades, research works involved the investigation of the member strength and development of the design approach for simply supported, continuous and T-beams containing large rectangular openings subjected to torsion, bending and shear forces. The proposed design method suggested the installation of diagonal steel reinforcement bars around the opening for providing the required strength. In recent years, Fiber Reinforced Polymers (FRP) have been widely used as an external bonded reinforcement system for upgrading and retrofitting of concrete structures. FRP as externally bonded reinforcement mainly used to repair and retrofit the damaged reinforced concrete member. However, very limited studies showed the application of the FRP laminates as external reinforcement around openings. Therefore, further investigations regarding the application of FRP laminates to strengthen the large openings in reinforced concrete members are very vital.In the last five decades, extensive research activities involved to determine the effects of openings in terms of shape (circular, square and rectangular), size and location (bending, shear, and torsion) on the strength and stiffness of RC beams. Effects of large square and circular openings placed at critical locations in bending and shear are identified as the main gaps. From literature review, it is obtained that almost in all of the available researches; beams were tested under monotonic loading. Beams subjected to fatigue loading are identified as the needed area for future research.

Hamdy, K. S.et al. [40] performed Finite Element Modeling FEM using ANSYS v.15 to explore the efficiency of strengthening using carbon Fiber Reinforced Polymer CFRP and basalt Fiber Reinforced Polymer BFRP sheets

for RC T-beams having shear zone large rectangular opening. Four strengthening schemes were discussed. It was concluded that introducing CFRP or BFRP sheets resulted in great increase in load carrying capacity and stiffness of the strengthened beams. Crack patterns and failure loads for the tested models were compared with an experimental study carried out by the authors and FEM results were in good agreement with experimental results**.** Different Strengthening schemes are illustrated in figures (2-9 to 2-12). B-O-S-CFRP-1 is strengthened by wrapping of the bottom cord only using one layer of CFRP sheet. B-O-S-CFRP-2 is strengthened by applying two horizontal side CFRP strips at bottom cord and confining of the bottom cord using one layer of CFRP, In addition 50 mm U-strips are applied to right and left of the opening for the beam stem only (not complete wrap). B-O-S-CFRP-3 is similar to B-O-S-CFRP-2 but additional longitudinal CFRP strip with 100 mm width was applied to the slab top surface above the opening. B-O-S-CFRP-4 is typically as B-O-S-CFRP-3 but additional horizontal strip with 100 mm width was applied to the beam soffit under the opening and extended 100 mm right and left. Also, the side vertical strips were completely wrapped around the web through pre-cut slots through the slab. B-O-S-BFRP was strengthened as B-O-S-CFRP-4 but with BFRP instead of CFRP. Figures from (2-22) to (2-26) show the finite element mesh and details of reinforcement.

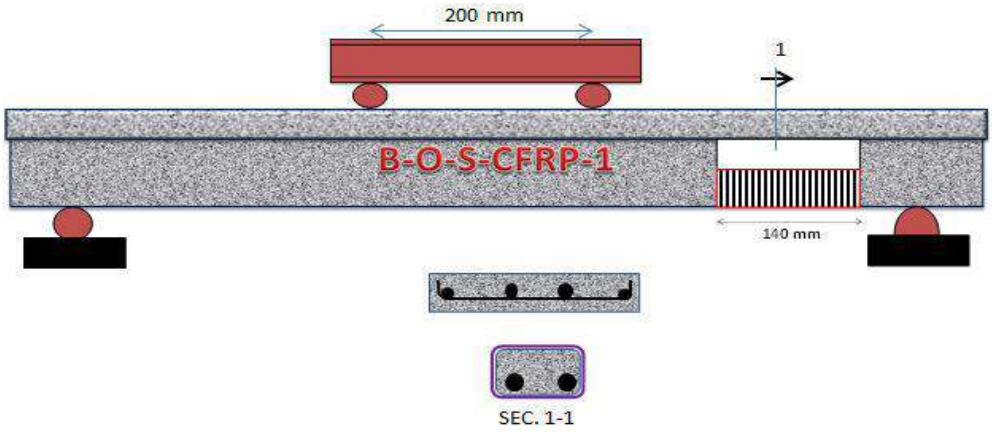

Figure (2-22): Strengthening scheme 1**Hamdy, K. S.et al. [40]**

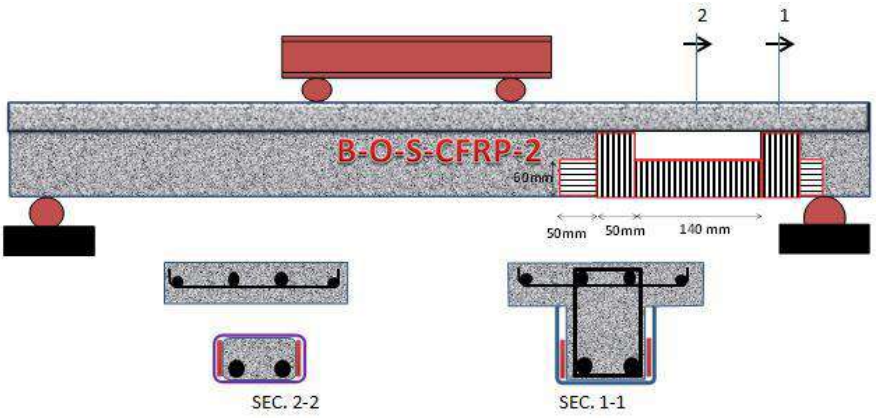

Figure (2-23): Strengthening scheme **.Hamdy, K. S.et al. [40]**

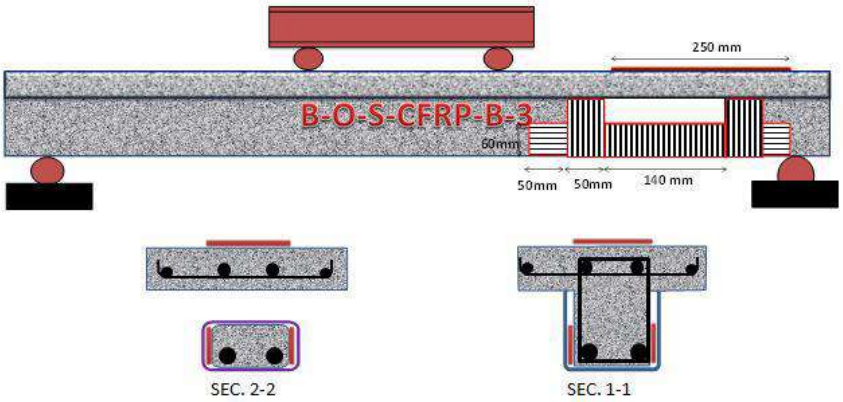

Figure (2-24): Strengthening scheme **Hamdy, K. S.et al. [40]**

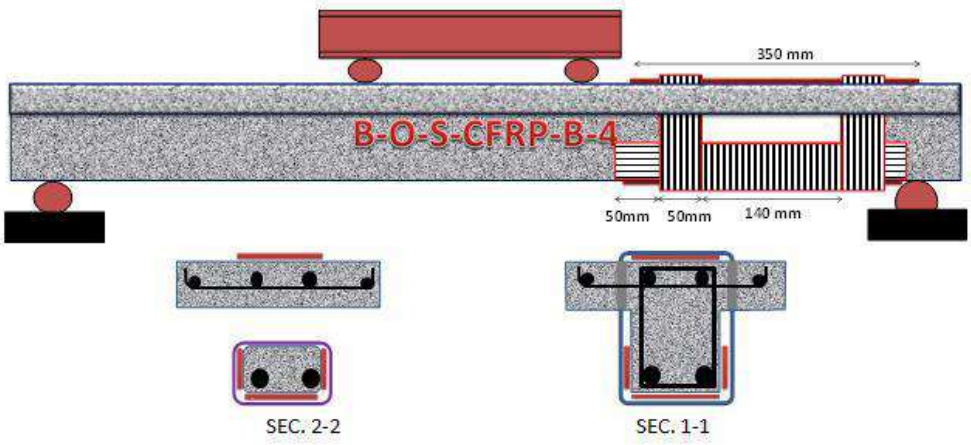

Figure (2-25): Strengthening scheme **Hamdy, K. S.et al. [40]**

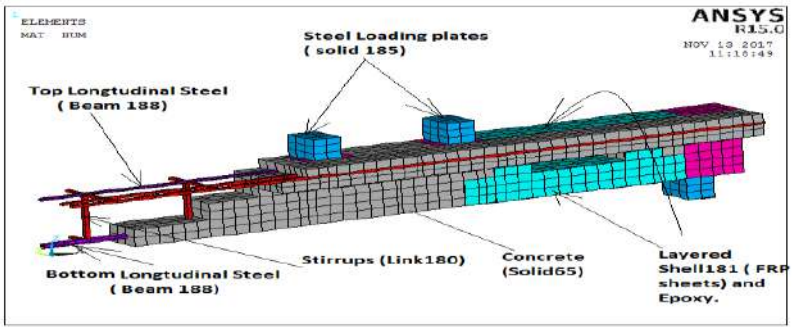

Figure (2-26): FE mesh (B-O-S-CFRP-4) 1**Hamdy, K. S.et al. [40]**

In the end, Finite element results were compared with experimental results. It is not efficient to wrap only the bottom cord of the opening with FRP sheets as the shear cracks start from the opening corners. The RC shallow T-beams with openings can behave as solid beams if they are properly strengthened. Modeling of longitudinal steel bars in ANSYS using beam elements is better than modeling them with link elements so that it can consider the dowel action in shear resistance. CFRP is more efficient than BFRP due to high modulus of elasticity and tensile strength; max % increase in ultimate load over control opened beam was 76.5% and 56.5% for CFRP and BFRP strengthened beams respectively.

WY Lu.et al., [41] examine the effect of carbon fiber reinforced polymer (CFRP) on the shear strengths of deep beams with web openings. A total of 18 high-strength concrete deep beams with web openings were tested. Twelve were externally wrapped with four layers of CFRP, six of them strengthened in the horizontal direction and the others in the vertical direction. The parameters of the configuration of CFRP, the sizes of the openings and the locations of the openings were covered in this study. The test results indicates the shear strengths of deep beams with openings sized 60×40 mm were about 16% higher than that with openings sized 68×68 mm. For deep beams with openings sized 60×40 mm, the lower the locations of openings the higher the shear strengths were. The test results also indicate the shear strengths of deep beams with web openings strengthened by CFRP wrapped in the vertical direction can be

enhanced by about 10%. However, the shear strengths of deep beams with web openings strengthened by CFRP wrapped in the horizontal direction can only be enhanced by about 6%. The shear strengths of deep beam, with different size and location of web openings and strengthened by different configuration of CFRP can be reasonably predicted by the empirical formulas of Kong and Sharp. The shear strengths of deep beams with web openings strengthened by CFRP wrapped in the vertical direction can be enhanced by about 10%. However, the shear strengths of deep beams with web openings strengthened by CFRP wrapped in the horizontal direction can only be enhanced by about 6%. Also**,** the shear strengths of deep beam, with different size and location of web openings and strengthened by different configuration of CFRP, can be reasonably predicted by the empirical formulas of Kong and Sharp (1977).

SHENG, T. F., [42] deals with the experimental study of the behavior of reinforced concrete deep beams with or without large rectangular openings as well as openings strengthened using externally bonded Carbon Fiber Reinforced Polymer (CFRP) composites in shear. The structural behavior, including the load deflection, cracking patterns, failure mode, and effectiveness of the CFRP wraps were investigated. A total of four specimens of beams with compressive strength of 35 MPa were tested to induce shear failure under 4 points loading test, which included one solid deep beam acted as a control beam (CB), one of which was tested without strengthening (US-BRO), and the remaining beams were strengthened with CFRP wraps in varying configurations around the opening (S-BRO-1, S-BRO-2). The beam had a cross section of 120 mm in width and 600 mm in depth as well as a length of 2400 mm. All the test specimens had a same geometry, main reinforcement arrangements and opening's location. All the preparatory works of specimen materials were conducted in Laboratory FKASA. The examined parameter was the effect of configurations of the CFRP wraps used for the shear strengthening. The inclusion of un-strengthened large rectangular openings in the shear zone of a

reinforced concrete deep beam leads to a reduction of ultimate beam strength by approximately 70%. The application of CFRP wraps with the presented strengthening configurations restricted the propagation of the diagonal crack and effectively increases ultimate load-carrying capacity as well as the ductility of the beam. The strength re-gains by U-shaped strengthening configuration around the openings was approximately 36% as compared to the beam with un-strengthened openings. However, the deep beam with U-shaped CFRP with horizontal fiber strengthened at the top and bottom chords of the openings were not capable to restore the control beam's original structural strength remarkably. The beam only managed to re-gain about 41% of the control beam's capacity.

Shakir, Q. et al., [43] based on experimental work included testing of thirteen specimens categorized into two groups. The first group included five beams: one is solid while the others are hollow beams with two openings of different sizes and locations. The second group included eight specimens strengthened with CFRP sheets in three systems to determine the best configuration of strengthening. The experimental results showed that the presence of openings (150*150) mm and (150*250) mm, which located flushed to the flange, led to a decrease in the load capacity by (43% and 64%) for the square and rectangular openings respectively. On the other hand, when the openings located in bottom location the reduction in capacity was found to be (48% and 70%) for the square and rectangular opening respectively. Also, the results of the test showed that the strengthening of the carbon strips led to improving in the structural capacity, where in the case of openings located flushed to the flange, there was an increased by (19% and 64%) for square and rectangular openings respectively. In contrary, in the case of opening located in the bottom location, the improvement in capacity was found to be (37% and 87%) for square and rectangular opening, respectively. This paper summarized a result of an experimental study on the strengthening of self-Compacting Reinforced Concrete T-deep beam with large opening by (CFRP) carbon fiber reinforced

polymer sheets. The full warp below opening (bandage) is necessary to provide the resistance, especially when the opening is located close to the bottom of the web. The strengthening with the CFRP sheets led to an improvement in structural capacity by (19% and 64%) for square and rectangular openings respectively, when located flushed to the flange while bottom location, was found the improvement in capacity by (37% and 87%) for square and rectangular openings respectively. Strengthening the interior faces of the opening corners with CFRP sheets did not contribute a significant improvement in the general behavior due to the comparison of CFRP sheets in the opposite side that desiring the resistance. Thus, it is recommended to adopt such configuration when using material strong in comparison as steel plates and angle.

El Maaddawy, T., & Sherif, S.,[44] presents the results of a research work aimed at examining the potential use of externally bonded carbon fiber reinforced polymer (CFRP) composite sheets as a strengthening solution to upgrade reinforced concrete (RC) deep beams with openings. A total of 13 deep beams with openings were constructed and tested under four-point bending. Test specimen had a cross section of 80 × 500 mm and a total length of 1200 mm. Two square openings, one in each shear span, were placed symmetrically about the mid-point of the beam. Test parameters included the opening size, location, and the presence of the CFRP sheets. The structural response of RC deep beams with openings was primarily dependent on the degree of the interruption of the natural load path. Externally bonded CFRP shear strengthening around the openings was found very effective in upgrading the shear strength of RC deep beams. The strength gain caused by the CFRP sheets was in the range of 35–73%. Figures (2-27) and (2-28) shows the test setup and strengthening system of the specimens respectively.

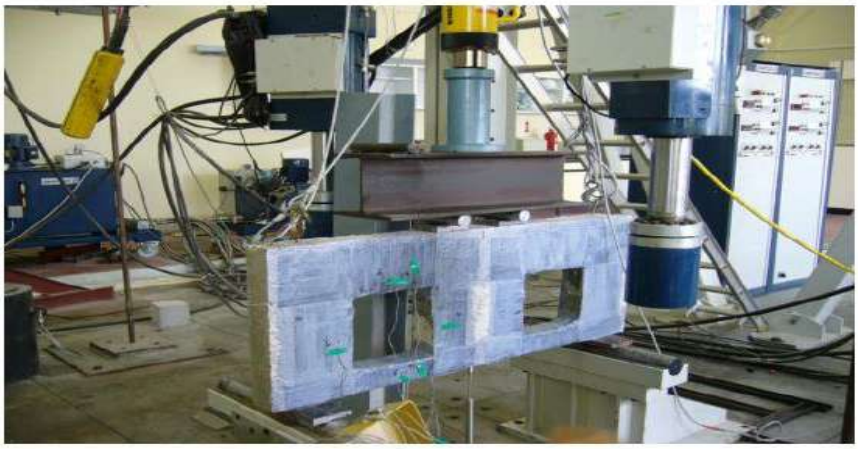

Figure (2-27): Test setup, **El Maaddawy, T., & Sherif, S., [44]**

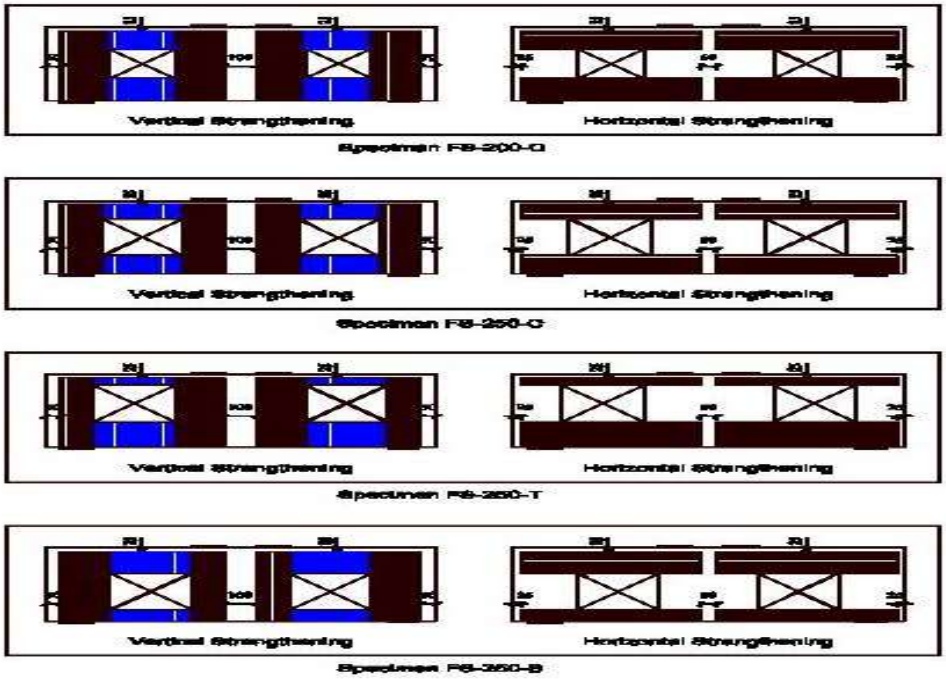

Figure (2-28): CFRP strengthening scheme (unit in mm), **El Maaddawy, T., & Sherif, S., [44]**

Hawileh, R. A.et al., [45] developing a 3D nonlinear finite element (FE) model that can simulate the response of reinforced concrete (RC) deep beams with openings strengthened in shear with carbon fiber reinforced polymer (CFRP) sheets. The opening is located at the midpoint of the shear span so that it fully interrupts the natural load path. The FE model is developed and the simulation environment is conducted using the commercial finite element code, ANSYS. The concrete material is modeled using solid elements that account for concrete

cracks and other material nonlinearities. Multilayer Shell elements are used to model the CFRP sheets along with their adhesive. Link elements are used to model the internal steel reinforcement. The FE model accounts for the bond behavior at the concrete-to-CFRP interface by introducing a layer of epoxy at the interface between the concrete and the CFRP. The results of the FE model are in good agreement with the experimental data. Four 3D nonlinear FE models are developed using the simulation environment, ANSYS 11.0 (2007). The developed FE models presented herein are based on the tested specimens in (El-Maaddawy & Sherif, 44) 2009 experimental program; hence they have the same dimensions, geometry and material configurations, boundary conditions, and loading. The concrete material was simulated using SOLID65 ANSYS (2007) elements. The steel bars reinforcements were modeled using LINK8 ANSYS 2007 element. The CFRP sheets are modeled using SHELL99 ANSYS 2007 element with elastic orthotropic material properties that have its own coordinate system, where the x-axis is in the direction parallel to the fibers. SHELL99 element is used to model layered applications of structural shell models. The element allows up to 250 layers and has eight nodes with six degrees of freedom at each node: translations in the x, y, and z directions and rotations about the x, y, and z-axes. In this study, the first layer of SHELL99 is used to simulate the epoxy resin at the concrete/CFRP sheet interface while the following layers are used to simulate the CFRP sheets, both horizontally and vertically depending on the location of the FRP element. The coordinate system for each layer of the SHELL99 elements is specified depending on the orientation of the CFRP fibers, horizontally or vertically. Based on the results of this study, the following conclusion can be drawn:

· The load-deflection response of the FE models is in a good agreement with the measured experimental response.

· The FE simulation models confirmed that the size of the opening and the presence of the CFRP strengthening have a significant influence on the performance of RC deep beams. The larger the opening size, the more likely the RC deep beam to fail prematurely. The CFRP strengthening around the openings resulted in up to a 75% increased the shear capacity.

· The developed FE models verified in this study could be used as an alternative to experimental testing, which is usually more costly and time extensive. The FE modeling of the problem can also serve as a numerical platform for performance prediction of RC deep beams with openings strengthened in shear with CFRP composites.

Lam, L., Hussain, Q. et al., [46] examines the effect of glass chopped strand mat fiber composites (GCSM) with the mechanical anchor on the shear strength of reinforced concrete deep beams. Two types of matrix system were used to provide stresses between the fibers and between the fiber composites-to-concrete interface. Epoxy and polyester resin were investigated and compared to find the suitable resin matrix. Mechanical expansion anchor system which was recently proposed by the author was used in this study. The experimental results indicated that using GCSM composites with mechanical anchors led to enhancement of load-carrying capacity and stiffness of the beams. Epoxy resin system was found to be more effective compared to Polyester resin. The ultimate shear capacity of the RC deep beams strengthened with epoxy system was increased up to 68% compared to the control specimen. Continuously wrapped the GCSM fiber composites over the bottom and both sides of the beam in the form of a U-wrapped provided additional anchorage at the bottom end of fiber composites. This leads to the prevention of debonding and the increase of loading capacity. Providing additional bond strength of the bond interface by using mechanical anchor found to be more effective since it leads to more usage of the composites. Strengthening technique using FRP wrapped with

mechanical anchors supposedly confined the compressive strut which is able to increase the loading capacity. A total of five beams were constructed to investigate the shear strengthening using glass chopped strand mat fiber with two different kinds of the matrix system. Epoxy resin and polyester resin were used in this study. The beams were 100 mm thick and 350 mm deep along with the total length of 1000 mm. All specimens were tested under single-point loading with a shear span of 420 mm giving a shear span-to-depth ratio (*a/h*) of 1.2. The longitudinal reinforcement consisted of two 12 mm diameter deformed bars. The compressive steel reinforcement consisted of three 6 mm round bars. The web reinforcement consisted of 6 mm smooth bars spaced at 150 mm and 100 mm in vertical and horizontal direction, respectively. The vertical web reinforcement was in the form of stirrups whereas the horizontal web reinforcement was longitudinal bars on both sides of the beams. Closely spaced vertical stirrups were used at both ends of the beams to avoid premature failure at these locations. Four beams strengthened using fiber composites with mechanical anchors were divided into two groups, group 1 and group 2, based on the different types of resin. Each group comprised two beams which were strengthened by side bonding (both-side) and by U jacketing (U-wrapped). Fully wrapping the FRP system around the section on all four sides was not investigated in this study due to the impractical usage. The cured fiber composite thickness of 2 mm along with the anchor spacing of 150 mm and 100 mm in vertical and horizontal direction was kept the same for all strengthened beams. The number in the specimen designation refers to the number of layers of GCSM fiber. The letters “P” and “E” refers to the polyester resin and epoxy resin, respectively. The letter “A” refers to “Strengthening in Both-Side Bonded” while the letter “B” refers to “Strengthening in U-Wrapped Scheme”. **Hussain, Q., & Pimanmas, A., [47]** presents the finite element analysis conducted on SFRP strengthened reinforced concrete (RC) deep beams. The analysis variables included SFRP material (glass and carbon), SFRP thickness

(3 mm and 5 mm), SFRP configuration and strength of concrete. The externally applied SFRP technique is significantly effective to enhance the ultimate load carrying capacity of RC deep beams. In the finite element analysis, realistic material constitutive laws were utilized which were capable of accounting for the non-linear behavior of materials. The finite element analysis was performed using computer software WCOMD. In the analysis, two dimensional eight-node reinforced concrete planar elements for concrete and planar elements with elastic-brittle behavior for SFRP were used to simulate the physical models. The concept of smeared cracking in concrete and steel was adopted over the element. The calculated finite element results are found to be in good agreement with the experimental results and to capture the structural response of both un-strengthened and SFRP strengthened RC deep beams. A comparison between the finite element results and experimental data proved the validity of the finite element models. Further, the finite element models were utilized to investigate the behavior of RC deep beams strengthened with different directions of SFRP Strips (vertical and horizontal). The vertical SFRP strips are found to be more effective than horizontal ones. Figure (2-29), shows the sketch of a typical RC deep beam specimen used in experimental investigation. The RC deep beams were designed in such a way to develop shear failure. The bottom steel bars were 2-DB12 (Yield strength = 410 MPa) and shear reinforcements were RB6 plain bars (yield strength = 240 MPa). The RC deep beams were cast using low strength (21.45 MPa) and high strength concrete (46.20 MPa). The casting of RC deep beams was performed in a vertical position.

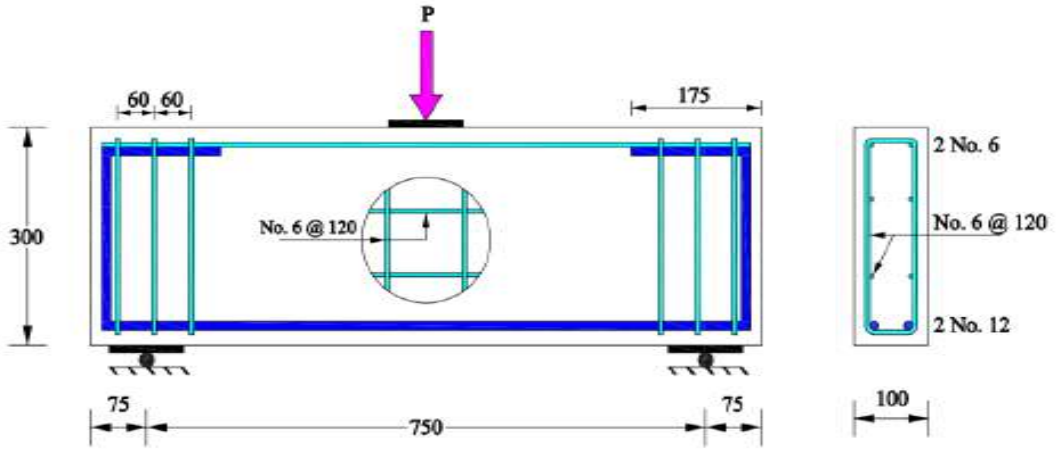

Figure (2-29): Details of test specimen (units in mm). **Hussain, Q., & Pimanmas, A. , [47]**

Hussain, Q., & Pimanmas, A., [48] also presents an experimental investigation performed on reinforced concrete (RC) deep beams with circular openings strengthened using externally bonded sprayed fiber reinforced polymer (SFRP) composites. The research parameters investigated were openings size, thickness of SFRP and orientation of SFRP. A total of 8 RC deep beams with circular openings were constructed and tested under three-point bending. Test specimen had a cross section of 100 x 500 mm and a total length of 1050 mm. Two circular openings, one in each shear span were placed symmetrically about the mid-point of the beam. SFRP was applied either on both lateral faced or on three faces (U-shaped) excluding the top face. An anchorage system was utilized to enhance the bond between concrete and SFPR. It was found that externally bonded SFRP and anchored with mechanical anchors are very effective to enhance the shear strength of deep beams. The strength gain caused by the SFRP was in the range of 64%-130%. Also, SFRP applied on 3 sides (U-shaped) was found to be more effective than 2-sided SFRP in shear strengthening.

Al-Ghanem, H. et al., [49] studies the shear and flexural behavior of reinforced concrete (RC) deep beams strengthened with externally bonded carbon fiber-reinforced polymers (CFRP). Using two types of CFRP composites including sheets and laminates, different configurations for shear and flexural

strengthening of deep beams were experimentally investigated. In total, twenty specimens of deep beams with cross-sectional dimensions of 190 mm width, 400 mm depth and an overall length of 1 900 mm were casted and tested to failure. Concerning the cracks' formation, failure's modes, ultimate strength and overall stiffness, the performance of the strengthened beams compared to the control beams were evaluated. From the test results, the effectiveness of CFRP technique on enhancing both the shear and flexural capacity of deep beams is verified; however, the efficiency differs variedly depending on the material and the strengthening scheme. Regarding the shear strengthening, using the continuous wrap of two sheets records the highest increase in the ultimate strength with a value exceeds 86% compared only to 36% with the inclined laminates. On the other hand, an enhancement of about 51% is achieved through the flexural strengthening with two layers of sheets and 26% when the laminates are used; both are accompanied by a divergent in the failure mode from flexure to shear**.** The effectiveness of CFRP composites on enhancing both the shear and flexural capacity of deep beams is verified; however, the efficiency differs variedly depending on the material and the strengthening scheme. Although the use of CFRP sheets for shear strengthening is found to be the most useful and practical system concerning the amount of material consumed and the ultimate strength attained, the other system of using the laminates is found to be almost equally effective. However, taking the economic aspect into consideration resulted in adopting the use of CFRP sheets rather than laminates. Regarding the shear strengthening, using the continuous wrap of two sheets records the highest increase in the ultimate strength with a value exceeds 86% over the control beams, even though the beams strengthened by one layer of sheet showed a nearly similar increase reached to about 79% over the control beams. Thus, it can be concluded that the use of one layer of CFRP sheets is more efficient for practical solutions. Orientation of carbon fibers is found to be a major factor in the influence of CFRP materials on the shear resistance of

strengthened beams. The CFRP laminates oriented at an angle of 45o with respect to the longitudinal axis of the beam are more effective than the horizontal ones in increasing the beam's ultimate strength. This can be verified as an increase of about 36% was recorded for the inclined laminates compared only to 10% when the horizontal laminates were used. Also, the use of CFRP sheets is found to be more effective than using CFRP laminates in enhancing the flexural resistance of deep beams.

Kumar, G. H., [50] deals with the study of deep beams containing openings and the validation of results with FEM model using ANSYS. A total of 5 deep beams with openings are casted without shear reinforcements and are tested under three-point loading. Test specimen has a cross section of 150x460 mm and a total length of 1200 mm. Two circular openings, one in each shear span, are placed symmetrically about the mid-point of the beam. The structural response of RC deep beams with openings was primarily dependent on the degree of the interruption of the natural load path. Externally bonded GFRP shear strengthening around the openings was found very effective in upgrading the shear strength of RC deep beams. The strength gain caused by the GFRP sheets was in the range of 68–125%. Finite element modeling of RC deep beams containing openings strengthened with GFRP sheets is studied using ANSYS and the results are compared with experimental findings. SOLID65 is used for the 3-D modelling of solids of Reinforced Concrete. BEAM188 is used as reinforcing bars, to model supports and under the load steel plate is used, which SOLID 45 is used. To model laminated composites SHELL 91 is used**.** A simply supported beam is considered having and overall length of 1200 mm with effective length of 900 mm. Size of the beam is 150 x 460 mm. Figure (2-30) shows the control beam with boundary conditions used in the analysis. Single point loading is applied at the midpoint of the beam. To get the accuracy of results mesh size considered as 25 mm as edge length.

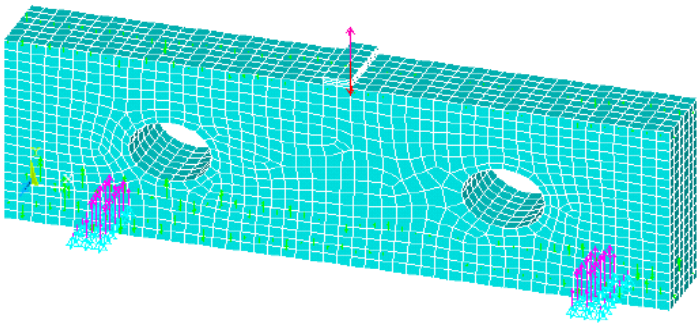

Fig. (2-30): Deep beam model in ANSYS. **Kumar, G. H., [50]**

longitudinal reinforcement and 6 mm diameter bars are used as stirrups. The tension reinforcement consists of 2 no's 12 mm diameter HYSD bars. Two bars of 8 mm of HYSD bars are also provided as hang up bars

Abdel-Kareem, A. H., [51] presents the experimental results of twenty-three reinforced concrete beams with rectangular web openings externally strengthened with Fiber Reinforced Polymers (FRP) composites bonded around openings. All tested beams had the same geometry and reinforcement details. At openings locations, the stirrups intercepted the openings were cut during fabrication of reinforcement cage to simulate the condition of inclusion of an opening in an existing beam. Several design parameters are considered including the opening dimensions and location in the shear zone, the wrapping configurations, and the amount and the type of the FRP composites in the vicinity of the openings. The wrapping configurations of FRP included: sheets, strips, U-shape strips, and U- shape strips with bundles of FRP strands placed at the top and sides of the beam forming a fan under the strips to achieve closed wrapping. The effect of these parameters on the failure modes, the ultimate load, and the beam stiffness were investigated. The shear contribution of FRP on the shear capacity of tested beams with web openings was estimated according to ACI Committee 440-08, Canadian Standards S6-06, and Khalifa *et al*. model and examined against the test results. A modification factor to account for the dimensions of opening chords was applied to the predicted gain in the shear capacity according to ACI 440-08 and CSA S6-06 for bonded Glass Fiber

Reinforced Polymers (GFRP) around openings. The analytical results after incorporating the modification factor into the codes guidelines showed good agreement with the test results. Span to depth ratio of 3.04. One opening was created on a side of the test specimens. At opening locations, each opening intercepted one or more of the stirrups. To simulate the condition of inclusion of an opening in an existing beam, these stirrups were cut during fabrication of the reinforcement cage. The FRP were bonded to the concrete at all surfaces around the openings such that the principal direction of fibers was oriented to interrupt the potential shear crack. Longitudinal FRP strips with fibers oriented in a direction parallel to the longitudinal axis of the beam were provided above and below each opening. Vertical FRP with different configurations and fibers oriented in a direction perpendicular to the longitudinal axis of the beam were wrapped around the opening chords, and adjacent to each vertical face of the opening. Four wrapping configurations for the vertical FRP, were used as follows; sheets, strips covered 50% of the opening chords length, U-shape strips left a clear distance 25 mm at the top of beam to account for the presence of a concrete slab, and U- shape strips with bundles of FRP strands placed at the top and sides of the beam forming a fan under the strips to achieve closed wrapping. The last two configurations of the vertical FRP were applied to the top opening chords only, while strips wrapped the bottom opening chords. The FRP sheets and strips had an overlap of about 50 mm. For all strengthened web openings, the number of layers for both vertical and horizontal FRP was the same and the width of vertical strips adjacent to the vertical faces of the opening was 75 mm. Different strengthened systems, included the wrapping configurations, the amount of FRP (number of applied layers), and the type of FRP (glass or carbon), were applied to web openings 150 x 450 mm. Other web openings with different dimensions and locations in the shear zone were strengthened by two layers from GFRP strips. configurations around openings. At failure, the U-shaped strips wrapped the top chord of the openings were detached from the

concrete surface near the point load. For sheets, strips, and U-shaped strips with bundles of FRP strands at the top and beam sides, the FRP ruptured at the onset of failure. For all tested beams the shear failure was accompanied by diagonal shear cracks between FRP bonded around the openings and the point load and the support. A modification factor (*Ko)* to address the effect of the dimensions of openings chords on the contribution of GFRP to shear resistance of strengthened web openings is defined as a function of chord width to chord height. Incorporating *Ko* into the predicted gain in the shear capacity equations from ACI 440-08 and CSA S6-06 guidelines results in a significantly improved correlation of the experimental results with the predicted results from the codes guidelines.

El-Kareim et al, [52] cared with T-shaped sections as they studied experimentally the behavior of flanged deep beams with web openings. This study aims to enrich the literature by reporting the experimental data of sixteen deep beams: twelve with flanged section (with or without opening) and four reference beams with rectangular section. The shear span to depth ratio (a/d) was 1.10. The openings in the beams' web had a constant depth (120 mm) and varied lengths (120 mm, 240 mm, and 360 mm). The effect of flange on the strength, stiffness, and deformation capacity of the tested beams was assessed. The results were analyzed in terms of cracking pattern, mode of failure, load–deflection behavior, deformations distribution, and strains in reinforcement. Prediction of the experimentally obtained behavior using finite element model was introduced. Assessment of ultimate strengths based on the available design equations and analytical models was also discussed. The test results clearly showed that the flange resulted in a significant gain in the strength and stiffness that cannot be ignored in the design. The FEA was shown to provide a reasonably accurate estimation of the experimental behavior for the tested beams. With the assumptions made herein, the modified compression field

theory (MCFT) prediction was the closest to the experimental results shown in Figure (2.31)

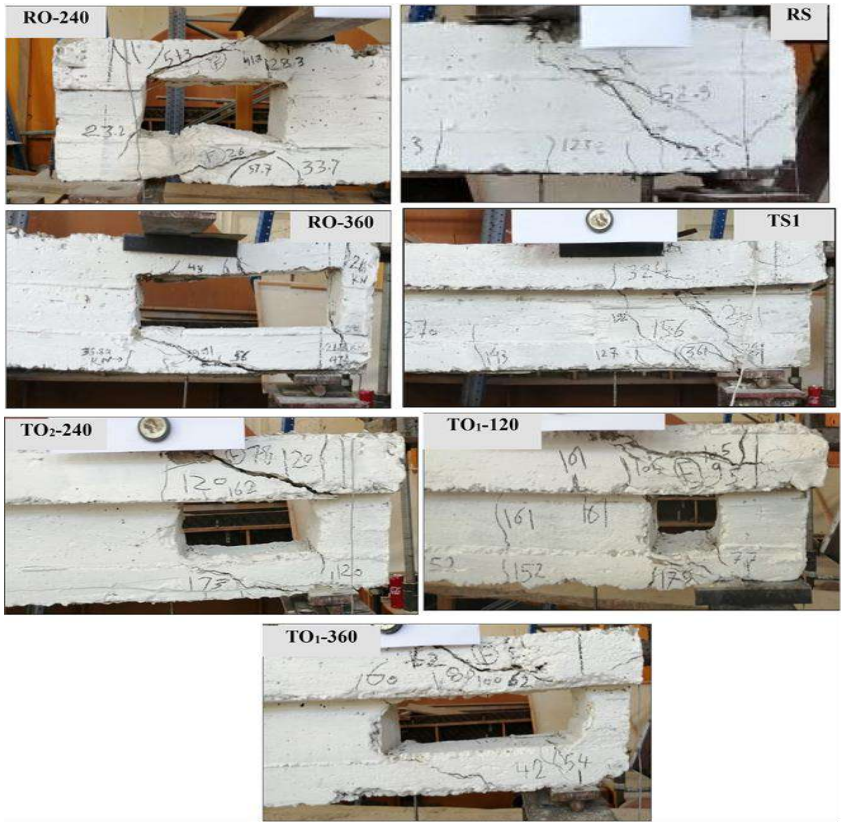

Figure (2-31): Failure mode for some representative beams. **El-Kareim et al, [52]**

Ghali MK et al, [53] studied numerically the Behavior of T-shaped deep beams with openings using different loading conditions. The studied parameters included flange dimensions, shear span to-depth ratio, concrete strength, size and location of openings, VL and HZ stirrups ratios and loading type. In addition, top and bottom-loaded deep beams were investigated. Increasing the flange depth by 50% and 100% increases the initial cracking load by 10% and 14% and the ultimate shear capacity by 16% and 22% respectively. The opening size controlled the appearance of the first diagonal crack load. Decreasing the opening size enhanced the first cracking load. Decreasing (a/d) by 16.7% and 41.7% increased the cracking load by 17% and 131% and the ultimate shear capacity by 13% and 115% respectively. Finally, the shear capacities for 71 test results have been calculated using an existing strut-and-tie model (STM). The

comparison showed that the STM model performs well in predicting the ultimate shear capacity. The overall average value of the ratio between NLFE and predicted strengths is 1.157. The applied Load and the Support Conditions of the Deep Beams is shown in Figure (2-32).

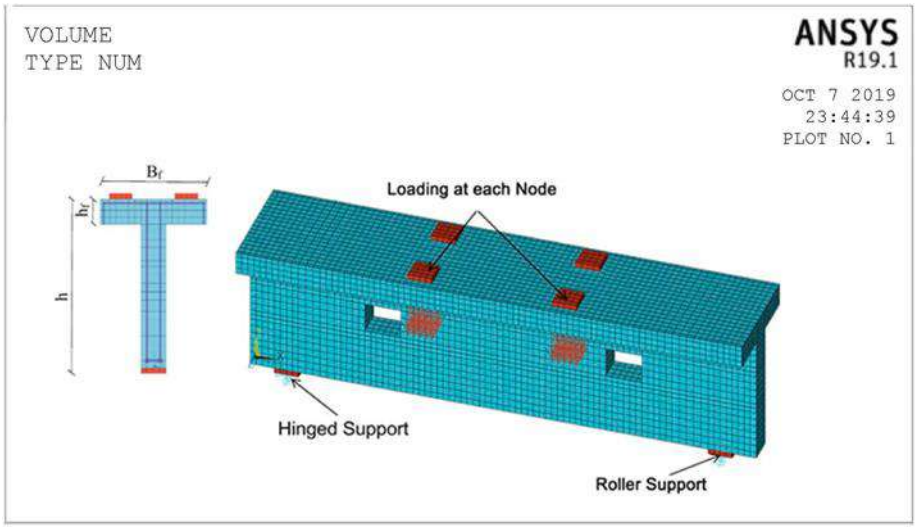

Figure (2-32): The applied load and the support conditions of the deep beams.

Ghali MK et al, [53]

Nasr Z. Hassan [54] analyzed thirty-nine specimens using finite element method (Ansys 14) to study the behavior of high–strength reinforced concrete deep beams with openings. Specimens are simply supported deep beams of effective span 1800 mm from support to support. An overhanging length of 240 mm from each support was to provide an adequate anchorage length of steel reinforcement and to prevent any local failure at support. Cross section dimensions of each beam are 120 mm width and 600 mm thickness. The specimens divided to three sets, Set A, consists of sixteen specimens divided as four groups with same opening dimension (60 mm x 60 mm) and different location directions (Horizontal, Vertical, Diagonal and Perpendicular to the diagonal), four specimens are in each direction. Set B, examines fifteen specimens consists of three Groups, all of them have same opening location and different opening shape, such that square or rectangle. Finally set C examines

eight specimens divided to two groups considering the behavior of the characteristic strength of concrete, one group contains four beams' specimens of normal strength concrete while, the other group contains four beams of high strength concrete. He concluded that as much more area of opening inside the central zone increases, the failure load decreases. Beams with normal strength concrete are more ductile than beams with high strength concrete, Cracks taken the strut and tie triangular shape, extents from supports to load plate, concentrated around openings corner and there are no cracks at the two zones after the supports. Stresses at mid – span increases linearly till it reached to first crack, then it increases non – linear taken the shape of parabola till it reached to failure where maximum stress found. At corners of openings the stress began from zero, reaches to maximum value at first crack then it returned to zero at failure. Stresses decreases as the size of opening increases.

Also, **Nasr Z. Hassan et al [55]** tested experimentally ten reinforced concrete deep beams The beams were simply supported on rigid steel plates of 800 mm apart (span length) and with overhanging 150 mm from each side, the total height of the beam and its thickness are 800 mm and 100 mm respectively. Shape, size and location of opening are considered in this study. The first beam is control beam without openings, three beams with square openings of 120 mm x 120 mm, with different locations, another three beams with rectangular openings 160 mm x 80 mm, with length in vertical direction, while the last three beams have rectangular openings 160 mm x 80 mm, with length in horizontal direction. Results indicated that all deep beam with opening have failure load less than its control beam. It also indicated that either moving of opening far from the imagine width path of forming strut member from concentrated load to each support of the deep beam as shown in Figure (2-33) or decreasing the opening size, the failure load decreases , bottom deflection decreases and corresponding ductility increases.

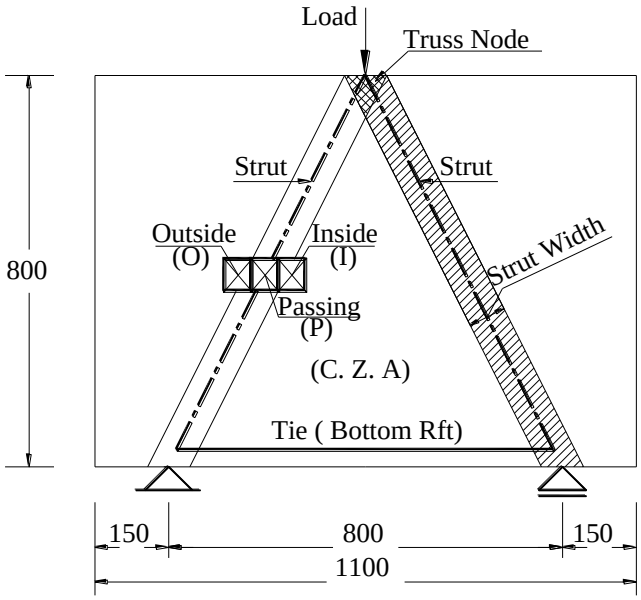

Figure (2-33): The locations of openings, **Nasr Z. Hassan et al [55]**

CHAPTER THREE
EXPERIMENTAL PROGRAM

3.1 Introduction

This chapter deals with the experimental program, properties of strengthening materials, and the material properties used in casting deep beams to study the behavior of eleven deep beams with and without openings strengthened vertically and horizontally with basalt fiber sheets. The openings have different shapes with constant area

3.2 Experimental Program

The experimental program consists of eleven deep beams divided into five groups as listed in Table (3-1). All beams have the same rectangular cross-section with dimensions of 150 mm wide,500 mm depth, and a length of 1000mm. The clear span of the tested deep beams was fixed at 850mm. **Group 1** consists of two deep beams without opening, one of them without strenghening and the other one strengthened horizontally using BFRP sheets, **group 2** consists of three deep beams with vertical rectangle openings with dimensions 100*200 mm, one of them is un strenghened and the others are strengthened vertically or horizontally with BFRP sheets, **group 3** consists of two deep beams with horizontal rectangle openings with dimensions 200*100 mm strengthened vertically or horizontally with BFRP sheets, **group 4** consists of two deep beams with circle openings with 160 mm diameter one o them strengthened vertically and the other strengthened horizontally using BFRP sheets and **group 5** consists of two deep beams with square openings having a length of 140 mm one o them strengthened vertically and the other strengthened horizontally using BFRP sheets, Figure (3-1) shows the concrete

dimenions and locations of openings in all deep beams, also Table (3-2) shows the concrete cross-section and the span of all group spesimens. Figures (3-2) through (3-6) show the details of reinforcement in all specimens (all dimensions in mm), the steel used for stirrups is mild steel with (F_y)=240 MPa with 6 mm diameter bars and high-tensile steel for longitudinal bars with (F_y)=360 MPa with 16 mm diameter at the top and have a rough surface to get more bonds between steel bars and concrete. The bottom reinforcement of the beams was two bars with 25mm diameter.

Table (3-1): The data of the tested beam

Group no.	Beam symbol	Type of opening	direction of opening	Size of opening	Location of opening	Strip width(mm)	No.of layers	Strip length (mm)	Strip direction
G1	B 1	-	-			–	–	–	–
	B 2	-	-		At both sides	100	2	1000	Hz
G2	B 3	rec	Vl	100*200		-	-	–	–
	B 4	rec	Vl	100*200		100	2	500	Vl
	B 5	rec	Vl	100*200		100	2	1000	Hz
G3	B 6	rec	Hz	200*100		100	2	500	Vl
	B 7	rec	Hz	200*100		100	2	1000	Hz
G4	B 8	circular	-	D=160		100	2	500	Vl
	B 9	circular	-	D=160		100	2	1000	Hz
G5	B 10	square	-	140*140		100	2	500	Vl
	B 11	square	-	140*140		100	2	1000	Hz

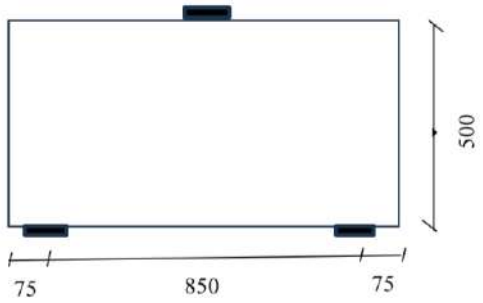

(a): Group 1

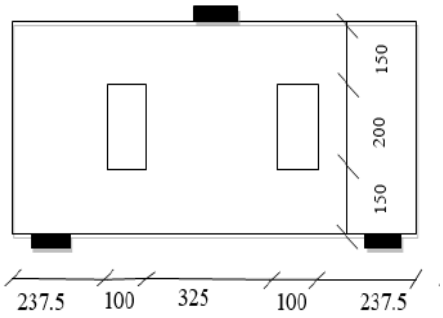

(b): Group 2

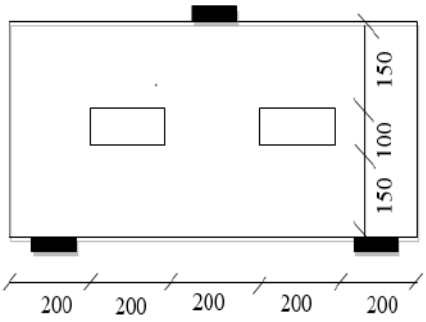

(c): Group 3

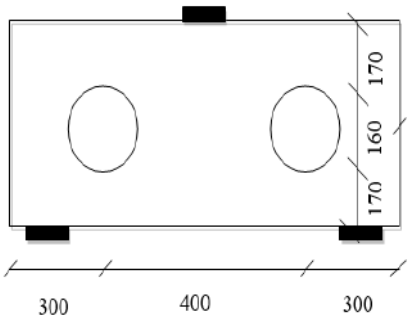

(d): Group 4

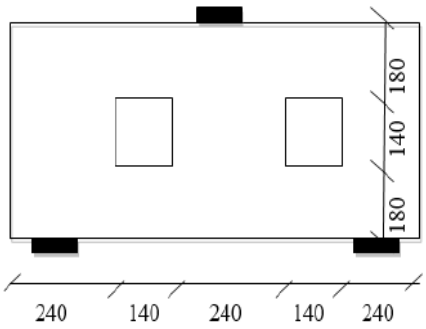

(e): Group 5

Figure (3-1): The concrete dimensions and the locations of openings in all group specimens.

Table (3-2) : The concrete cross section and the span of all the beams.

Beam	L_t	L	b	a	h	a/h	L /h
B	1000	850	150	425	500	0.85	1.7

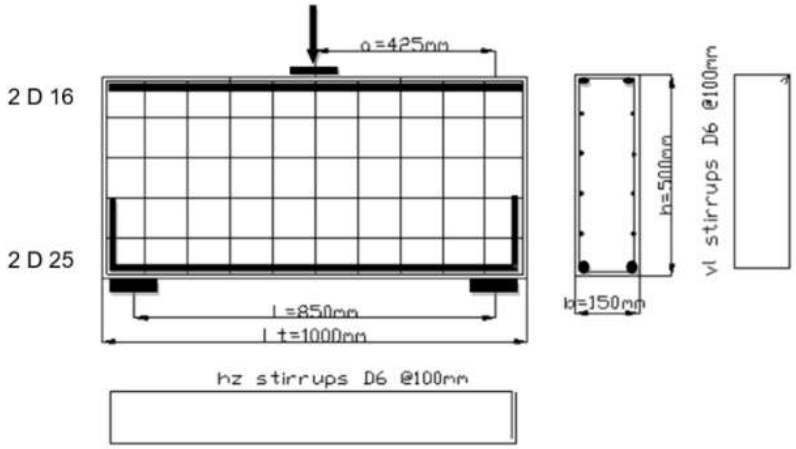

Figure (3-2): Details of reinforcement for group 1

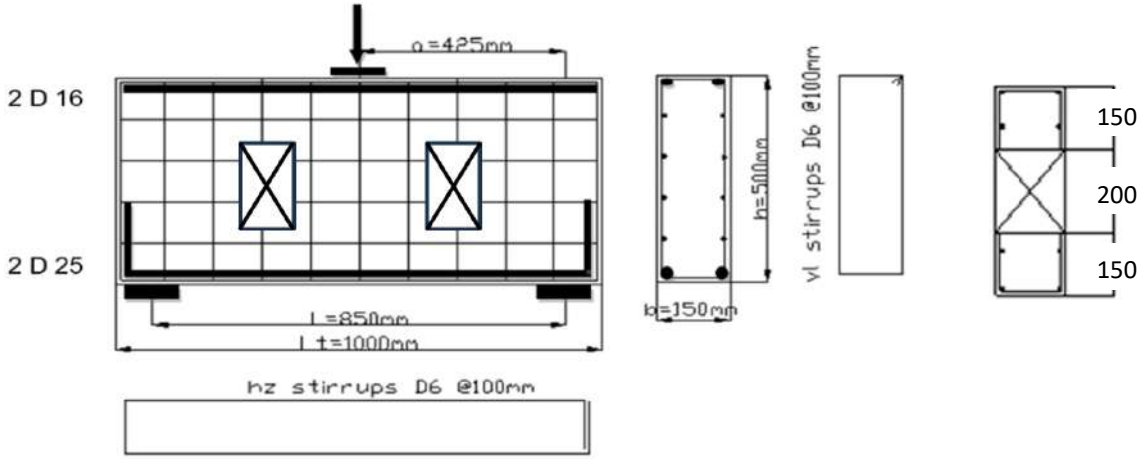

Figure (3-3): Details of reinforcement for group 2

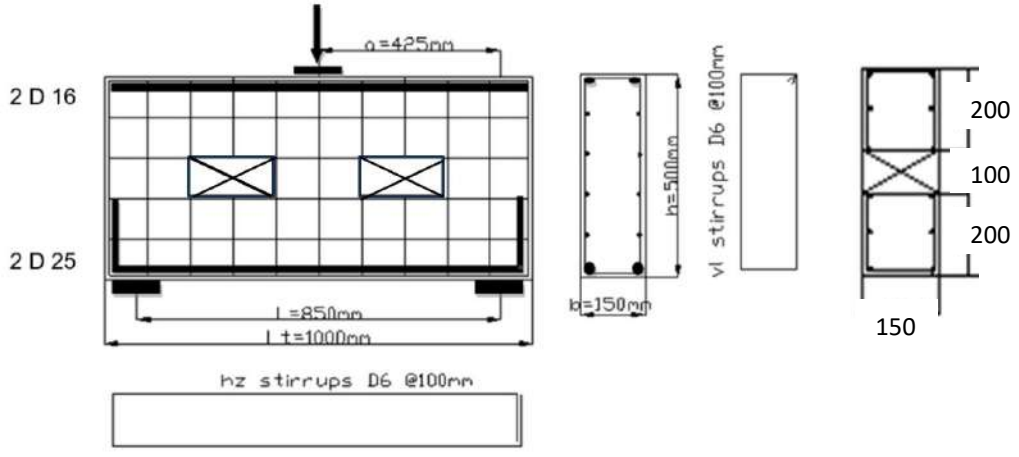

Figure (3-4): Details of reinforcement for group 3

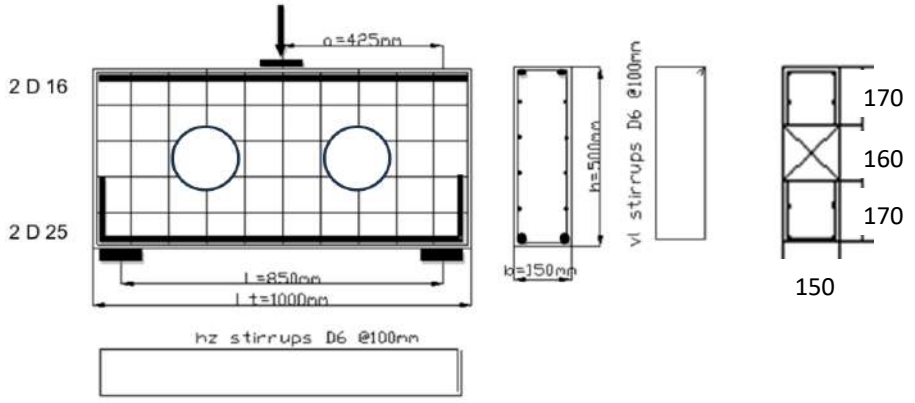

Figure (3-5): Details of reinforcement for group 4

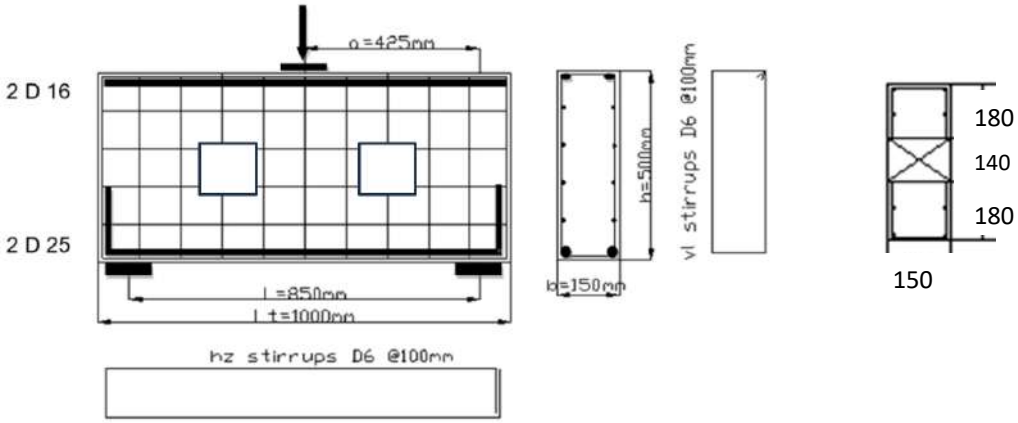

Figure (3-6): Details of reinforcement for group 5

Strengthening System of Beams.

Figure (3-7) presents a schematic of the BFRP plan employed for external shear strengthening. Two layers of longitudinal BFRP sheets with a 100 mm x 1000 mm size and fibers orientated parallel to the longitudinal axis of the beam were glued to the concrete above and below each opening. Additionally, two layers of BFRP sheets with fibers orientated vertically were wrapped behind the chords on the right and left for each opening with a size of 100 mm and a length of 500 mm, and they were placed next to each vertical face of the openings with fibers oriented vertically for each opening.

(a): Group 1 strengthing system

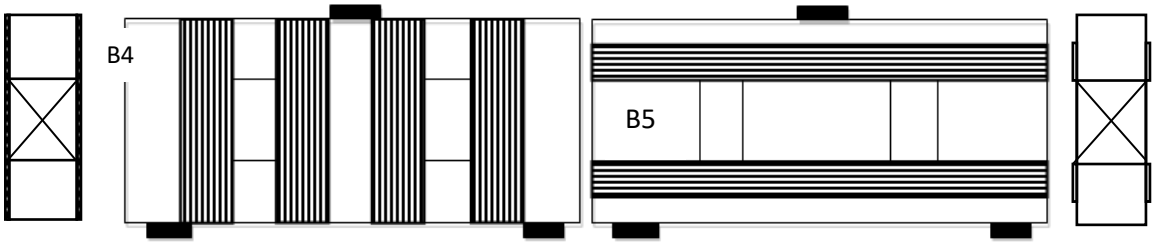

(b): Group 2 strengthing system

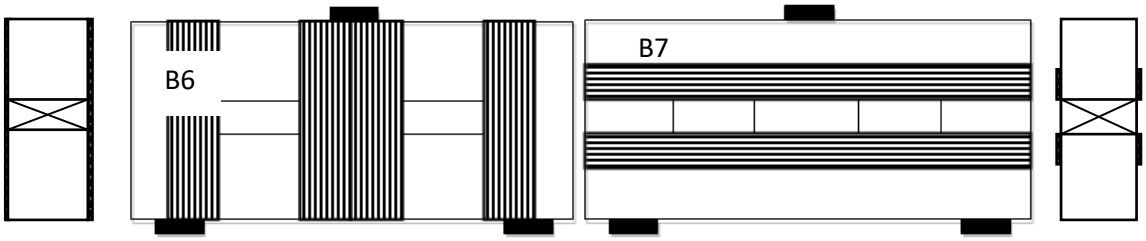

(c): Group 3 strengthing system

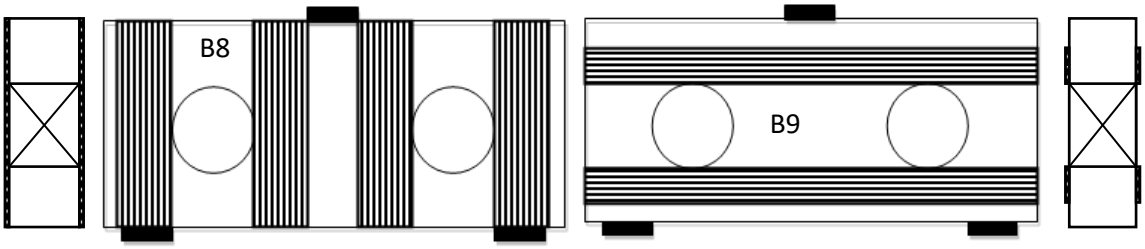

(d): Group 4 strengthing system

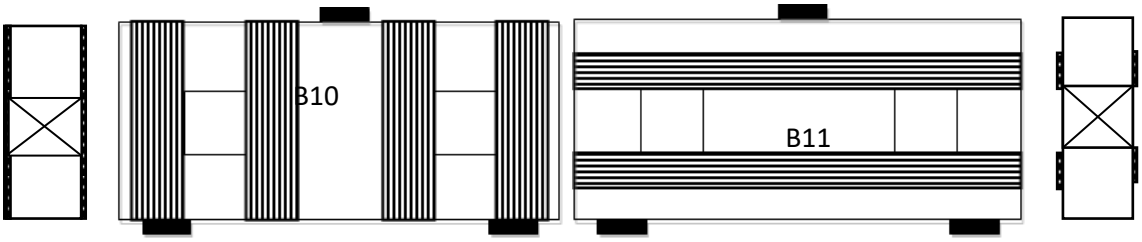

(e): Group 5 strengthing system

Figure (3-7): The deep beams strengthening systems.

3.3 Materials Used in Strengthening Deep Beams.

The strengthening system consists of two-row materials: basalt fiber and resin (epoxy resin)

3.3.1 Basalt Fiber

Basalt called (UD fabrics) are a kind of high-performance engineering material used as externally bonded structural strengthening of concrete, masonry, or wood members, which is used in conjunction with an appropriate leveling mortar or putty and structural adhesive to improve the flexural or shear strength of the member. Figure (3-8) shows the basalt fiber sheet used in this study and basalt fiber components are shown in Table (3-3).Three specimens were cut into size 100mm and roughed with sand as shown in Figure (3-9) to simulate the bond between sheets and concrete, then the strain gauges turned to it in the middle and the specimens have been tested in tensile machine until failure and the tensile force, the strain reading have been recorded, the stress -strain relationship shown in Figure (3-10). The properties of basalt fiber sheets from tests and data sheet are shown in Table (3-5)

Figure (3-8): Basalt fiber

Table (3-3): Components of the used basalt fibers

Chemical components	SiO_2	Al_2O_3	CaO	MgO	$Na_2O + K_2O$	TiO_2	$Fe_2O_3 + FeO$	Others
Percentage by mass	51.6 -59.3	14.6 - 18.3	5.9 - 9.4	3.0 - 5.3	3.6 - 5.2	0.8 - 2.25	9.0 - 14.0	0.09 - 0.13

Figure (3-9): The specimen of basalt fiber roughed with sand

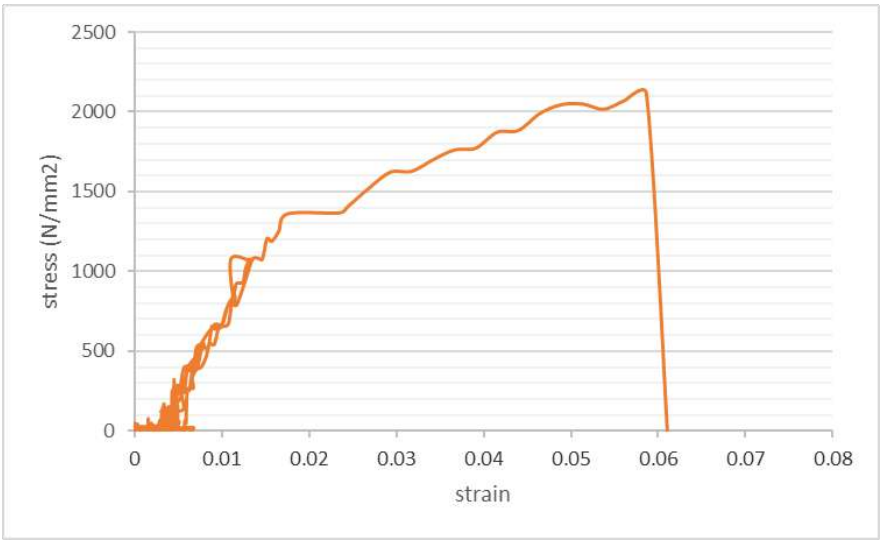

Figure (3-10): Stress-strain curve for basalt fibers

Table (3-5): Properties of basalt fibers

Type	Tensile strength (MPa)	Elongation at failure (%)	Tensile modulus (GPa)	Fabric density (g/m^2)
BWUD-400	2148.19	6.1	50.5	400

3.3.2 Resin

The used resin is epoxy-based impregnating resin of type Sikadur – 330 have been used to externally strengthen the reinforced concrete deep beams The properties of epoxy used are shown in Table (3-6).

Table (3-6): Properties of epoxy

Type	Mixing Ratio by Weight	Tensile strength (MPa)	Flexural Modulus (MPa)
Sikadur-330	A: B 4: 1	30	3800

3.4 Preparation of Deep Beams

The preparation of beams included the preliminary tests of the different materials used. In this part, the general properties of the concrete mix were also listed .the preparation of the test specimens also included the procedure of the concrete beams casting.

3.4.1 Used Materials

The beams tested in this experimental program were cast of concrete made of local materials .Cement was ordinary portland cement ,fine and coarse aggregates were composed of siliceous sand and good dolomite clean from impurities and well graded ,normal mild steel used for stirrups and high grade steel for longitudinal bars were locally produced bars. Preliminary tests were undertaken to determine the properties of the different materials.

3.4.1.1 Aggregate

Seive analysis ,spesific gravity,absorption and miosture content of both fine and coarse aggregate and dry –rodded unit weight of coarse aggregate are physical properties of the aggregate . The coarse aggregate used was crushed dolomite with maximum nominal size of 20 mm as shown in figure (3-11).the properties of coarse aggregate are shown in Table (3-7). The properties of the sand are listed in Table (3-8) .The grading of the sand has shown that the sand was medium size lying in zone I according to the Egyptian standard spesifications no.1109/2000 .

Figure (3-11): The used coarse and fine aggregate.

Table (3-7): The properties of used coarse aggregate

Test	Results	Specification Limit *
Specific gravity	2.48	-
Unit Weight	1.48	-
Materials Finer than no 200 Sieve	0.44	Less than 4 %
Absorption	1.6	Less than 2.5%
Abrasion (Los Anglos)	15.8	Less than 30 %
Crushing Value	18.6	Less than 30 %
Coefficient of impact %	13	Less than 45 %

* Egyptian Standard Specifications no: 1109/2002.

Table (3-8): The properties of fine aggregate

Test	Results	Limits *
Specific Gravity	1.70	-
Unit Weight	2.38	-
Materials Finer than no 200 Sieve	1.36	Less than 4 %

* Egyptian Standard Specifications no: 1109/2002.

3.4.1.2 Cement

Since the cement is the most active component in concrete and usually has the greatest unit cost, its selection and proper use is important to obtain the most economical balance with the desired properties for a particular concrete mixture. Physical and chemical properties characteristics of cement influence the properties of the hardened concrete. The cement used in this investigation is ordinary portland cement. The tests have shown the suitability of the cement for use in reinforced concrete applications. Chemical and physical properties of the used cement are shown in Table (3-9)

Table (3-9): The properties of the used cement

Properties		Test results	Limits of the E.S.S*
Fineness (m^2/Kg)		330	
Expansion (mm)		1.0	Not more than10
Initial Setting Time (mins)		125	Not less than 60min
Final Setting Time (mins)		170	Not more than10hrs
Compressive Strength(MPa)	7days	21.7	Not less than 10
	28 days	49.6	42.5- 62.5
Chemical Compositions	SiO_2	21.64%	
	$Al2O_3$	3.85%	
	$Fe2O_3$	5.67%	
	CaO	62.33%	
	MgO	2.27%	
	So_3	1.58%	
	L.O.I	2.07%	
	Na_2O	0.4%	
	K_20	0.19 %	

* Egyptian Standard Specifications no: 4756-1 /2009

3.4.1.3 water

Clean tap drinking water is used in this work. It is clean and free from impurities.

3.4.1.4 Steel Reinforcement

Steel used was normal mild steel for stirrups with a yield strength of 240 N/mm^2 with 6 mm diameter smooth and round bars. The steel used for reinforcement was high tensile steel with yield strength 360N/mm^2 with 16 and 25mm diameter and have a rough surface to get more bonds between steel bars and concrete.

3.4.2 Concrete Mix Properties

One concrete mix was used for the beams to obtain normal-strength concrete Table (3-10) presents the mix proportions by weight for 1 m^3 of concrete for normal strength concrete.

Table (3-10): The mix proportions by weight for 1 m^3 for N.S.C

Mix proportions of normal-strength concrete					
Volume	Coarse aggregate	Fine aggregate	Cement	Water	w/c
1 m^3	1400 kg	600Kg	350 kg	190 liters	0.54

3.4.3 Casting of Deep Beams

Wooden and Steel forms are used in casting the beams. Inside the forms, a plastic sheet is glued to the forms to preserve the mixing water. A mechanical mixer with a capacity of 0.125 m^3 is used to mix the concrete. The sides of the form are removed after 24 hours from the casting date. Water is sprayed for the concrete curing. Figure (3-12) shows the preparation of the specimens for casting, while Figures (3-13) to Figure (3-19) show the casting of the specimens. The fine and coarse aggregate are put into the mixer and mixed; the cement is added and followed by water. Then the contents are

mechanically mixed for a 5-minute period. The concrete is mechanically compacted externally using a vibrator to ensure full compaction inside the form. At the end of the casting operation, the specimen surface is leveled.

Figure (3-12): Preparing of the specimens for casting.

Figure (3- 13): Reinforcement details of deep beams

Figure (3-14) Wooden and steel form used in casting the specimen

Figure (3-15): The used mixer

Figure (3-16): Casting of specimens

Figure (3-17): A mechanical vibrator to ensure full compaction of concrete.

Figure (3-18): The beams after casting and leveling the surface.

Figure (3-19): The cubes and cylinders after casting and leveling the surface.

3.4.4 Concrete Compressive and Tensile Strength

The compressive strength of concrete was determined by compression tests carried out on standard cubes with dimensions 150x150x150 mm**,** standard cubes were cast with the beams and tested after 28 days to get the concrete compressive strength for the beams .Cylinders also were cast and tested to get

the tensile strength of the concrete. Figure (3-20) shows the modes of failure of cubes and cylinders. Tables (3-11) and (3-12) show the results of cubes and cylinders respectively.

Figure (3-20): The modes of failure of cylinders and cubes.

Table (3-11): Test results of cubes

Cube number	Load(KN)	Compressive strength (N/mm^2)
After 7 days		
1	360	16
2	402	17.8
3	365	16.2
average		16.7
After 28 days		
4	566	25.15
5	576	25.9
6	564	25.1
average		25.4

Table (3-12): Test results of cylinder

Cylinder number	Load (KN)	Tensile strenght (N/mm^2)
1	239	3.4
2	159	2.25
3	215.2	3.05
average		2.9

3.5 Strengthening of Deep Beams

Before bonding the composite fabric onto the concrete surface, the required region of the concrete surface was grinding and smoothed with a grinding and smoothing machine as shown in Figure (3-21). Once the surface was prepared to the required standard, the epoxy resin was mixed in accordance with manufacturer's instructions. Mixing was carried out in a plastic container and was continued until the mixture was in uniform color. When this was completed and the fabrics had been cut to size, the epoxy resin was applied to the concrete surface as shown in Figure (3-22). The composite fabric was then placed on top of epoxy resin coating and the resin was squeezed through the roving of the fabric with the roller. Air bubbles entrapped at the epoxy/concrete or epoxy/fabric interface were to be eliminated as shown in Figure (3-23). Then the second layer of the epoxy resin was applied as shown in Figure (3-24) and BFRP sheet was then placed on top of epoxy resin coating and the resin was squeezed through the roving of the fabric with the roller as shown in Figure (3-25) and the above process was repeated. During hardening of the epoxy, a constant uniform pressure was applied on the composite fabric surface to extrude the excess epoxy resin and to ensure good contact between the epoxy, the concrete and the fabric. This operation was carried out at room temperature. Concrete beams strengthened with basalt fiber fabric were cured for 24 hours at room temperature before testing. Also Figure (3-26) shows the final strengthened deep beam.

Figure (3-21): Grinding and smoothing with grinding machine.

Figure (3-22): Epoxy resin applied to the concrete surface

Figure (3-23): The composite fabric placed on top of epoxy resin coating

Figure (3-24): The second layer of the epoxy resin

Figure (3-25): The resin was squeezed through the roving of the fabric

Figure (3-26): The final strengthened deep beams.

3. 6 Test Setup of Deep Beams

The structural testing frame in the concrete testing laboratory of the National Center of Housing Research and Building has been used for testing. The frame mainly consisted of a horizontal I–beam fixed to two vertical columns. The columns are resting on the floor. Two horizontal angles are used to support the measuring dial gages. The specimens are simply supported on two I-beams where they are supported on the frame by welding to produce two line supports. The clear span between the two supports is 850 mm; one hydraulic loading jack with a capacity of 500 KN is used at the mid-span of the beam. A load cell is placed underneath the loading jack. The load cell is connected to a digital display screen to read the applying loads. The test setup and loading system are shown in Figure (3-27).

3.7 Measuring Devices

3.7.1 Displacement Devices

Vertical deflection was measured at the mid-span of the beams and at the third of the beam by linear variable distance transducer(LVDT). The data acquisition system used to record the deflection measurment underneath the bottom of the beam at mid and under-opening.Figure (3-28) shows the location of deflection measurments.

3.7.2 Strain Devices:

Electrical strain gauges are installed to measure the strains in the steel, glass, and hybrid–reinforcing bars. The strain gauge type is "TOKYO type FLA-6-11"with a gauge length of 6mm, their electrical resistance is 119.8 ± 0.20 ohm, and their gauge factor is 2.12±1.0 %. For each beam two strain gauges are installed at the middle part of one of the bottom bars and at vertical stirrups as shown in Figures (3-29) to Figure (3-33). The strain gauges are connected to a strain meter device with an accuracy of 1×10^{-6}. the strain gauges were

covered by a waterproof coating to protect them from water and damage during the casting of concrete.

Figure (3-27): The test setup and loading system.

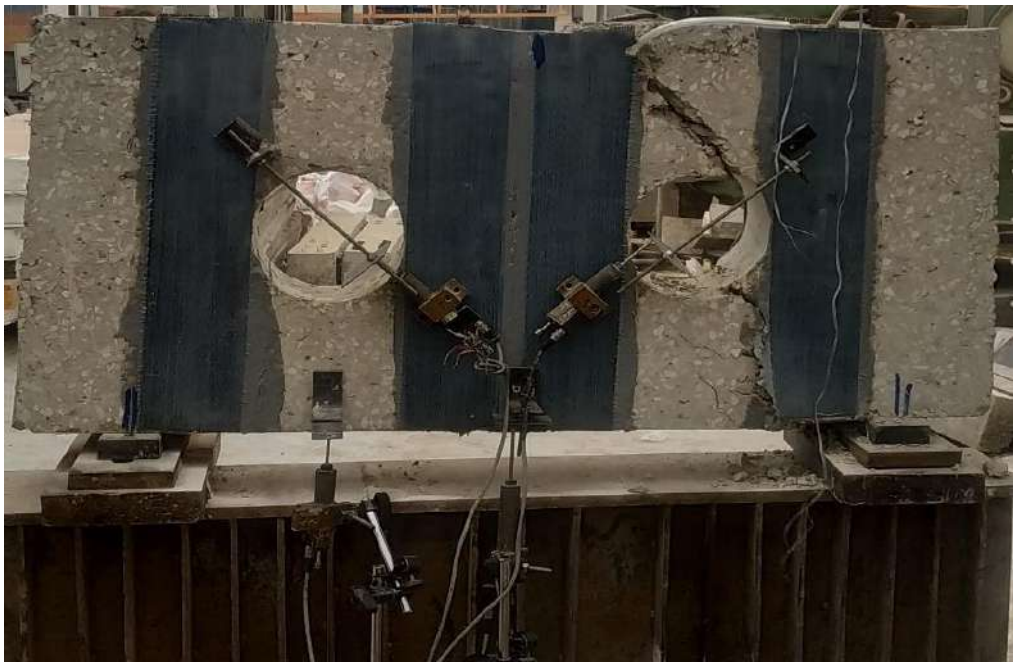

Figure (3-28): The location of deflection measurements.

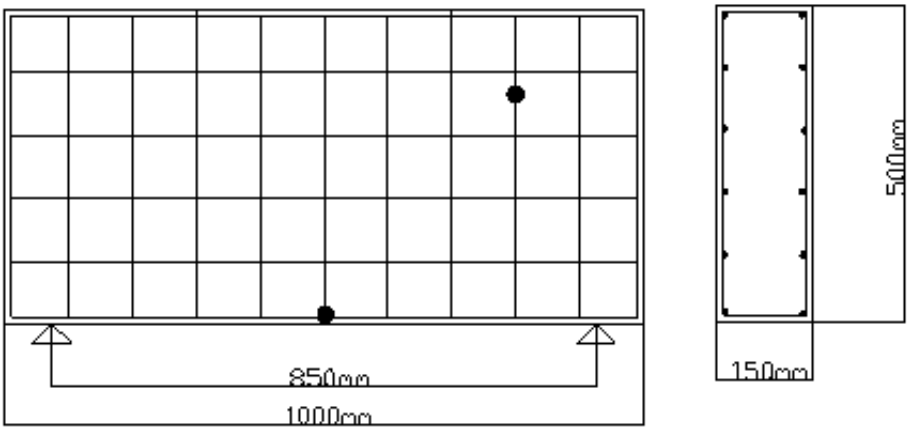

Figure (3-29): The strain gauges positions in beams without opening

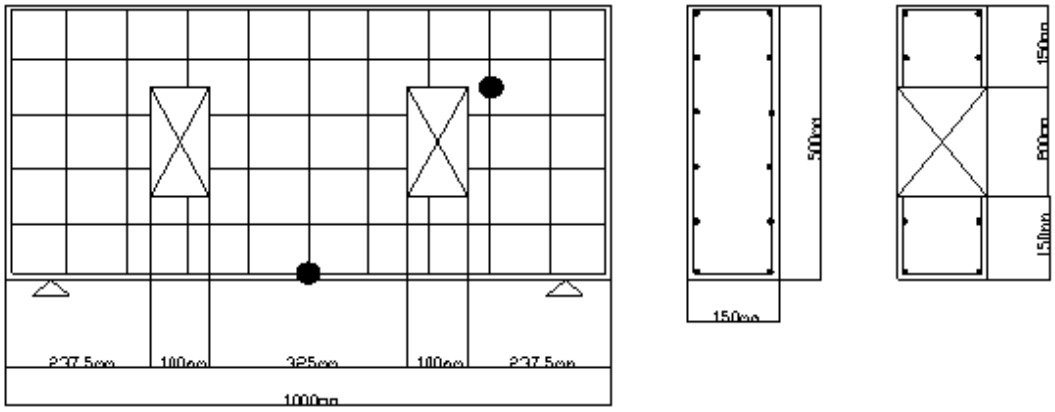

Figure (3-30):The strain gauges positions in beams with vertical opening

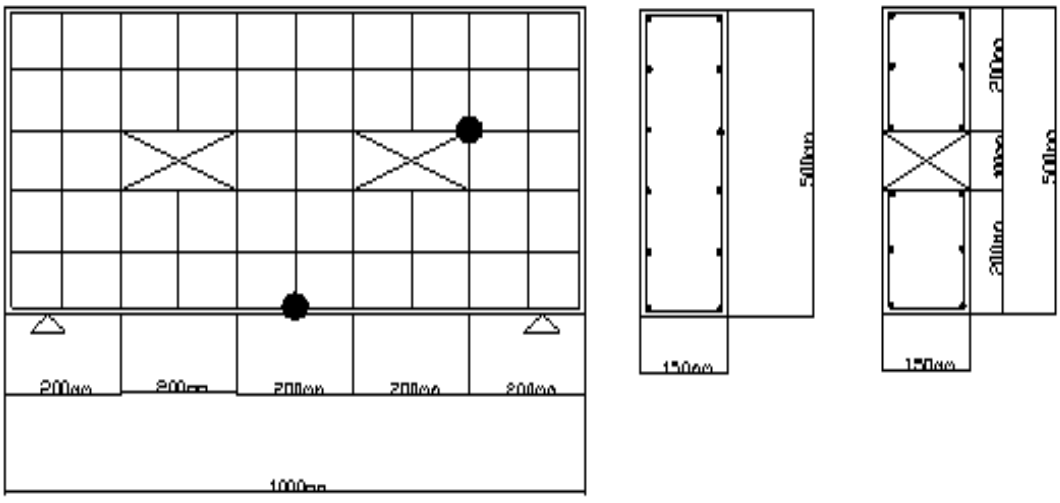

Figure (3-31): The strain gauges positions in beams with horizontal opening

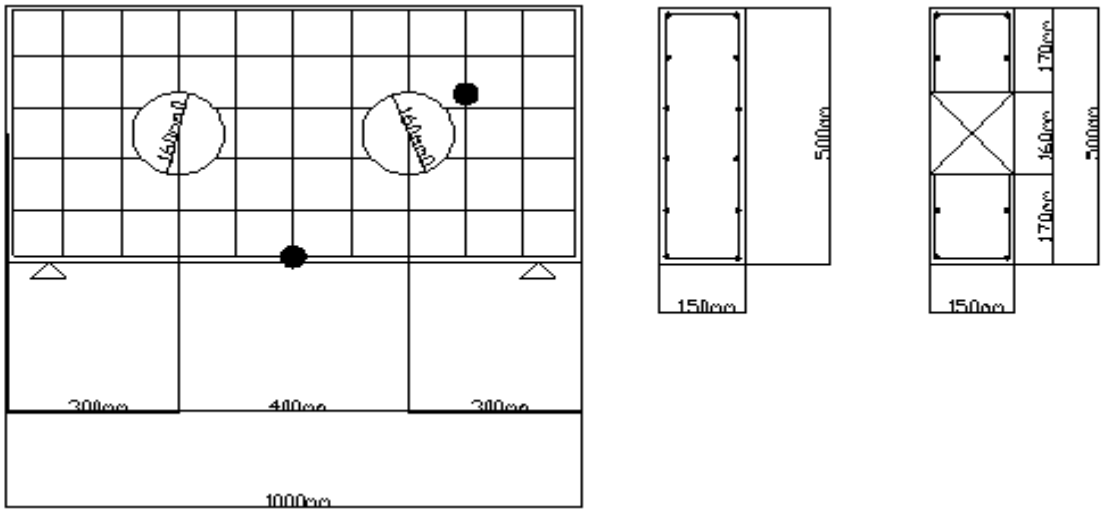

Figure (3-32): The strain gauges positions in beams with circular opening

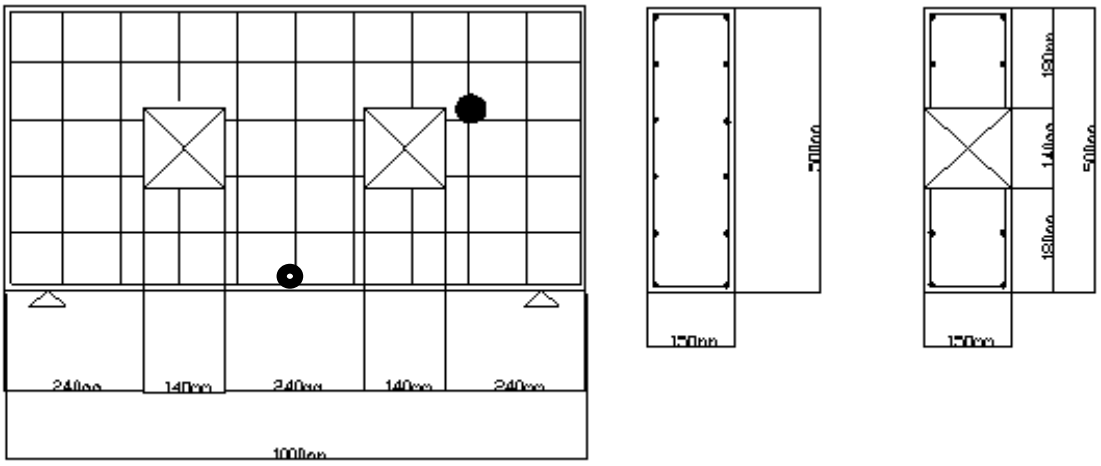

Figure (3-33): The strain gauges positions in beams with square opening

CHAPTER FOUR
EXPERIMENTAL RESULTS

4.1 Introduction

This chapter describes the experimental results for the reinforced beams. The behavior of test specimens is investigated for the studied parameters. The parameters are the orientations of BFRP strips, strengthening the deep beams with different types of openings using basalt fiber strips and strengthening deep beams without openings. The observed measurements included the following:

1- Load measured by the load cell.
2- Mid and under openings deflections measured by LVDT.
3- Reinforcement strain measured by strain gages.

The behaviors of the beams are evaluated by studying the following parameters:

1- The crack pattern and the modes of failure.
2- The cracked and failure loads.
3- The load-deflection relationship.
4- The load – strain relationship.

4.2 Experimental Results of The Tested Deep Beams:

Table (4-1) shows the results of all beams, cracking load and corresponding deflection, failure load with its corresponding deflection, and the failure modes.

4.2.1 Cracks Pattern and Modes of Failure

The tested beams showed several different modes of failure and crack patterns. Figures from (4-1) to (4-11) show the crack pattern for all tested beams.

Table (4-1): Summary of the results

Beam no.	P crack (kN)	Δ cr (mm)	P failure (kN)	Δ f (mm)	Failure mode
B1	262	1.54	451.8	2.5	Shear -compression
B2	347	1.7	636.28	4.2	Diagonal shear- tension
B3	178	2.64	298.69	4.14	Diagonal-shear splitting
B4	194	2.67	298.5	4.02	2 separate diagonal-shear cracks above and below the openings
B5	250	2.1	360	4.2	Diagonal-shear splitting
B6	210	3.93	353.9	4.9	2 separate diagonal-shear cracks above and below the openings
B7	380	3.78	456.82	4.56	FRP-rupture
B8	181	1.53	351.9	2.9	2 separate diagonal-shear cracks above and below the openings
B9	310	2.8	322.53	3.5	Diagonal-shear failure-concrete cover splitting
B10	240	3.2	312.5	3.98	2 separate diagonal-shear cracks above and below the openings
B11	325	3.9	356.42	4.7	Diagonal-shear splitting

4.2.1.1 Beam (B1)

At the reference beam, B1 diagonal cracks were observed at the loading point toward the edge of the beam until the support as shown in Figure (4-1). The cracks begin from the inner to the outer edge near the support. B1 showed typical diagonal shear failure. The first diagonal crack appeared at 262 kN (58% of the failure load). with the increase of load, diagonal cracks increase along the beam span then the cracks near the support opened, the beam failed at a load of 451.8 kN.

.

Figure (4-1): Crack pattern at failure (B1)

4.2.1.2 Beam (B2)

At the strengthened solid deep beam, B2 two diagonal cracks were observed at the loading point towards the edge of the beam until the support as shown in Figure (4-2). Beam (2) showed atypical diagonal failure. The first diagonal crack appeared at 347 KN (about 54.5% of the failure load). with the increase of load diagonal cracks started to increase along the beam span, then the middle cracks opened and wider and the beam failed at a load of 636.3 KN.

Figure (4-2): Crack pattern at failure (B2)

4.2.1.3 Beam (B3)

By studying the crack pattern of deep beam with openings (B3) shown in Figure (4-3), It was noted that the diagonal cracks first existed surrounding the openings and then spread out to the loading point and supports. The first diagonal crack appeared at 141 KN (about 47.2% of the failure load), with the increase of load diagonal cracks started to increase along the beam span then the cracks in the middle opened and wider and the beam failed at a load of 298.7 KN.

Figure (4-3): Crack pattern beam at failure (B3)

4.2.1.4 Beam (B4)

In beam B4 the cracks were diagonally propagated at the bottom of the opening to the support as shown in Figure (4-4). The first diagonal crack appeared at 194 kN (about 65% of the failure load), with the increase of load diagonal cracks started to increase along the beam span then the cracks in the middle opened and wider and the beam failed at a load of 298.5 kN.

Figure (4-4): Crack pattern at failure (B4)

4.2.1.5 Beam (B5)

In deep beam B5 the cracks were diagonally propagated at the bottom of the opening to the support as shown in Figure (4-5). The first diagonal crack appeared at 250 KN (about 65.5% of the failure load), with the increase of load diagonal cracks started to increase along the beam span then the cracks in the middle opened and wider and the beam failed at a load of 381.4 KN.

Figure (4-5): Crack pattern of (B5) at failure

4.2.1.6 Beam (B6)

The crack pattern shows that there are two diagonal cracks spread toward the load point as shown in Figure (4-6). The first diagonal crack appeared at 210 kN (about 59.3% of the failure load) With the increase of load diagonal cracks started to increase along the beam span then the cracks in the middle opened and wider and the beam failed at a load of 353.9 kN.

Figure (4-6): Crack pattern of the beam (B6) at failure

4.2.1.7 Beam (B7)

Figure (4-7) shows the crack pattern at failure for beam B7 (strengthened with horizontal BFRP strips), the crack pattern shows that there are 2 diagonal cracks propagated towards the load point leading to the spalling of the sheet from the concrete. The first diagonal crack appeared at 380 KN (about 83.2% of the failure load), with the increase of load diagonal cracks started to increase along the beam span then the cracks in the middle opened and wider and the beam failed at a load of 456.82KN.

Figure (4-7): Crack pattern of beam B7 at failure

2.4.1.8 Beam (B8)

Figure (4-8) shows the crack pattern of beam B8(circular opening strengthened with BFRP strips), it is clear that the cracks were diagonally propagated at the bottom of the opening to the support**.** The first diagonal crack appeared at 181KN (about 51.4% of the failure load).with the increase of load diagonal cracks started to increase along the beam span then the cracks in the middle opened and wider and the beam failed at a load of 352KN.

Figure (4-8): Crack pattern of beam B8 at failure

2.4.1.9 Beam (B9)

Figure (4-9) shows the crack pattern of beam B9(circular opening strengthened with horizontal BFRP strips) at failure, the cracks were diagonally propagated at the bottom of the opening to the support. The first diagonal crack appeared at 310KN (about 96% of the failure load). with the increase of load diagonal cracks started to increase along the beam span then the cracks in the middle opened and wider and the beam failed at a load of 322.5KN.

Figure (4-9): Crack pattern of beam B9 at failure

2.4.1.10 Beam (B10)

Figure (4-10) shows the crack pattern of beam B10 (square opening strengthened with vertical BFRP strips), the crack pattern in beam B10 showed mainly three cracks on the left and right sides of the beam which appeared initially at the loading point and then the crack on the left side propagates towards the support during the test until the failure of the beam and finally the concrete crush and then the cover separated from the top of the beam at left side. The first crack appeared at 240KN (about 77% of the failure load), with the increase of load diagonal cracks started to increase along the beam span then the cracks in the middle opened and wider and the beam failed at a load of 312.5KN.

Figure (4-10): Crack pattern of beam B10 at failure

2.4.1.11 Beam (B11)

Figure (4-11) shows the crack pattern of beam B11 (square openings strengthened with horizontal BFRP strips), the crack pattern in beam B11 showed only one crack on the left of the beam which appeared initially at the point of load and propagated to the support during the test till the failure of the beam. This crack appeared at 325KN (about 91% of the failure load), with the increase of load diagonal cracks

started to increase along the beam span then the cracks in the middle opened and wider and the beam failed at a load of 356.4KN.

Figure (4-11): Crack pattern of beam B11 at failure

4.2.2 Load-Deflection Relationships:

The relationship of load-deflection at mid span and under the opening at left side is plotted for each specimen. The results are organized in Figures from (4-23) to (4-34), deflection curves for all specimens have almost the same profile where the first part of the curves steeper than the second part, the failure is brittle (shear failure) for all beams.

4.2.2.1 Beam (B1)

Figure (4-12) shows the load - deflection relationship for beam (B1) at middle of the deep beam, the curve showed a bilinear behavior that appeared in all deep beams, the first part was nearly a straight line till the cracking load then, after cracking, the load increased till a sudden drop in load occurred, at the same load increment the deflection increased rapidly with high reduce in stiffness. The deflection at cracking load was 1.45 mm while the deflection at failure load was

2.5 mm

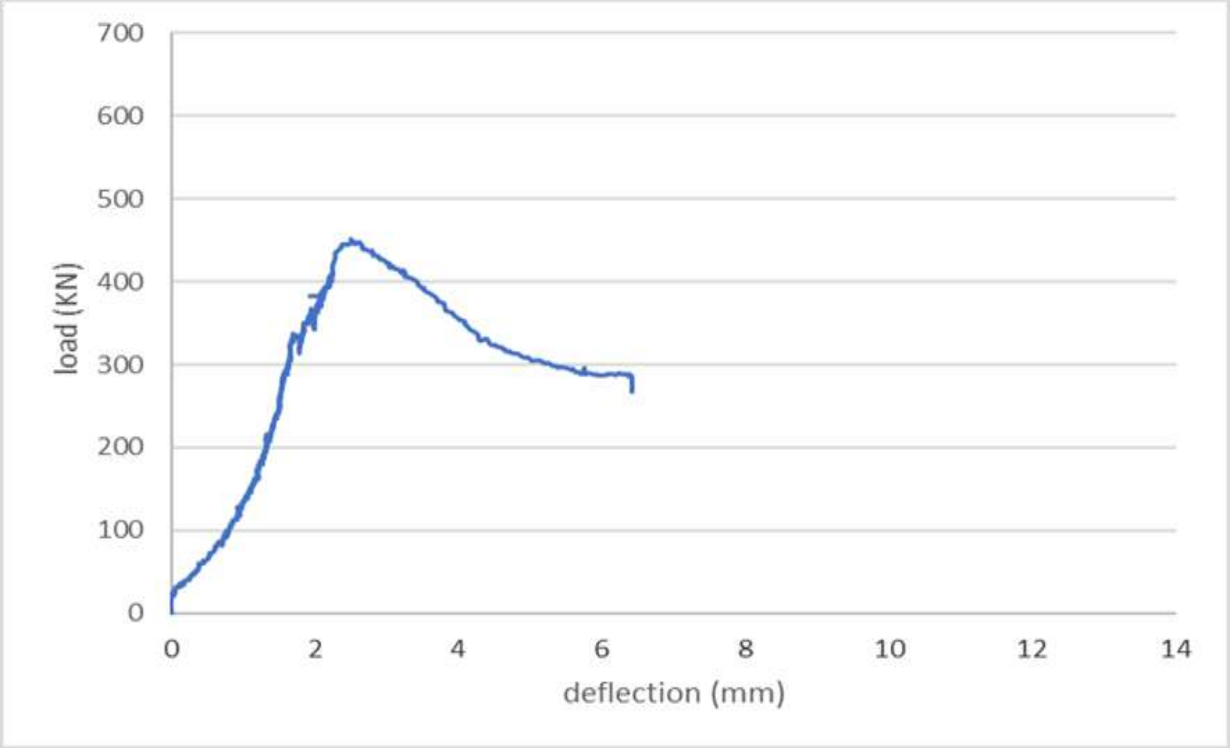

Figure (4-12): Load deflection curves for beam (B1)

4.2.2.2 Beam (B2)

Figure (4-13) shows the load - deflection relationship for deep beam (B2) strengthened with BFRP strips at middle of the deep beam, the curve showed a linear behavior at the first part was nearly a straight line till the cracking load then, after cracking, the load increased till a sudden drop in load occurred, at the same load increment the deflection increased rapidly with high reduce in stiffness. The deflection at cracking load was 1.7 mm while the deflection at failure load was 4.2 mm

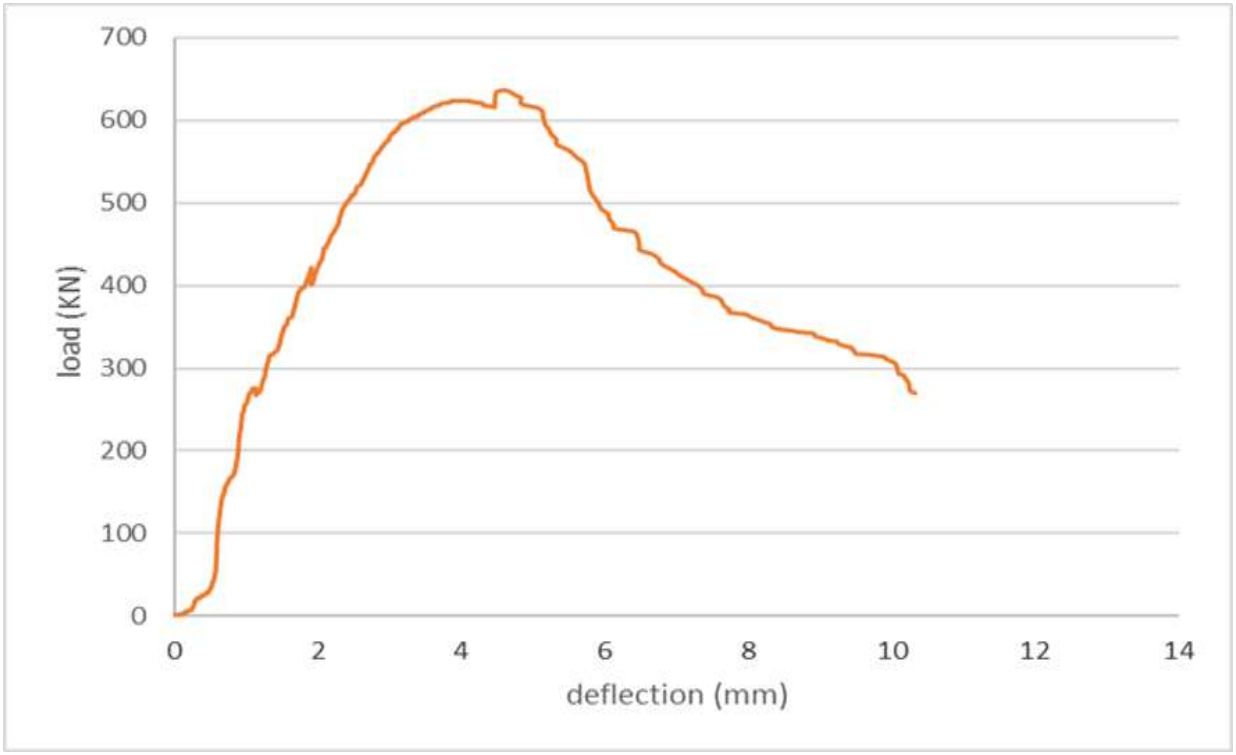

Figure (4-13): Load- deflection curve for beam (B2)

4.2.2.3 Beam (B3)

Figure (4-14) shows the load - deflection relationship for deep beam (B3) deep beam with rectangular openings) at middle of the deep beam, the curve showed a linear load deflection response indicating a higher rate of crack initiation, widening, and growth. A linear behavior at the first part was nearly a straight line till the cracking load then, after cracking, the load increased till a sudden drop in load occurred, at the same load increment the deflection increased rapidly with high reduce in stiffness. The deflection at cracking load was 2.6 mm while the deflection at failure load was 4.14 mm.

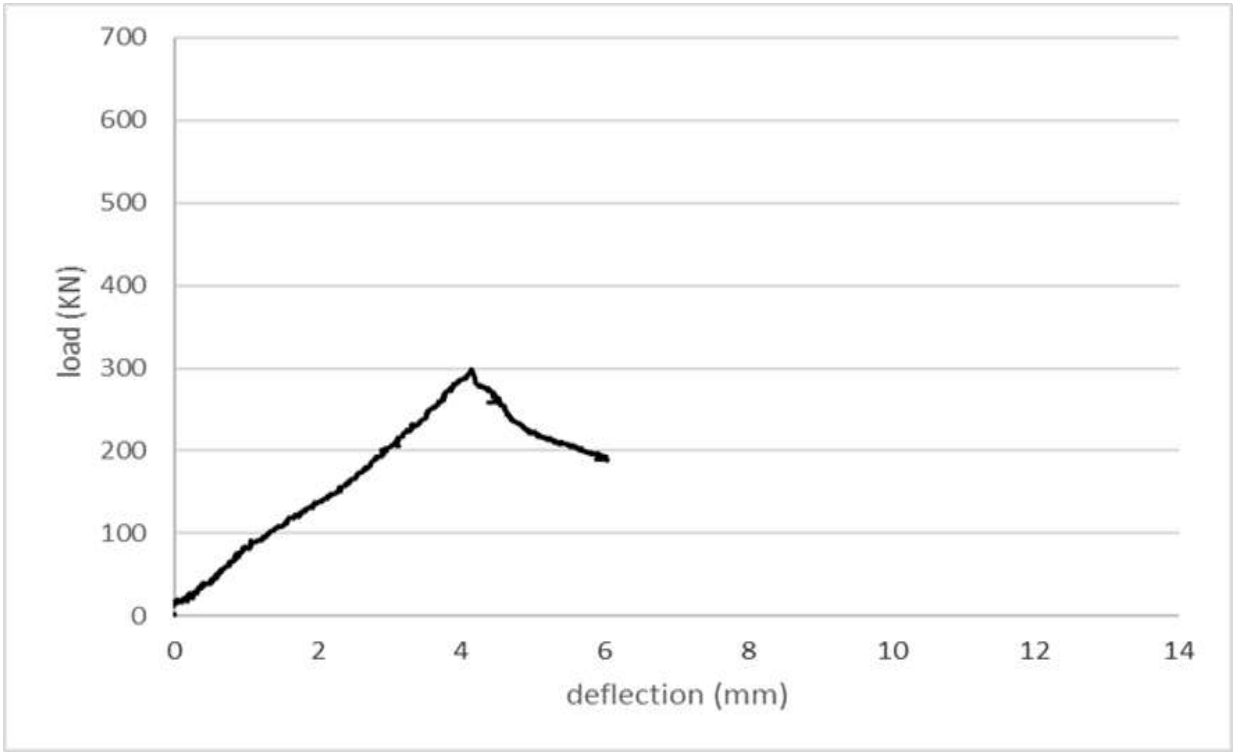

Figure (4-14): Load- deflection curve for beam (B3)

4.2.2.4 Beam (B4)

Figure (4-15) shows the load - deflection relationship for deep beam (B4) with openings strengthened vertically with BFRP strips at middle of the deep beam, the curve showed a linear load deflection response indicating a higher rate of crack initiation, widening, and growth. A linear behavior at the first part was nearly a straight line till the cracking load then, after cracking, the load increased till a sudden drop in load occurred, at the same load increment the deflection increased. rapidly with high reduce in stiffness. The deflection at cracking load was 2.67 m while the deflection at failure load was 4.02 mm.

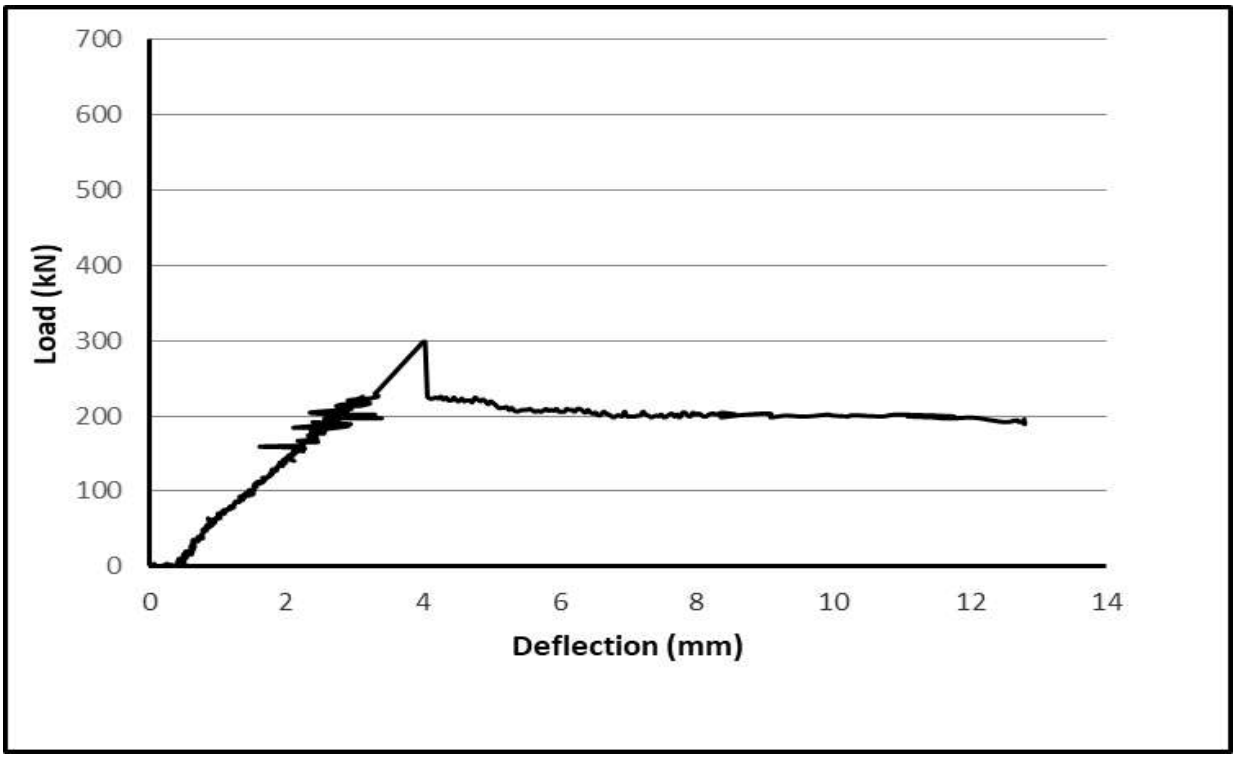

Figure (4-15): Load - deflection curves for beam (B4)

4.2.2.5 Beam (B5)

Figure (4-16) shows the load - deflection relationship at middle for deep beam (B5) with vertical openings strengthened with vertical BFRP strips, the curve showed a linear load deflection response indicating a higher rate of crack initiation, widening, and growth. A linear behavior at the first part was nearly a straight line till the cracking load then, after cracking, the load increased till a sudden drop in load occurred, at the same load increment the deflection increased rapidly with high reduce in stiffness. The deflection at cracking load was 2.1 mm while the deflection at failure load was 4.2 mm.

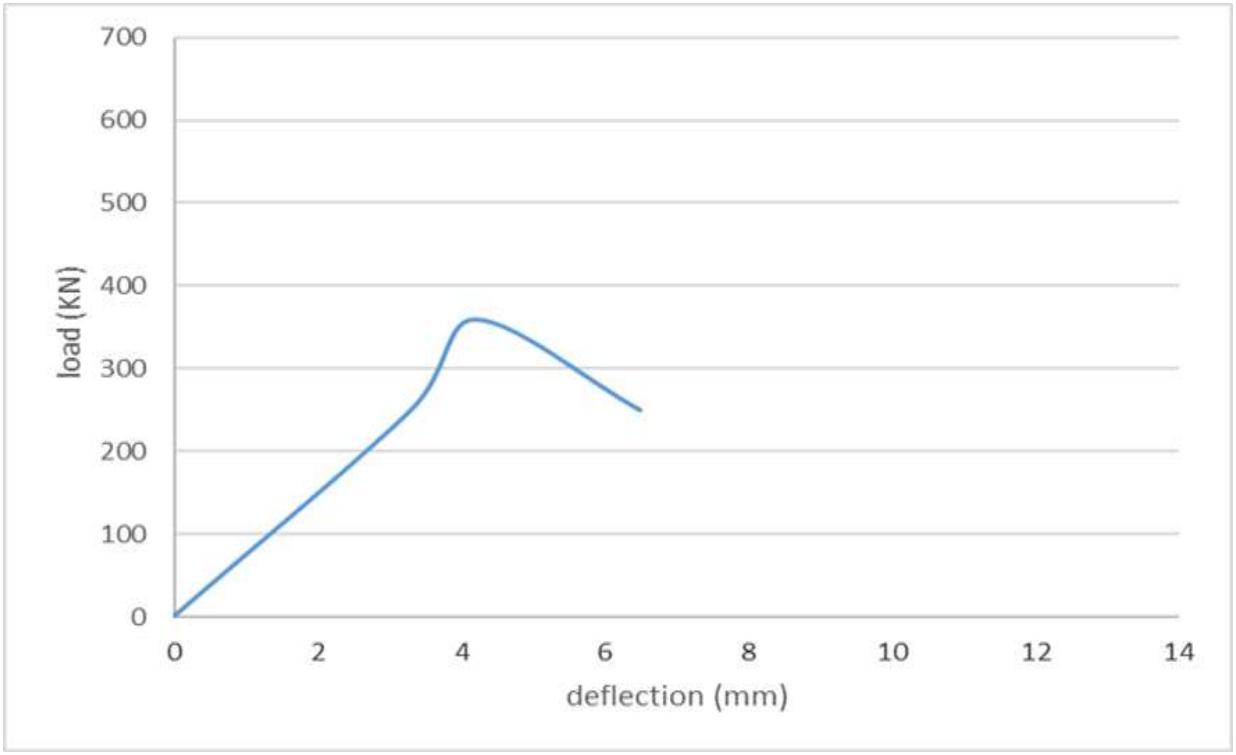

Figure (4-16): Load - deflection curves for beam (B5)

4.2.2.6 Beam (B6)

Figure (4-17) shows the load - deflection relationship for deep beam (B6) with horizontal strengthened with vertical BFRP strips openings at middle of the deep beam and under openings, the curve showed a linear load deflection response indicating a higher rate of crack initiation, widening, and growth. A linear behavior at the first part was nearly a straight line till the cracking load then, after cracking, the load increased till a sudden drop in load occurred, at the same load increment the deflection increased rapidly with high reduce in stiffness. The deflection at cracking load was 3.93mm while the deflection at failure load was 4.9 mm.

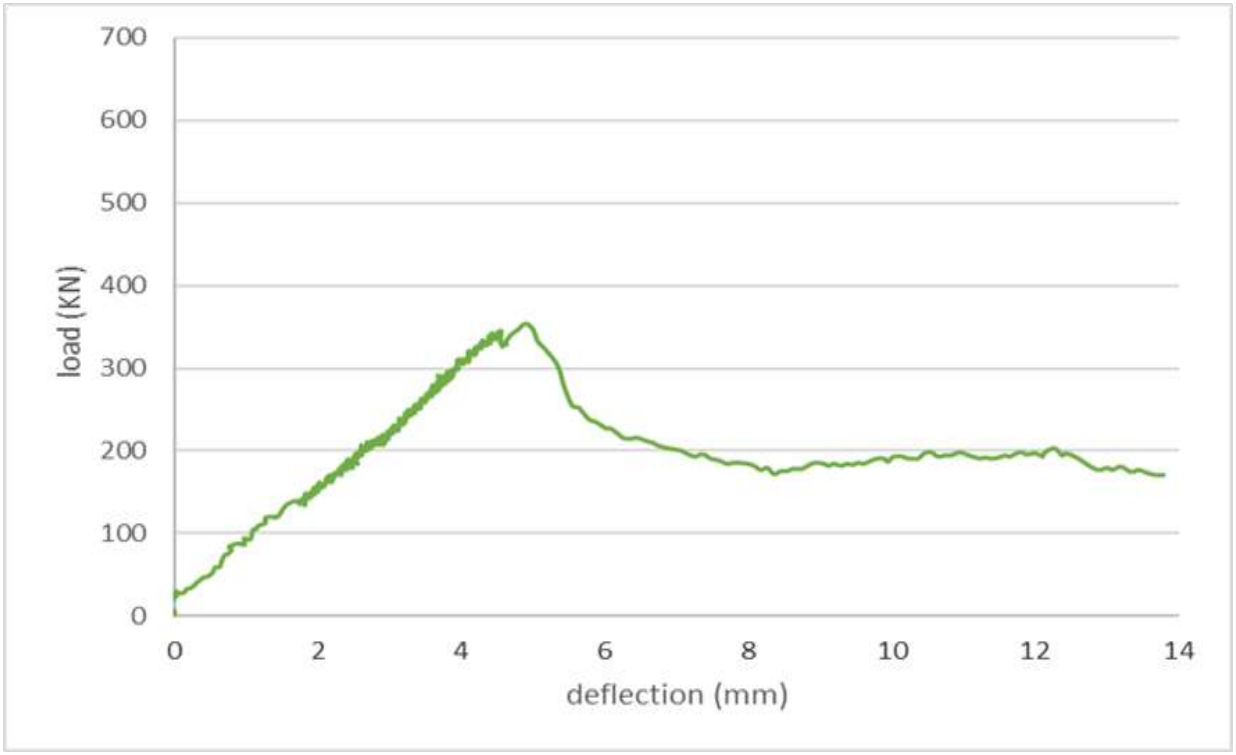

Figure (4-17): Load-deflection curves for beam (B6)

4.2.2.7 Beam (B7)

Figure (4-18) shows the load - deflection relationship for deep beam (B7) with horizontal openings strengthened by horizontal BFRP strips at middle of the deep beam, the curve showed a linear load deflection response indicating a higher rate of crack initiation, widening, and growth. A linear behavior at the first part was nearly a straight line till the cracking load then, after cracking, the load increased till a sudden drop in load occurred, at the same load increment the deflection increased rapidly with high reduce in stiffness. The deflection at cracking load was 3.78 mm while the deflection at failure load was 4.56 mm.

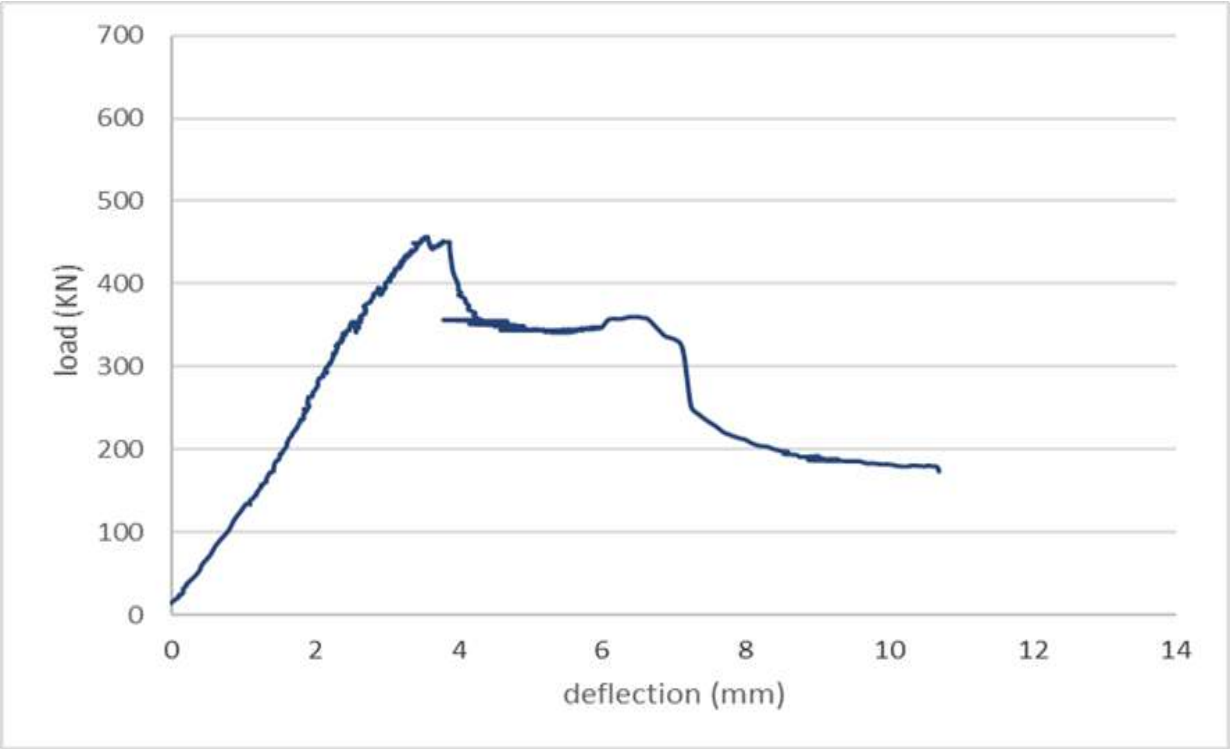

Figure (4-18): Load deflection curves for beam (B7)

4.2.2.8 Beam (B8)

Figure (4-19) shows the load - deflection relationship for deep beam (B8) with circular openings strengthened by vertical BFRP strips at middle of the deep beam, the curve showed a linear load deflection response indicating a higher rate of crack initiation, widening, and growth. a linear behavior at the first part was nearly a straight line till the cracking load then, after cracking, the load increased till a sudden drop in load occurred, at the same load increment the deflection increased rapidly with high reduce in stiffness. The deflection at cracking load was 1.53 mm while the deflection at failure load was 2.9 mm.

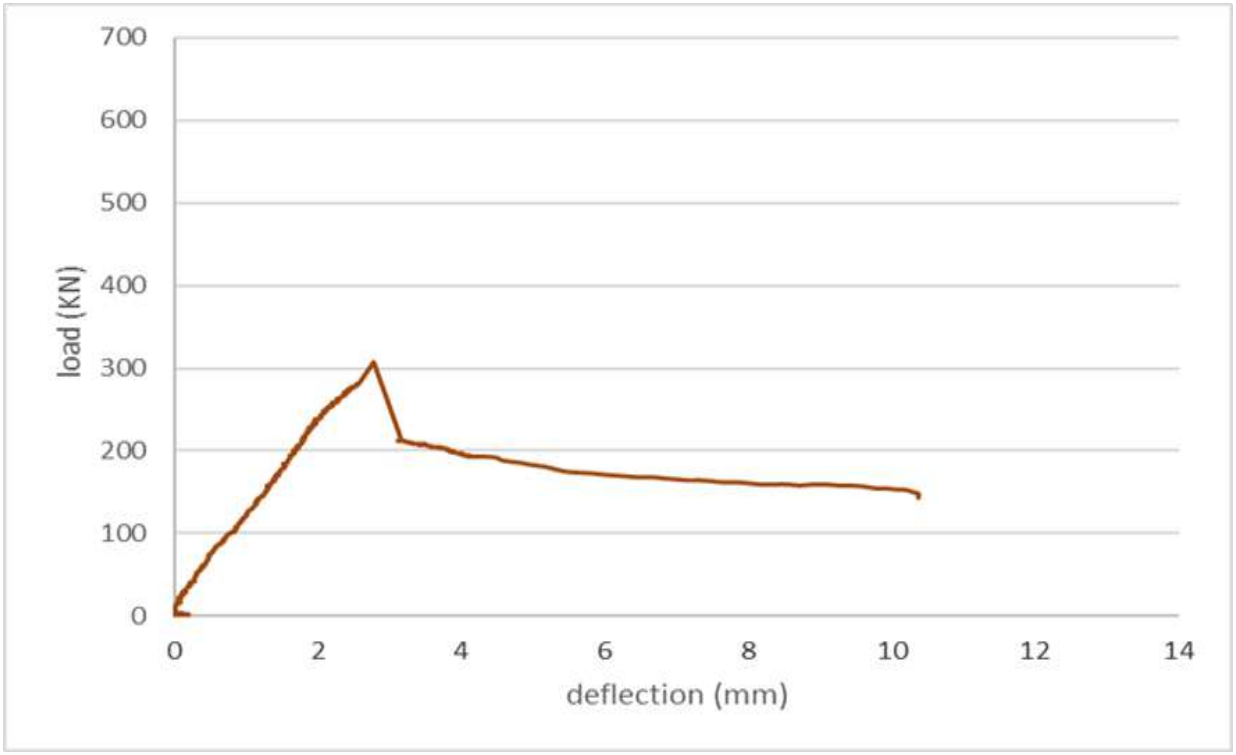

Figure (4-19): Load deflection curves for beam (B8)

4.2.2.9 Beam (B9)

Figure (4-20) shows the load - deflection relationship for deep beam (B9) with circular openings strengthened by horizontal BFRP strips at middle of the deep beam, the curve showed a linear load deflection response indicating a higher rate of crack initiation, widening, and growth. A linear behavior at the first part was nearly a straight line till the cracking load then, after cracking, the load increased till a sudden drop in load occurred, at the same load increment the deflection increased rapidly with high reduce in stiffness. The deflection at cracking load was 2.8 mm while the deflection at failure load was 3.5mm.

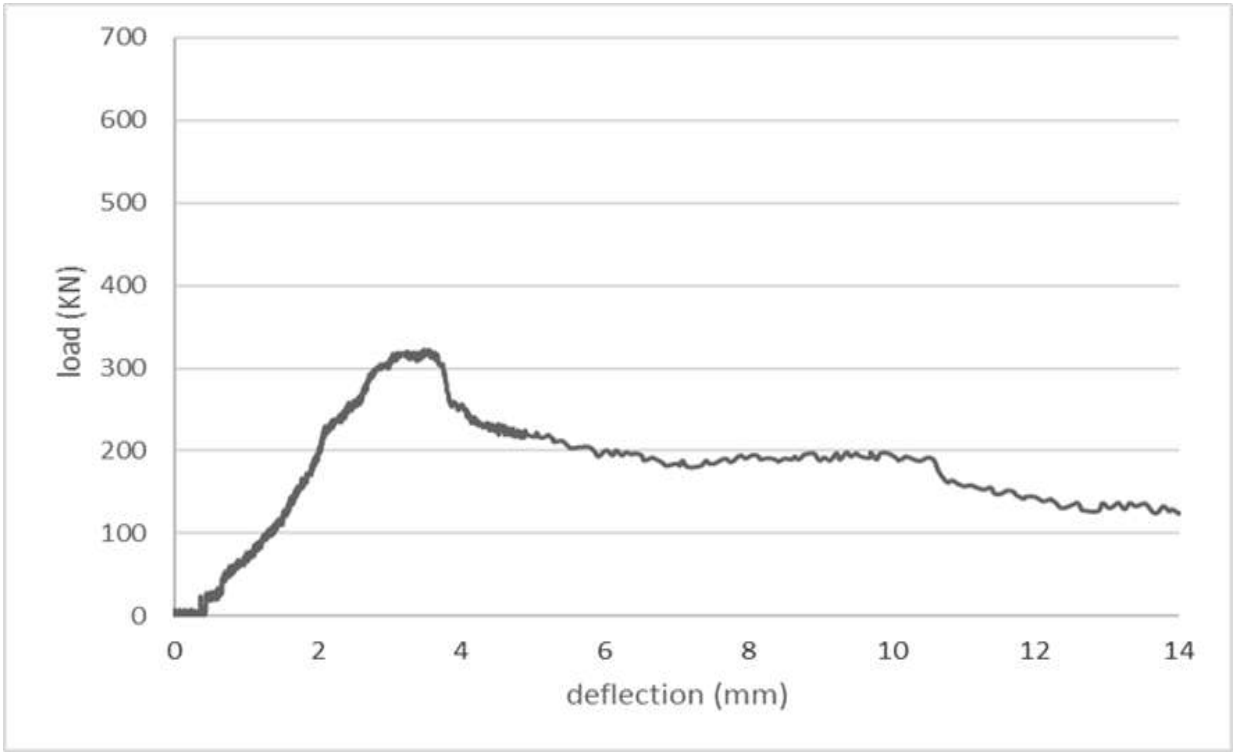

Figure (4-20): Load deflection curves for beam (B9)

4.2.2.10 Beam (B10)

Figure (4-21) shows the load - deflection relationship for deep beam (B10) with square openings strengthened by vertical BFRP strips at middle of the deep beam, the curve showed a linear load deflection response indicating a higher rate of crack initiation, widening, and growth. A linear behavior at the first part was nearly a straight line till the cracking load then, after cracking, the load increased till a sudden drop in load occurred, at the same load increment the deflection increased rapidly with high reduce in stiffness. The deflection at cracking load was 3.2 mm while the deflection at failure load was 3.98 mm.

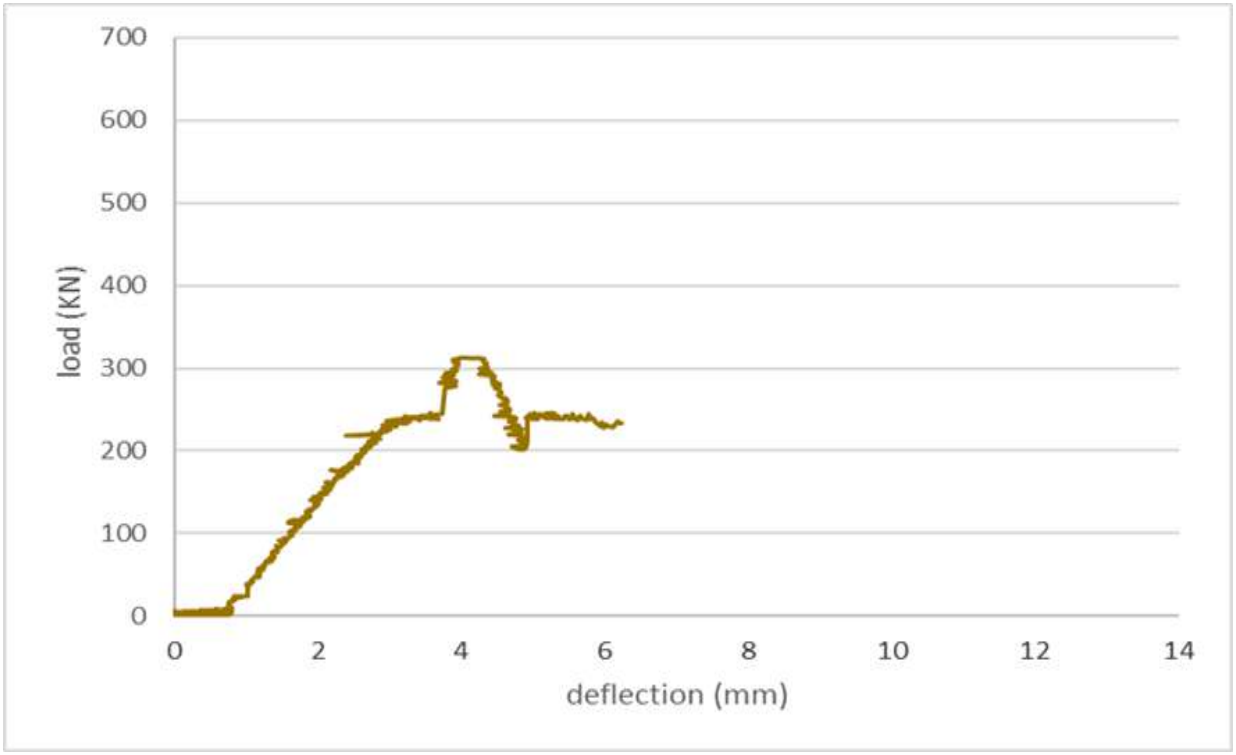

Figure (4-21): Load -deflection curves for beam (B10)

4.2.2.11 Beam (B11)

Figure (4-22) shows the load - deflection relationship for deep beam (B11) with square openings strengthened by horizontal BFRP strips at middle of the deep beam, the curve showed a linear load deflection response indicating a higher rate of crack initiation, widening, and growth. A linear behavior at the first part was nearly a straight line till the cracking load then, after cracking, the load increased till a sudden drop in load occurred, at the same load increment the deflection increased rapidly with high reduce in stiffness. The deflection at cracking load was 3.9 mm while the deflection at failure load was 4.7 mm.

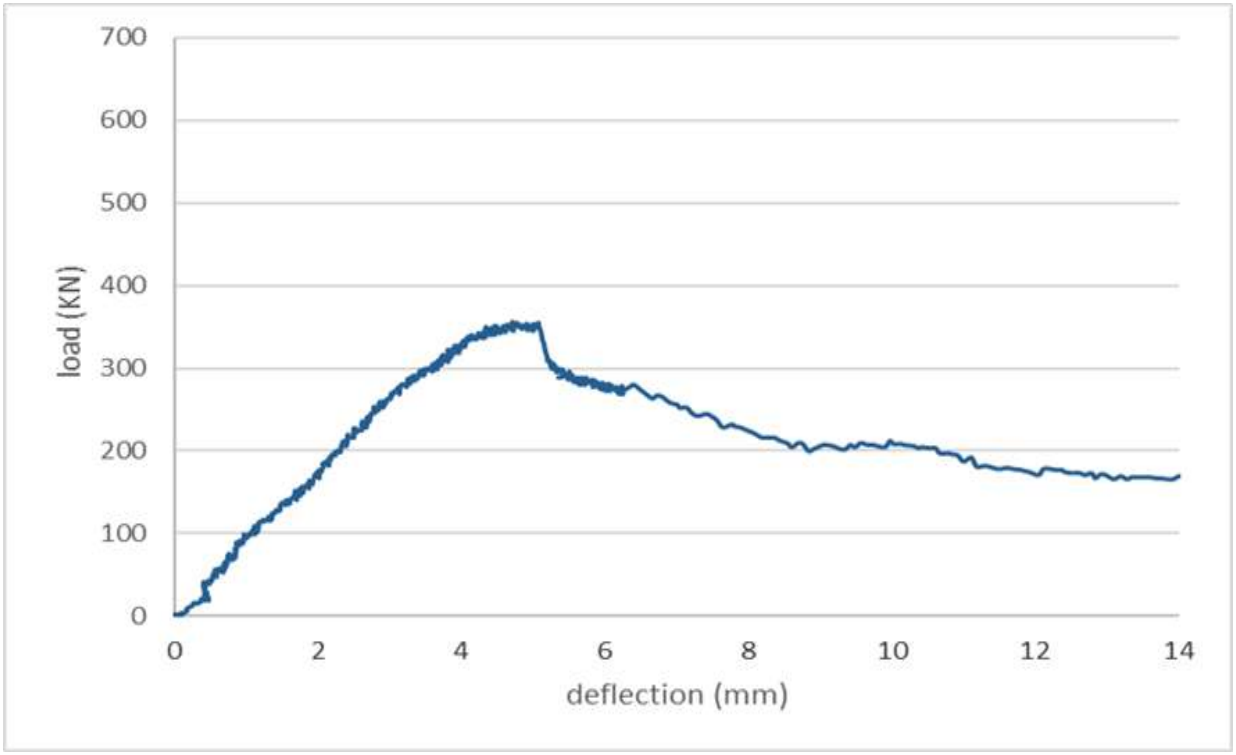

Figure (4-22): load deflection curves for beam (B11)

4.2.3 Reinforcement Strains

The steel strains were recorded at the point of mid-span of the flexural reinforcement and at top of the opening stirrups using electrical strain gages. The solid deep beams showed a typical load-steel strain relationship. Also, deep beams with openings showed a typical load-steel strain relationship for deep beams with openings. Figures from (4-23) to (4-34) show the load- strain curves for all tested beams as following:

4.2.3.1 Beam (B1)

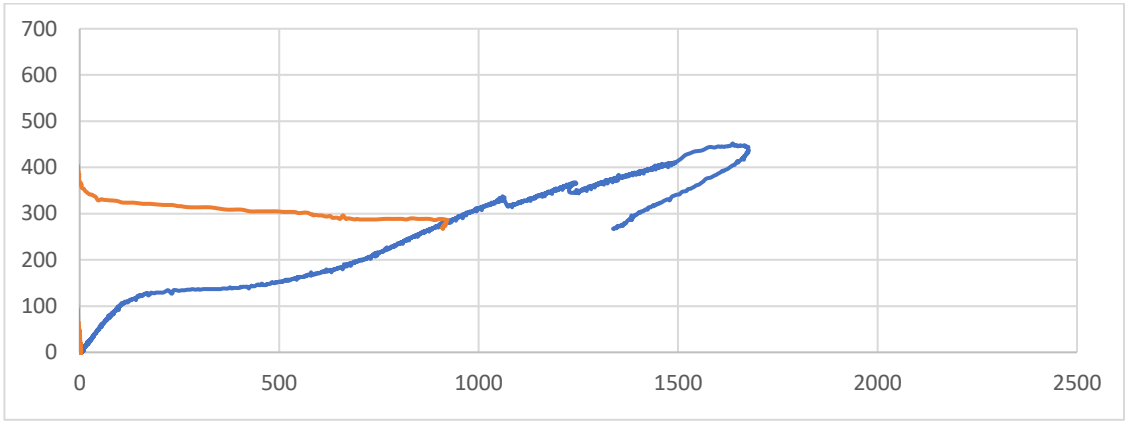

Figure (4-23): Load -strain curves for beam (B1)

4.2.3.2 Beam (2)

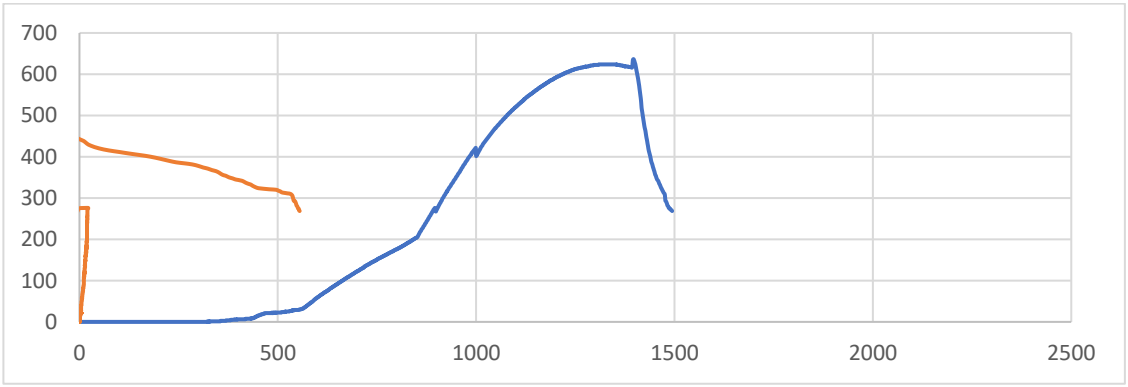

Figure (4-24): Load strain curves for beam (B2)

4.2.3.3 Beam (B3)

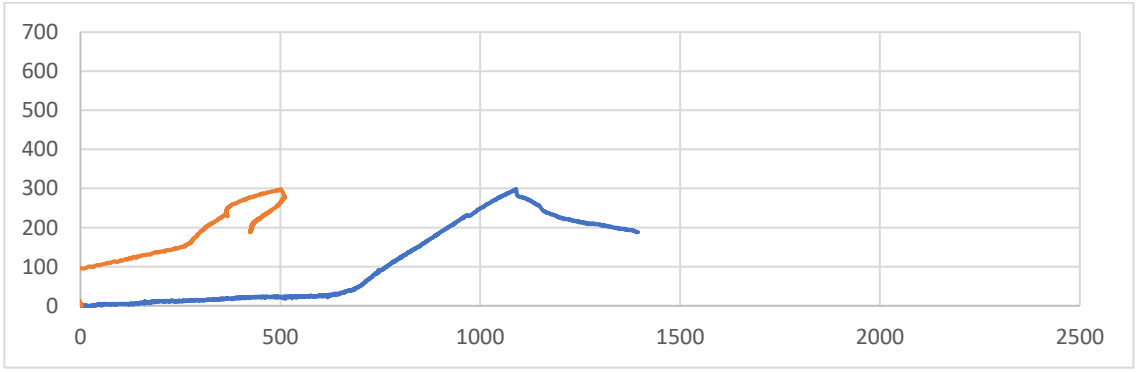

Figure (4-25): Load strain curves for beam (B3)

4.2.3.4 Beam (B4)

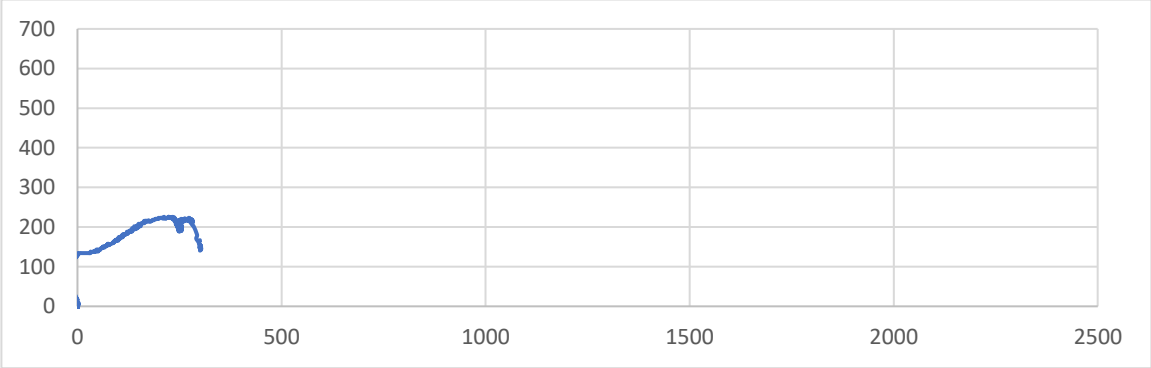

Figure (4-26): Load strain curves for beam (B4)

4.2.3.5 Beam (B6)

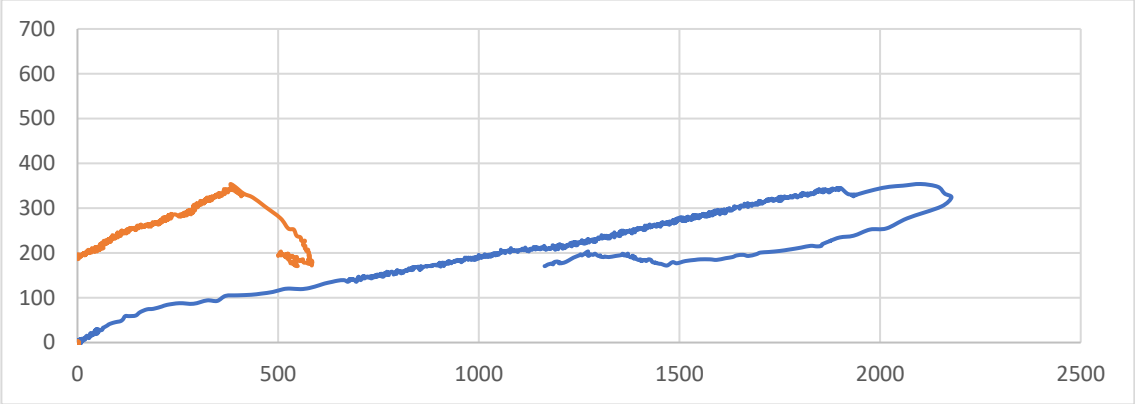

Figure (4-27): Load -strain curves for beam (B6)

4.2.3.7 Beam (B7)

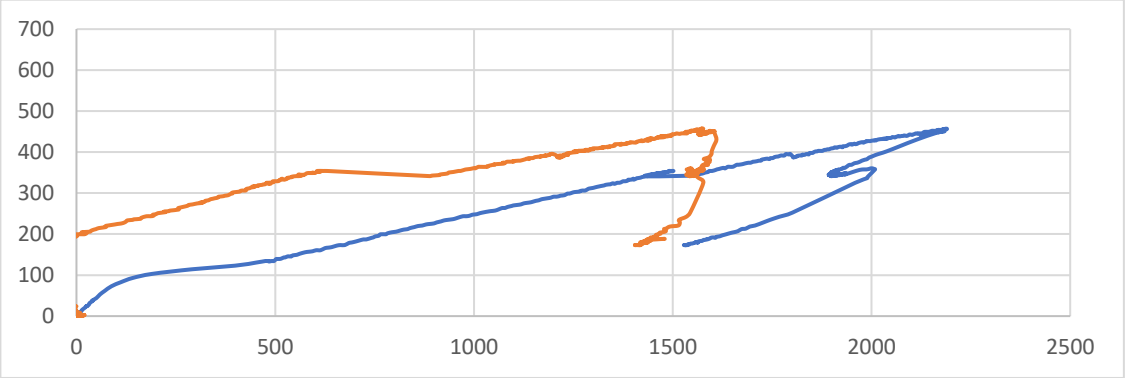

Figure (4-28): Load-strain curves for beam (B7)

4.2.3.8 Beam (B8)

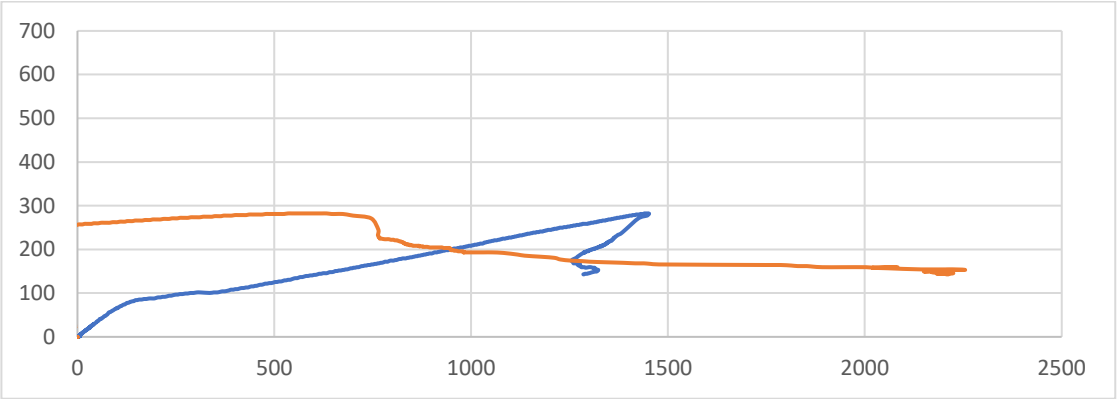

Figure (4-29): Load -strain curves for beam (B8)

4.2.3.9 Beam (B9)

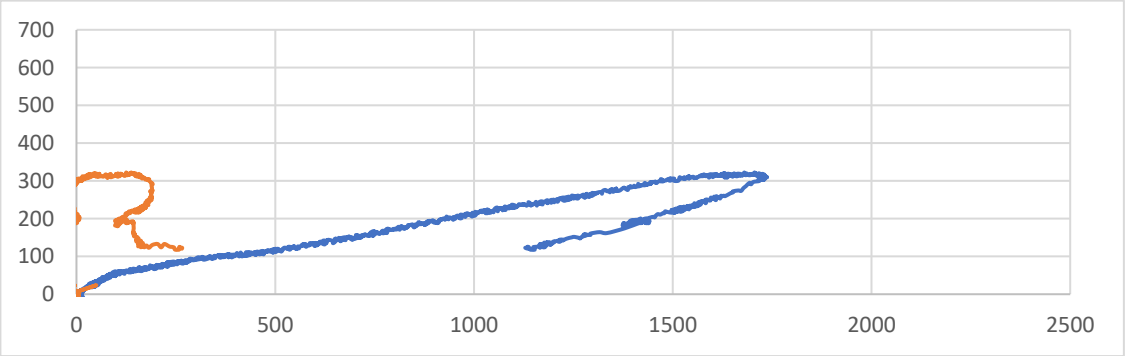

Figure (4-30): load -strain curves for beam (B9)

4.2.3.10 Beam (B10)

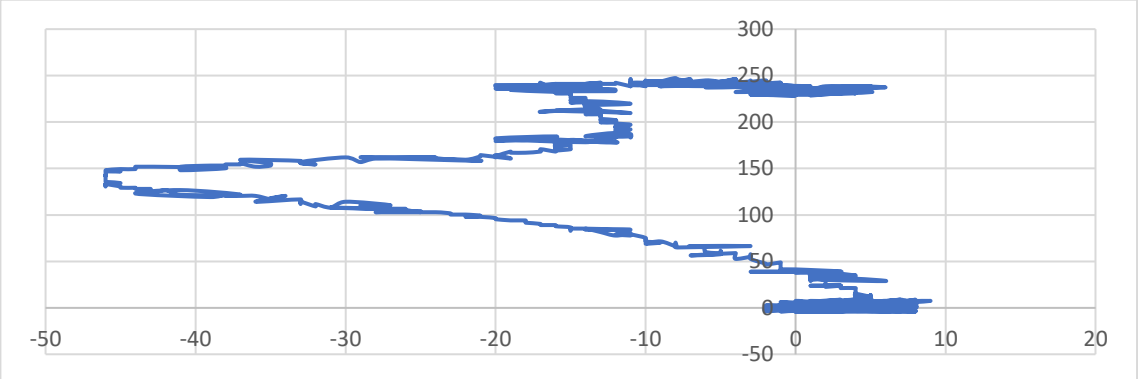

Figure (4-31): Load -strain curves for beam (B10)

CHAPTER FIVE
ANALYSIS AND DISCUSSION OF EXPERIMENTAL RESULTS

5.1 Introduction

This chapter describes the discussion for the analysis of the obtained results for the reinforced deep beams. The behavior of test specimens is investigated for the studied parameters. The parameters are the opening shapes and the orientation of basalt fiber strips. The behaviors of the beams are evaluated by studying the effect of strengthening the deep beams without opening using basalt fiber strips, the effect of strengthening the deep beams with pattern, using basalt fiber strips, the effect of strengthening orientation of basalt fiber strips (vertical and horizontal) on the cracks pattern, modes of failure, the cracked and failure loads, the load-deflection relationship, the load – strain relationship, the deflected shape profile of the tested beams, stiffness of the deep beams, energy absorption capacity and ductility index for the deep beams.

5.2 Cracks Pattern and Modes of Failure

Failure modes in deep beams can be categorized into five expected types: Steel bars yielding, concrete crushing in compression, shear reinforcement failure without BFRP rupture, BFRP layer rupture, and debonding, **Knight M et al., [56]**. The tested beams showed different crack patterns as shown in chapter four. The tested beams' failure

modes are diagonal shear with some differences in crack width and envelope according to the types of opening and direction of strengthen strips. The effects of different used parameters on crack pattern and mode of failure are discussed as follows:

5.2.1 Effect of Strengthening the Deep Beams Without Opening Using Basalt Fiber Strips on The Crack Pattern.

Figure (5-1) shows the crack pattern of the reference beam B1 and beam B2. From the crack pattern obtained, diagonal shear cracks were formed at the edge of the beam near the support and propagated toward the loading points. On the other hand, no flexural cracks were traced from the beam during the experimental testing up to beam failure. Meanwhile, the crack pattern in beam B2 (beam with no opening strengthened with horizontal basalt strips) showed two independent diagonal cracks from the loading point to the support and one flexure crack. This means that the BFRP strips change the failure mode from diagonal shear failure to shear-flexure failure.

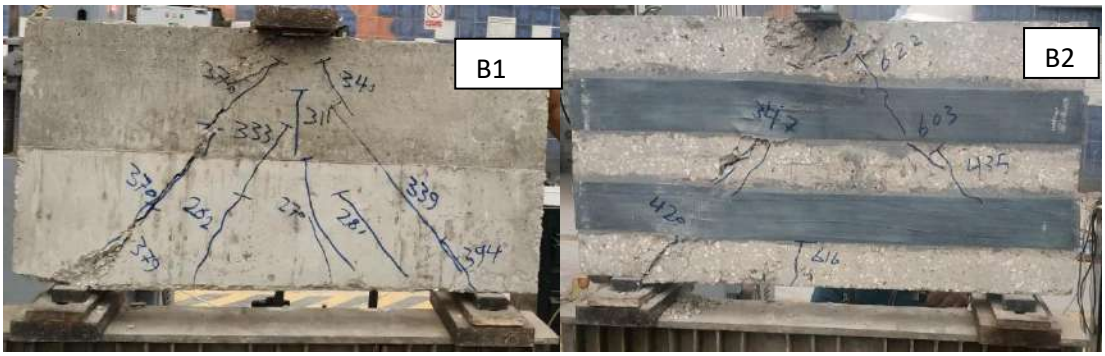

Figure (5-1): Crack pattern for deep beams without openings

5.2.2 Effect of Strengthening the Deep Beams with Opening Using Basalt Fiber Strips on Crack Pattern

By studying the crack patterns and failure modes for beams B3, B4, and B5, as shown in Figure (5-2). It was found that the cracks in beam (B3) with the

rectangular opening show that diagonal cracks were initiated and formed at the corner of the openings, at the top near the loading point, and at the bottom near the support, respectively. Similarly, cracks that were found in beam (B4) propagated diagonally at the bottom of the opening towards the support. With an increase in the load applied, new additional shear cracks were formed below the openings towards the support, while (B5)- strengthened with horizontal basalt strips has a greater number of cracks and is much wider than that in reference beams with no strengthened strips.

Figure (5-2): Crack pattern of deep beams with vertical rectangle openings

5.2.3 Effect of Opening Shapes Strengthen with Horizontal Basalt Fiber Strips on The Crack Pattern.

Figure (5-3) shows the crack patterns with sample numbers B5, B7, B9, and B11 which were studied for different opening shapes having the same area (vertical

rectangular, horizontal rectangular, circular, and square) respectively. Cracks were found propagated diagonally at the bottom of the opening towards the support in beam B5. With an increase in the load applied, new additional shear cracks were formed below the openings towards the support, as shown in the Figures. As illustrated in Figures, the crack pattern of beam B9 was found to be almost similar to those obtained in beam B5. However, the diagonal cracks at the bottom of the openings propagated towards the support were more severe than beam B5 which leads to crushing of concrete at the edge of the beam. In beam B7 the crack pattern shows that there are two diagonal cracks propagated toward the load point leading to the spalling of the sheet from the concrete. However, the crack pattern in beam B11 showed only one crack on the left side of the beam which appeared initially at the loading point and propagated towards the support during the test until the failure of the beam.

Figure (5-3): Crack patterns for beams strengthened with horizontal BFRP strips.

5.2.4 Effect of Opening Shapes Strengthen with Vertical Basalt Fiber Strips on The Crack Pattern.

Figure (5-4) shows the crack pattern of B4, B6, B8, and B10 which studied the Effect of opening shapes strengthening with vertical basalt fiber strips. Cracks were found propagated diagonally at the bottom of the opening towards the support in beam B4. With an increase in the load applied, new additional shear cracks were formed below the openings towards the support, as shown in the Figures. As illustrated in Figures, the crack pattern of beam B6 was found almost similar to those obtained in beam B4. However, the diagonal cracks at the bottom of the openings propagated towards the support were more severe than the beam which led to the crushing of concrete at the edge of the beam. In beam b8 the crack pattern shows that there are two diagonal cracks propagated toward the load point leading to the spalling of the sheet from the concrete. However the crack pattern in beam B10 showed two cracks on the right and on the left side of the beam under the openings, the crack on the left appeared initially at the loading point and propagated towards the support during the test until the failure of the beam. In the vertical strengthening in all types of openings, the cracks were confined diagonally between two vertical strips above and below the opening, in addition to they were deep cracks deeper than their counterparts in the horizontal strengthening, and also in the vertical strengthening, no cracks appeared from under the strips, unlike the horizontal one, in which the cracks appeared under the basalt fibers. The vertical strengthening hid the inclined cracks that start from the top under the load.The vertical strengthening using BFRP prevented cracks on both sides of the openings, right and left, changing its path to be under the openings and above, as it divided the deep beam horizontally into two sections of deep beams, one upper and the other lower making two triangles, one above and one below, while the horizontal strengthening did not do that, but rather

preserved the same shape as the distribution of cracks in the form of one triangle with the full height of the deep beam, and this is what happened in the horizontal openings.

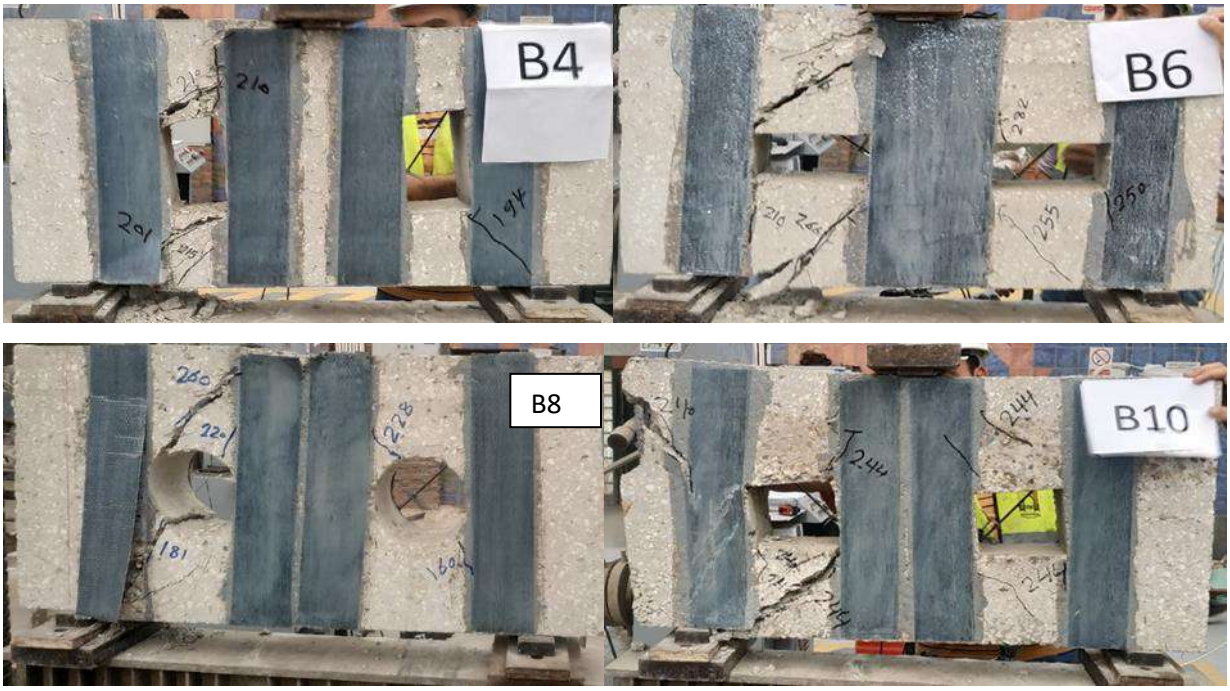

Figure (5-4): Crack patterns for beams strengthened with vertical BFRP strips.

5.2.5 Effect of Strengthening Orientation of Basalt Fiber Strips on The Crack Pattern.

By comparing Figures in Chapter Four for B4 with B5, B6 with B7, B8 with B9, and B10 with B11 we can find that all those beams have the same crack pattern. Still, in beams strengthened with horizontal strips, the cracks were smaller than that in those beams which strengthened with vertical strips which means that the orientation of strips did not change the behavior of failure of deep beams.

5.3 Load-Deflection Relationship

The relationship of load-deflection is plotted for each specimen in chapter four. The results are organized in Figures from (5-5) to (5-12).

5.3.1 Effect of Strengthening the Deep Beams Without Opening Using Basalt Fiber Strips on Load Deflection Curves.

Figure (5-5) shows the load-deflection curves for deep beams without opening. by comparing the load-deflection curves of B1 and B2, it was noticed that the strengthen and non-strengthen beams have the same behavior (semi-linear up to failure load then the load decreases with a curvature of the curve up to failure), the deflections are the same up to failure load in non-strengthen beam then increased rapidly in strengthen beam.

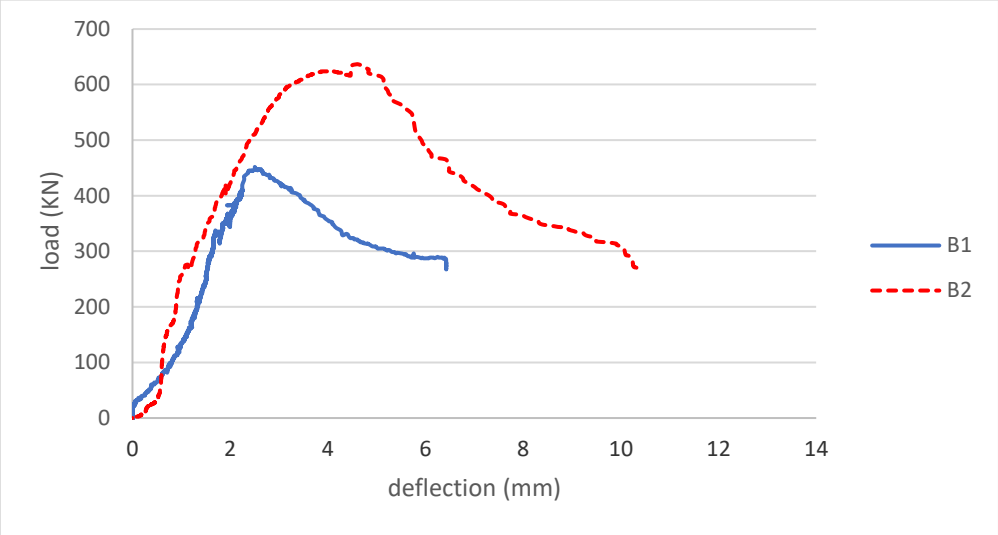

Figure (5-5): Load-deflection curves for beams without opening.

5.3.2 Effect of Strengthening the Deep Beams with Opening Using Basalt Fiber Strips on Load-Deflection Curves.

Figure (5-6) shows the load-deflection curves of deep beams B3, B4, and B5, by studying these Figures it has been observed that a non-linear load-deflection response was observed indicating a higher rate of crack initiation, widening, and growth. The behavior of the load-deflection curve is still the same when the deep beam is strengthened with BFRP strips in the case of horizontal and vertical strips. the behavior of deep beams with openings is different from the behavior of

deep beams without openings where the deflection of deep beam with openings is higher than that in the deep beam without openings at the initial stage with a lower slope of the load-deflection curves for deep beams with openings.

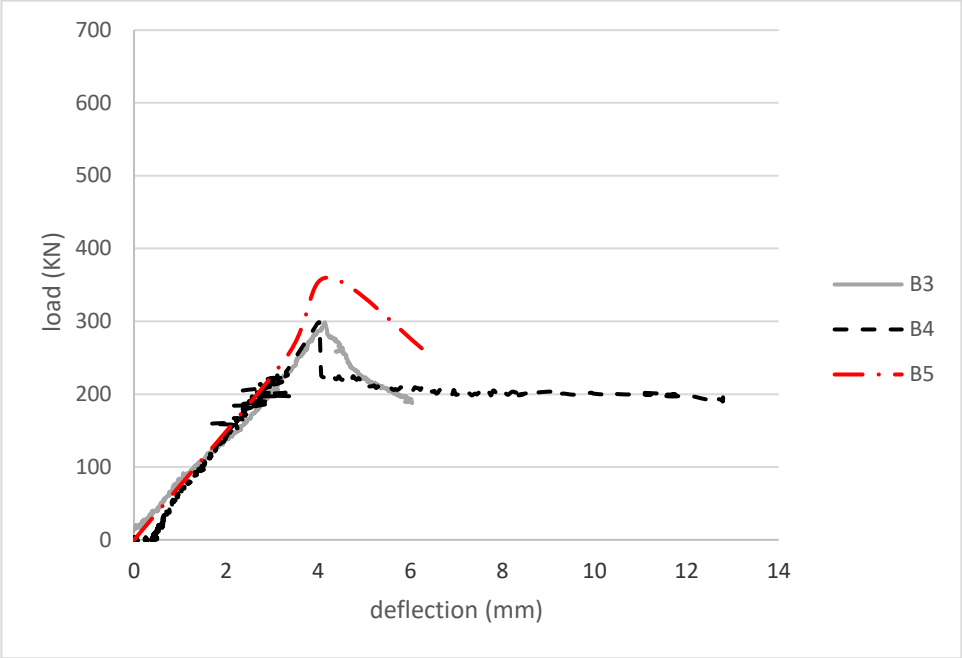

Figure (5-6): Load-deflection curves for beams with vertical rectangular opening

5.3.3 Effect of Opening Shapes Strengthen with Horizontal Basalt Fiber Strips on Load Deflection Curves.

The load-deflection curves of deep beams strengthen with horizontal BFRP strips are drawn in Figure (5-7) which showed that the deflections of strengthened beams (B5, B7, B9, and B11) are lower than that in non-strengthened beams (B1 and B3) and a higher initial slope up to failure load in strengthened beams than that in non- strengthened beams. All beams have the same behavior, linear up to failure then the curve has anon linear behavior.

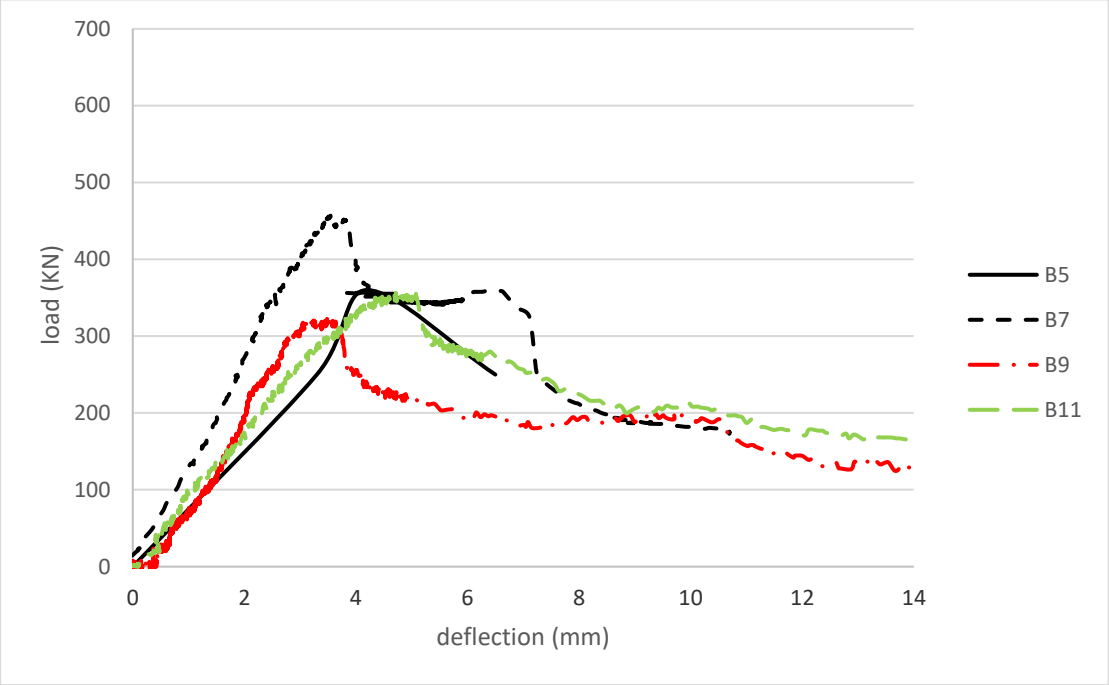

Figure (5-7): Load-deflection curves for beams with different types of openings strengthened with horizontal strips.

5.3.4 Effect of Opening Shapes Strengthen with Vertical Basalt Fiber Strips on Load Deflection Curves.

The load-deflection curves of deep beams strengthened with vertical BFRP strips are drawn in Figure (5-8) which shows that the deflections of strengthened beams (B4, B8, and B10) are lower than that in non-strengthened beams (B1 and B3) and a higher initial slope up to failure load in strengthened beams than that in non- strengthened beams. While in deep beam B6, the deflection at initial stage is higher than the deflection of non-strengthened deep beams (B1and B3). All beams have the same behavior, linear up to failure then the curve has anon linear behavior.

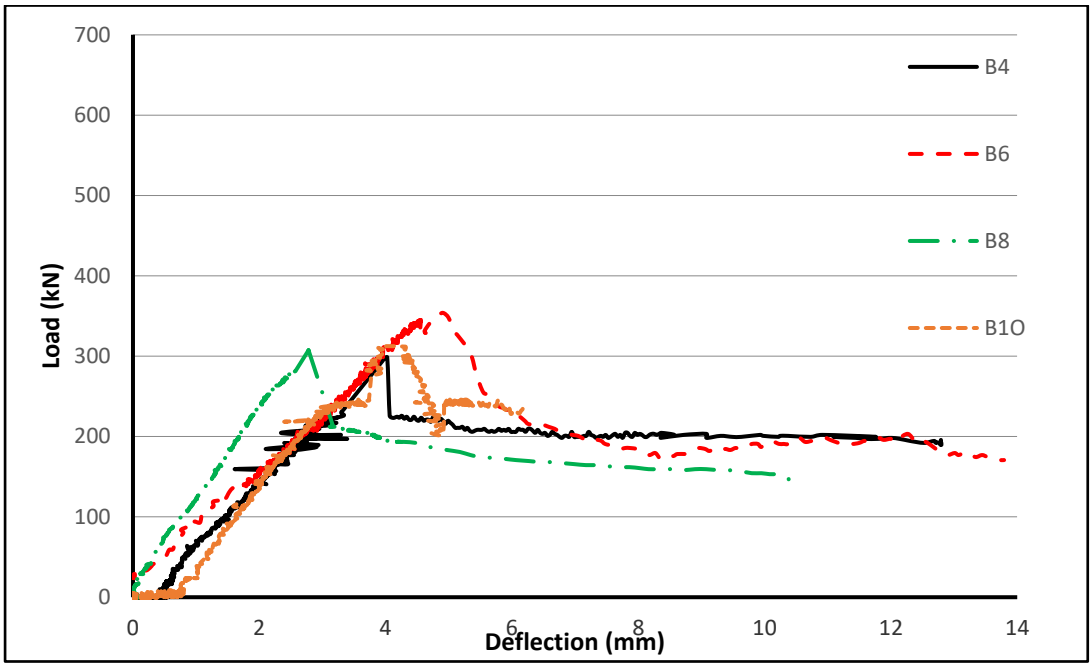

Figure (5-8): Load-deflection curves for beams with different types of openings strengthened with vertical strips.

5.3.5 Effect of Strengthening Orientation of Basalt Fiber Strips on Load-Deflection Curves.

The load–deflection curves of specimens of groups vertical openings, horizontal openings, circular, and square are shown in Figures. (5-9) to (5-12), respectively. From these figures, we can observe that in the deep beams with vertical, circular and square openings, there is no different effect on the load-deflection curve behavior in case of vertical from horizontal strength where the curve is linear up to the failure load then the load decrease with a non-linearity form until failure of the beam despite of that same behavior, the failure load in case of horizontal strength is higher than that in vertical strengthening by (20,5,14 %) respectively. Whereas, in the case of the horizontal openings, the behavior of the horizontal strengthening is completely different from the vertical strengthening, as the slope of the line in the horizontal is greater than in the vertical, also after reaching the

maximum load, the behavior remains different in both cases. In the slope of the line or even the maximum load, while in the horizontal BFRP strips, the maximum load increased by (36%). Hence, Horizontal strength improves the failure load in the range of (8-54) % while vertical strength improves the failure loads in the range of (0-18) % only.

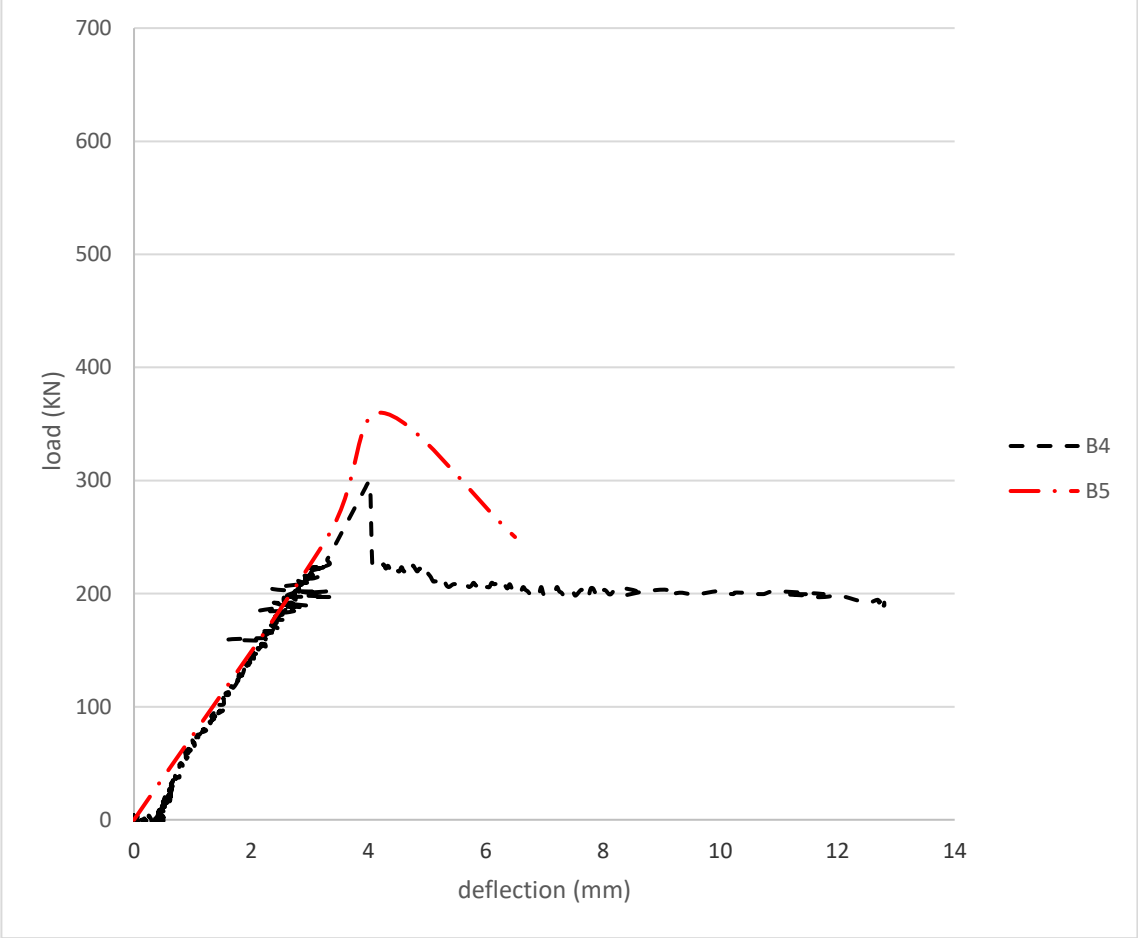

Figure (5-9): Load-deflection for beams with vertical rectangular openings strengthened with vertical and horizontal strips.

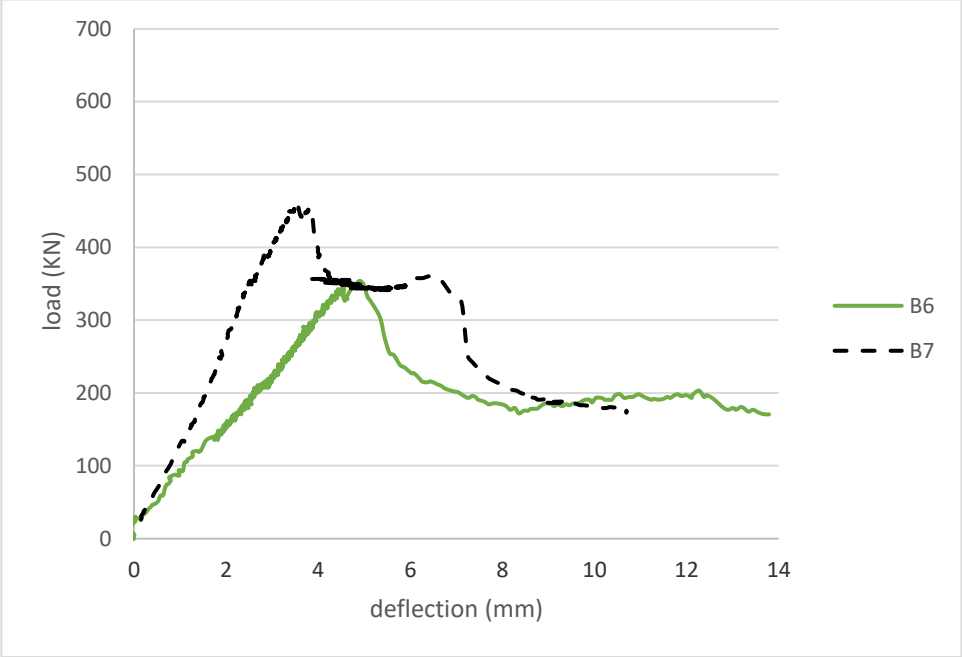

Figure (5-10): Load-deflection for beams with horizontal rectangular opening strengthened with vertical and horizontal strips.

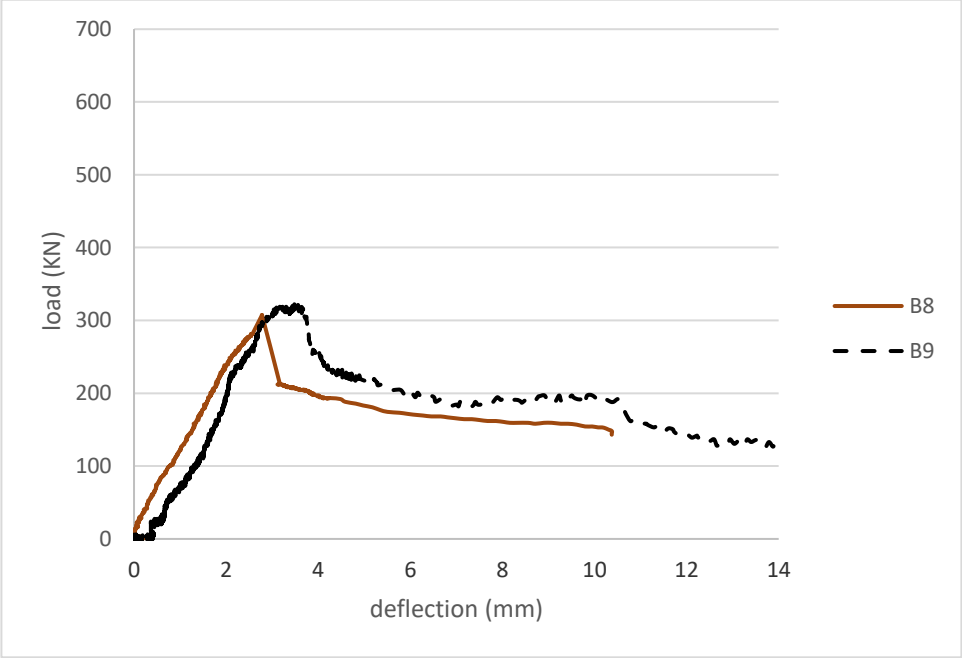

Figure (5-11): Load-deflection for beams with circular opening strengthened with vertical and horizontal strips.

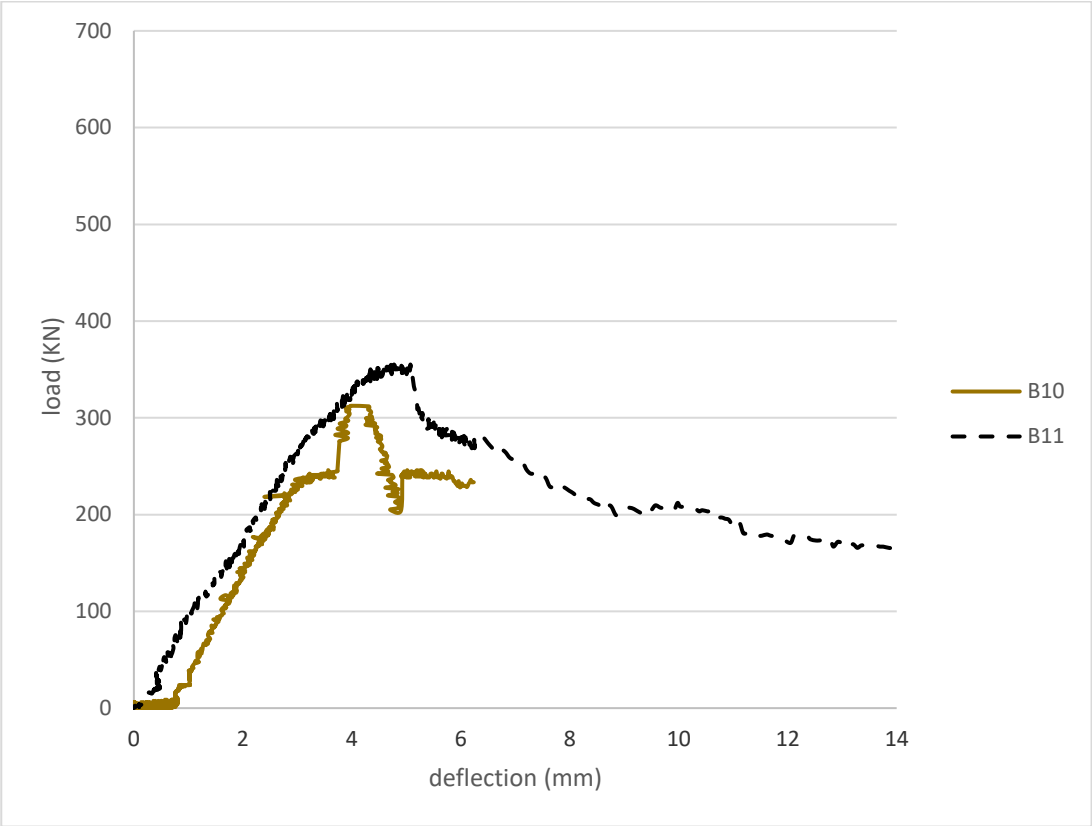

Figure (5-12): Load-deflection for beams with square opening strengthened with vertical and horizontal strips.

5.4 Cracked and Failure Loads.

All the results of crack loads and failure loads are summarized in Table (5-1), while Figure (5- 13) shows the variation of both crack load and the failure load, respectively for all tested specimens. The horizontal axis of both figures defines each specimen configuration and the vertical axis crack load and the failure load. The cracking loads in the strengthened beams are formed at a higher load compared to the ones in the control beams. By studying the cracking and failure loads shown in Figure (5-13), it was observed that the cracking load in the strengthened beams is created at a higher load compared to the cracking loads in the non-strengthened beams. Where, in non-strengthened beams with and without

openings, the cracking load appears at nearly 59% of the failure load while in strengthened beams with an opening the cracking load appears at nearly 69.4, 83.2, 96.1 and 91.2% of the failure load for beams B5, B7, B9, and B11 respectively.

This means that using BFRP horizontally in deep beams with openings delays the cracks while in (B2) the cracking load appears at nearly 54.5% of the failure load. This means that BFRP in strengthening deep appeared the cracks earlier than that in non-strengthened deep beams. By studying the values in Table (5-1) which shows the different failure loads concerning B3, it was found that the vertical opening reduces the failure load by 34% while providing basalt fiber strips, and, the strength has been increased by about 21.8% also, BFRP in deep beams with horizontal openings increased the strength by 34.7% which means that the beam returned to its original capacity. In beams B9 and B11, the strength was increased by 7.6% and 16.4% respectively. Also, Figure (5-14) shows the different failure loads concerning B1, by comparing B2 with beam B1 (control) it was found that the strength of the beam increased by 41%. while the beam with a horizontally strengthened opening gains strength by 1% when compared to the non-strengthened beam B1.but in beams with vertical, circular, and square openings the failure loads did not reach the failure loads in B1, therefore, the BFRP increases the capacity of solid deep beams by 41% while BFRP increases the capacity of deep beams with openings by (7.6- 34.7) when strengthening the openings horizontally by it.

Table (5-1): Values of cracking and failure loads

Beam No.	Cracking load (p_{cr}) (KN)	Failure load (p_f) (KN)	$(\frac{pcr}{pf})$
B1	270	451.8	59.76 %
B2	347	636.28	54.5 %
B3	178	298.69	59.6 %
B4	194	298.5	64.99 %
B5	250	360	69.4 %
B6	210	353.9	59.3 %
B7	380	456.82	83.2 %
B8	181	351.9	51.4 %
B9	310	322.53	96.1%
B10	240	312.5	76.8%
B11	325	356.42	91.2 %

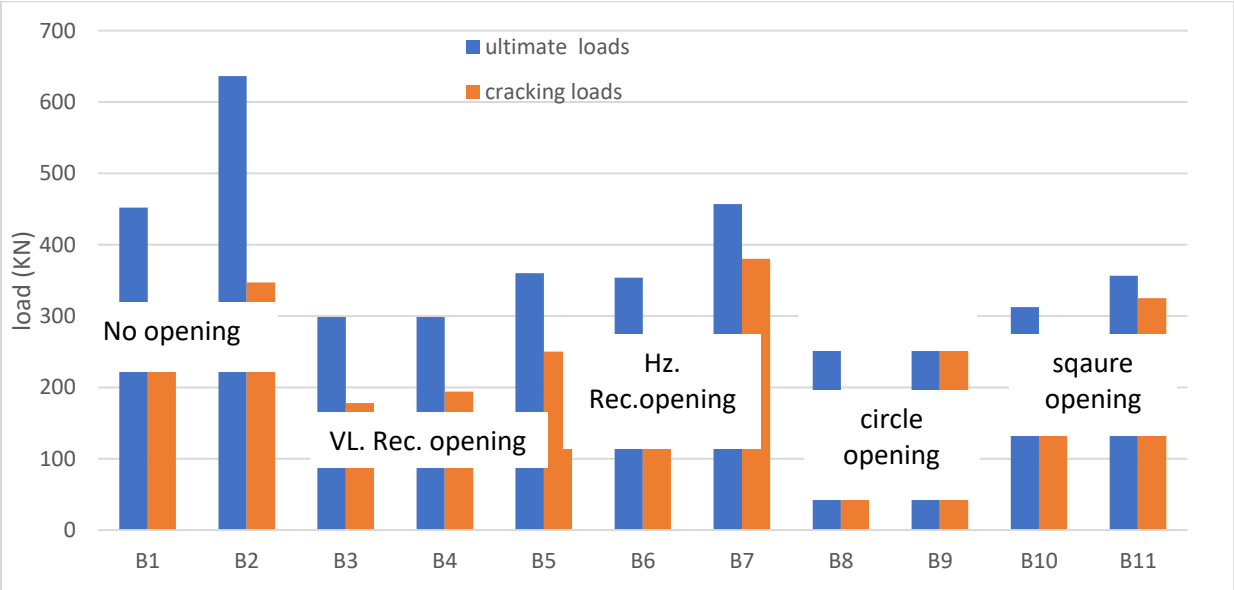

Figure (5-13): The cracking and failure loads for all specimen

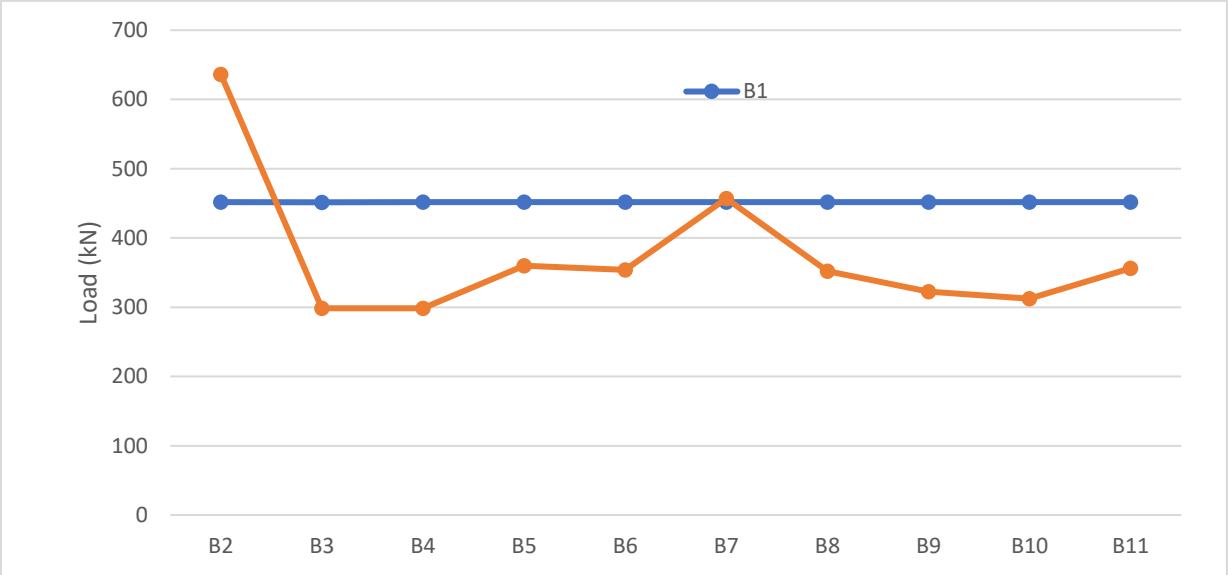

Figure (5-14): The different failure loads concerning B1.

5.5.1 Effect of Strengthening the Deep Beams without Opening Using Basalt Fiber Strips on Cracking Load and Failure Load.

Figure (5-15) shows the values of cracking and failure loads for solid deep beams without openings, it is obvious that strengthening deep beams without openings make the first crack appear earlier than in non-strengthened deep beams, where the crack in non-strengthened deep beams appeared at nearly 60% of maximum loads and the first crack in strengthened beam appeared at nearly 54% of the maximum load also strengthening deep beams horizontally by basalt fiber strips give a higher failure load than non-strengthened nearly by 41% .that means that strengthening using basalt fiber reinforced polymer strips is very effective in strengthening and we can use it as an alternative to carbon fibers in strengthening deep beams to save the environment from pollution.

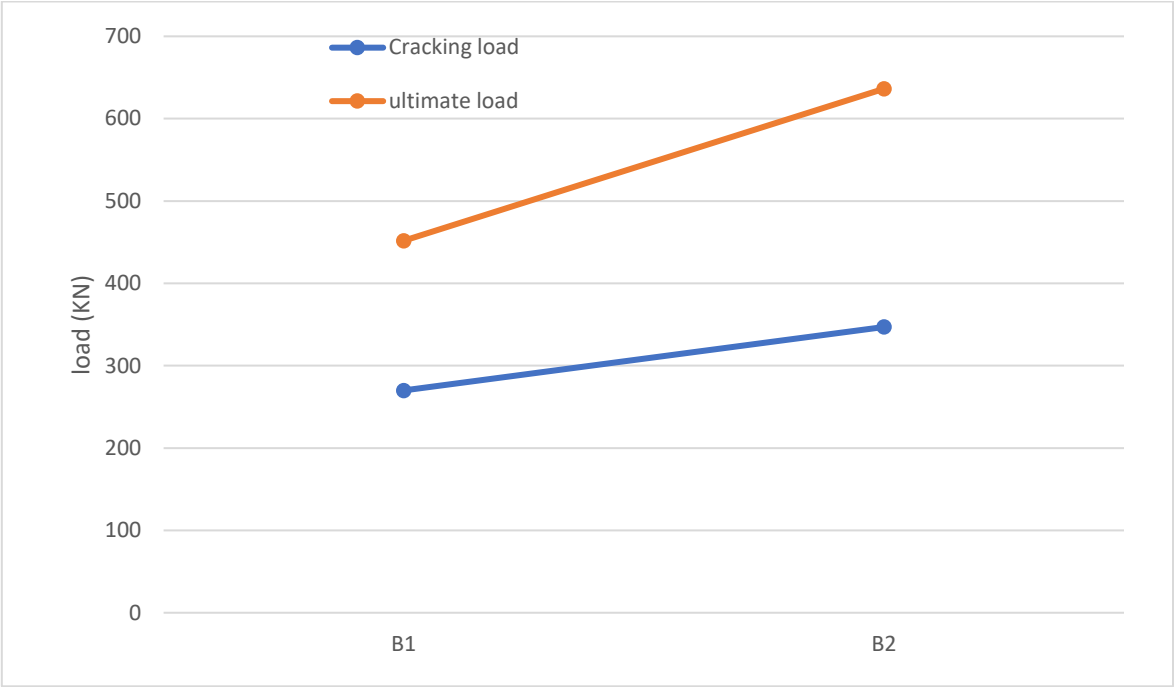

Figure (5-15): The cracking and failure loads for deep beams without openings.

5.5.2 Effect of Strengthening the Deep Beams with Opening Using Basalt Fiber Strips on Cracking Load and Failure Load.

Figure (5-16) shows the values of cracking and failure loads for deep beams with vertical rectangular openings, it is obvious that openings in deep beams decrease the ultimate and cracking loads and first crack appears nearly at the same stage for solid and deep beam with openings (59% of failure loads), but when the openings strengthened with vertical BFRP strips the first crack appeared later than in non- strengthened beam. also, strengthening the deep beam with horizontal BFRP strips makes the first crack appear later than in vertical strengthening deep beams with openings.

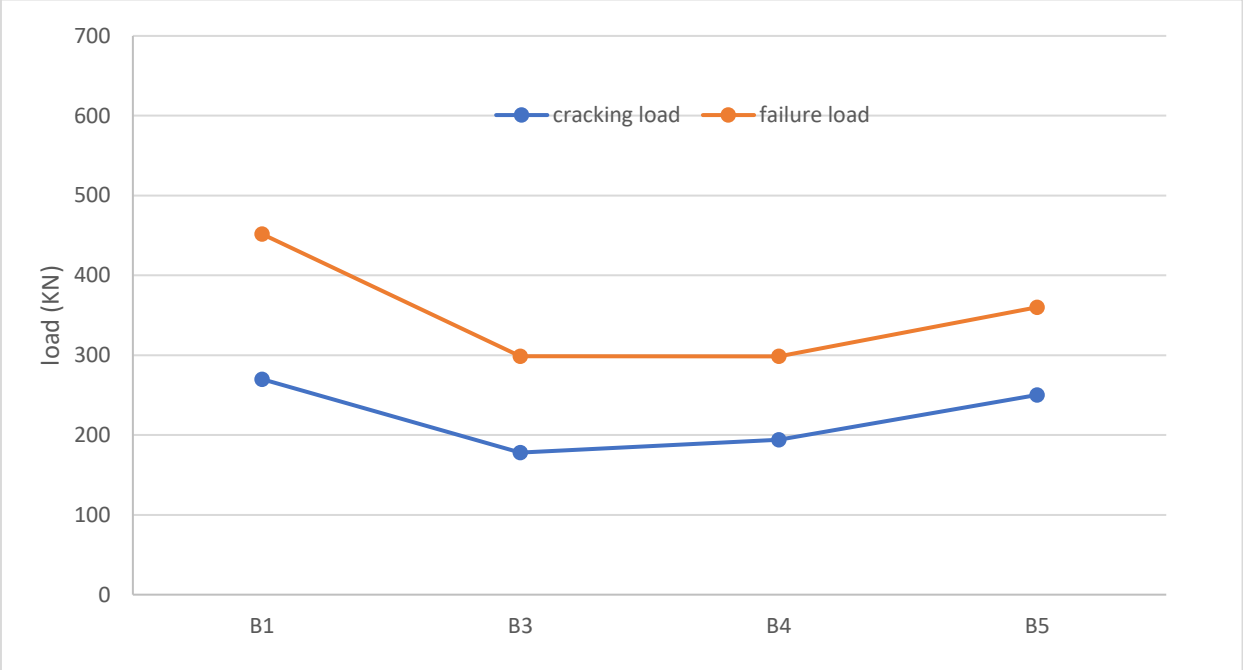

Figure (5-16): The cracking and failure loads for deep beams with rectangular openings.

5.5.3 Effect of Opening Shapes Strengthened with Horizontal Basalt Fiber Strips on Cracking Load and Failure load.

Figure (5-17) show the cracking and failure load for different types of openings strengthened with BFRP strips, it is obvious that the cracking load appears at nearly 69.4, 83.2, 96.1 and 91.2% of the failure load for beams B5, B7, B9, and B11 respectively. This means that using BFRP horizontally in deep beams with openings delays the cracks. Vertical openings have the least ratio of first crack/ failure load while circular openings has the highest ratio while the deep beam with horizontal openings has the highest failure load then the deep beam with vertical openings after that the deep beam with square openings and the last is the deep beam with circular openings, therefore the best type of openings is the horizontal one with the same value of area for all types of openings.

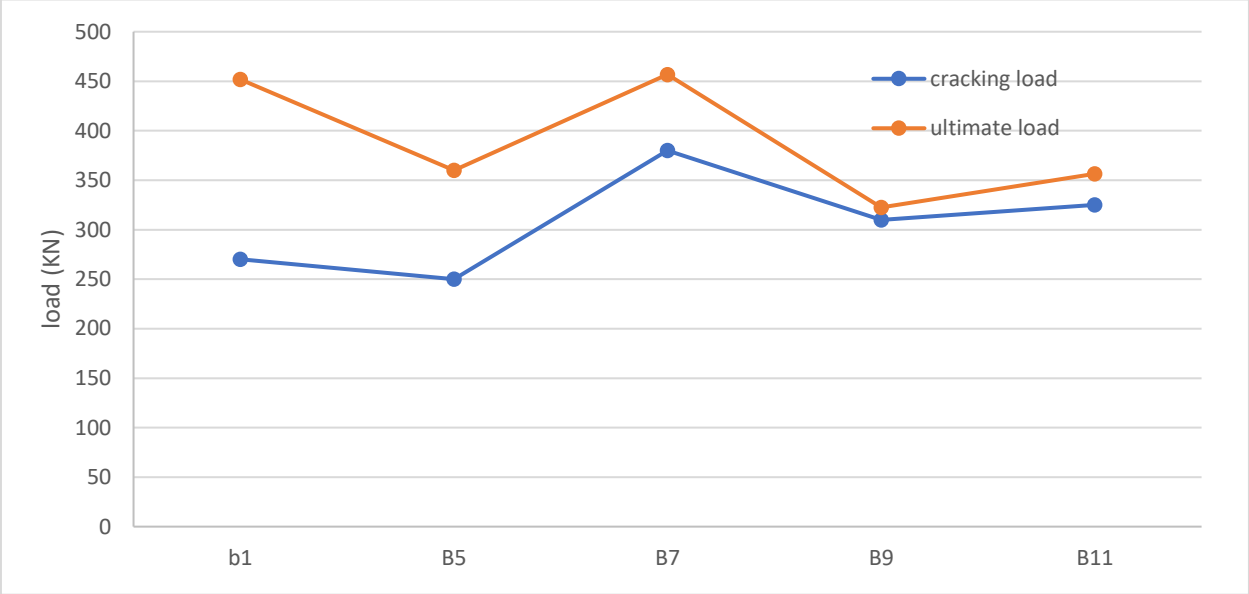

Figure (5-17): The cracking and failure loads for deep beams with horizontal strengthening openings.

5.5.4 Effect of Opening Shapes Strengthen with Vertical Basalt Fiber Strips on Cracking Load and Failure Load

Figure (5-18) shows the cracking and failure load for different types of openings strengthened with vertical BFRP strips, it is obvious that the cracking load appears at nearly 65, 59.3, 51.4 and 76.8 % of the failure load for beams B4, B6, B8, and B10 respectively. This means that using BFRP horizontally in deep beams with openings delays the cracks. circular openings have the lowest ratio of first crack/ failure load while square openings have the highest ratio the deep beam with horizontal openings has the highest failure load then the deep beam with circular openings after the deep beam with square openings and the last is the deep beam with vertical rectangular openings, therefore the best type of openings is the horizontal one with the same value of area for all types of openings.

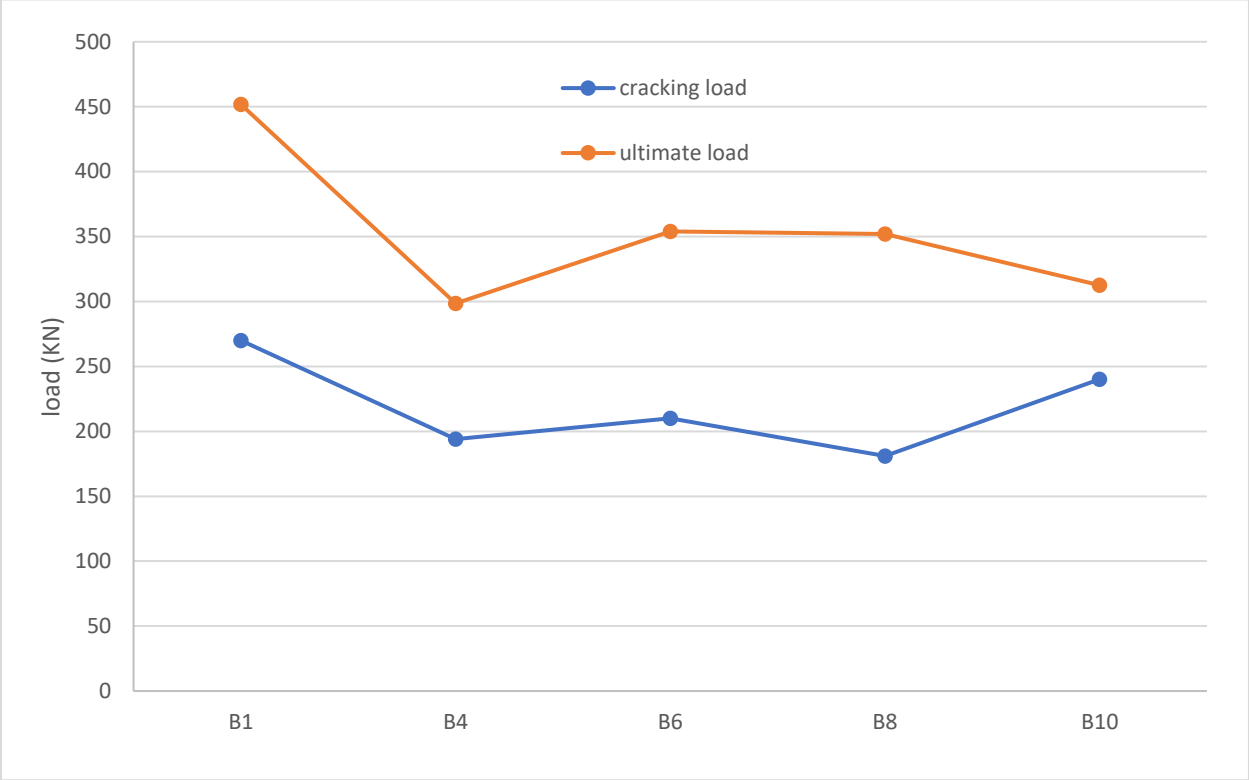

Figure (5-18): The cracking and failure loads for deep beams with vertical BFRP strip openings.

5.5.5 Effect of Strengthening Orientation of Basalt Fiber Strips on Cracking Load and Failure Load

Figures from (5-19) to (5-22) show the comparison of horizontal and vertical strength for different types of openings, it is obvious that the failure load in case of horizontal strength is higher than that in vertical strengthening by (20,36,5,14 %) for vertical rectangular, horizontal rectangular, circular, and square respectively. Hence, Horizontal strength improves the failure load in the range of (8-54) % while vertical strength improves the failure loads in the range of (0-18) % only. Also, horizontal strength for different types of openings make the first crack appeared later than deep beams with vertical strengthening.

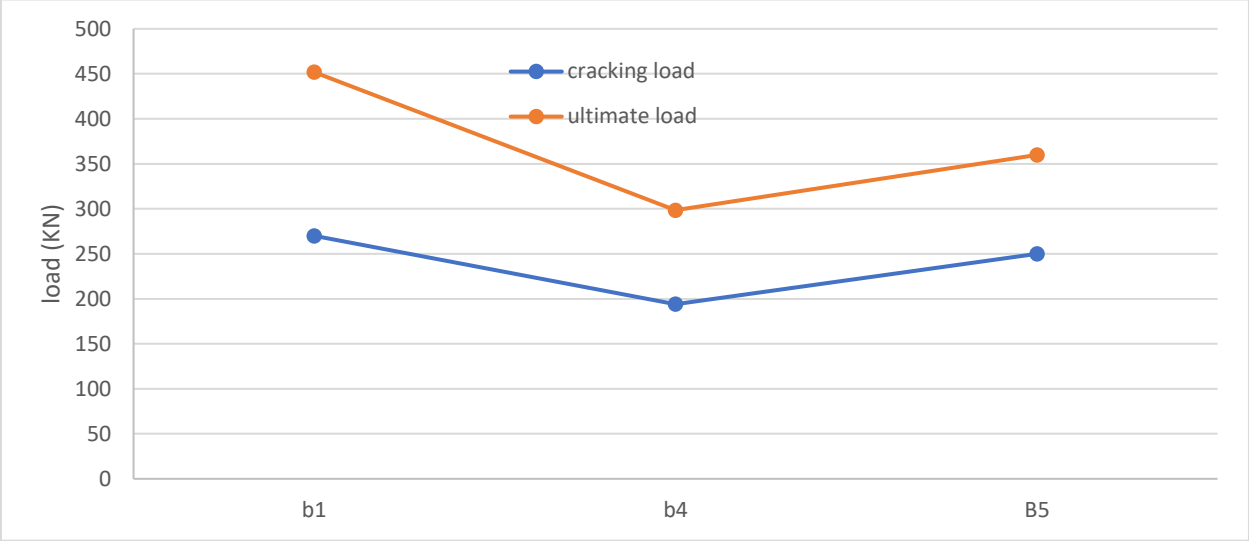

Figure (5-19): The cracking and failure loads for deep beams with vertical rectangular openings.

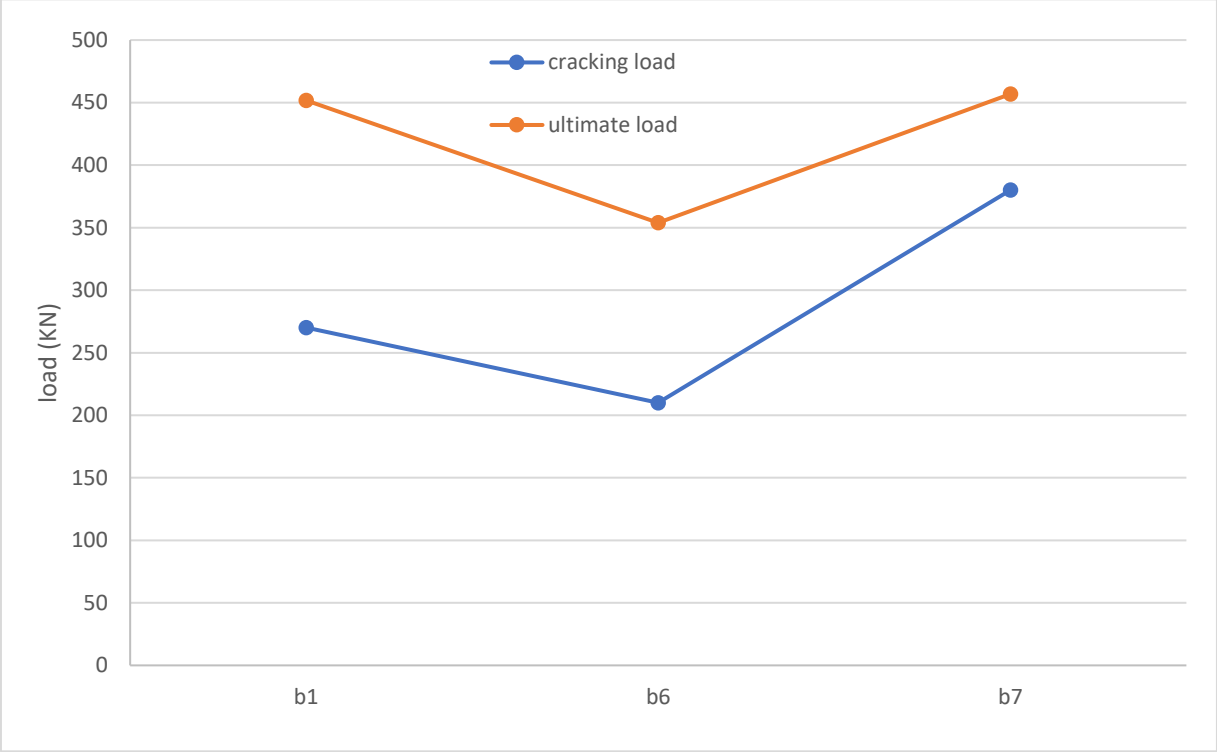

Figure (5-20): The cracking and failure loads for deep beams with horizontal rectangular openings.

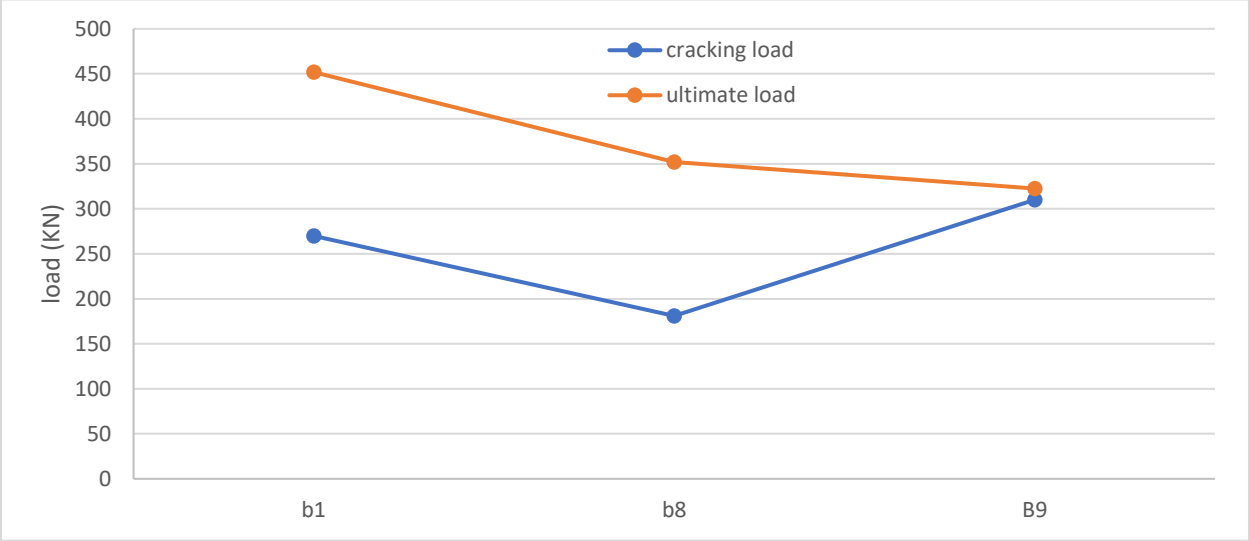

Figure (5-21): The cracking and failure loads for deep beams with circular openings.

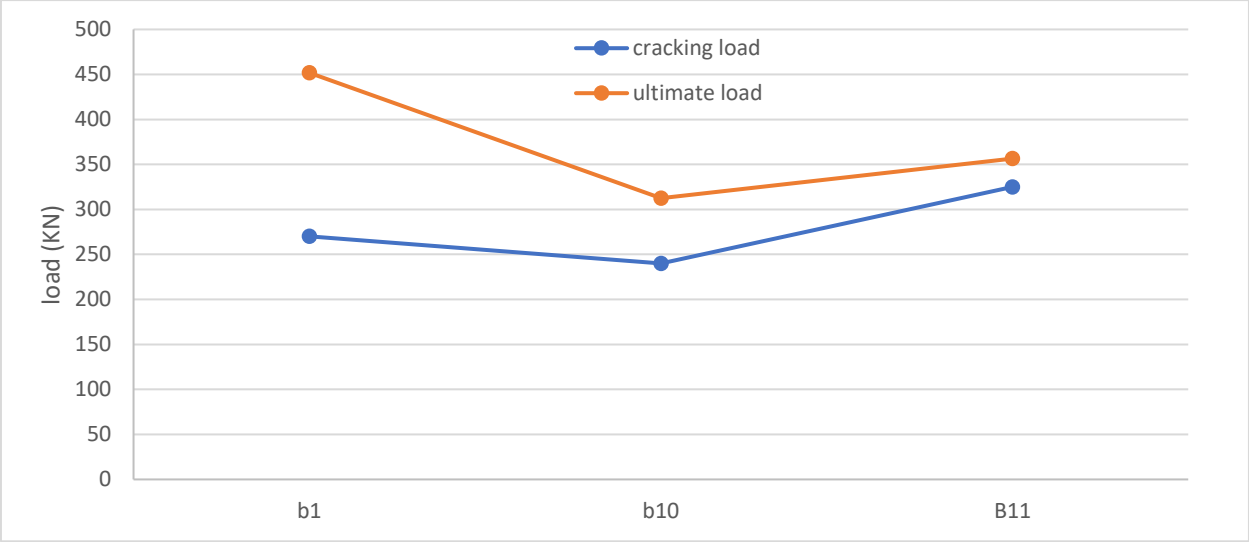

Figure (5-22): The cracking and failure loads for deep beams with square openings.

5.5 Energy Absorption Capacity

The energy absorption of the beam members is calculated as the area enclosed by the load-deflection curves. Figure (5-23) shows the different values of the energy

absorption capacities for all beams. From this Figure, it is seen that the energy absorption capacity is increased when the beam is strengthened with basalt fiber strips of about 156 % in the case of deep beams without opening. While the openings in the deep beams decrease the energy by 34% of the origin total energy, the vertical strength increases the energy by 45,83,19 and 59% of the value of the non-strengthened beam for deep beams with vertical, horizontal, circle, and square openings respectively. Horizontal strength also increases the energy by 52,57,40 and 70% for deep beams with vertical, horizontal, circle, and square openings respectively as listed in Table (5-2). Also, horizontal strength was more than the vertical strength by 5, 18, and 7% for vertical, circle, and square openings respectively while in the case of horizontal rectangle opening the total energy of vertical strength was more than in horizontal strength by 16%.

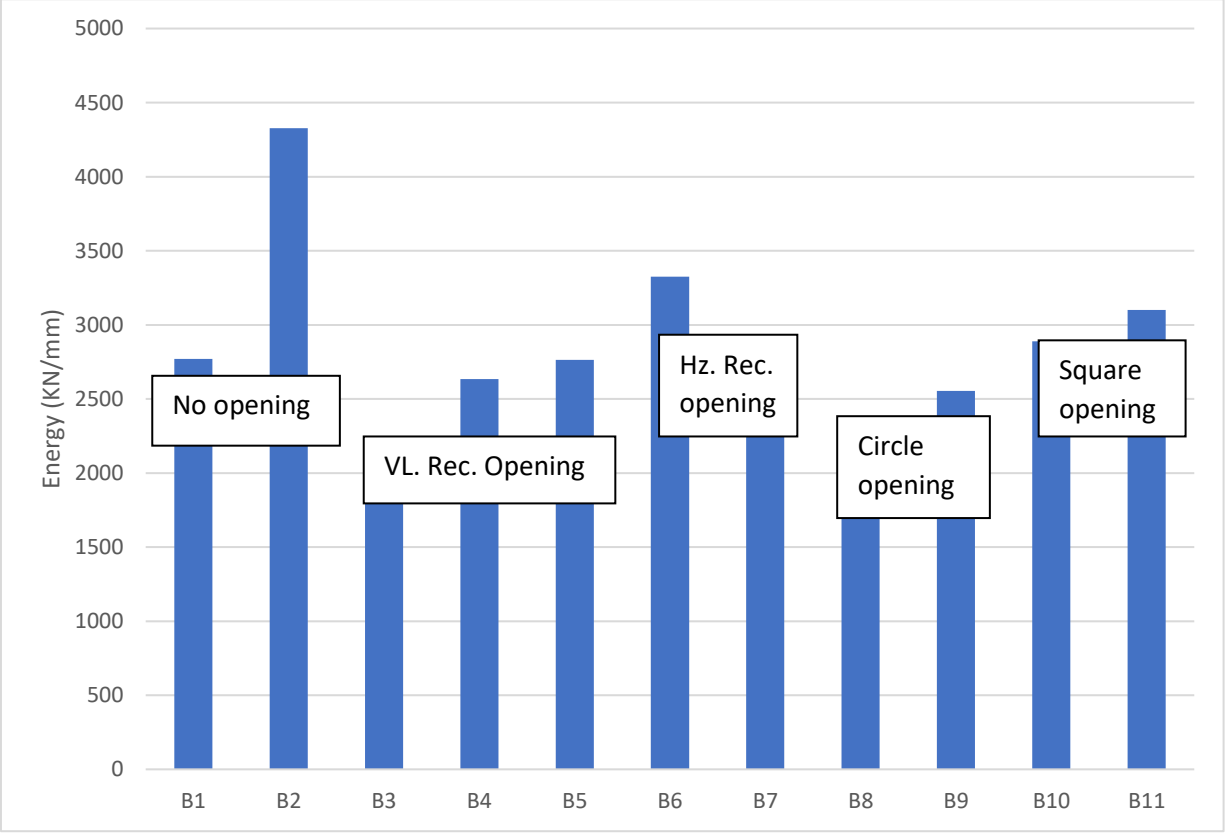

Figure (5-23): Energy absorption capacities for all specimens

5.6 Measure of Ductility

Ductility reflects the adequacy of the reinforced concrete members to realize and disperse energy before failure **Al-Gasham. T.S et al., [57-60**], and it is an indication of the amount of inelastic deformation. There are various ways to determine the ductility in flexure **Abbass A. et al., [61, 62]**, (deformation at max. load/total elastic deformation), Ductility factor may also be defined as the ratio of deflection at failure to the deflection at yield or the first crack while ductility can also be used to compare energy absorption under impact and other types of loads **Abid S R et al., [63-68]**. Among this approaches, the method proposed by (sadea G.et al., [69] is more fit for deep beams since the others relymainly on the strain yield of tensile reinforcing bars that is absent in the deep beams because of brittle shear failure. In this study, the ductility factor (DF) is calculated as a ratio of absorbed energy (i.e., the entire area beneath the load-deflection curve) to the energy absorbed up to the service load. As mentioned before in reinforced concrete elements, a force equating 70-75% of the failure load could be taken as a service load **Tan K H.et al., [70], Jabir et al., [60]** as shown in Equation (5.1) and Figure (5-24). The determined ductility factors for all beams are recorded in Table (5-2). The energy absorption can be found by calculating the area under the curve (ET) of the total deformation (load–defection curve), which is calculated utilizing **Simpson's rule**, Equation (5.2) for all beam specimens. by studying the values of ductility listed in the Table (5-2), it is obvious that the ductility of strengthened solid deep beams is more than the ductility of non-strengthened deep beams which means that the BFRP strips enhance the behavior of solid deep beam by increasing the ductility of the beam.

$$\mu_E = \frac{ET}{E@75\%\ of\ ultimate\ load} \tag{5.1}$$

$$ET = \frac{Pi+P(i+1)}{2} * (\Delta(i+1) - \Delta i) \tag{5.2}$$

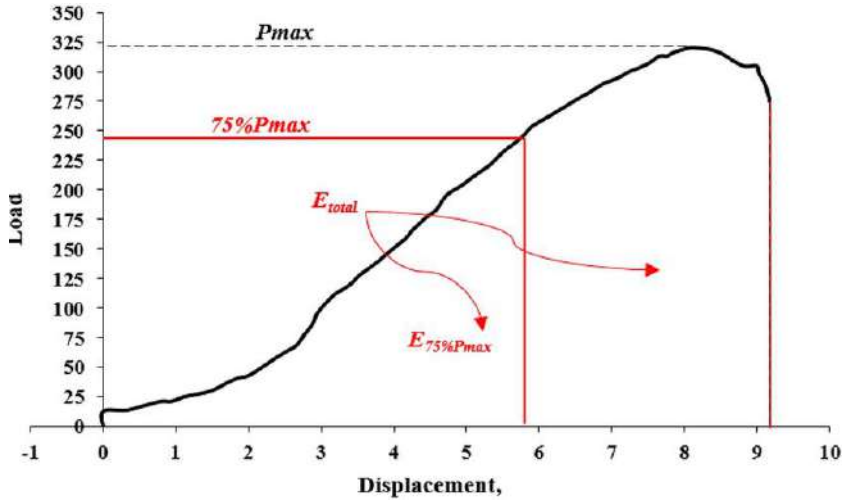

Figure (5-24): Illustration of measure of ductility

Table (5-2): Values of total energy, energy at 0.75 of max. load and ductility index

Beam no.	Total area (E_T)	$E_{0.75\ P\ max}$	Ductility index
B1	2770.25	609.7	4.54
B2	4328.13	557	7.77
B3	1820.7	375.5	4.84
B4	2633.64	2112.67	1.24
B5	2763.5	700	3.94
B6	3325.6	750.3	4.43
B7	2854.1	412	6.92
B8	2169.47	516.5	4.2
B9	2554.3	252.7	10.1
B10	2888.2	515.75	5.6
B11	3100.1	411	7.54

5.7 Deflection Shapes of the Beams

The deformed shapes are drawn by measuring the deflection at three points: at mid-span, at 333 and 667 mm from the left support which represents the third of the span from the left and right side.

5.7.1 Effect of Strengthening the Deep Beams Without Opening Using Basalt Fiber Strips on Deflection Shape Profiles.

Figure (5-25) shows the deflection shape profile for solid deep beams B1 and B2. From this Figure, it can be concluded that the strengthened beam is more ductile than the non-strengthened one. the deflected shape of deep beam B1 is a smooth curve while the shape of B2 is a convex shape. This means that Hz BFRP strips increased the deflection and did not enhance the deflected shape profile of the deep beams.

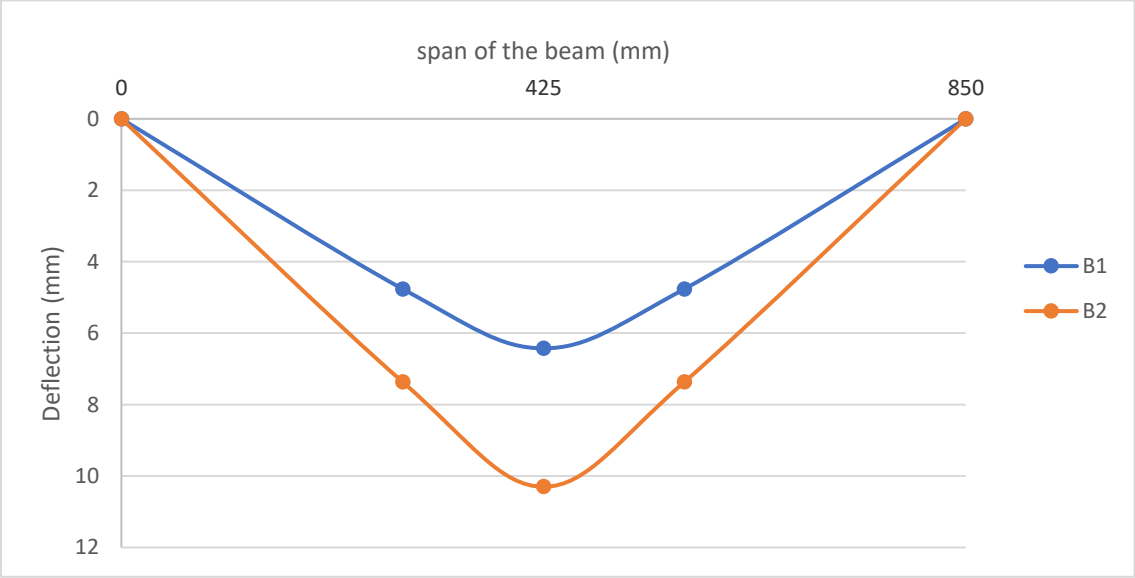

Figure (5-25): Deformed shape for deep beams without openings strengthened with horizontal BFRP strips.

5.7.2 Effect of Strengthening the Deep Beams with Opening Using Basalt Fiber Strips on Deflection Shape Profile.

Figure (5-26) shows the deflected shapes of beams (B1, B3, B4, and B5), It is obvious that the deflections of the deep beams with openings are greater than the deflection in deep beams without openings, especially under the openings. The deflection profile of the deep beam without openings is parabolic in shape. The deep beams strengthened with vertical and horizontal basalt fiber strips give higher deflection than that in deep beams without strengthening. The deflection profile for both deep beams (B3 and B5) is the same parabolic shape while B4 has a sharp shape. Horizontal strength is better in shape of deflection than vertical strength.

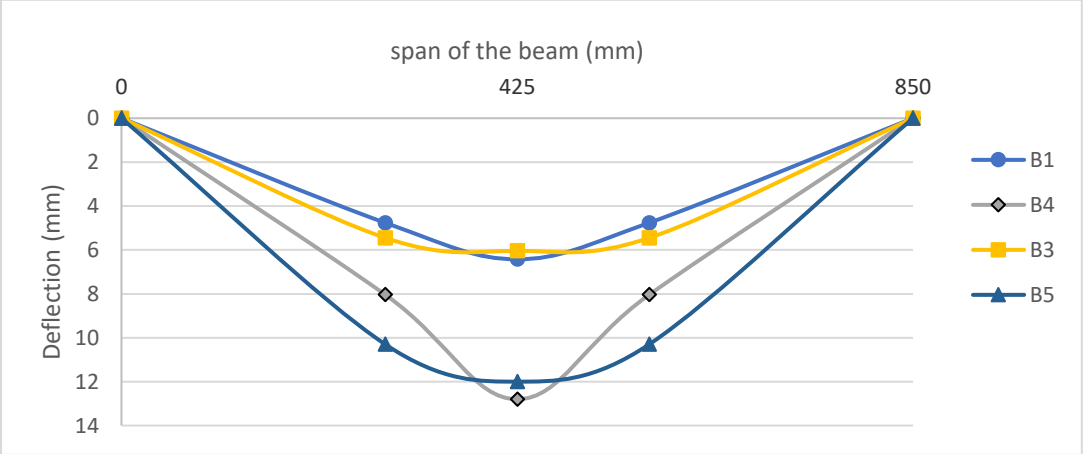

Figure (5-26): Deformed shape for deep beams with vertical rectangular openings strengthened with BFRP strips.

5.7.3 Effect of Opening Shapes Strengthened with Vertical Basalt Fiber Strips on Deflected Shape Profiles.

Figure (5-27) shows the deflected shapes for deep beams with different types of openings strengthened with vertical BFRP strips, from this figure, it is obvious that horizontal rectangular openings have the highest deflection followed by

vertical openings then circular openings finally the least value of deflection at failure is the square openings. but in the horizontal openings, this high measure of deflection is due to the break under the openings of the deep beam at failure not due to the real ductility of that deep beam. In deep beam B6, the deflected shape profile is a line not curve because the value of deflection is not due to areal ductility but it is due to abreak under the openings.

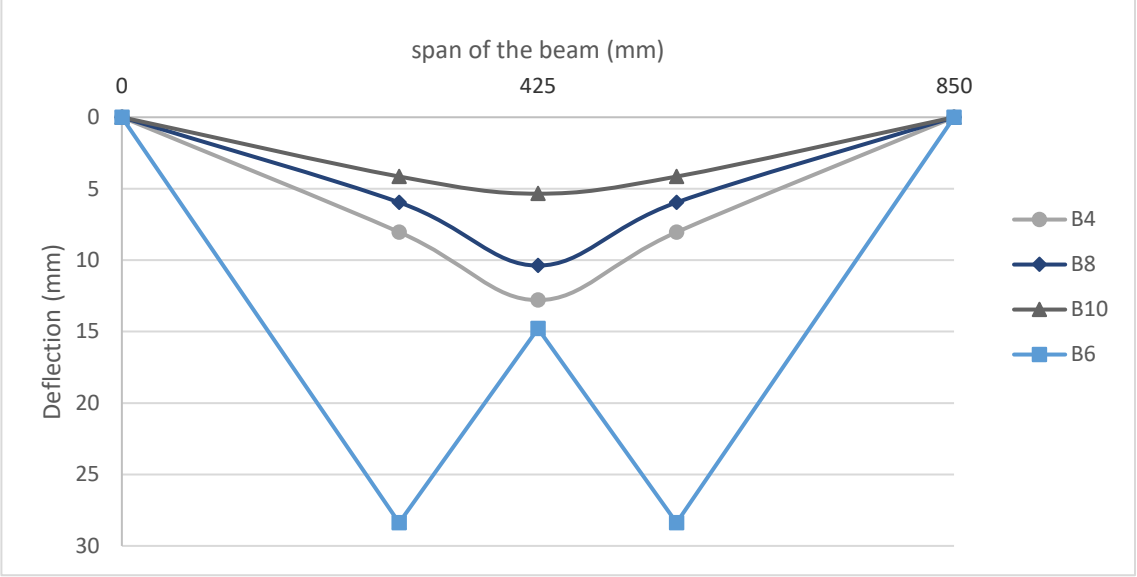

Figure (5-27): Deformed shape for deep beams with different types of openings strengthened with horizontal BFRP strips.

5.7.4 Effect of Opening Shapes Strengthened with Horizontal Basalt Fiber Strips on Deflected Shape Profiles.

Figure (5-28) shows the deflected shapes for deep beams with different types of openings strengthened with horizontal BFRP strips, from this Figure, it is obvious that square openings have the highest deflection followed by circular openings then vertical openings finally the least value of deflection at failure is the horizontal rectangular openings.

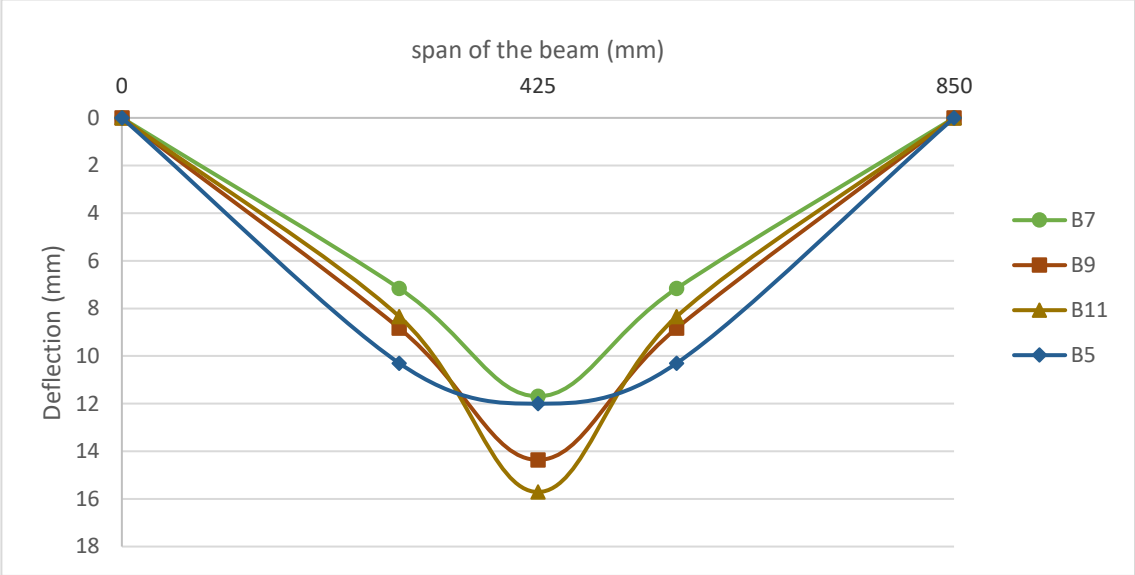

Figure (5-28): Deformed shape for deep beams with different types of openings strengthened with horizontal BFRP strips.

5.7.5 Effect of Strengthening Orientation of Basalt Fiber Strips on Deflected Shape Profiles.

Figures from (5-29) to (5-32) show the deflected shapes for deep beams with different types of openings strengthened with vertical and horizontal BFRP strips, from these Figures, it is obvious that deep beams with rectangular openings, vertical strength has a higher deflection than horizontal strength while in other types of openings, the horizontal strength has a higher deflection than the vertical strength. Deep beams with horizontal strength have a sharp shape while deep beams with vertical strength have semi parabolic shape. In deep beams with vertical rectangular openings, the horizontal strength is better than the vertical one also in deep beams with horizontal rectangular openings, the deflected shape of the horizontal strength is better than in the shape in the case of vertical strength whereas in B6 (deep beam with Vl. Strength), there is a break under the openings. In deep beams with circular openings, the deflection shape is the same in

horizontal and vertical strength but with a higher deflection in horizontal strength while in deep beams with square openings the shape of vertical strength is better than the shape for horizontal strength but with a lower deflection.

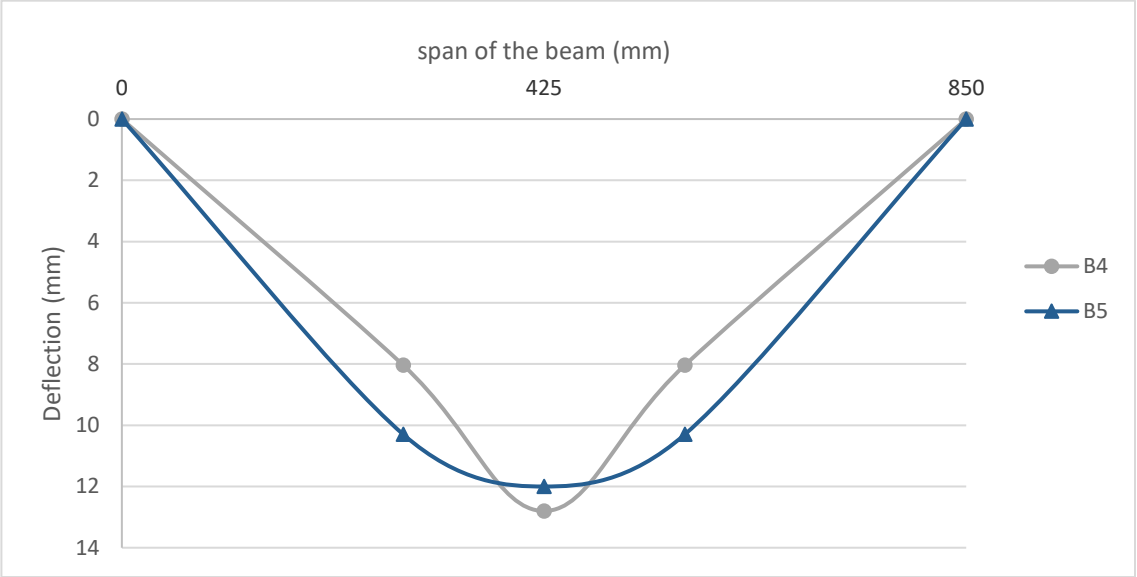

Figure (5-29): Deformed shape for deep beams with vertical rectangular opening

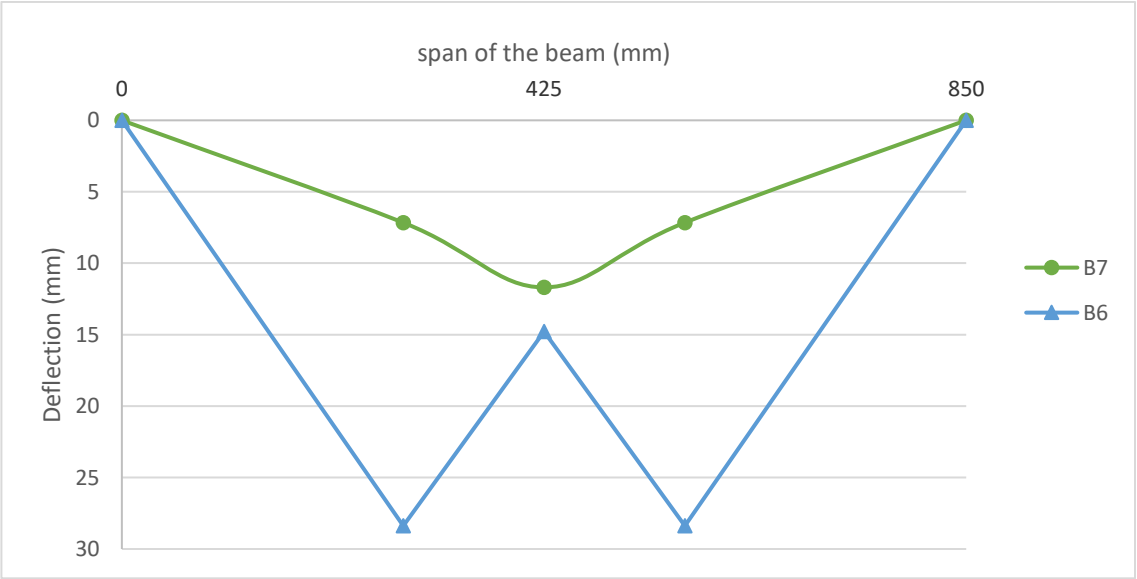

Figure (5-30): Deformed shape for deep beams with horizontal rectangular opening

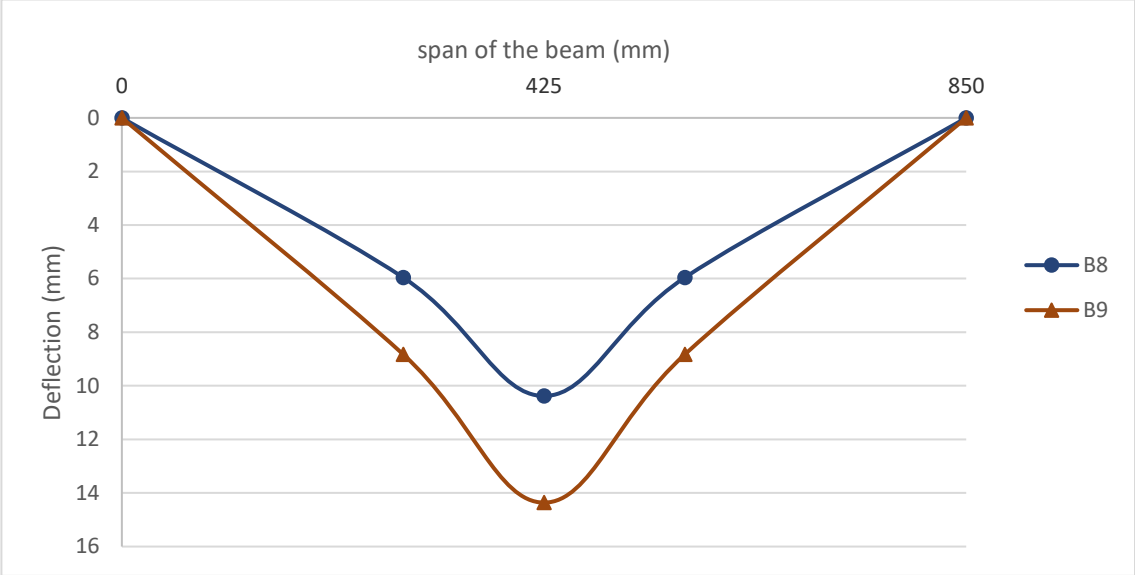

Figure (5-31): Deformed shape for deep beams with circular opening

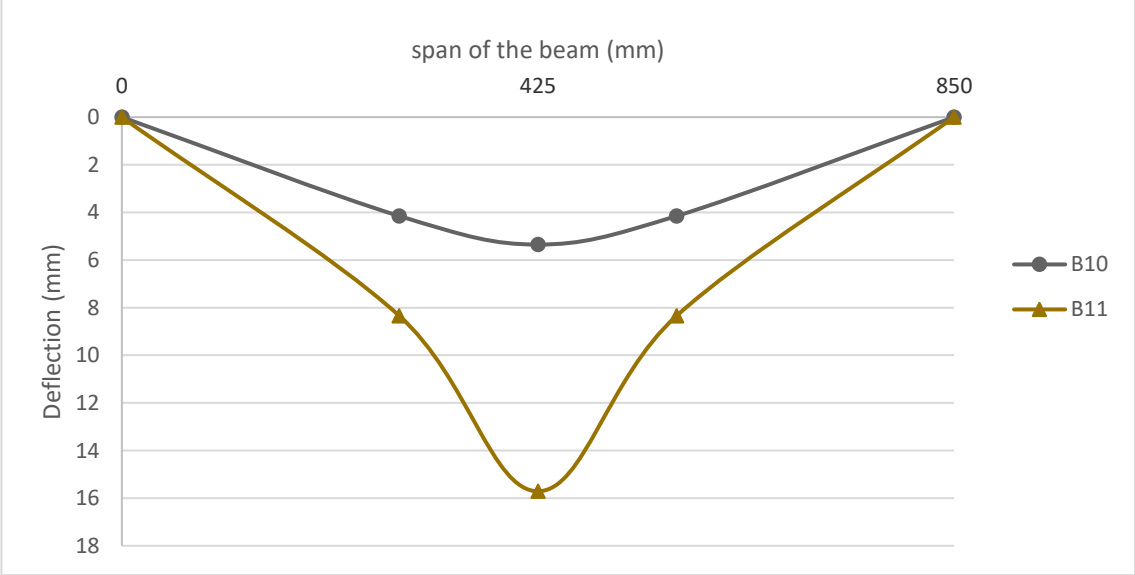

Figure (5-32): Deformed shape for deep beams with square opening

5.8 Reinforcement Strains

The deep beams with and without openings showed a typical load-steel strain relationship, while the beams strengthened with BFRP-strips showed different load strain curves. Table (5-3) shows the values of yield strain for steel bars, and

the percentage of the strain that occurred in the bars according to yield for the different types of openings in deep beams. By studying the values in the Table, it is obvious that deep beams with and without openings don't reach the yield strain at bottom reinforcement except in B8 the main steel reached the yield strain and more. while strain at the opening is more than the strain in the bottom bars and reaches the yield in most of the deep beam specimens which indicates the shear behavior of deep beams. In the deep beam B4, the strain is very low which means that the beam did not work effectively, and the failure was due to weakness in the concrete, also B3 did not reach to yield in steel and the failure occurred due to compression failure in concrete.

5.9 Stiffness of The Deep Beams

The stiffness of the beams can be calculated as the ratio between the force and deflection (F/Δ). Figure (5-33) and Table (5-3) show the values of stiffness of the deep beams tested at the stage of cracking load and the stage of failure load. By studying these values, it is obvious that the beams without openings have a higher stiffness than those in beams with openings, the stiffness increased at the ultimate stage than that in the cracking stage in beams without BFRP strips of about (3 and 7) % for B1 and B3 respectively but in beams strengthen with BFRP strips the stiffness decreased at ultimate stage than that in cracking stage. in non-strengthened beams the stiffness at cracking stage nearly the same at the ultimate stage while in strengthen beams the stiffness at ultimate stage bigger than it in cracking stage except for beam with horizontal rectangular opening the stiffness are the same in the two-stage, generally the BFRP increase the stiffness at the cracking stage. The horizontal strength of deep beams without openings reduces the stiffness by 16% at the maximum strength. While the horizontal strength of

deep beams with openings increased the stiffness by 25,39,28 % for vertical rectangular openings, horizontal rectangular and circular openings respectively but in deep beams with square openings, the stiffness decreased by 13%. Vertical strength decreases the stiffness by 5,17,8% in the case of deep beams with vertical, horizontal and square openings respectively whereas the stiffness increased by 56 % in case of deep beam with circular openings.

Table (5-3) : The strains, and stiffness values of all beams.

Beam No.	$(\varepsilon_u/\varepsilon_y)$ %		Stiffness at cracking (kN.mm)	Stiffness at ultimate (kN.mm)
	At opening	At middle		
B1	139.75	51.22	175.32	180.72
B2	118.83	30.83	204.12	151.49
B3	96	28.38	67.42	72.14
B4	25.25	21	72.66	68.45
B5	110	42	100	90.80
B6	181.5	32.5	53.43	59.98
B7	182.5	89.44	100.52	100.17
B8	121	125.2	118.30	112.94
B9	144.75	14.77	110.71	92.15
B10	112	22	64.34	66.10
B11	153	24	65	62.52

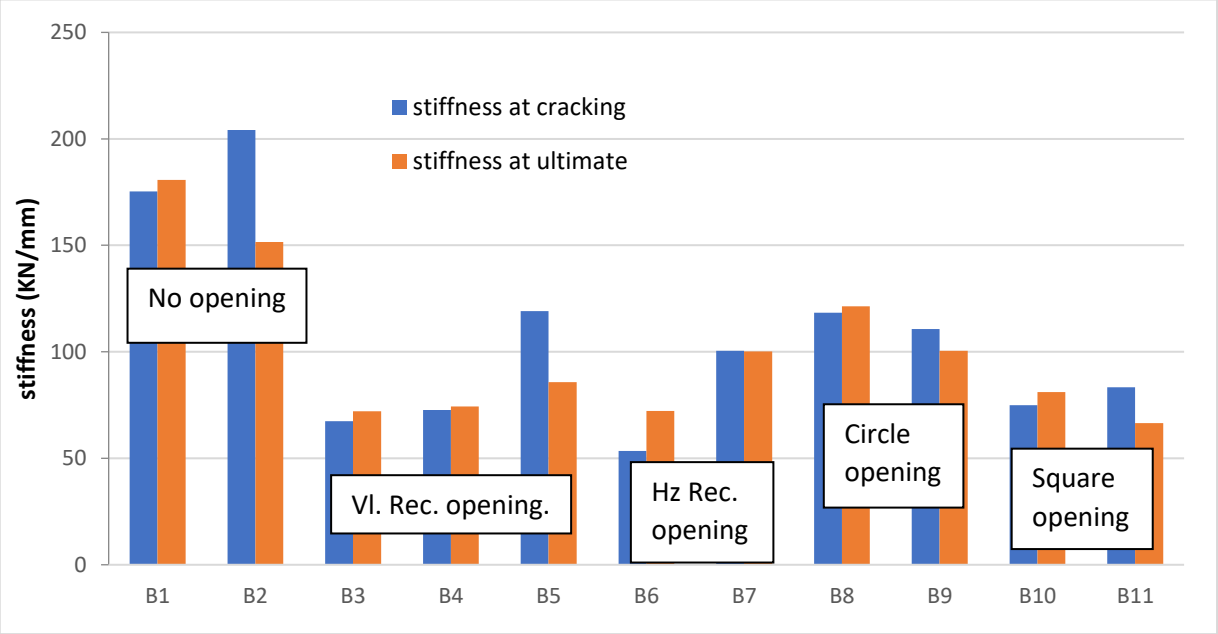

Figure (5-33): Stiffness at cracking and stiffness at failure load for all specimens

CHAPTER SIX
FINITE ELEMENT ANALYSIS

6.1 Introduction

This chapter presents a simulation of the deep beam specimens illustrated in previous chapters using finite element analysis by ANSYS 19 R2**[72]**, and discusses the data obtained from FEA (ANSYS 19.0), The test results were compared with the predicted failure load obtained from the American Code **ACI 318-08 [2]**. Moreover, a numerical analysis was carried out using a nonlinear finite element program (ANSYS19.0) to discover all the factors in this study. The analysis and data output of the ANSYS19.0 are compared with the experimental samples, and the result of the comparison of experimental data and the ANSYS19 data is presented, also, new parameters were added using ANSYS and the results are compared with the equations illustrated later in this chapter.

6.2 Finite Element Analysis

6.2.1 General

The finite element method (FEM) is a process, in which finite degrees of freedom are approximated to be an assemblage of elements each with a specified number of unknowns. In recent years, the use of finite element analysis has increased due to progressing knowledge and capabilities of computer software and hardware. It has now become the choice method to analyze concrete structural components. The use of computer software to model these elements is much faster and extremely cost-effective. A finite element model was developed to simulate all beams in this study, from linear through nonlinear response and up to failure, using the software package

ANSYS19.0 R2. Comparisons were done for the load-deflection relationship at the mid-span of the beam, failure loads, reinforcement steel strain, and crack patterns at failure. Modeling simplifications and assumptions developed during this research are presented below.

6.2.2 Modeling Assumptions

The following are the modeling assumptions made for the deep beam models in the present study to provide reasonably good simulations for the behavior:

1. Concrete and steel are modeled as isotropic and homogeneous materials.
2. Poisson's ratio is assumed constant throughout the loading history.
3. Steel is assumed to be an elastic-perfectly plastic material and identical in tension and compression.
4. A perfect bond exists between concrete and steel reinforcement.
5. The BFRP material is assumed to be especially orthotropic-transversely isotropic. That is, the material properties in the two directions that are both perpendicular to the fiber direction are identical.
6. The BFRP fabric is assumed to carry stress along its axis only.
7. Time-dependent nonlinearities such as creep, shrinkage, and temperature change are not included in this study.

6.2.3 Selection of Element Type Using Ansys

In this section, the description of element types used for all materials used in Ansys models is presented. These materials are concrete, steel reinforcement, loading and supporting plates, and carbon fiber reinforced polymer (BFRP). Elements used in thesis models are widely used and recommended by ANSYS and previous researchers, **Jaya Jothi et al[73-79]**

6.2.3.1 Concrete

An eight-node solid element, Solid65, was used to model the concrete. The solid element has eight nodes with three degrees of freedom at each node: translations in the nodal local x, y, and z directions. The element is capable of plastic deformation, cracking in three orthogonal directions, and crushing.

The geometry and node locations for this element type are shown in Figure (6-1), [ANSYS 2019-R2]

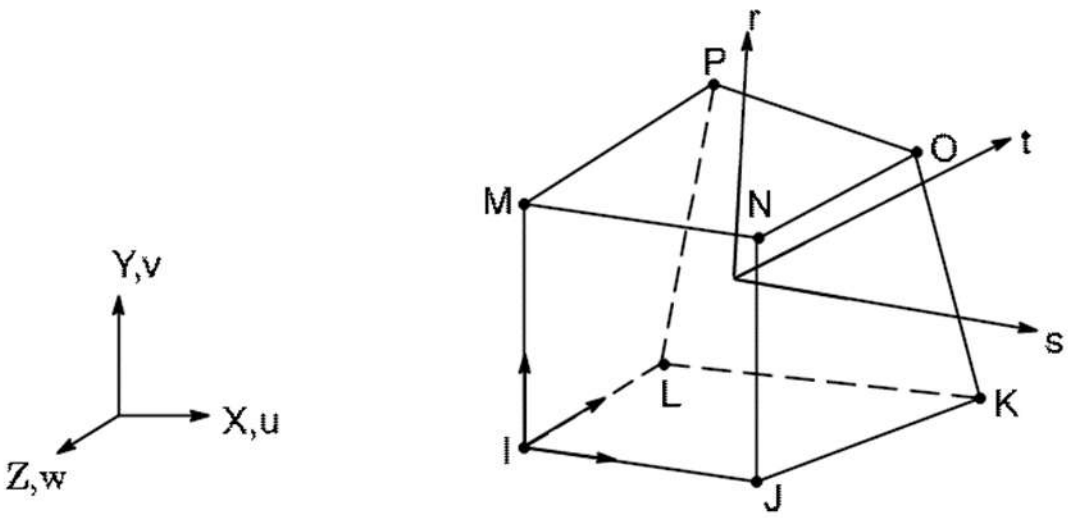

Figure (6-1): SOLID 65: 3-D reinforced concrete solid (ANSYS 19.0)

6.2.3.2 Steel Reinforcement

A Link180 element was used to model steel reinforcement. The element is a uniaxial tension-compression element with three degrees of freedom at each node: translations in the nodal x, y, and z directions. Plasticity, creep, rotation, large deflection, and large strain capabilities are included. This element is shown in Figure (6-2), [ANSYS, 2019].

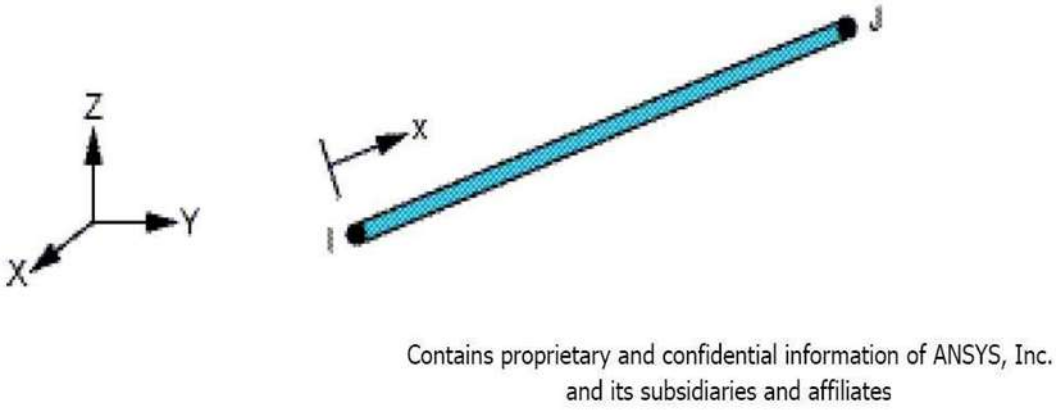

Figure (6-2): Link180: 3-D spar (Ansys 19.0)

6.2.3.3 Steel Plates Element

An eight-node solid element, SOLID45, used for steel plates.Steel plates added at loading and supports locations, in the finite element models, to provide a more even stress distribution over the loading areas and prevent locale failure of concrete at these locations. The element defined with eight nodes having three degrees of freedom at each node, translations in the nodal x, y, and z directions. The geometry and nodes locations for this element type shown in Figure (6-3).

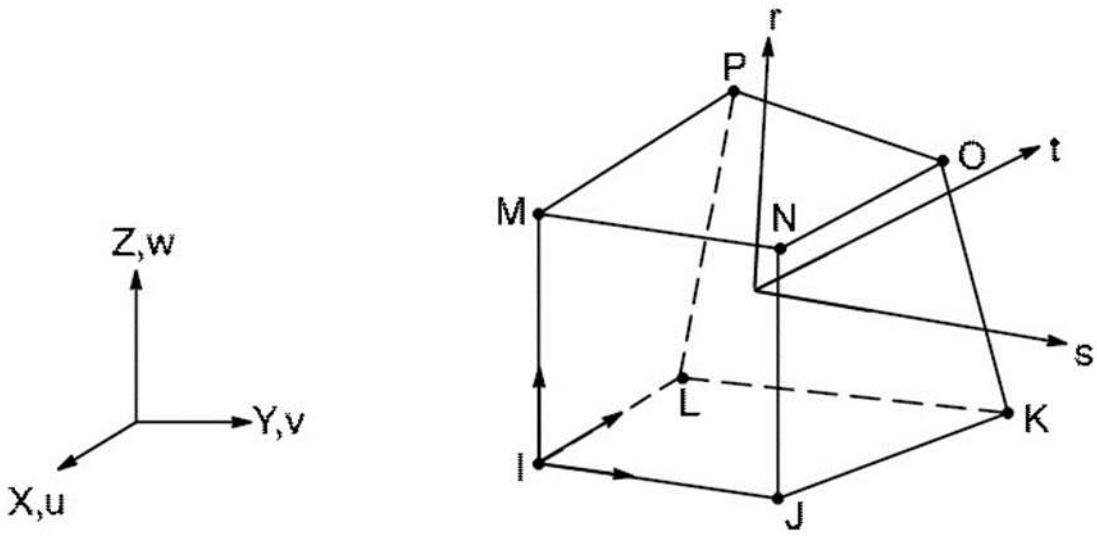

Figure (6-3) SOLID45: 3-D solid (ANSYS19.0)

6.2.3.4 Basalt Fiber Reinforced Polymer (BFRP)

In this section, we simulate the strips using two elements, solid 186 The Solid186 element is used for the modeling of basalt fibers as avolume. This element is defined by eight nodes having three degrees of freedom at each node as shown in Figure (6-4): translations in the nodal x, y, and z directions. The element is capable of plasticity, hyper elasticity, stress stiffening, creep, large deflection, and large strain capabilities.solid186 is available in two forms: Homogeneous Structural Solid (default); and Layered Structural Solid. And then epoxy is simulated as a volume with solid65 as a material.

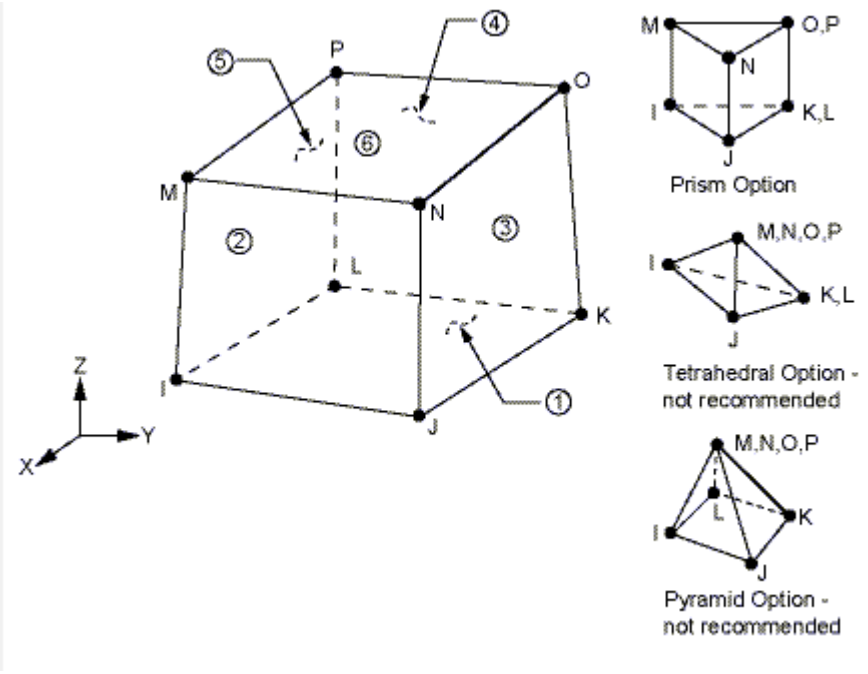

Figure (6-4): Solid 186 3-D solid (ANSYS19.0)

6.2.4 Materials properties

6.2.4.1 Concrete

Development of a model for the behavior of concrete is a challenging task. Concrete is a quasi-brittle material and has different behavior in compression and tension. The tensile strength of concrete is typically 8-15% of the compressive strength, **Shah, et al. [80].** In compression, the stress-strain curve for concrete is linearly elastic up to about 30 percent of the maximum compressive strength. Above this point, the stress increases gradually up to the maximum compressive strength. After it reaches the maximum compressive strength σcu, the curve descends into a softening region, and eventually crushing failure occurs at an ultimate strain ε cu. In tension, the stress-strain curve for concrete is approximately linearly elastic up to the maximum tensile strength. After this point, the concrete cracks and the strength decreases gradually to zero, **Bangash [81].** Figure (6-5) shows atypical stress-strain curve for normal weight concrete, **Bangash [81]**.

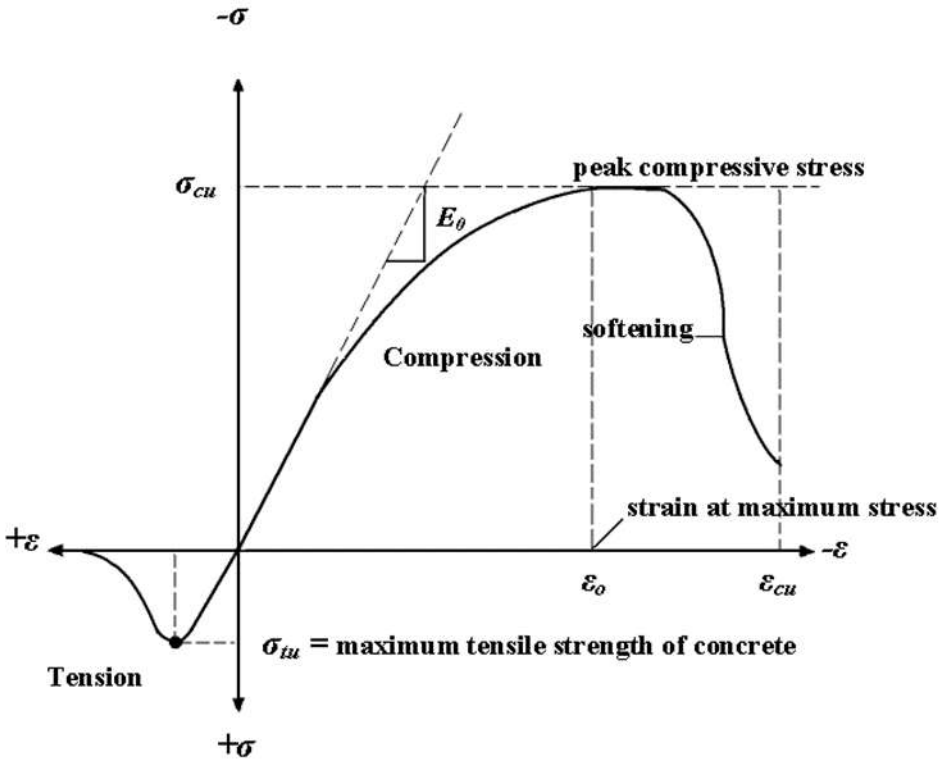

Figure (6-5): A typical stress-strain curve for normal-weight concrete **Bangash [81].**

To model the concrete, ANSYS requires the following input data:

- Elastic modulus (E_c).
- Ultimate uniaxial compressive strength (σ_{cu}).
- Ultimate uniaxial tensile strength (σ_{tu}).
- Poisson's ratio (υ).
- Shear transfer coefficient (β_t) for open and closed cracks.
- Compressive uniaxial stress-strain relationship for concrete

In this study, the ultimate cubic compressive strength of the concrete (*fcu*) was 25.0MPa. According to the Egyptian Code of Practice (ECP 203-2007) the corresponding elastic modulus $Ec = 4400\sqrt{fcu}$ =22000.0 MPa. Moreover, the tensile strength *fctr* =0. $6\sqrt{fcu}$ = 3 MPa. Poisson's ratio for concrete equals 0.2. The shear transfer coefficient, βt, represents the conditions of the crack face. The value of βt ranges from 0.0 to 1.0, with 0.0 representing a smooth crack. (complete loss of shear transfer) and 1.0

representing a rough crack (no loss of shear transfer) (ANSYS 19.0).

The value of βt for open cracks used in many studies of reinforced concrete structures varied between 0.05 and 0.25, **Bangash [81].** The shear transfer coefficient used in this study was equal to 0.3 for open cracks and 0.9 for closed cracks. Equation (6.1) presents the uniaxial compressive stress-strain relationship for concrete. This equation is used to plot the multi-linear isotropic stress-strain curve for the concrete until ultimate compressive strength.

$$\sigma = \frac{Ec \,.\, \varepsilon}{1+\left(\frac{\epsilon}{\epsilon 0}\right)2} \qquad (6.1)$$

Where; σ = stress at any strain ε

εo = strain at the ultimate compressive strength =*2fcu/Ec=0.0025*

Five points are used to represent the stress-strain curve using the Equation (6.1) starting from the elastic stress limit (0.3 *fcu*) up to the ultimate stress limit (*fcu*=30MPa). However, the ideal stress-strain curve softened after reaching the ultimate strength; this portion is not used in the finite element material model, as the negative slope portion will lead to convergence problems. In this study, the negative slope was ignored and a last point corresponds to ultimate strain equal to 0.003 at peak stress *fcu*= 30MPa where an assumption was made of perfectly plastic behavior after reaching maximum stress. The resulting multilinear isotropic stress-strain curve for the concrete used in this study is shown in Figure (6-6)

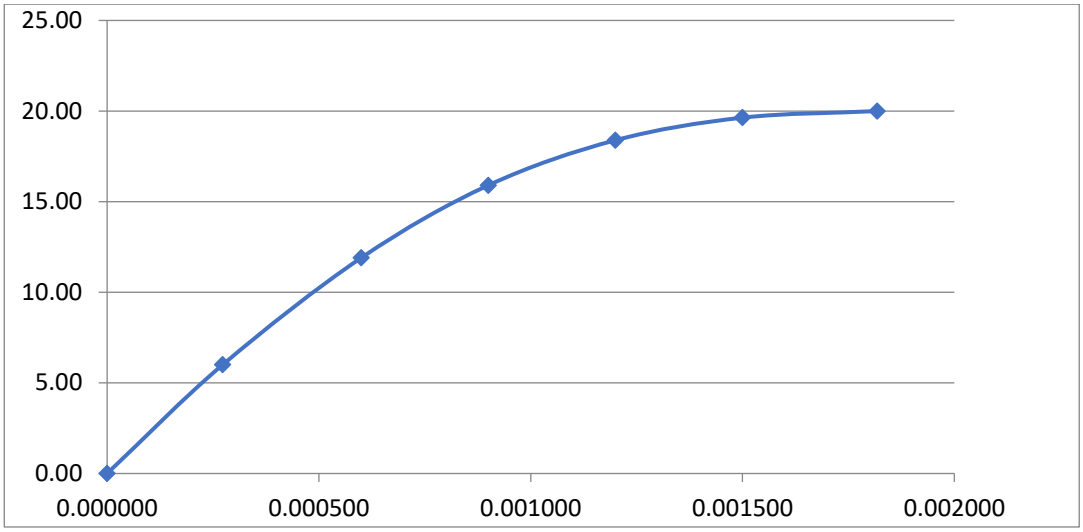

Figure (6-6): Stress strain curve used to model the concrete.

Failure Criteria for Concrete

The model is capable of predicting failure for concrete materials. Both cracking and crushing failure modes accounted for. The two input strength parameters, ultimate uniaxial tensile and compressive strengths, needed to define a failure surface for the concrete. Consequently, a criterion for failure of the concrete due to a multiaxial stress state can be calculated (William and Warnke 1975).A three-dimensional failure surface for concrete shown in Figure(6-7). The most significant nonzero principal stresses are in x and y directions, represented by σ_{xp} and σ_{yp} respectively. Three failure surfaces shown as projections on the σ_{xp}-σ_{yp} plane. The mode of failure is a function of the sign of σ_{zp} (principal stress in z direction). For example, if σ_{xp} and σ_{yp} are both negative (compressive) and σ_{zp} is slightly positive (tensile), cracking would be predicted in a direction perpendicular to σ_{zp}. However, if σ_{zp} is zero or slightly negative, the material is assumed to crush (ANSYS 19.0).

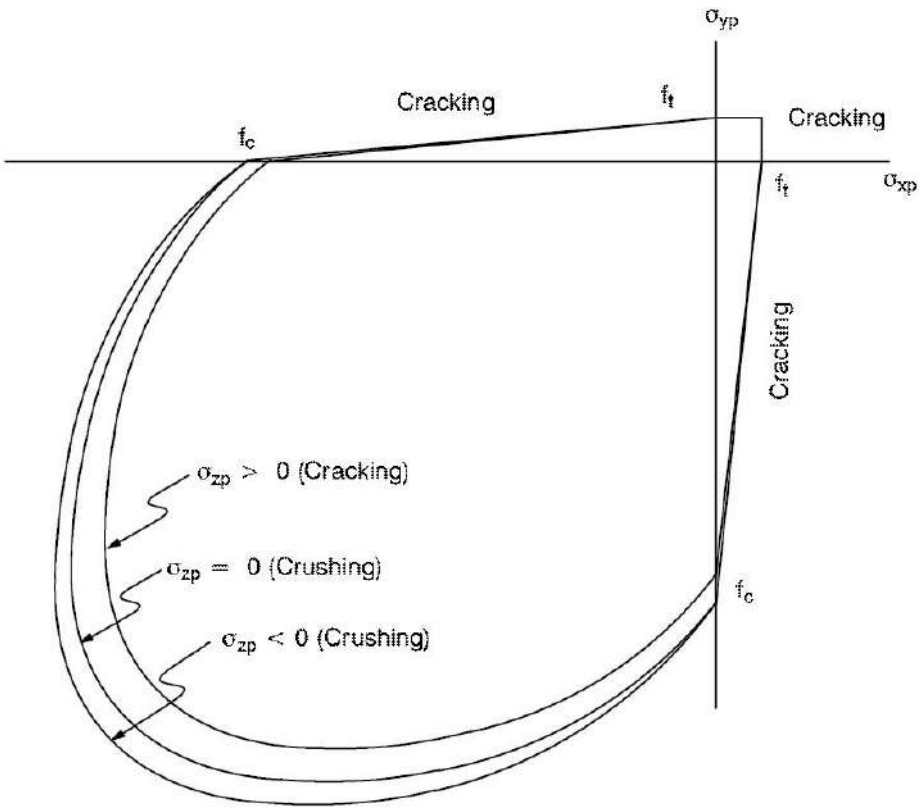

Figure (6-7): 3-D failure surface for concrete (ANSYS 19.0)

6.2.4.2 Reinforcement and Steel Plates

The test specimens was constructed with the high strength steel (grade 52). Properties of the steel reinforcement used in this FEM study follow the design material properties used for the experimental investigation. The finite element model for rebar was assumed to be a bilinear isotropic elastic-perfectly plastic material and identical in tension and compression as shown in Figure(6-8). Material properties for the steel reinforcement for all specimens in this study are as follows:

Elastic modulus (E_s) = 200,000 MPa, Poisson's ratio (ν) = 0.3 Yield stress (f_y) = 360 MPa, Elastic tangent modulus = 0.0.The steel plates, added to the finite element model, were assumed linear elastic materials with elastic modulus equal to 200,000 MPa, and Poisson's ratio of 0.3.for the shear reinforcement tow values of yield stress will used the first is the same as above((f_y) = 360 MPa) and the second with (f_y) = 240 MPa

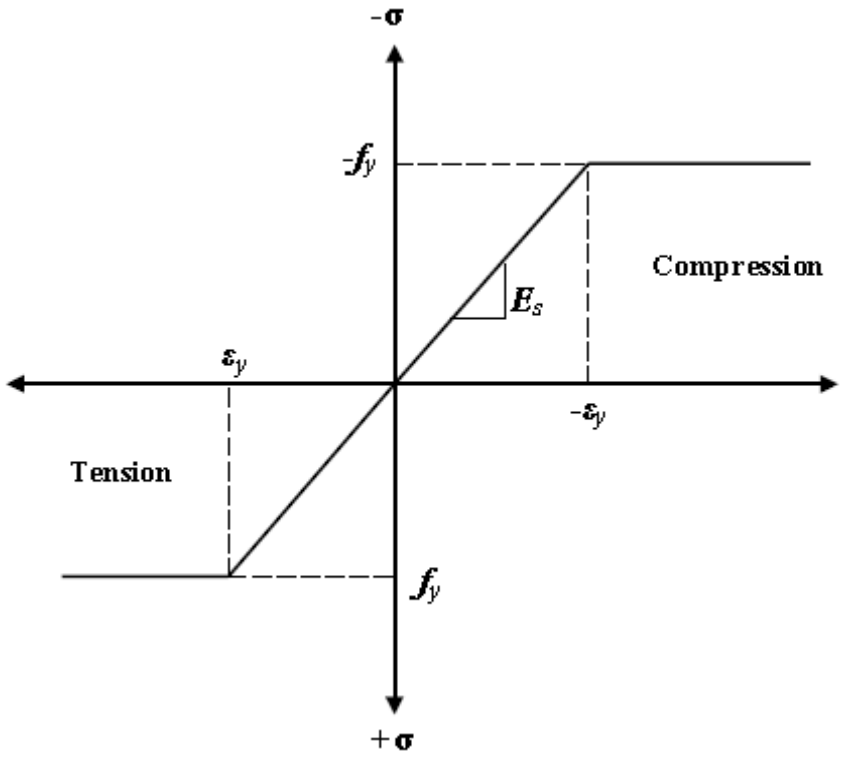

Figure (6-8) Stress-strain curve for steel reinforcement

6.2.4.3 Basalt Fiber Strips and Resin Properties

The used resin is epoxy (Sikadur 330) had a tensile strength of 25 N/mm2 and an ultimate elongation of 1.5%. the layer of epoxy is assumed to have a thickness of 0.3mm. According to the results of testing the basalt fiber strips, the sheet has a typical thickness of 0.4mm, an average tensile strength of 894MPa, an elastic modulus of 50.5GPa, and with maximum elongation of 1.33%. The cured BFRP composite sheet was treated as an elastic orthotropic material up to failure to simulate its natural behavior. The elastic orthotropic material properties used are [Ex = 50.5GPa, Ey,z= 3.8 GPa, νxy,xz = 0.4, νyz = 0.3, Gxy,xz= 18GPa, and Gyz =19.4GPa

6.2.5 The Loading System , and Meshing

To ensure that the model acts in the same way as the experimental specimen, boundary conditions needed to apply where the supports and loads exist. The supports modeled as a fixed support. The nodes on the support plates given constraints in all degrees of freedom, applied as constant values of zero. The force, applied at the loading steel plate, applied across all nodes of the loading plate. The force applied at each node on the plate is 1/8 of the applied force. Figure (6-9) shows the loading and boundary conditions of the specimen. The specimen consists of a beams with constant width 150 mm, total height 500 mm with a total length 1000mm, and variable types of opening After construction of model with volumes, areas, lines, a finite element analysis requires meshing of the model. The model then divided into a number of small elements, and after loading, stresses and strains calculated at integration points of these small elements , **Chapelle, D., & Bathe, K. J.[82]**

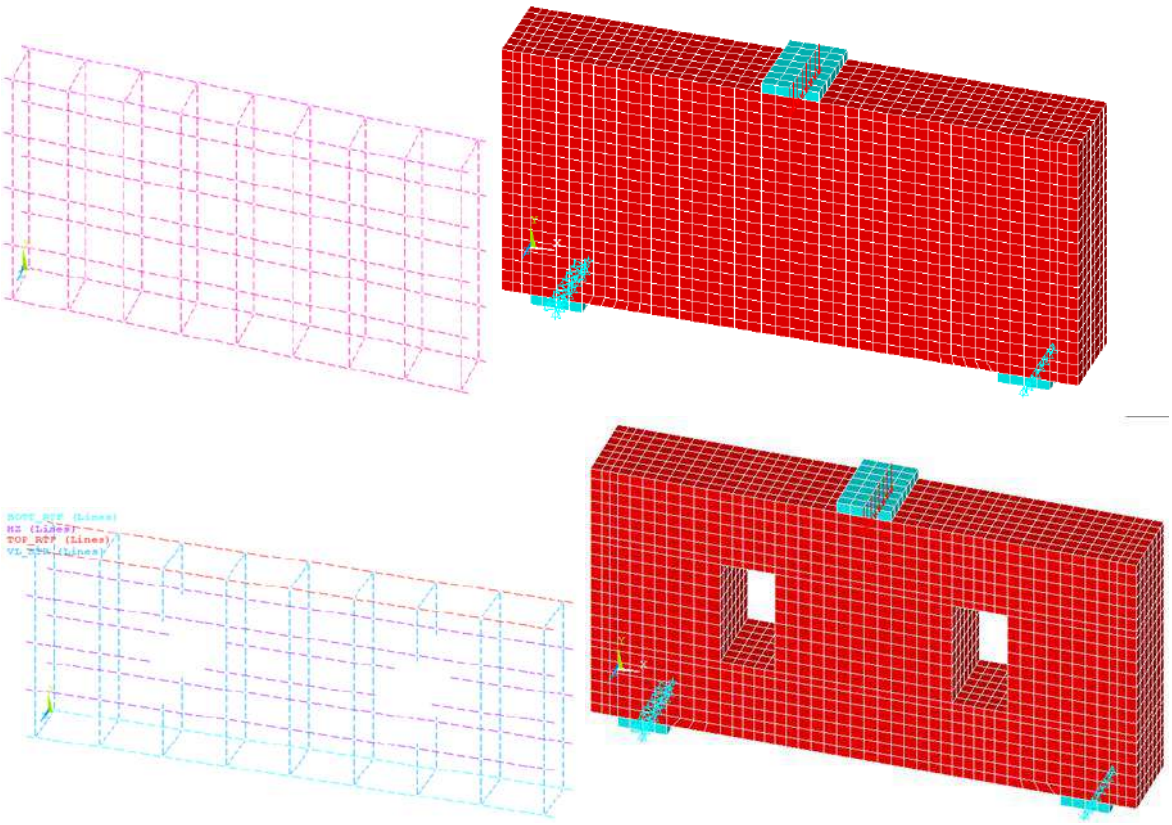

Figure (6-9): The loading system, and meshing, for specimens in ANSYS

6.3 Verification of Results Using Finite Element

6.3.1 Comparison of The Experimental nd Finite Element Results

The goal of the comparison of the FE model and the experimental results is to verify the FE model (ANSYS 19.0) results. In addition to ensure that, the elements, material properties and convergence criteria are adequate to model all beams in this study in accordance to the following comparisons:

1) Cracks pattern as shown in figures(6-10) to (6-20)
2) Load-deflection relationship
3) Failure load

Another results from ANSYS are:stress in concrete , maximum stress, and strain in BFRP strips and stress and strain in steel at failure

6.3.1.1 Crack Patterns for Beams

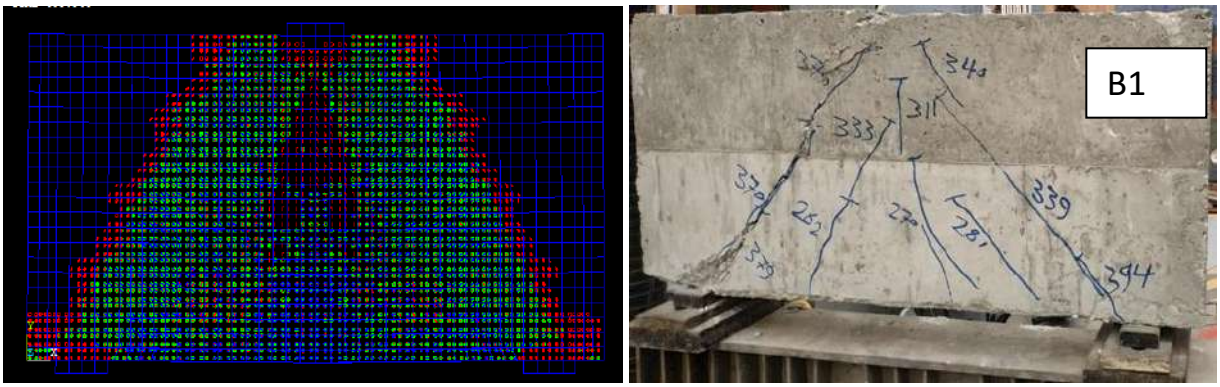

Figure (6-10): Comparison of cracks from ANSYS and test for B1

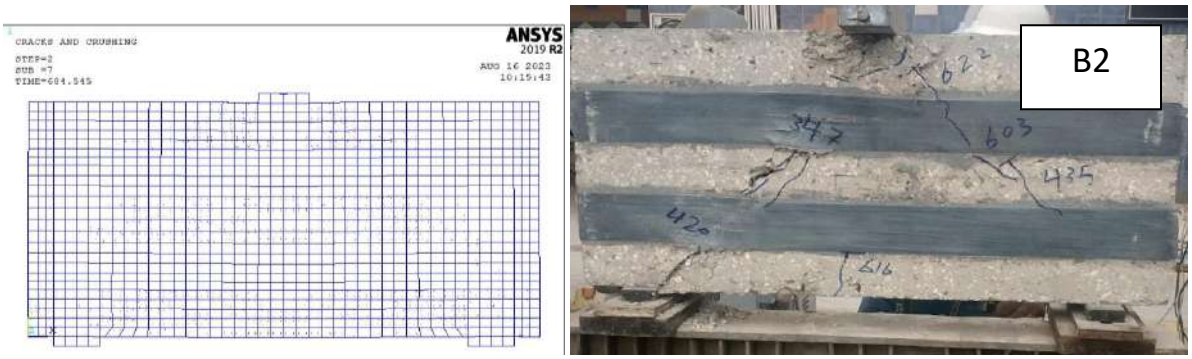

Figure (6-11): Comparison of cracks from ANSYS and test for B2

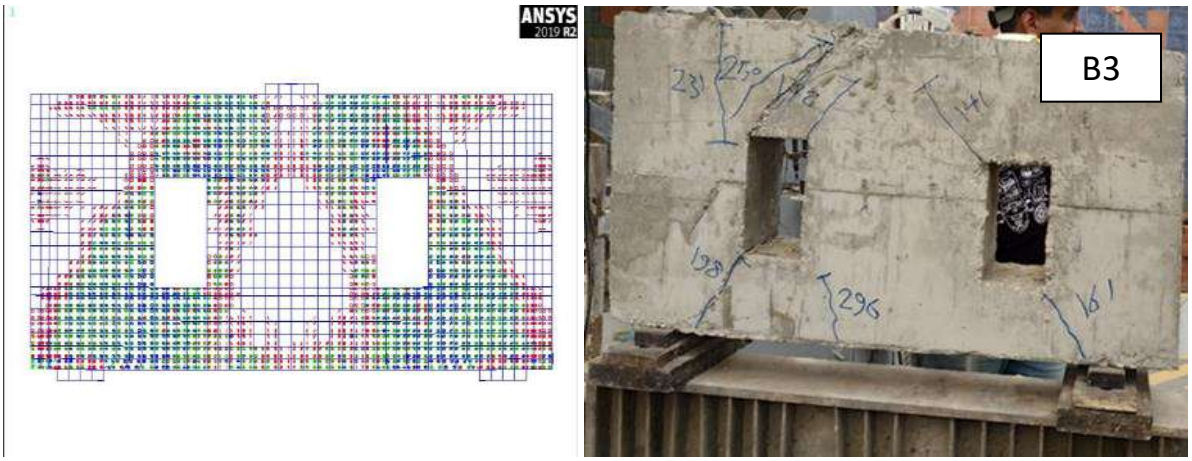

Figure (6-12): Comparison of cracks from ANSYS and test for B3

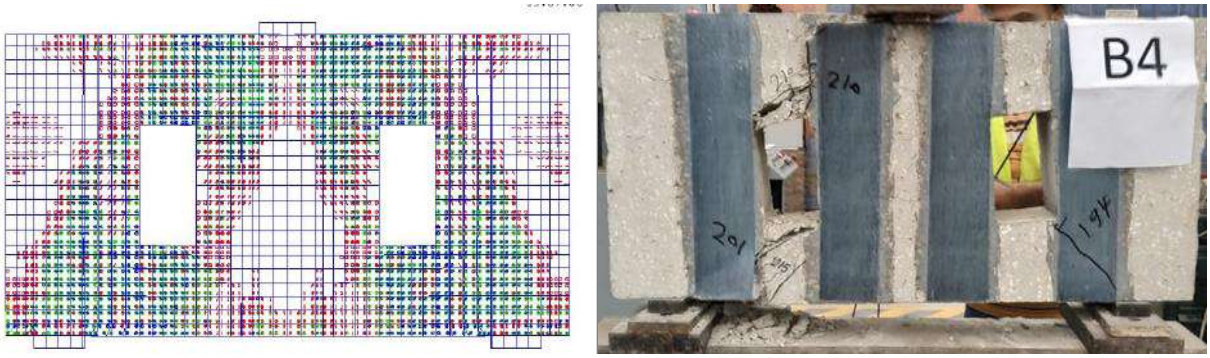

Figure (6-13): Comparison of cracks from ANSYS and test for B4

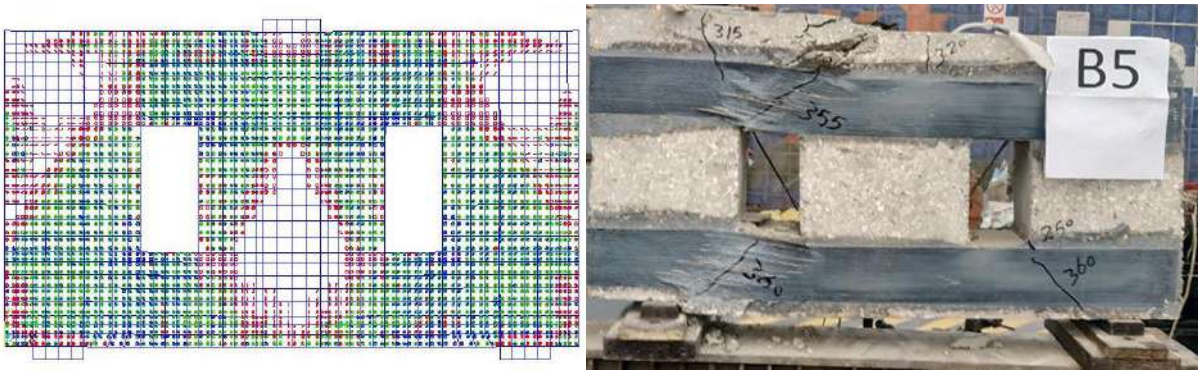

Figure (6-14): Comparison of cracks from ANSYS and test for B5

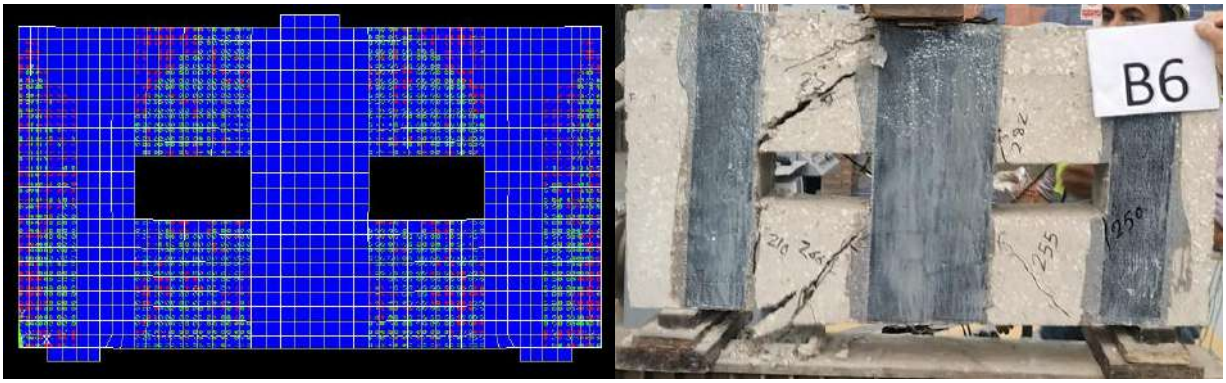

Figure (6-15): Comparison of cracks from ANSYS and test for B6

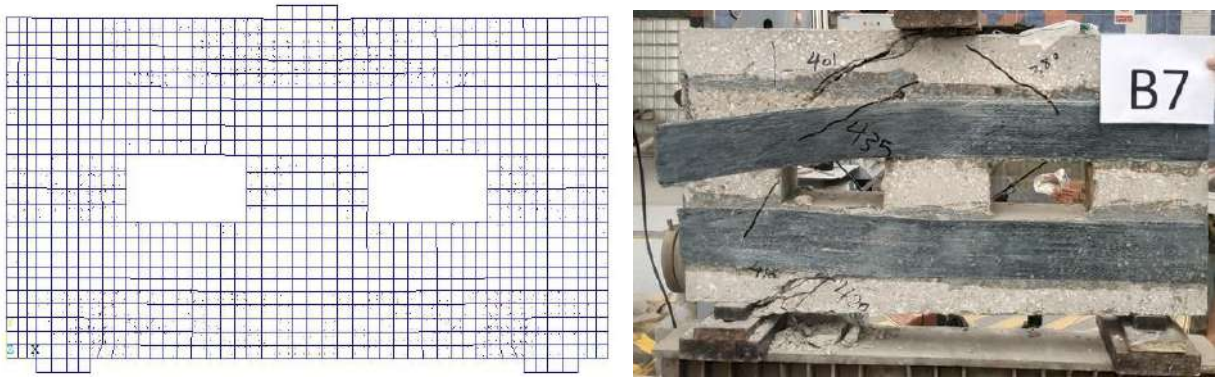

Figure (6-16): Comparison of cracks from ANSYS and test for B7

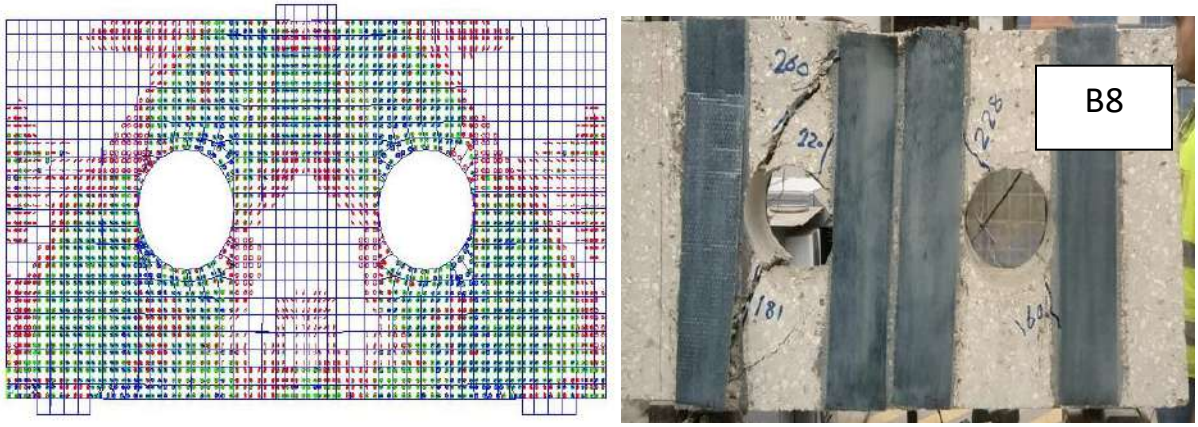

Figure (6-17): Comparison of cracks from ANSYS and test for B8

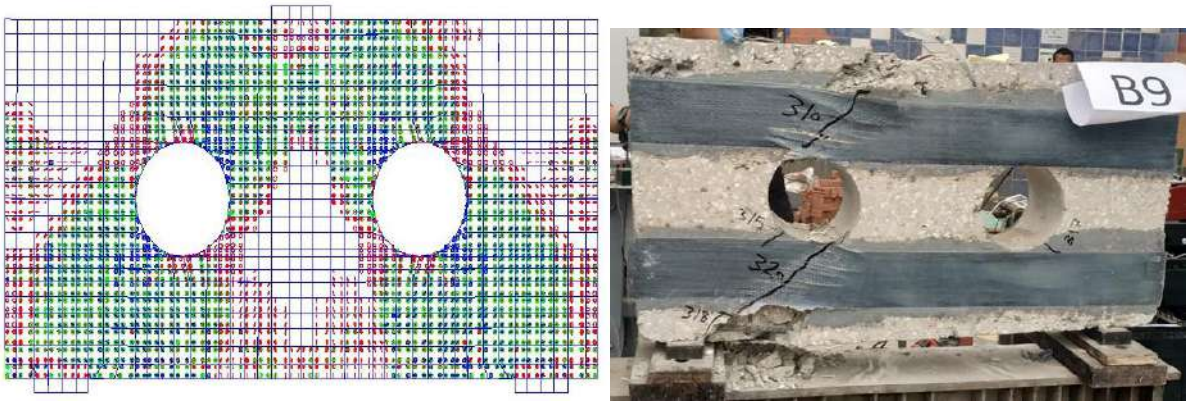

Figure (6-18): Comparison of cracks from ANSYS and test for B9

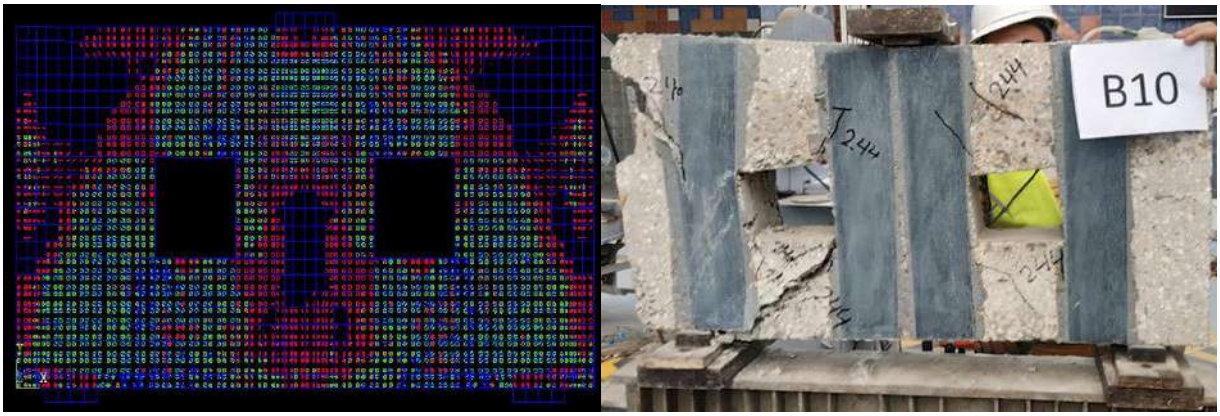

Figure (6-19): Comparison of cracks from ANSYS and test for B10

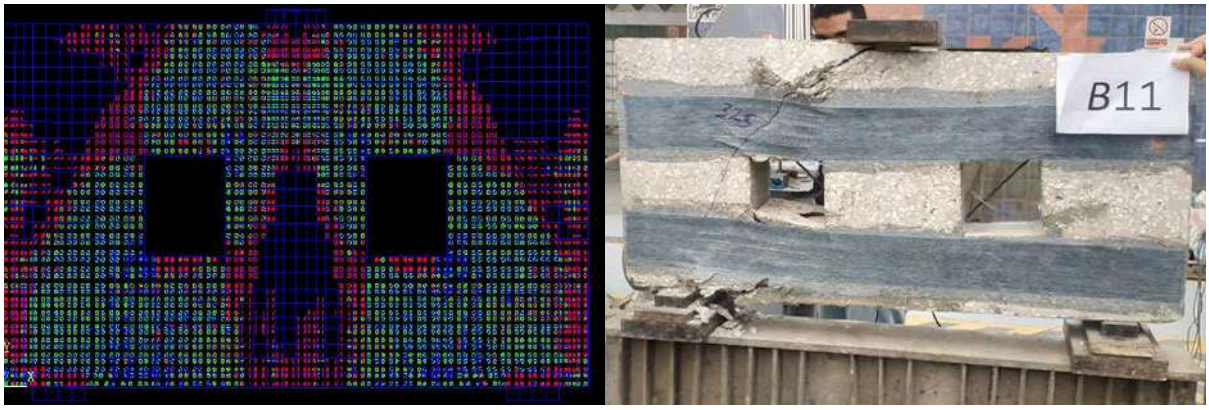

Figure (6-20): Comparison of cracks from ANSYS and test for B11

6.3.1.2 Load Deflection Relationship

The deflection versus load sup-steps, calculated using FEA, shown in contour lines. The contour lines for all the specimens have the same shape but differ in the value.. The maximum deflection recorded at the end of every load increment, and then it plotted upon the experimental load-deflection relationship. The full non-linear load-deflection curves for all experimental specimens shown in Figure(6-21)through Figure (6-31) and the full data explained in Table (6-1).

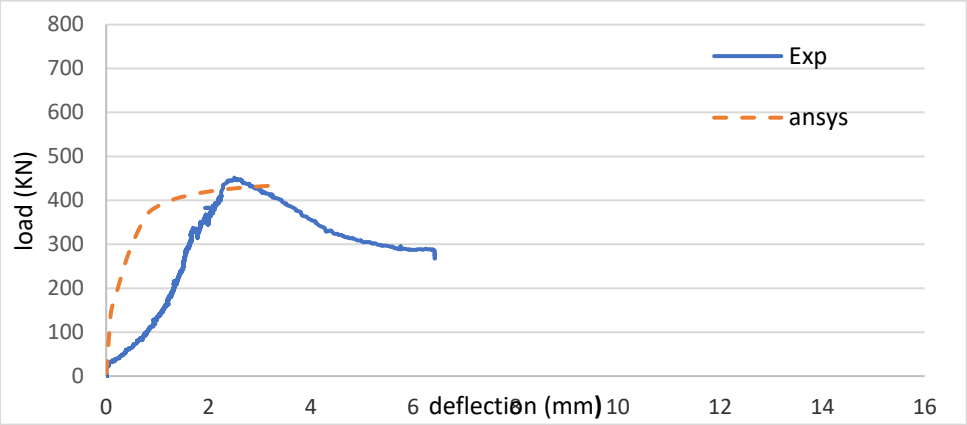

Figure (6-21): Comparison of load -deflection curves from Ansys and experimental for B1

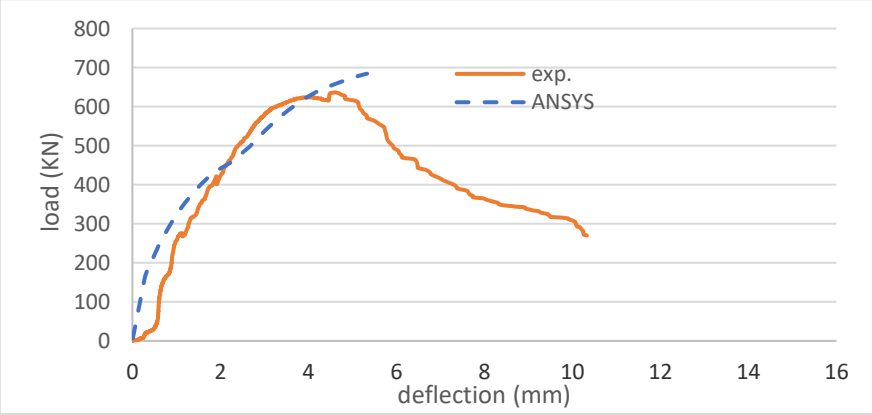

Figure (6-22): Comparison of load -deflection curves from Ansys and experimental for B2

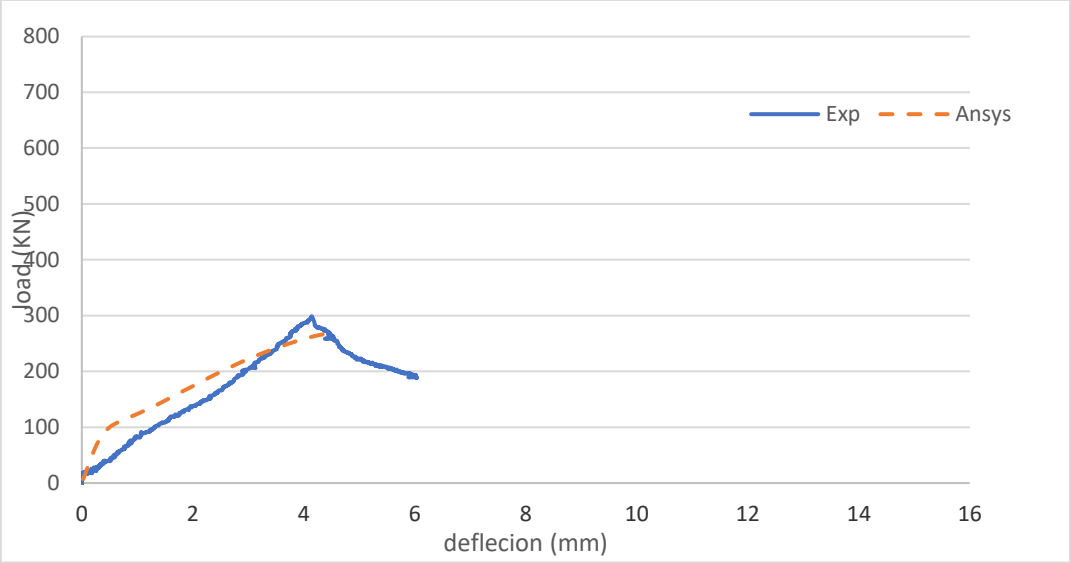

Figure (6-23): Comparison of load -deflection curves from Ansys and experimental for B3

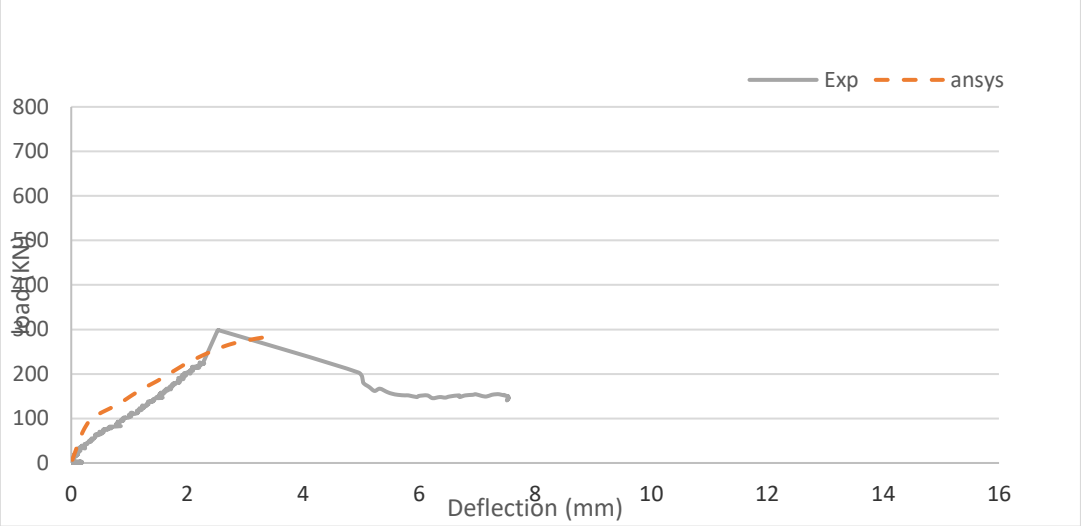

Figure (6-24): Comparison of load -deflection curves from Ansys and experimental for B4

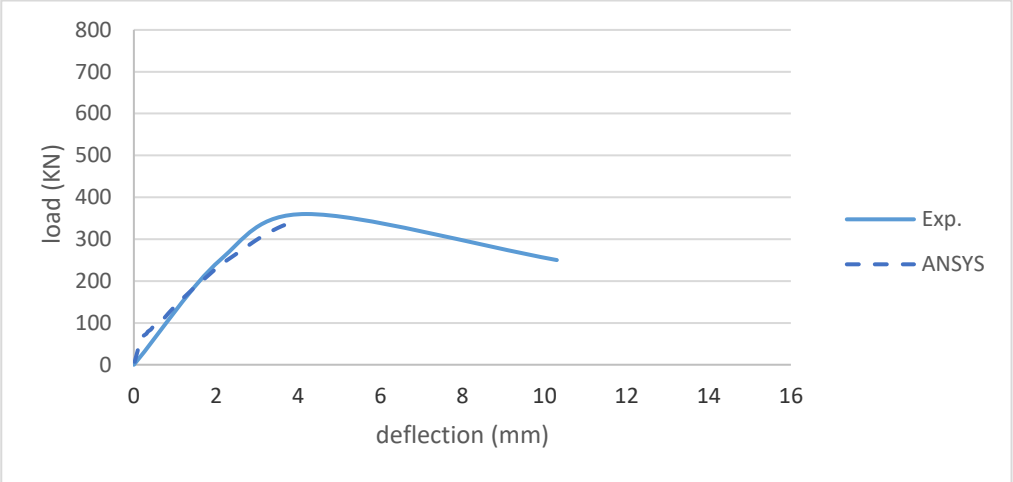

Figure (6-25): Comparison of load -deflection curves from nsys and experimental for B5

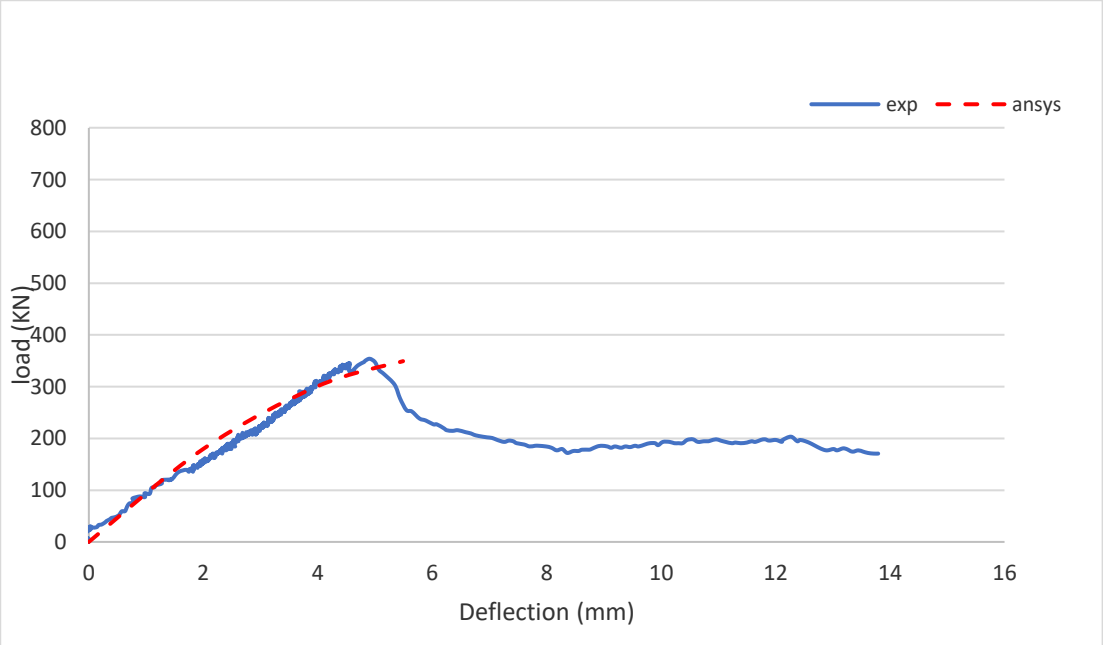

Figure (6-26): Comparison of load -deflection curves from Ansys and experimental for B6

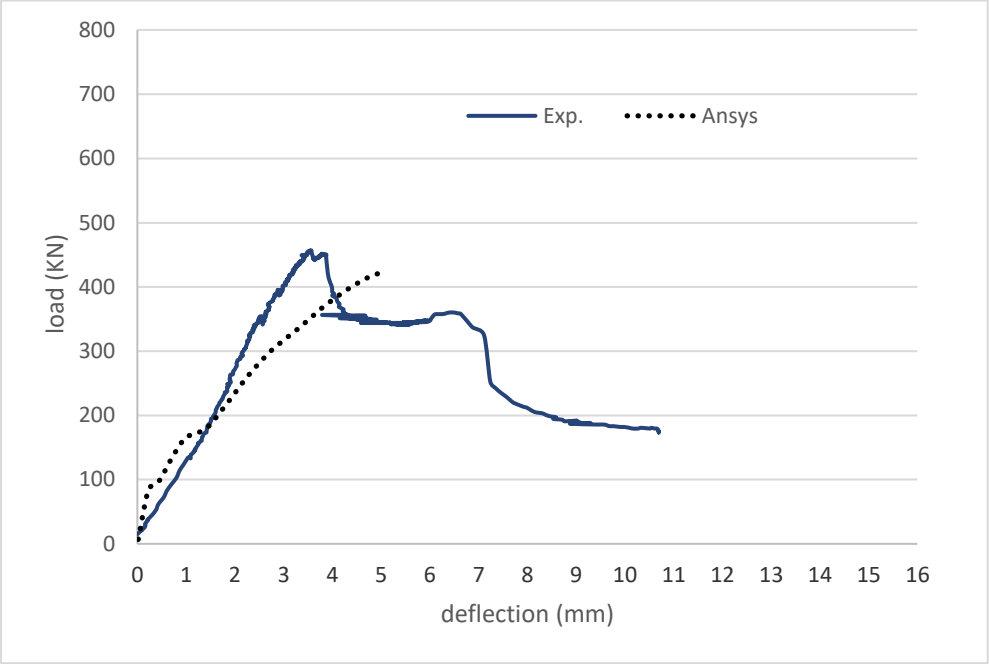

Figure (6-27): Comparison of load -deflection curves from Ansys and experimental B7

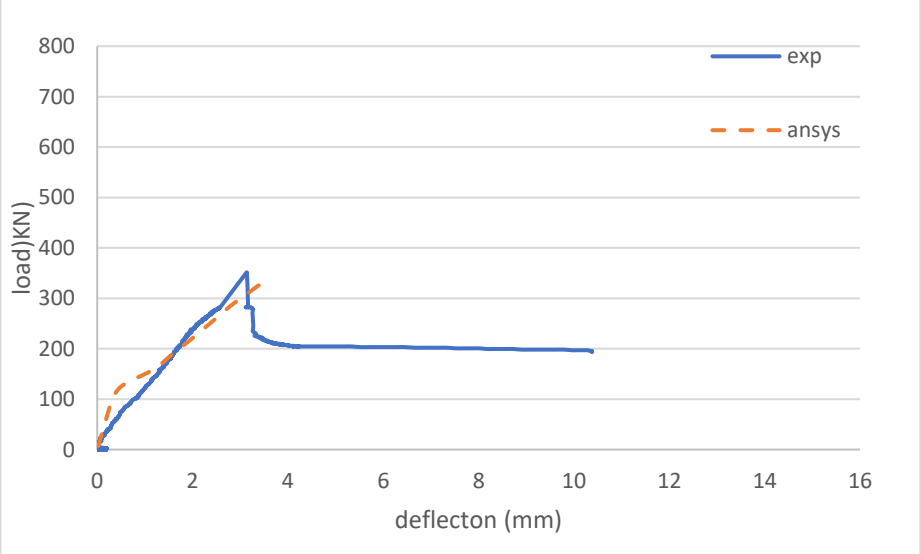

Figure (6-28): Comparison of load -deflection curves from Ansys and experimental for B8

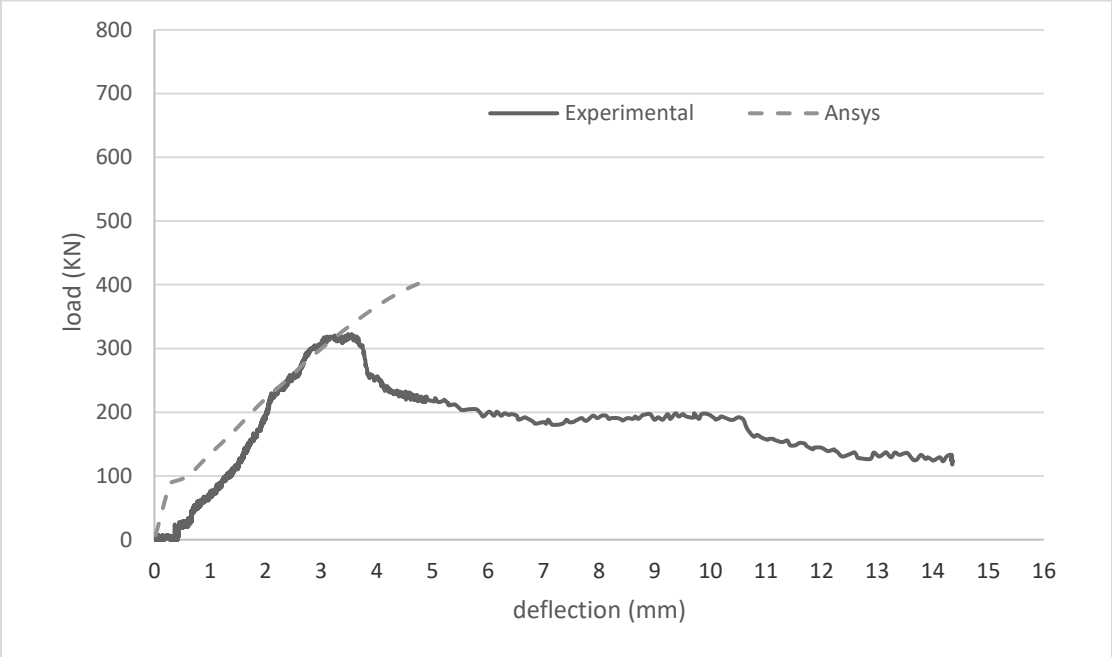

Figure (6-29): Comparison of load -deflection curves from ansys and experimental B9

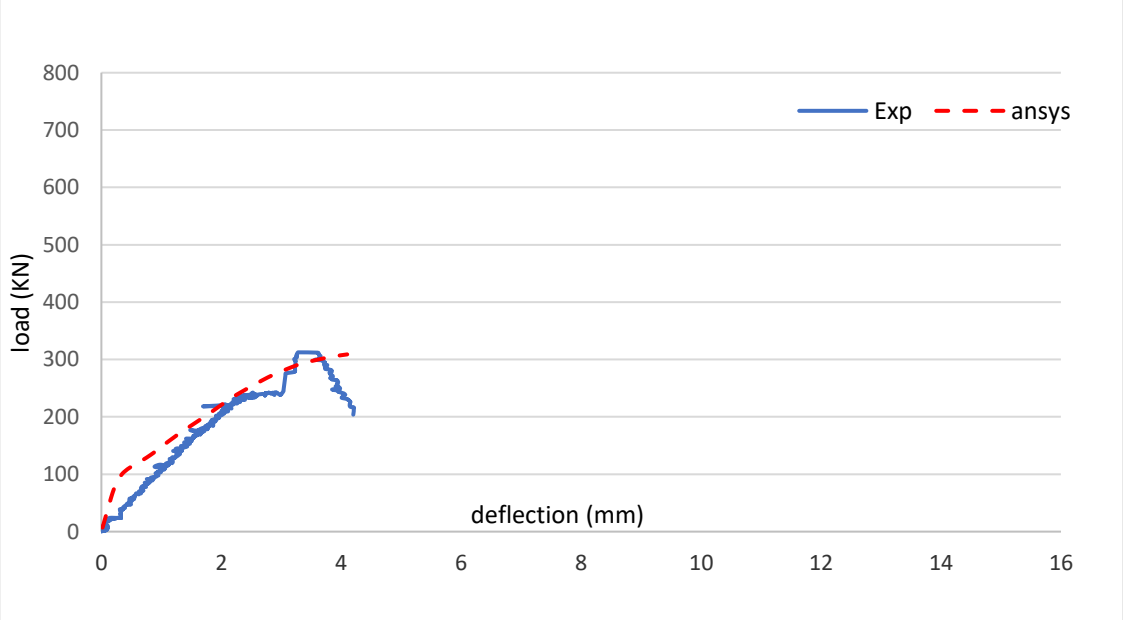

Figure (6-30): Comparison of load -deflection curves from Ansys and experimental B10

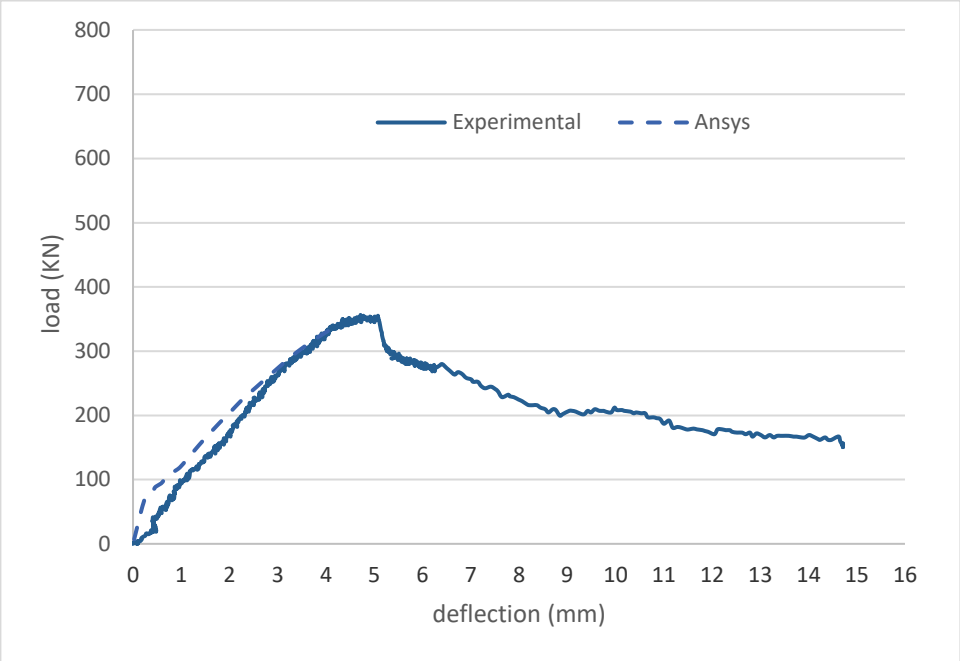

Figure (6-31): Comparison of load -deflection curves from ansys and experimental B11

6.3.1.3 Failure Load

The ultimate failure load obtained from the FEA (ANSYS 19.0-R2) is close to that obtained from the experimental test as explained in Table (6-1) that has presented a comparison between the analytical and experimental results. It can be concluded that the analytical model is nearly the same as the experimental result in solid deep beam (B1), also (B3) with openings which isn't strengthened with BFRP, so we could expect the ultimate load for other types of openings (horizontal, circular, and square). In the beam (B4), the ultimate load could not reach its full shear strength predicted by the analytical model. This is because this beam failed untimely by rotation of three distinct segments in the shear span. deep beams strengthened vertically by BFRP (B4,B6,B8,B10) For these specimens, the ratio of the experimental to finite element shear strength was in the range of 0.88–1.04. This suggests that a strength reduction factor of 0.96

should be adopted for strengthen RC deep beams with vertical BFRP to account for a possible change in the mode of failure. The ratio of the experimental to analytical strength of all horizontally strengthened specimens varied between 0.8 and 1.08. This suggests that a strength reduction factor of 0.94 should be adopted for strengthening RC deep beams with horizontal BFRP to account for a possible change in the mode of failure. it can be stated that the analytical procedure can give reasonable shear strength prediction for RC deep beams with openings strengthened with BFRP strips. Also deflection have an average 0.97 with a standard deviation of 0.12.

Table (6-1): experimental and Ansys results

No.	symbol	Experimental results		ANSYS19 results		$\frac{Pexp}{PAns}$	$\frac{\Delta\ exp}{\Delta Ans}$
		load	deflection	load	deflection		
		Pfail (KN)	Δ fail (mm)	P fail (KN)	Δ fail (mm)		
1	B1	451.8	2.5	428.9	2.53	1.05	0.99
2	B2	636.28	4.2	618	3.74	1.03	1.12
3	B3	298.6	4.14	281.4	4.5	1.06	0.92
4	B4	298.5	4.02	339	3.8	0.88	1.06
5	B5	360	4.2	341.5	3.9	1.05	1.08
6	B6	353.9	4.9	341	4.9	1.04	1.00
7	B7	456.8	4.56	423	5	1.08	0.91
8	B8	351.9	2.9	355	3.48	0.99	0.83
9	B9	322.5	3.5	401	4.74	0.8	0.74
10	B10	312.5	3.98	320	4.6	0.98	0.86
11	B11	356.4	4.7	339	4.22	1.05	1.10
					Average	1	0.97
					Standard	0.09	0.12
					Coefficient of variation	0.09	0.13

6.4 Stress in Concrete

6.4.1 Deep Beam B1

Stress in solid deep beam B1 resulting from ANSYS 2019 shows a perfect shape of stresses in deep beams as it shows a strut and tie shape, strut have a bottle shape with a large wide. compression in diagonals ranging from -47.3 to -4.8 MPa and tension in the bottom of the deep beams with value of 37.6 MPa as shown in Figure (6-32)

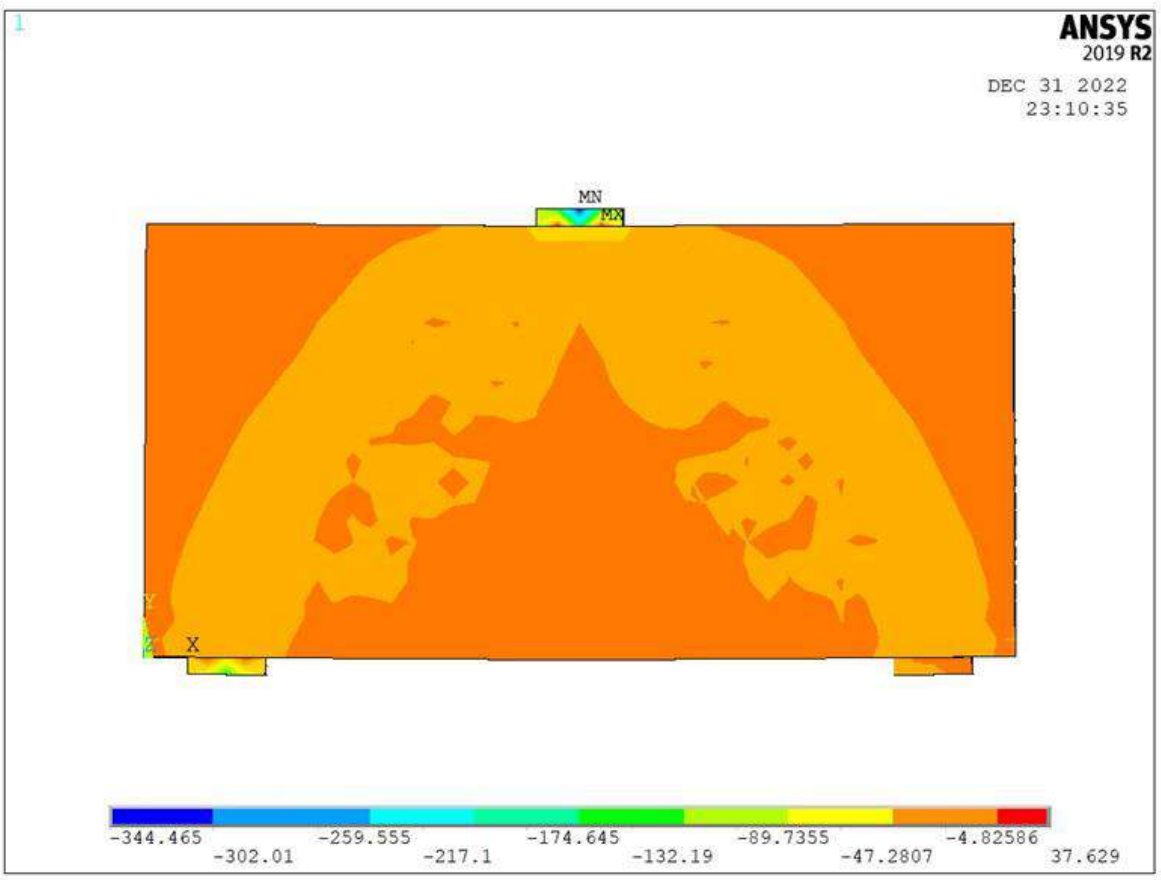

Figure (6-32): Stress in concrete in B1

6.4.2 Deep Beam B2

Stress in solid deep beam strengthened with BFRP strips (B2) resulting from ANSYS 2019 shows a perfect shape of stresses in deep beams as it show a strut

and tie shape, with a bottle shape less wide than the wide in strut exciting in B1 compression in diagonals ranging from -22.7 to -10 MPa which is nearly 0.48 of the stress obtained in B1 and tension in the bottom of the deep with a small value of 1 MPa beams as shown in Figure (6-33)

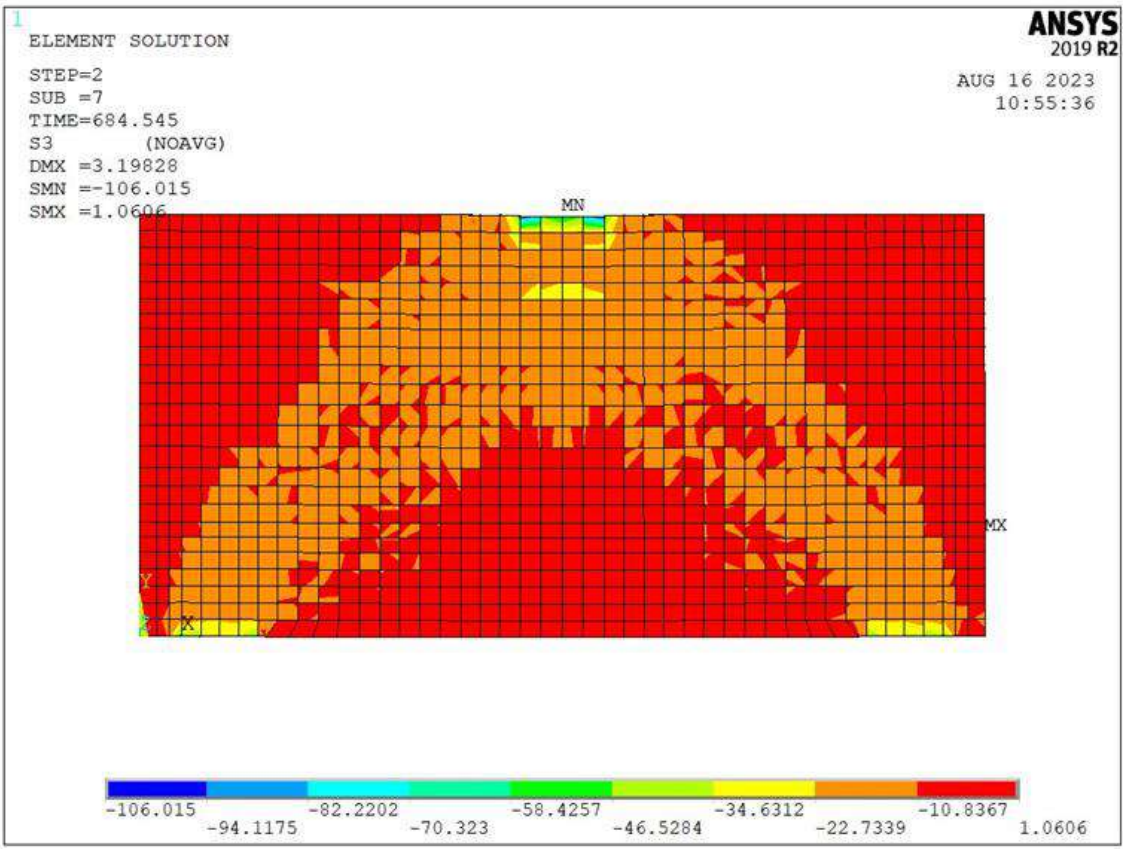

Figure (6-33): Stress in concrete in B2

6.4.3 Deep Beam B3

Stress in deep beam with vertical rectangular opening (B3) resulting from ANSYS 2019 shows a perfect shape of stresses in deep beams with openings as it shows a concentration in stress at the corner of openings, right at top and left at bottom of the openings. Compression in the corners of openings ranging from -33 to -8 MPa and tension in the bottom of the deep with a small value of 15.4 MPa

beams as shown in Figure (6-34)

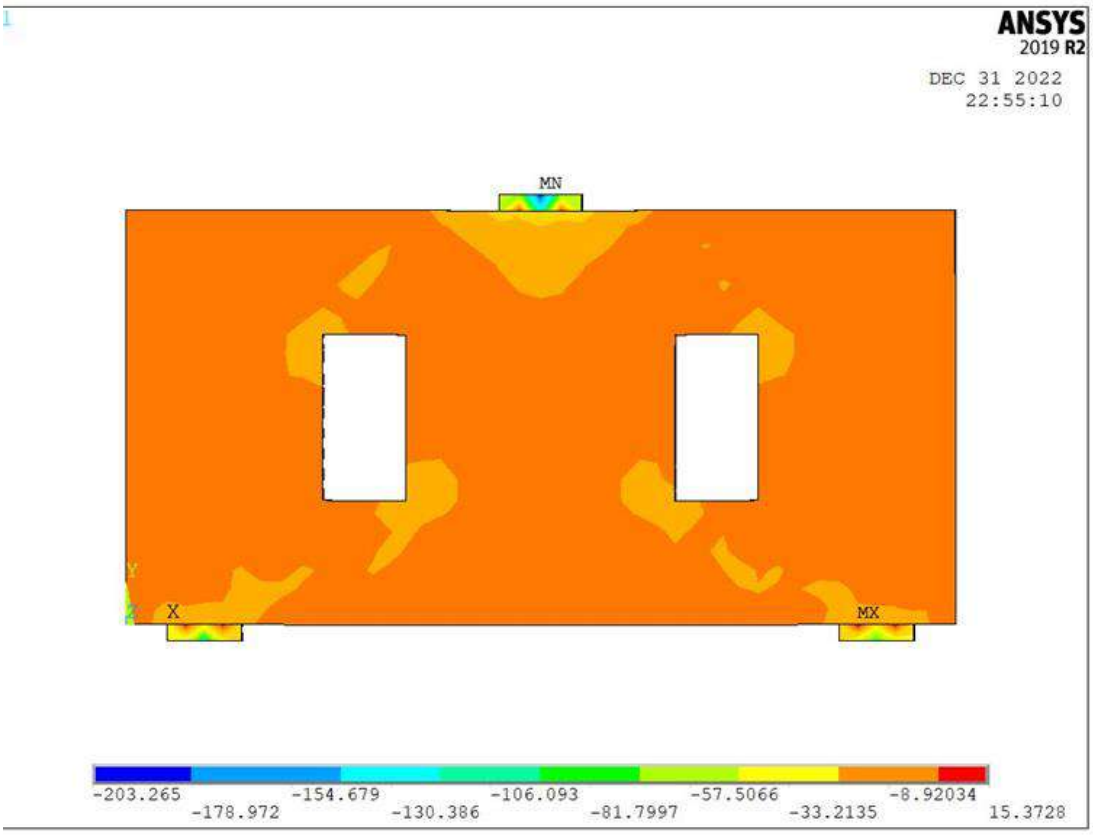

Figure (6-34): Stress in concrete in B3

6.4.4 Deep Beam B4

Stress in deep beam with vertical rectangular opening strengthen with vertical BFRP strips (B4) resulting from ANSYS 2019 shows a perfect shape of stresses in deep beams with openings as it show a concentration in stress at the corner of openings ,compression in the top of openings ranging from -41.8 to -12 MPa which is nearly 1.24 of the stress obtained in B3 and tension in the bottom of the deep with a small value of 14.3MPa beams as shown in Figure (6-35)

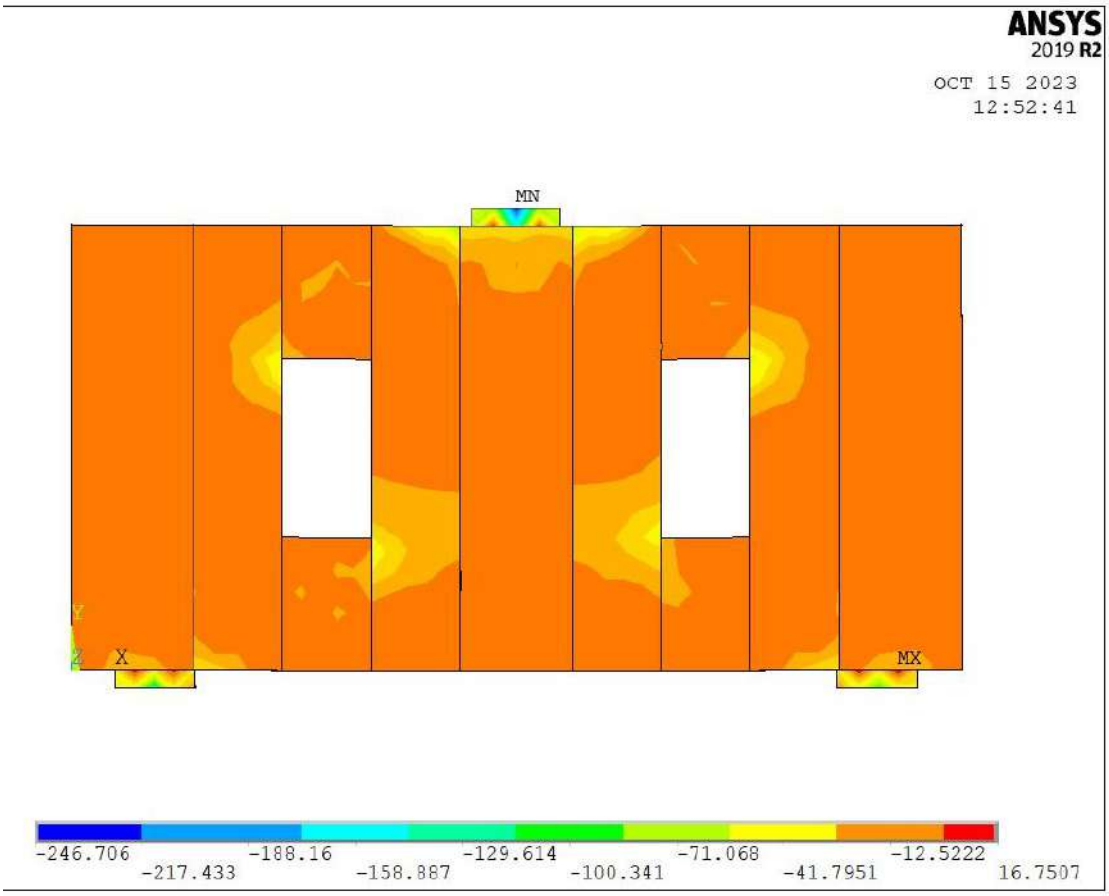

Figure (6-35): Stress in concrete in B4

6.4.5 Deep Beam B5

Stress in deep beam with vertical rectangular opening strengthen with horizontal BFRP strips (B5) resulting from ANSYS 2019 shows a different shape of stresses in deep beams with openings as it show 2 strut shapes up and bottom at the corners of openings, compression in the top of openings ranging from -34 to -7 MPa and tension in the bottom of the deep with a small value of 19.3MPa beams as shown in figure (6-36)

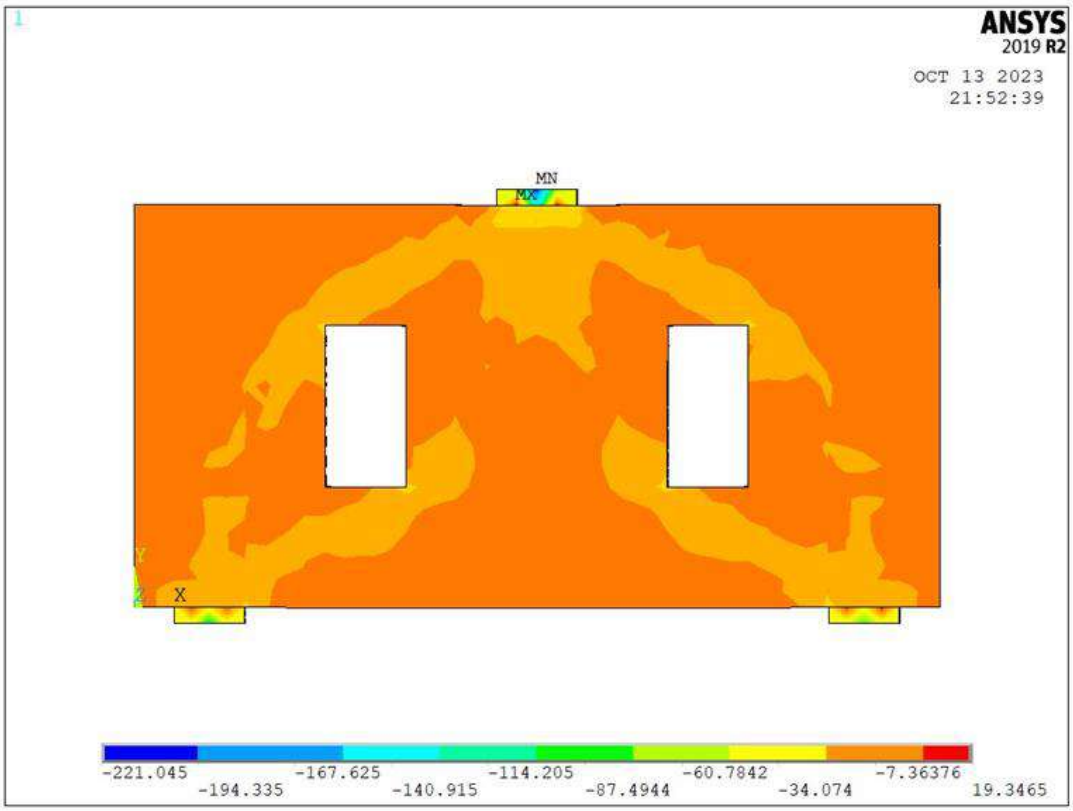

Figure (6-36): Stress in concrete in B5

6.4.6 Deep Beam B6

Stress in deep beam with horizontal rectangular opening strengthen with vertical BFRP strips (B6) resulting from ANSYS 2019 shows a perfect shape of stresses in deep beams with openings as it shows a concentration in stress at the corner of openings, compression in the top of openings ranging from -247to -88 MPa and tension in the bottom of the deep with a small value of 71MPa beams as shown in figure (6-37)

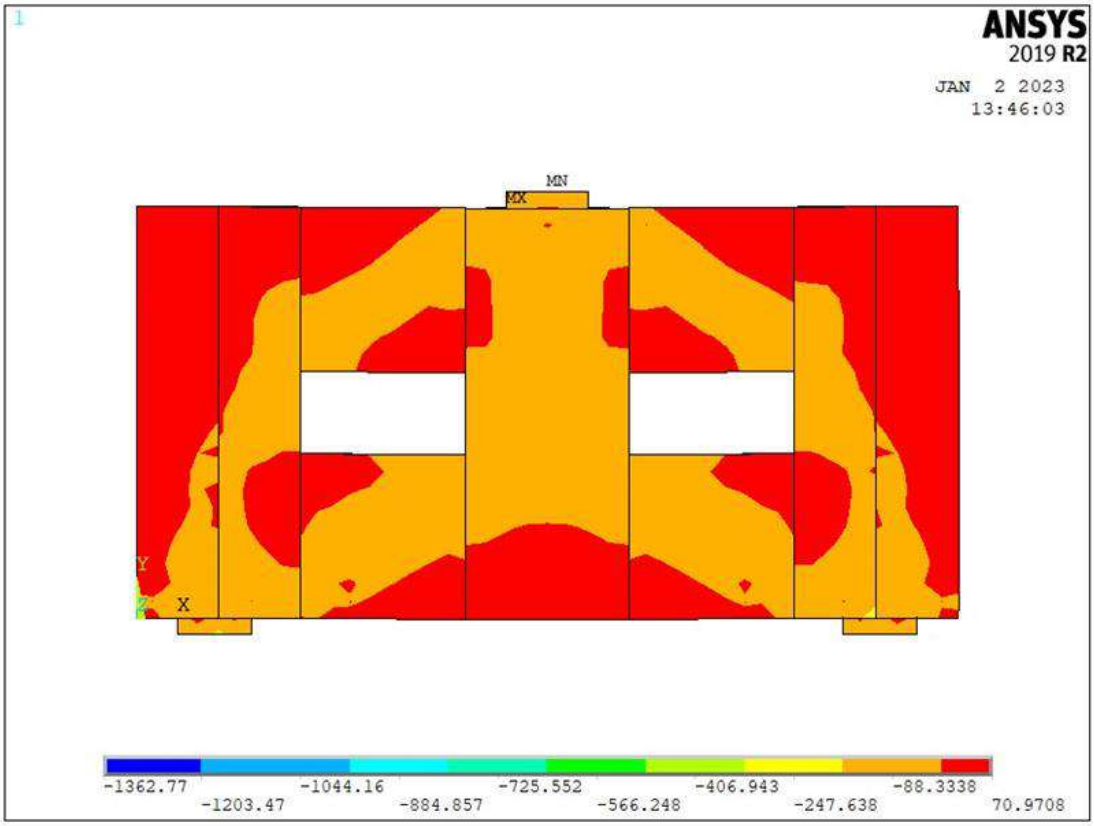

Figure (6-37): Stress in concrete in B6

6.4.7 Deep Beam B7

Stress in deep beam with horizontal rectangular opening strengthen with horizontal BFRP strips (B7) resulting from ANSYS 2019 shows a perfect shape of stresses in deep beams with openings as it shows a concentration in stress at the corner of openings, compression in the top of openings ranging from -43 to -12 MPa and tension in the bottom of the deep with a small value of 18 MPa beams as shown in figure (6-38)

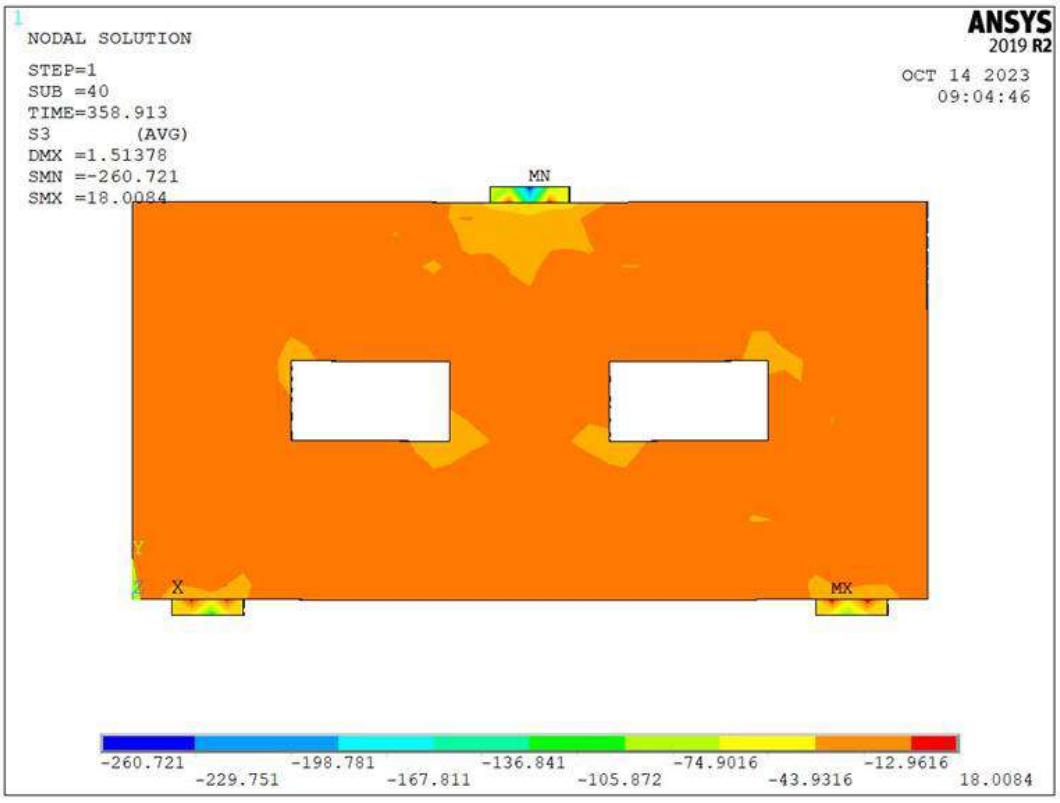

Figure (6-38): Stress in concrete in B7

6.4.8 Deep Beam B8

Stress in deep beam with circular opening strengthen with vertical BFRP strips (B8) resulting from ANSYS 2019 shows a perfect shape of stresses in deep beams with openings as it show a concentration in stress at the corner of openings ,compression in the top of openings ranging from -52to -15 MPa and tension in the bottom of the deep with a small value of 21.6MPa beams as shown in figure (6-39)

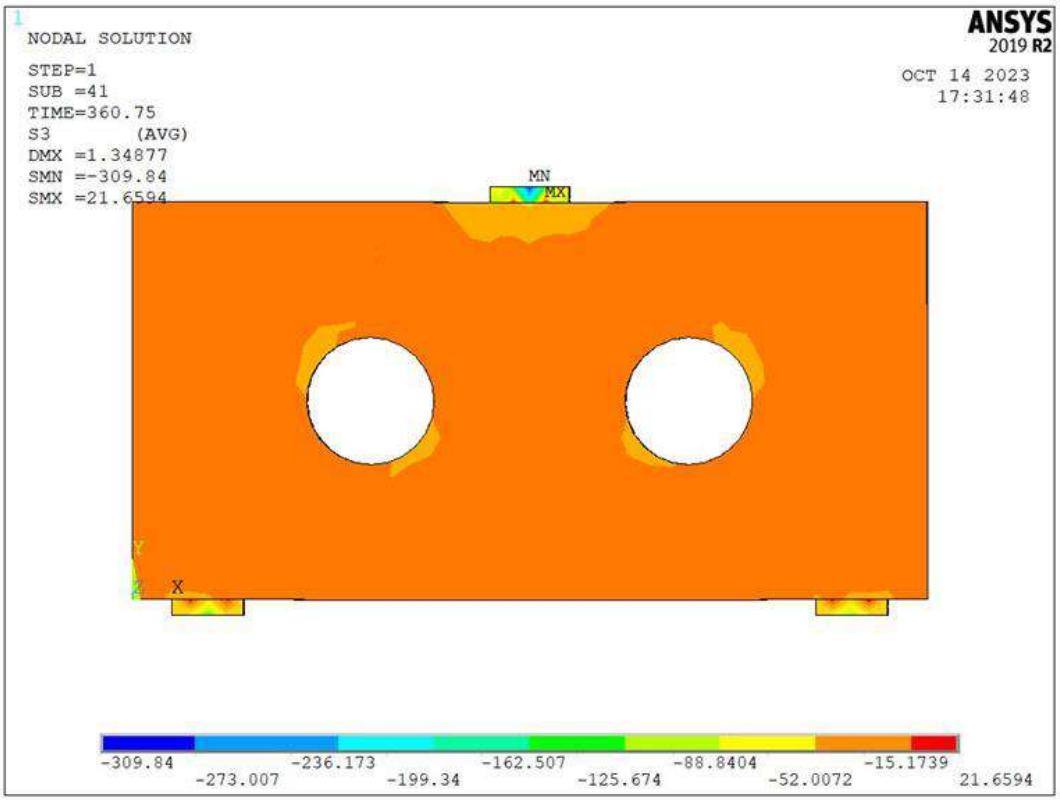

Figure (6-39): Stress in concrete in B8

6.4.9 Deep Beam B9

Stress in deep beam with circular opening strengthen with horizontal BFRP strips (B9) resulting from ANSYS 2019 shows a perfect shape of stresses in deep beams with openings as it show a concentration in stress at the corner of openings ,compression in the top of openings ranging from -56 to -11 MPa which means that horizontal BFRP increase the stress about 8% than that stresses in beams with vertical BFRP strips and tension in the bottom of the deep with a small value of 33.2 MPa beams as shown in Figure (6-40)

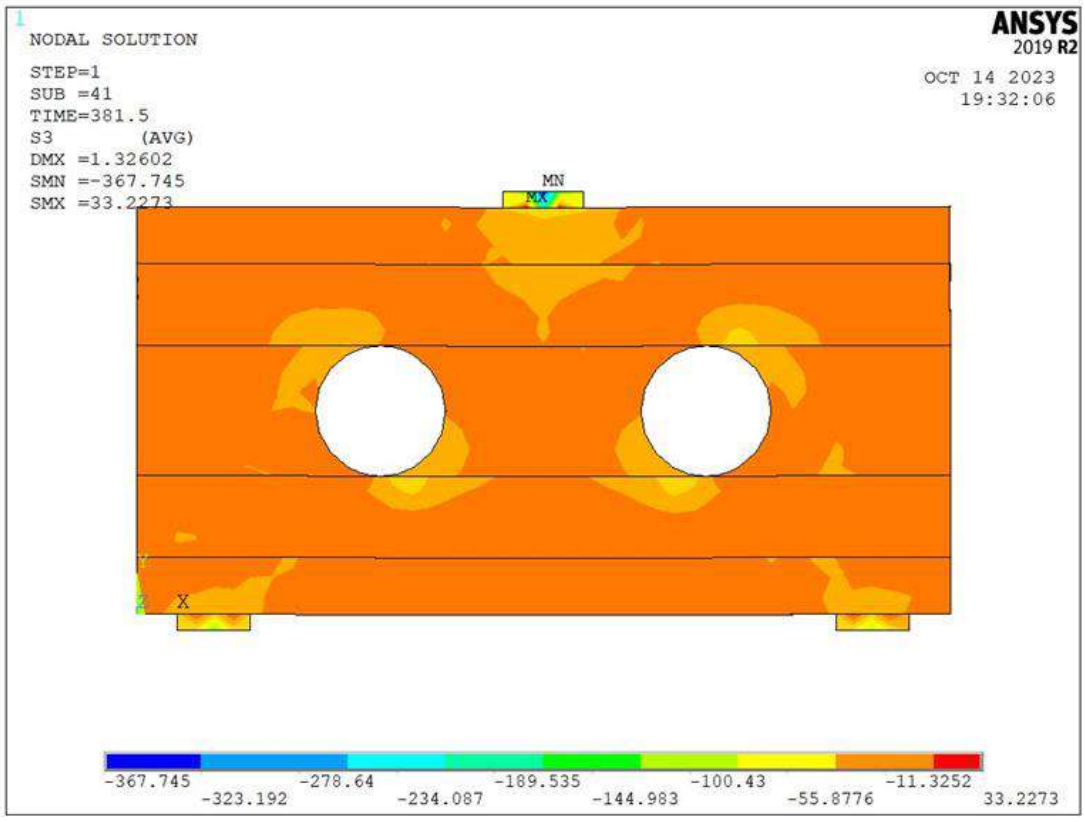

Figure (6-40): Stress in concrete in B9

6.4.10 Deep Beam B10

Stress in deep beam with square opening strengthen with vertical BFRP strips (B9) resulting from ANSYS 2019 shows a perfect shape of stresses in deep beams with openings as it show a concentration in stress at the corner of openings ,compression in the top of openings ranging from -50.4 to -7.5 MPa and tension in the bottom of the deep with a small value of 35 MPa beams as shown in figure (6-41)

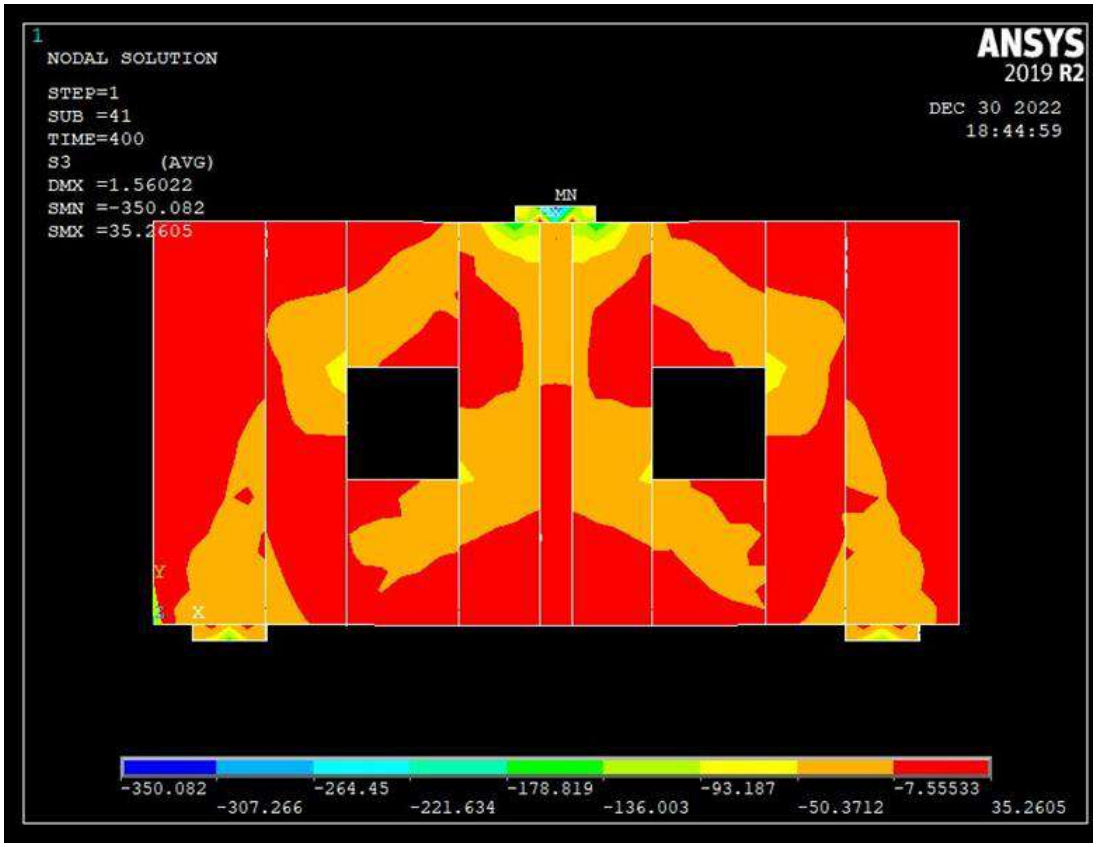

Figure (6-41): Stress in concrete in B10

6.4.11 Deep Beam B11

Stress in deep beam with square opening strengthen with horizontal BFRP strips (B11) resulting from ANSYS 2019 shows a perfect shape of stresses in deep beams with openings as it show a concentration in stress at the corner of openings ,compression in the top of openings ranging from -40 to -3.7 MPa which means that the horizontal BFRP strips decrease the stresses about 20% of the value obtained from beam B10 which is strengthened by vertical BFRP strips and tension in the bottom of the deep beam with a value of 34 MPa(nearly the same of B10) as shown in figure (6-42)

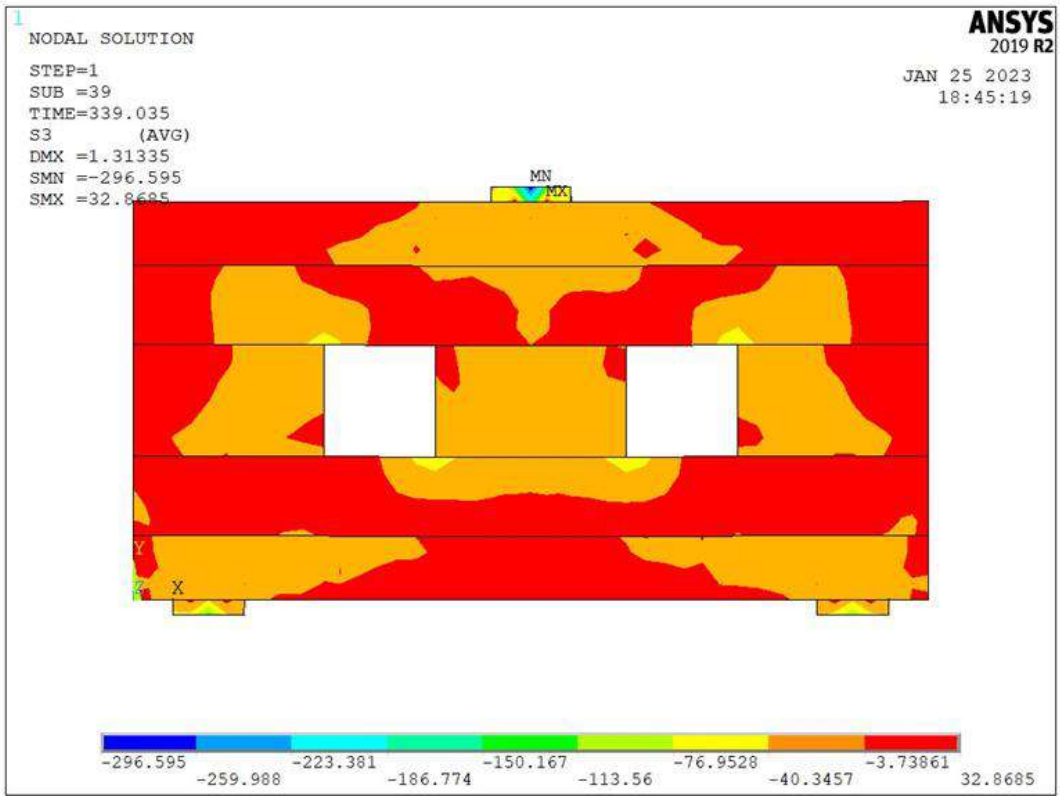

Figure (6-42): Stress in concrete in B11

6.5 Stress and Strain in Steel at Failure

6.5.1 Stress and Strain at B2

Figure (6-43) shows the stress and ultimate strain in steel reinforcement of the deep beam B2, from this figure it can noted that the ultimate stress is 320 MPa which means that the failure occurred mainly due to shear in the horizontal direction and some of vertical stirrups. Also, the value of ultimate strain (0.004) that appeared in horizontal reinforcement shows that the steel reached to the yield in horizontal steel before vertical steel.

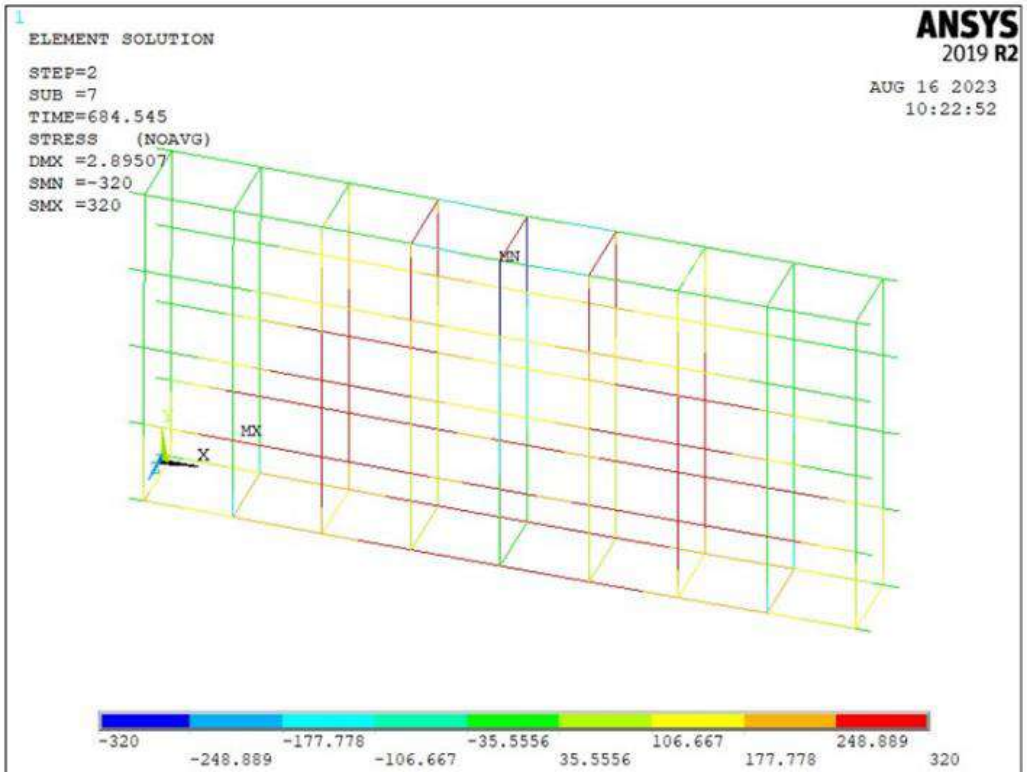

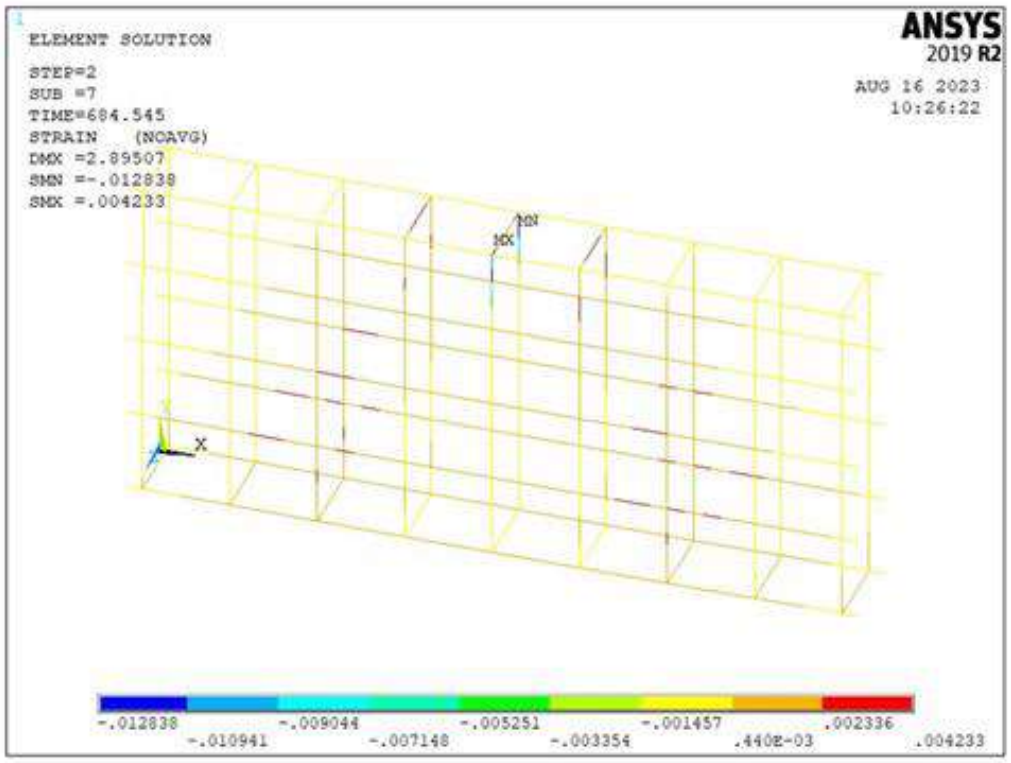

Figure (6-43): Stress and strain in steel at failure in beam B2

6.5.3 Stress and Strain at B3

Figure (6-44) shows the stress and ultimate strain in steel reinforcement of the deep beam B2, from this figure it can noted that the ultimate stress is 320 MPa which means that the failure occurred mainly due to shear in the horizontal direction and some of vertical stirrups. Also, the value of ultimate strain (0.004) that appeared in horizontal reinforcement shows that the steel reached to the yield in horizontal steel before vertical steel.

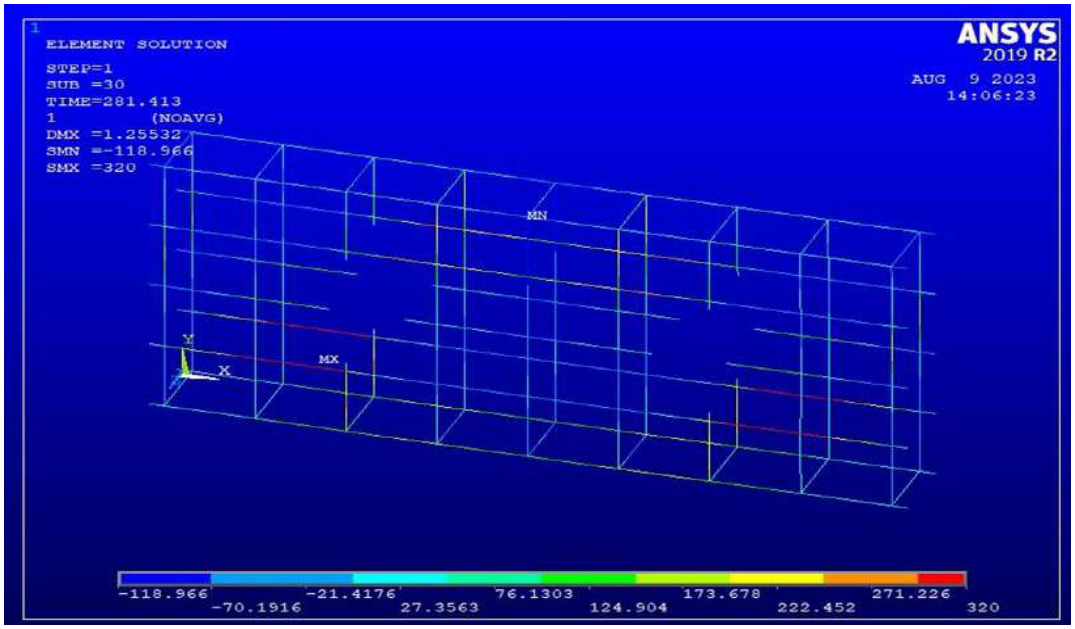

Figure (6-44): Stress and strain in steel at failure for beam B3

6.5.4 Stress and Strain at B4

Figure (6-45) shows the stress and ultimate strain in steel reinforcement of the deep beam B2, from this figure it can noted that the ultimate stress is 280 MPa which means that the failure occurred mainly due to shear in the horizontal direction and some of vertical stirrups. Also, the value of ultimate strain (0.004) that appeared in horizontal reinforcement shows that the steel reached to the yield

in horizontal steel before vertical steel.

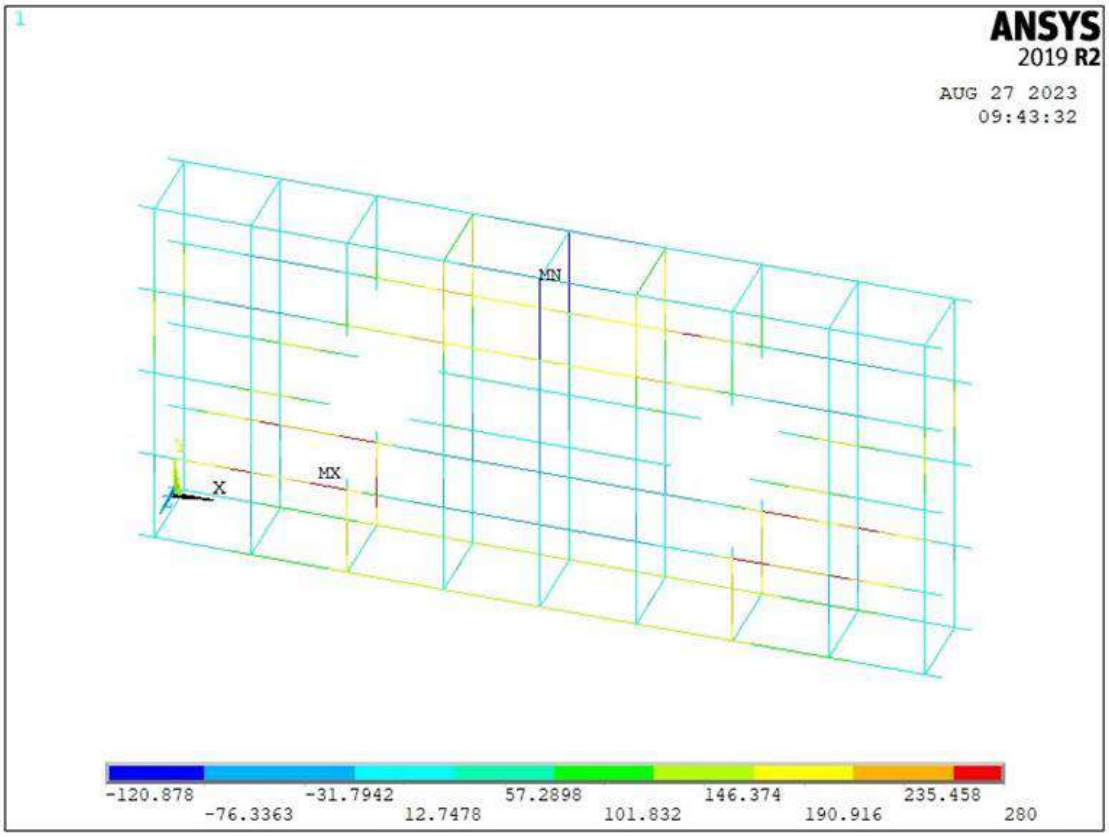

Figure (6-45): Stress in steel at failure for beam B4

6.5.5 Stress and Strain at B5

Figure (6-46) shows the stress and ultimate strain in steel reinforcement of the deep beam B2, from this figure it can noted that the ultimate stress is 322.6MPa which means that the failure occurred mainly due to shear in the horizontal direction and some of vertical stirrups. Also, the value of ultimate strain (0.0016) that appeared in horizontal reinforcement shows that the steel didn't reach to the yield in horizontal steel.

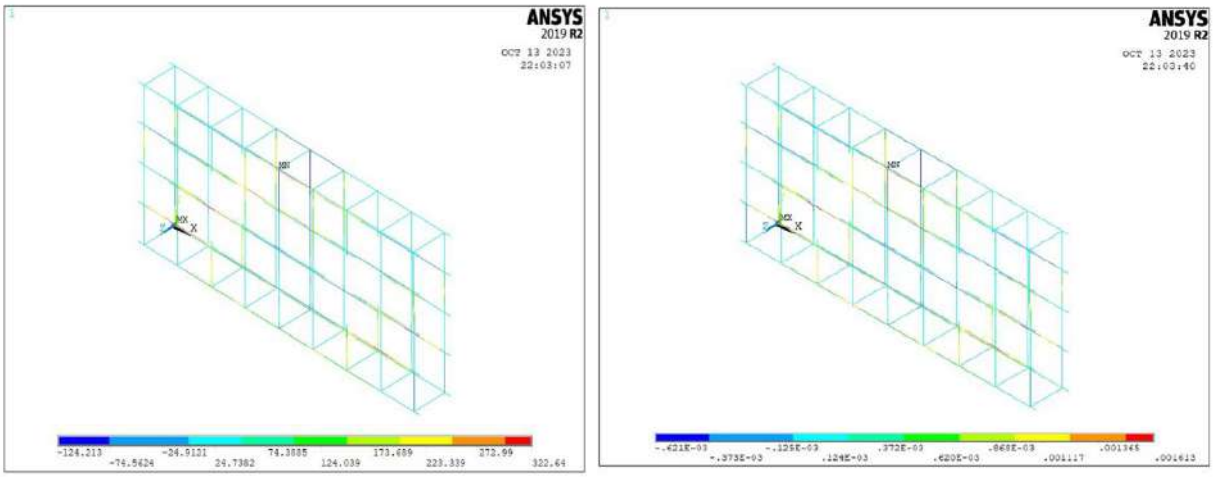

Figure (6-46): Stress and strain in steel at failure for beam B5

6.5.6 Stress and Strain at B6

Figure (6-47) shows the stress and ultimate strain in steel reinforcement of the deep beam B2, from this figure it can noted that the ultimate stress is 322.6MPa which means that the failure occurred mainly due to shear in the horizontal direction and some of vertical stirrups. Also, the value of ultimate strain (0.0033) that appeared in vertical reinforcement shows that the steel reach to the yield stress in vertical steel.

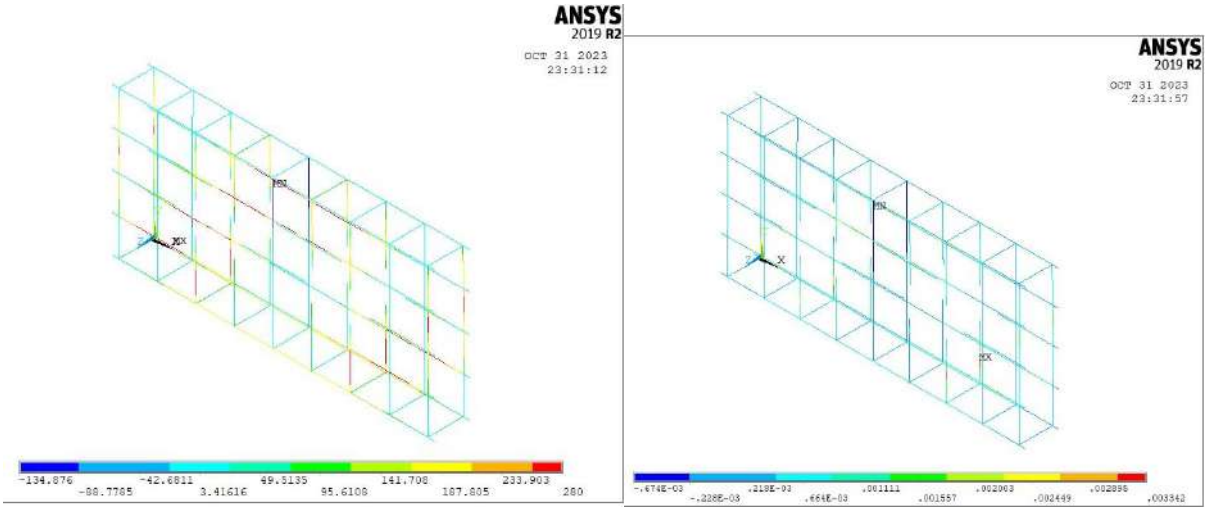

Figure (6-47): Stress and strain in steel at failure for beam B6

6.5. 7 stress and strain at B7

Figure (6-48) shows the stress and ultimate strain in steel reinforcement of the deep beam B2, from this figure it can noted that the ultimate stress is 280 MPa which means that the failure occurred mainly due to shear in the horizontal direction and some of vertical stirrups. Also, the value of ultimate strain (0.003) that appeared in horizontal reinforcement shows that the steel reached to the yield in horizontal steel.

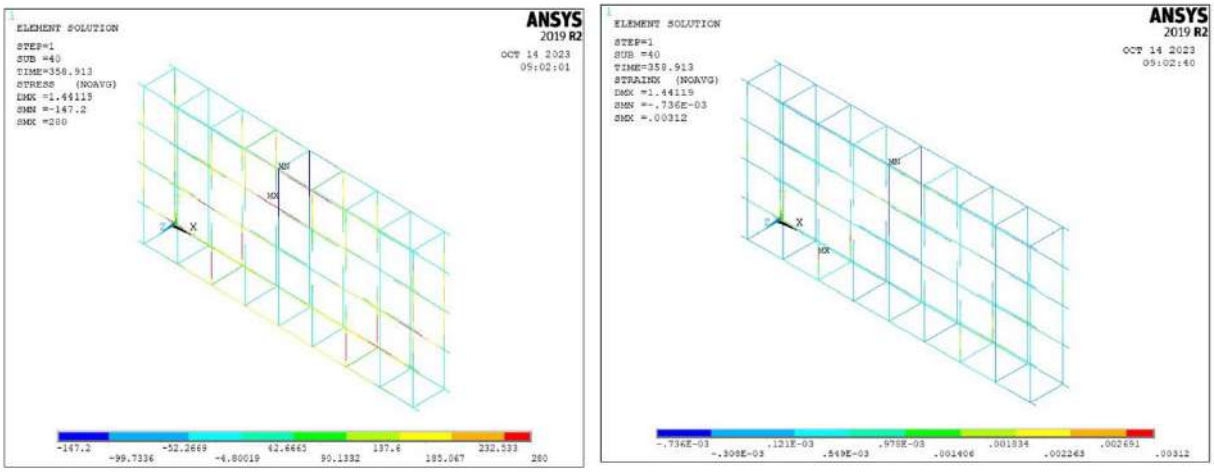

Figure (6-48): Stress and strain in steel at failure for beam B7

6.5.8 Stress and Strain at B8

Figure (6-49) shows the stress and ultimate strain in steel reinforcement of the deep beam B2, from this figure it can noted that the ultimate stress is 280 MPa which means that the failure occurred mainly due to shear in the horizontal direction and some of vertical stirrups. Also, the value of ultimate strain (0.0015) that appeared in horizontal reinforcement shows that the steel didn't reach to the yield in horizontal steel.

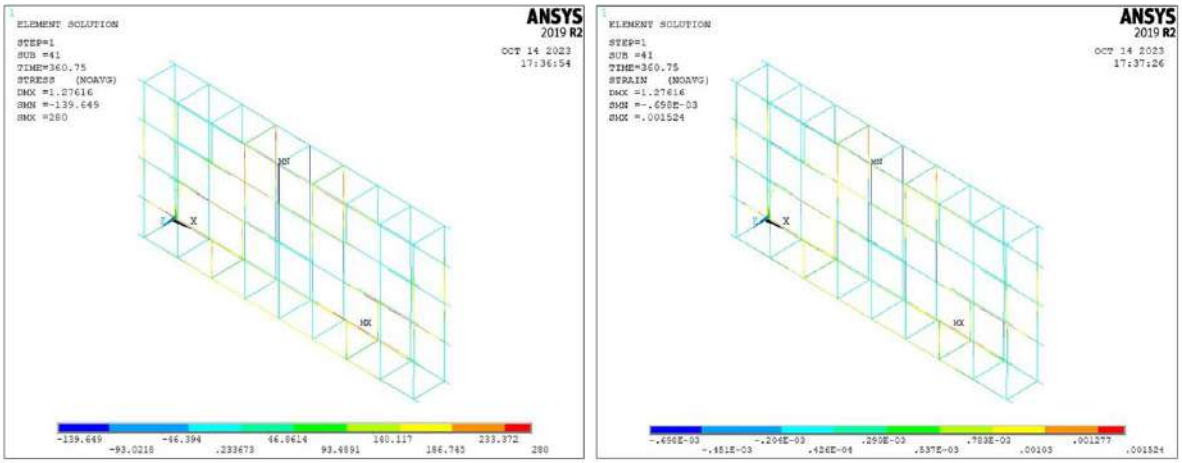

Figure (6-49): Stress and strain in steel at failure for beam B8

6.5.9 Stress and Strain at B9

Figure (6-50) shows the stress and ultimate strain in steel reinforcement of the deep beam B9, from this figure it can noted that the ultimate stress is 280 MPa which means that the failure occurred mainly due to shear in the horizontal direction and some of vertical stirrups. Also, the value of ultimate strain (0.0023) that appeared in horizontal reinforcement shows that the steel reach to the yield stress in horizontal steel.

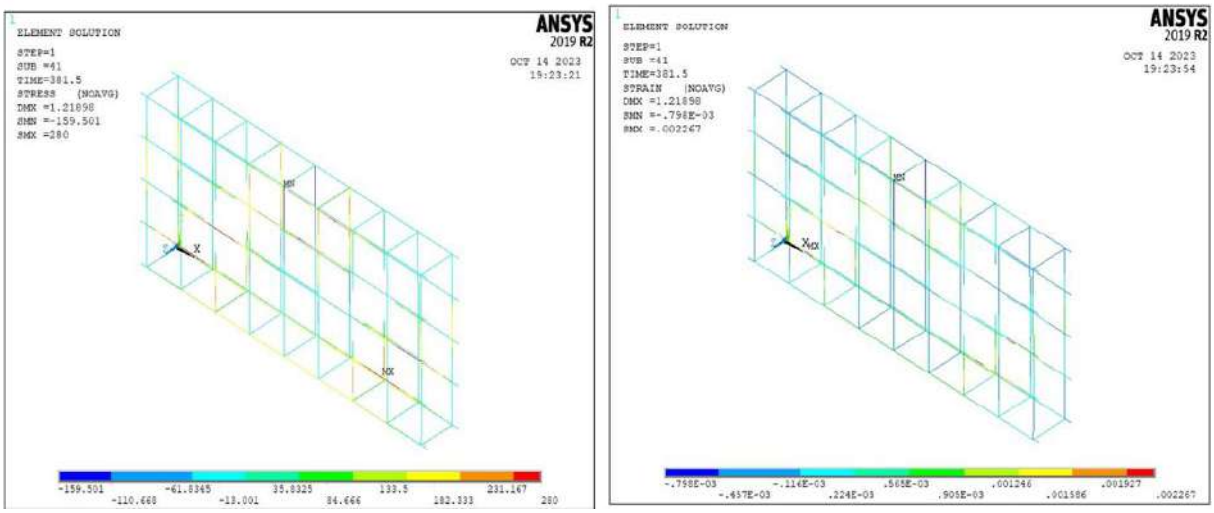

Figure (6-50): Stress and strain in steel at failure for beam B9

6.5.10 Stress and Strain at B10

Figure (6-51) shows the stress and ultimate strain in steel reinforcement of the deep beam B10, from this figure it can noted that the ultimate stress is 280 MPa which means that the failure occurred mainly due to shear in the horizontal direction and some of vertical stirrups. Also, the value of ultimate strain (0.0017) that appeared in horizontal reinforcement shows that the steel reach to the yield stress in horizontal steel.

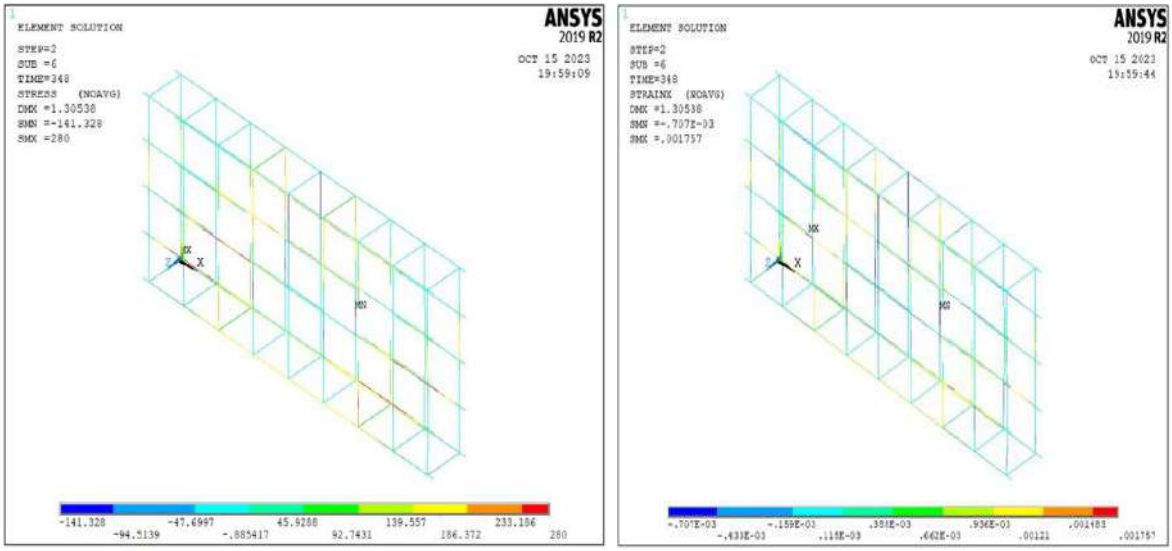

Figure (6-51): Stress and strain in steel at failure for beam B10

6.5.11 Stress and Strain at B11

Figure (6-52) shows the stress and ultimate strain in steel reinforcement of the deep beam B11, from this figure it can noted that the ultimate stress is 324.7 MPa which means that the failure occurred mainly due to shear in the horizontal direction and some of vertical stirrups. Also, the value of ultimate strain (0.0016) that appeared in horizontal reinforcement shows that the steel reach to the yield stress in horizontal steel.

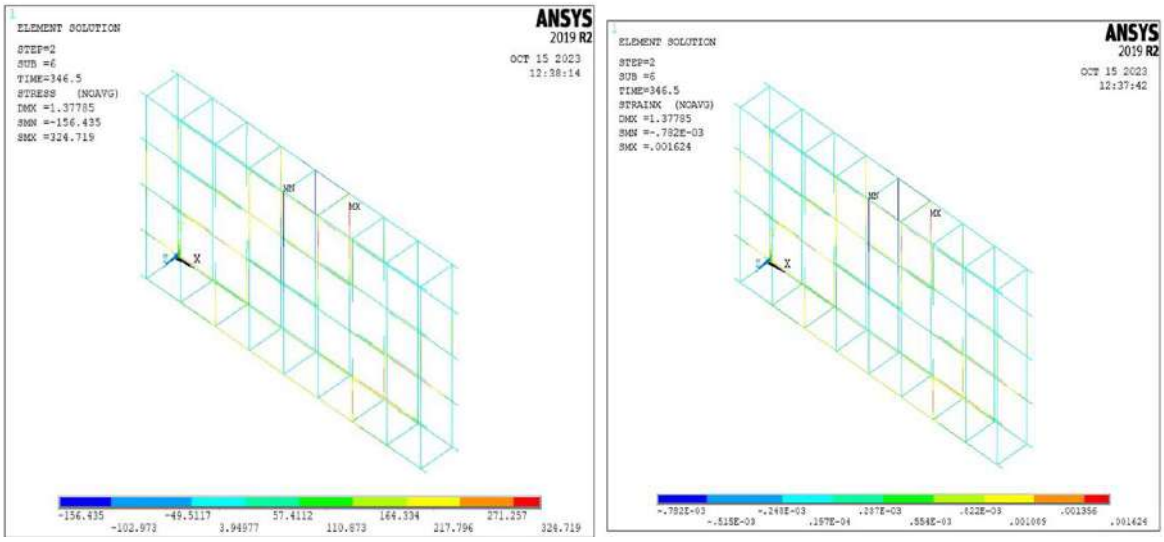

Figure (6-52): Stress and strain in steel at failure for beam B11

6.6 Maximum Stress in BFRP Strips

6.6.1 Maximum Stress in BFRP Strips at B2

Figure (6-53) shows the stresses in basalt strips, from this figure it can see that there is a stress concentration in the middle of the BFRP sheet increased at bottom of the beam toward the supports with a maximum value of 259.6 MPa at the end of the sheet and minimum value of 28.6 MPa at the strips on the top of the beam with a variation of 231 MPa.

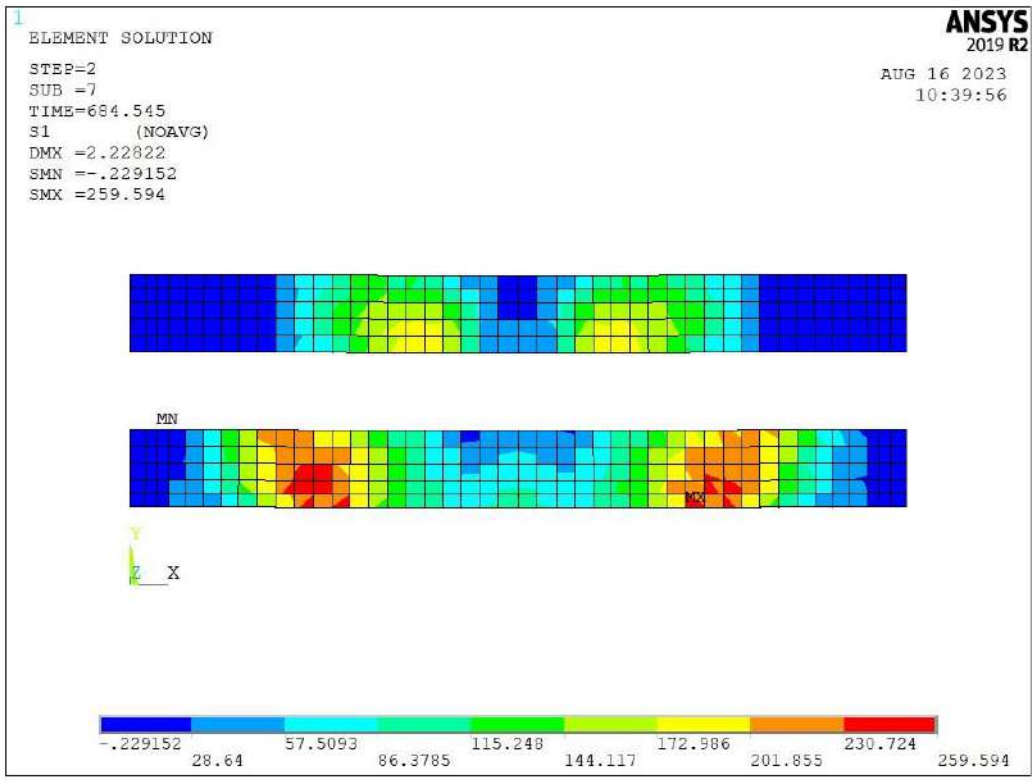

Figure (6-53): Stress in basalt fiber strips at failure for beam B2

6.6.2 Maximum Stress in BFRP Strips at B4

Figure (6-54) shows the stresses in basalt strips, from this figure it can see that there is a stress concentration distributed over 3 zones at the corner of the opening top and bottom with values of -41.8, -27.4 and -13 MPa from closest to farthest from the opening respectively. With a small tension value of 1.3 MPa in other places in the basalt sheet.

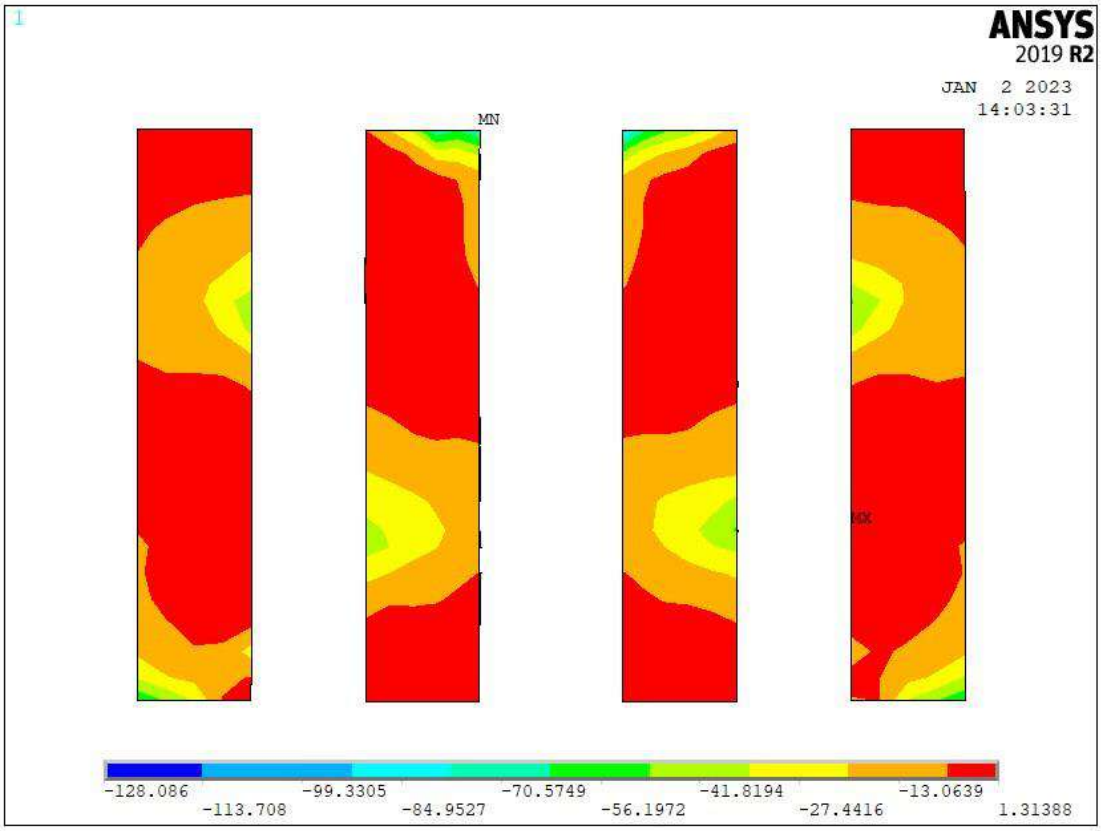

Figure (6-54): Stress in basalt fiber strips at failure for beam B4

6.6.3 Maximum Stress in BFRP Strips at B5

Figure (6-55) shows the stresses in basalt strips for deep beam B5, from this figure it can see that stress in the sheet at top of the openings have a concentration in the middle of the beam unlike the basalt sheet at the bottom of the openings, it has a stress concentration at the edges of the beam not in the middle of it with a maximum value of 164.4 MPa at the bottom sheet and a minimum value of -1 MPa that means that the sheet at the top of opening has a tension stress in the middle and compression with a small value at the outer edge of the sheet ,while the sheet at bottom of the openings the stresses are tension in the outer of the sheet and compression with a small value in the middle of the sheet.

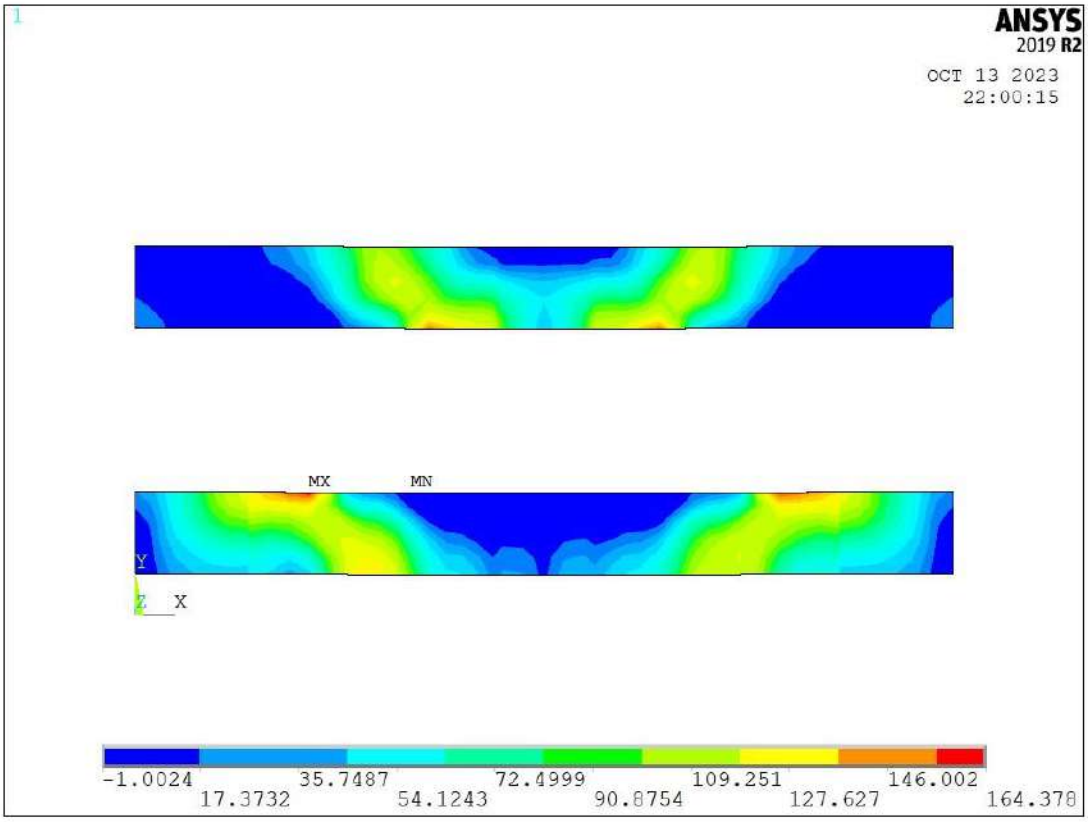

Figure (6-55): Stress in basalt fiber strips at failure for beam B5

6.6.4 Maximum Stress in BFRP Strips at B6

Figure (6-56) shows the stresses in basalt strips, from this figure it can see that there is a stress concentration distributed over 4 zones at the corner of the top of opening with values of -39, -29, -19 and -9 MPa from closest to farthest from the opening respectively. Also, at the corner of the bottom of the openings, the stress concentration distributed at 3 zones with values of -29, -19 and -9 MPa with a small tension value of 0.9 MPa in other places in the basalt sheet at the top and bottom of the basalt sheet.

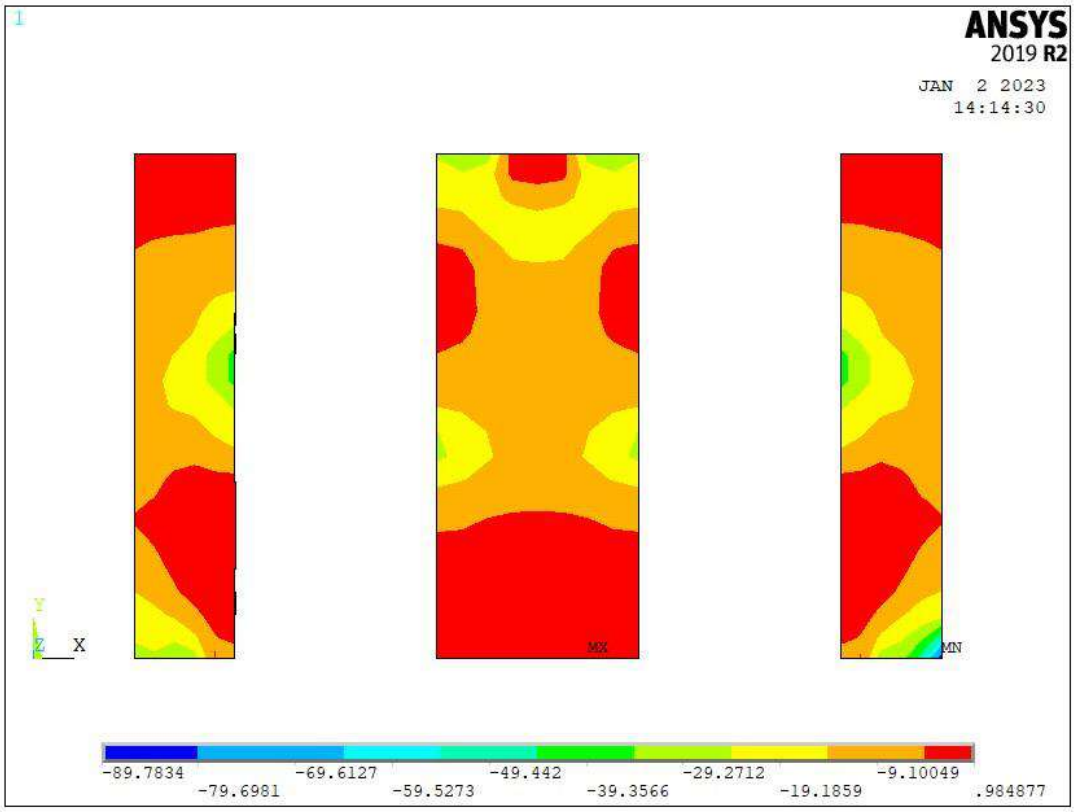

Figure (6-56): Stress in basalt fiber strips at failure for beam B6

6.6.5 Maximum Stress in BFRP Strips at B7

Figure (6-57) shows the stresses in basalt strips for deep beam B7, from this figure it can see that stress in the sheet at top of the openings have a concentration in the middle of the beam unlike the basalt sheet at the bottom of the openings, it has a stress concentration at the edges of the beam not in the middle of it with a maximum value of 276.5 MPa at the bottom sheet and a minimum value of -0.7 MPa that means that the sheet at the top of opening has a tension stress in the middle and compression with a small value at the outer edge of the sheet ,while the sheet at bottom of the openings the stresses are tension in the outer of the sheet and compression with a small value in the middle of the

strips of BFRP.

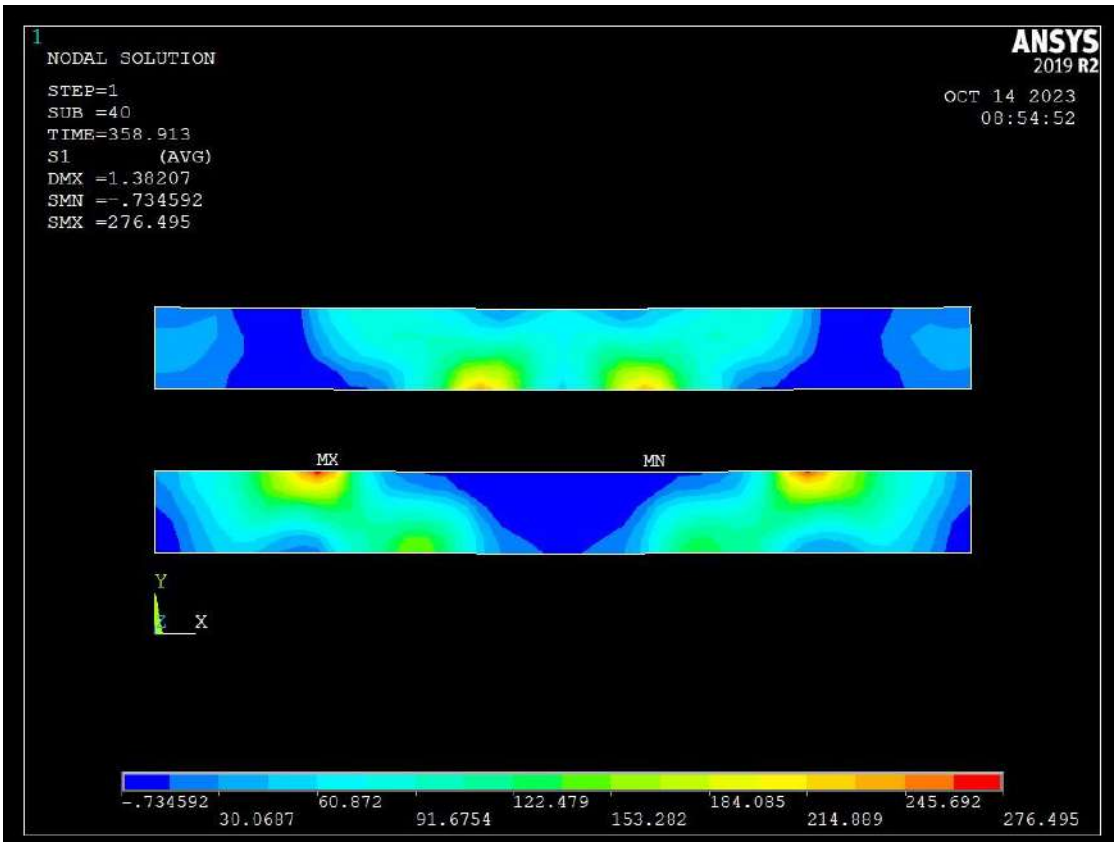

Figure (6-57): Stress in basalt fiber strips at failure for beam B7

6.6.6 Maximum Stress in BFRP Strips at B8

Figure (6-58) shows the stresses in basalt strips in beam B8, from this figure it can see that there is a stress concentration at the outer strips with a maximum value of 155 MPa at the bottom of the strips. While, the inner strips have a concentration in stress at the top of the sheet with a maximum value of 120.4 MPa with a small compression value of 0.8 MPa in other places in the basalt sheet at the top and bottom of the basalt sheet.

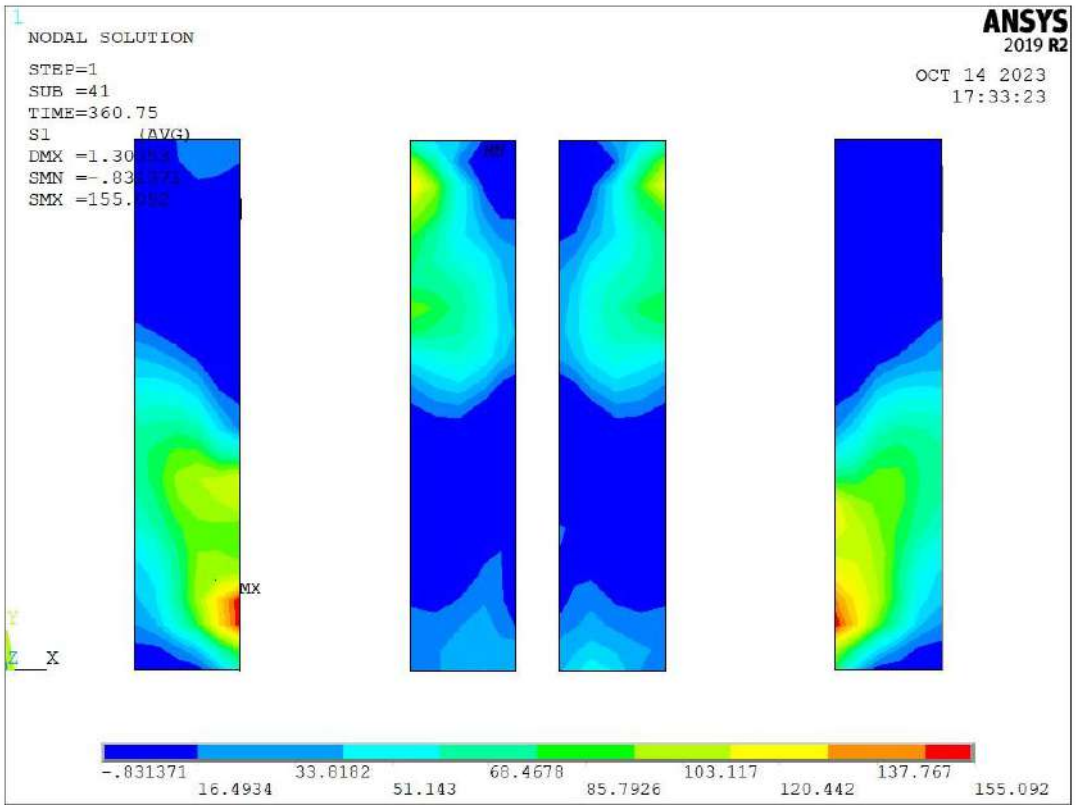

Figure (6-58): Stress in basalt fiber strips at failure for beam B8

6.6.7 Maximum Stress in BFRP Strips at B9

Figure (6-59) shows the stresses in basalt strips for deep beam B9, from this figure it can see that stress in the sheet at top of the openings have a concentration in the middle of the beam unlike the basalt sheet at the bottom of the openings, it has a stress concentration at the edges of the beam not in the middle of it with a maximum value of 202 MPa at the bottom sheet and a minimum value of -0.5 MPa that means that the sheet at the top of opening has a tension stress in the middle and compression with a small value at the outer edge of the sheet ,while the sheet at bottom of the openings the stresses are tension in the outer of the sheet and compression with a small value in the middle of the sheet.

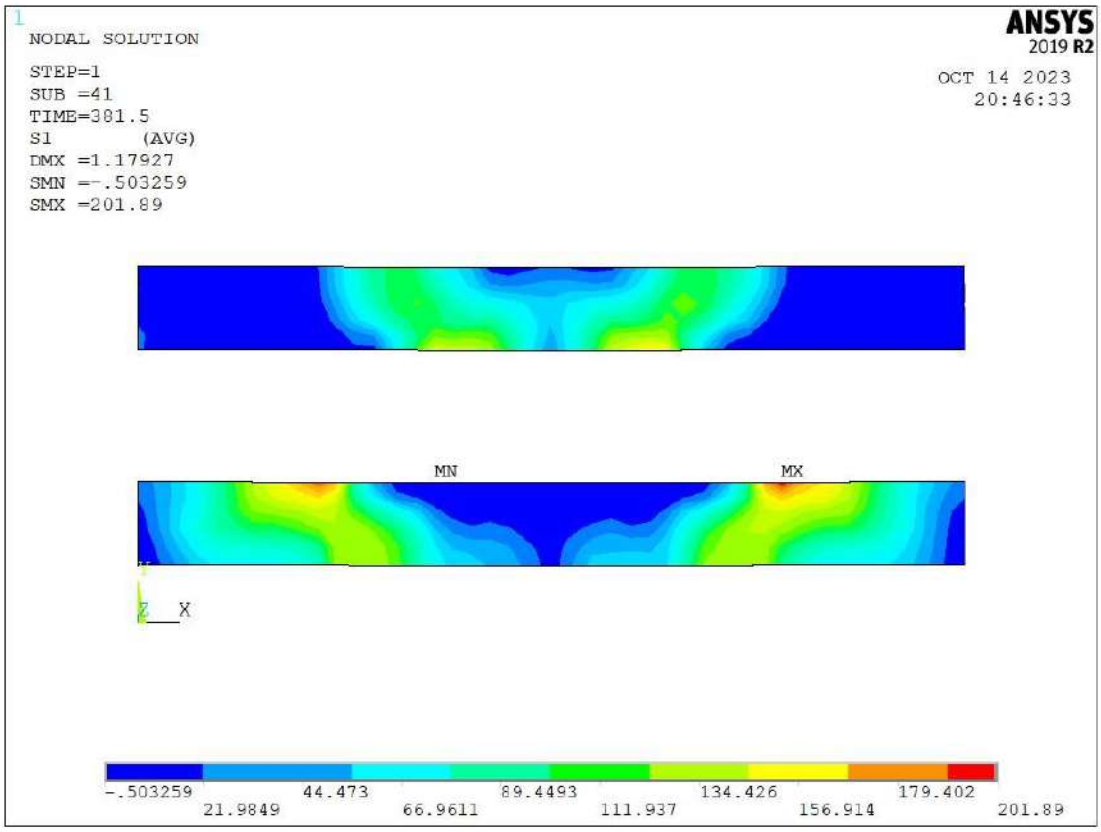

Figure (6-59): Stress in basalt fiber strips at failure for beam B9

6.6.8 Maximum Stress in BFRP Strips at B10

Figure (6-60) shows the stresses in basalt strips in beam B8, from this figure it can see that there is a stress concentration at the outer strips with a maximum value of 164 MPa at the bottom of the strips. While, the inner strips have a concentration in stress at the top of the sheet with a maximum value of 109MPa with a small compression value of -0.9 MPa in other places in the basalt sheet at the top and bottom of the basalt sheet.

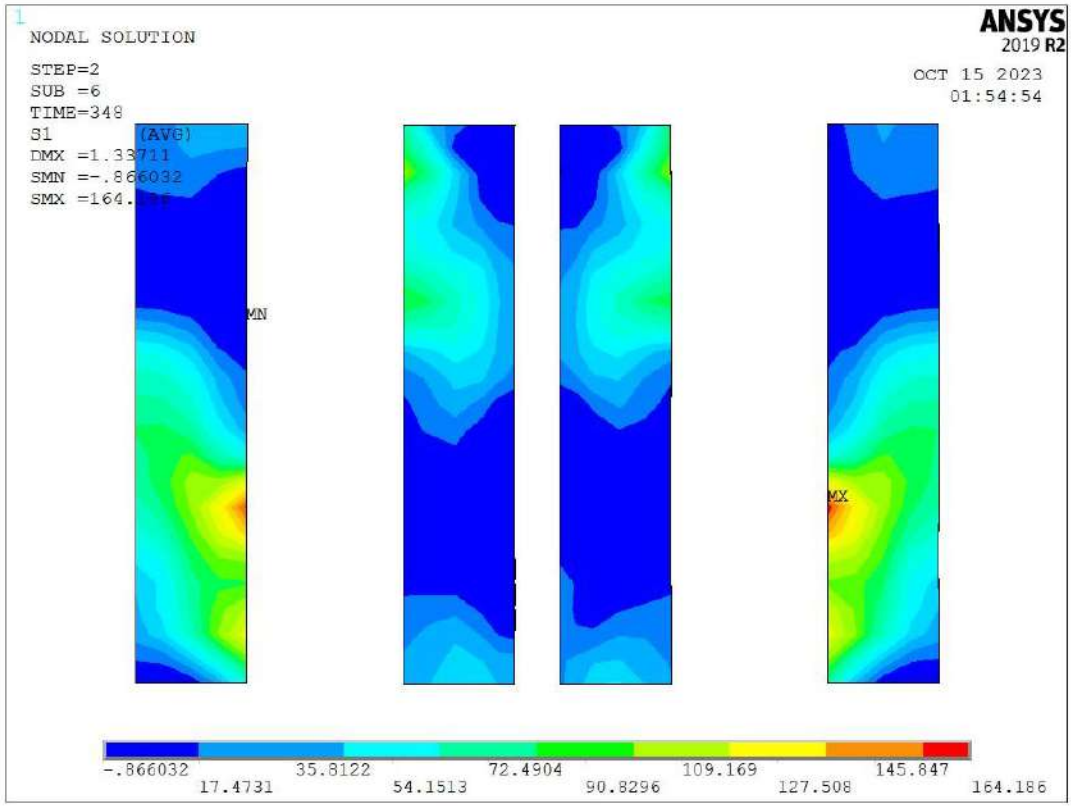

Figure (6-60): Stress in basalt fiber strips at failure for beam B10

6.6.9 Maximum Stress in BFRP Strips at B11

Figure (6-61) shows the stresses in basalt strips for deep beam B11, from this figure it can see that stress in the sheet at top of the openings have a concentration in the middle of the beam unlike the basalt sheet at the bottom of the openings, it has a stress concentration at the edges of the beam not in the middle of it with a maximum value of 203.4 MPa at the bottom sheet and a minimum value of -1.2 MPa that means that the sheet at the top of opening has a tension stress in the middle and compression with a small value at the outer edge of the sheet ,while the sheet at bottom of the openings the stresses are tension in the outer of the sheet and compression with a small value in the middle of the sheet.

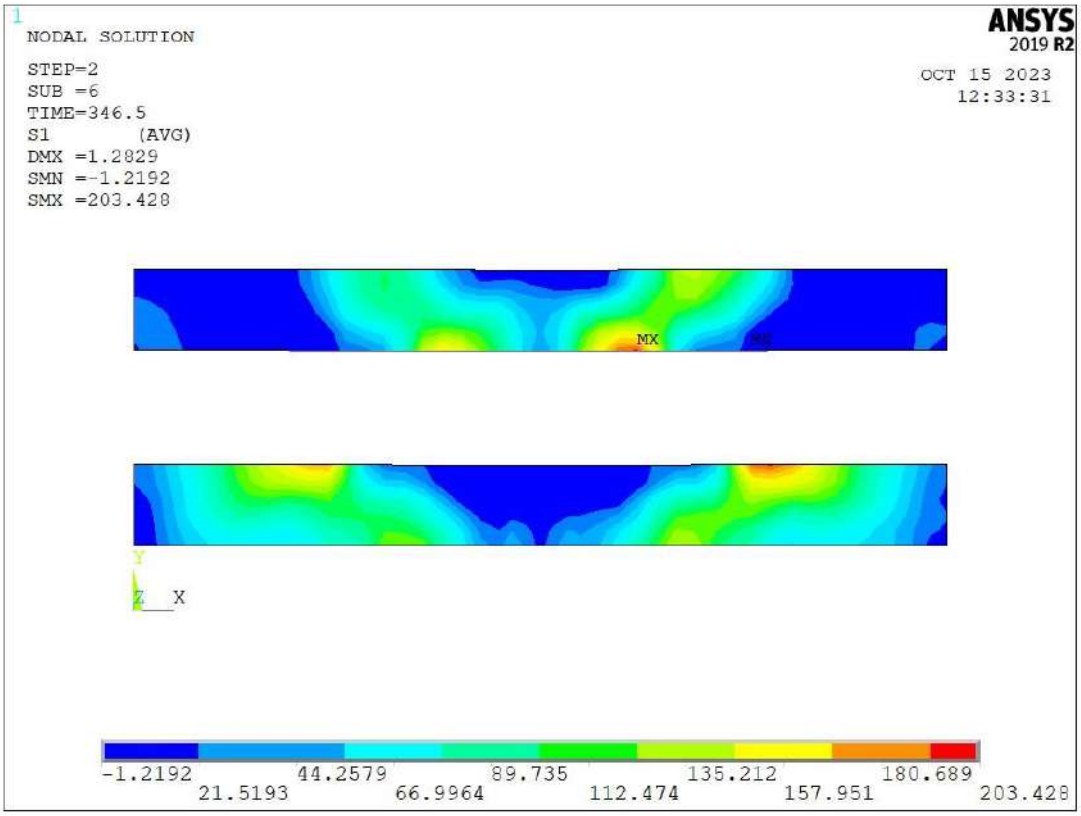

Figure (6-61): Stress in basalt fiber strips at failure for beam B11

6.7 Strain in BFRP strips

6.7.1 Strain in BFRP Strips of B2

Figure (6-62) show the strain distribution at failure of deep beam B2 which is strengthened by horizontal basalt fiber strips, by studying this figure it can see that distribution of strain is similar to the distribution of stress in the basalt fiber strips. At the top strips, the strain concentrated at the middle of the sheet while in the bottom sheet, the strain concentrated at the outer of the sheet with a maximum value of 0.013 that means that the basalt sheet doesn't reach to its full capacity where the elongation at failure is 0.025.

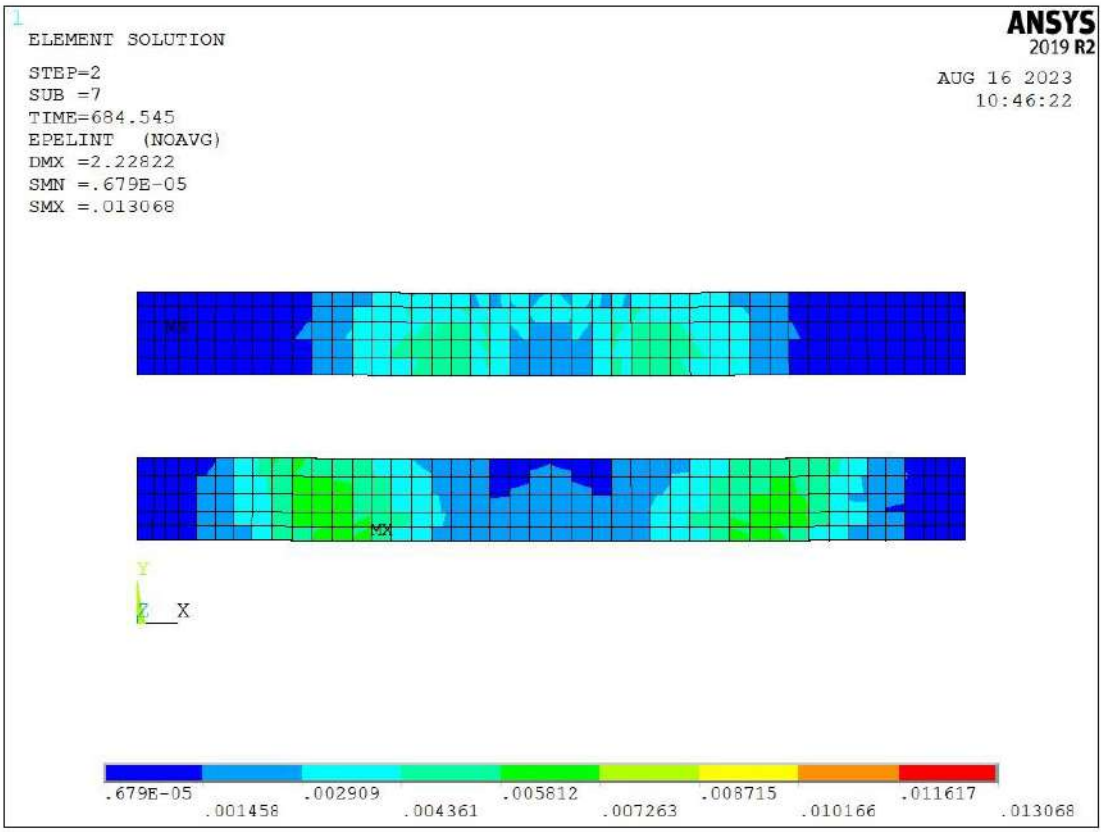

Figure (6-62): Strain in basalt fiber strips at failure for beam B2

6.7.2 Strain in BFRP Strips of B4

Figure (6-63) show the strain distribution at failure of deep beam B4 at x-direction and y-direction, by studying this figure it can see that distribution of strain is similar to the distribution of stress in the basalt fiber strips with a maximum value of 0.015 in x- direction and a maximum value of 0.01 in y-direction that means that the basalt sheet doesn't reach to its full capacity where the elongation at failure is 0.025.

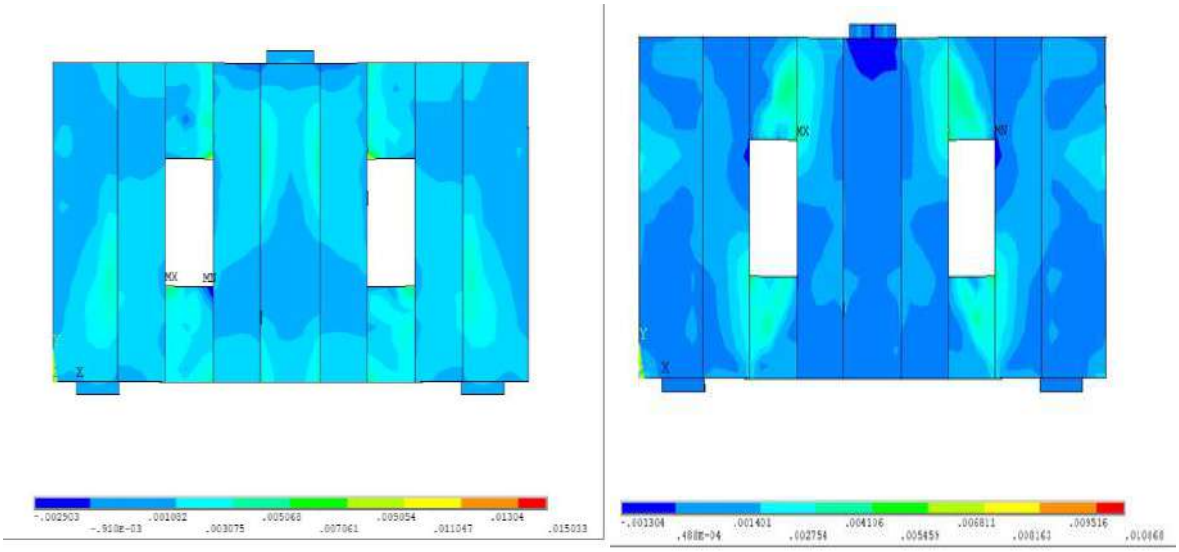

(a): strain in x- direction (b): strain in y- direction

Figure (6-63): Strain in basalt fiber strips at failure for beam B4

6.7.3 Strain in BFRP Strips of B4

Figure (6-64) show the strain distribution at failure of deep beam B5 at x-direction and y-direction, by studying this figure it can see that distribution of strain is similar to the distribution of stress in the basalt fiber strips with a maximum value of 0.003 in x- direction and a maximum value of 0.001 in y-direction that means that the basalt sheet doesn't reach to its full capacity where the elongation at failure is 0.025.

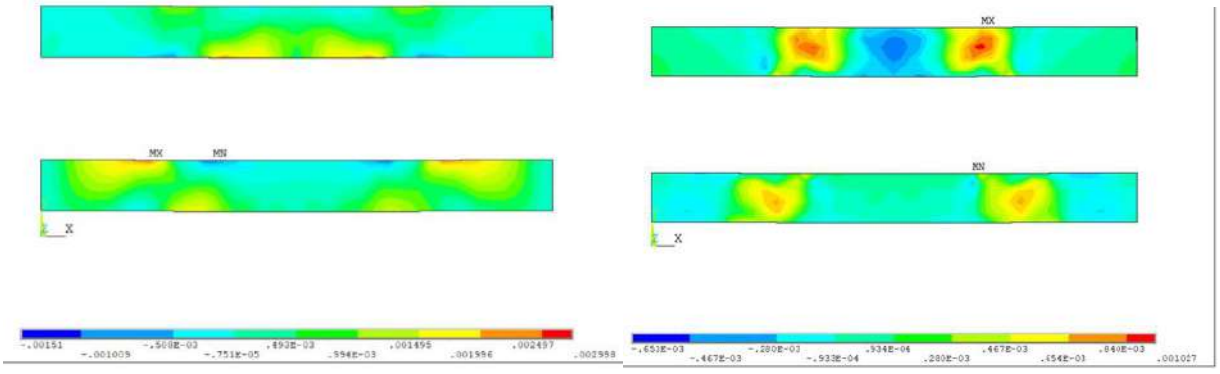

(a): strain in x- direction (b): strain in y- direction

Figure (6-64): Strain in basalt fiber strips at failure for beam B5

6.7.4 Strain in BFRP Strips of B6

Figure (6-65) show the strain distribution at failure of deep beam B5 at x-direction and y-direction, by studying this figure it can see that distribution of strain is similar to the distribution of stress in the basalt fiber strips with a maximum value of 0.002 in x- direction and a maximum value of 0.0027 in y-direction that means that the basalt sheet did not reach its full capacity in y-direction where the elongation at failure is 0.025.

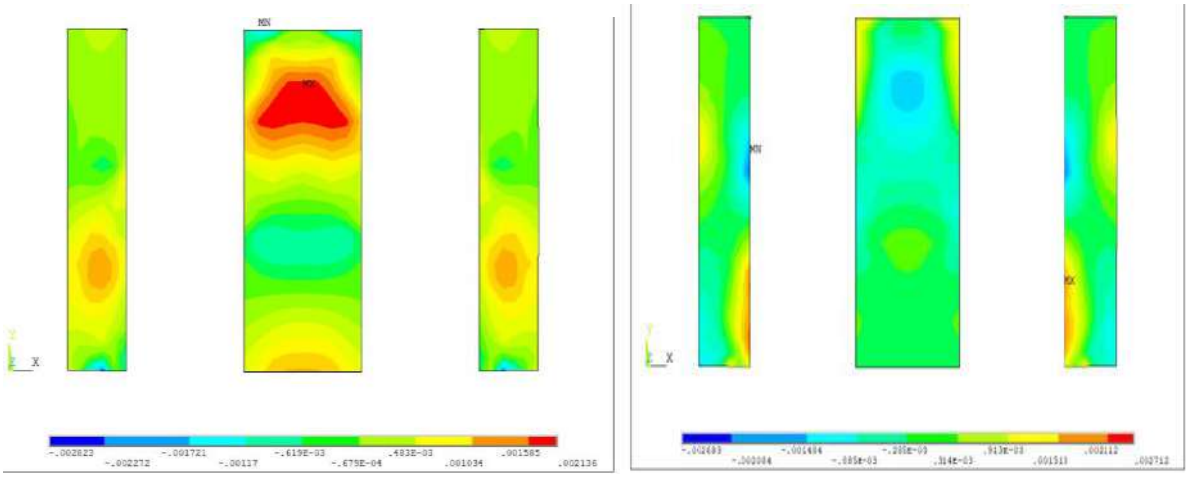

(a): strain in x- direction (b): strain in y- y-direction

Figure (6-65): Strain in basalt fiber strips at failure for beam B6

6.7.5 Strain in BFRP Strips of B7

Figure (6-66) show the strain distribution at failure of deep beam B7 at x-direction and y-direction, by studying this figure it can see that distribution of strain is similar to the distribution of stress in the basalt fiber strips with a maximum value of 0.0049 in x- direction and a maximum value of 0.001 in y-direction that means that the basalt sheet reaches to its full capacity in y-direction where the elongation at failure is 0.025.strain at x- direction is bigger than the strain at y- direction by 4.9.

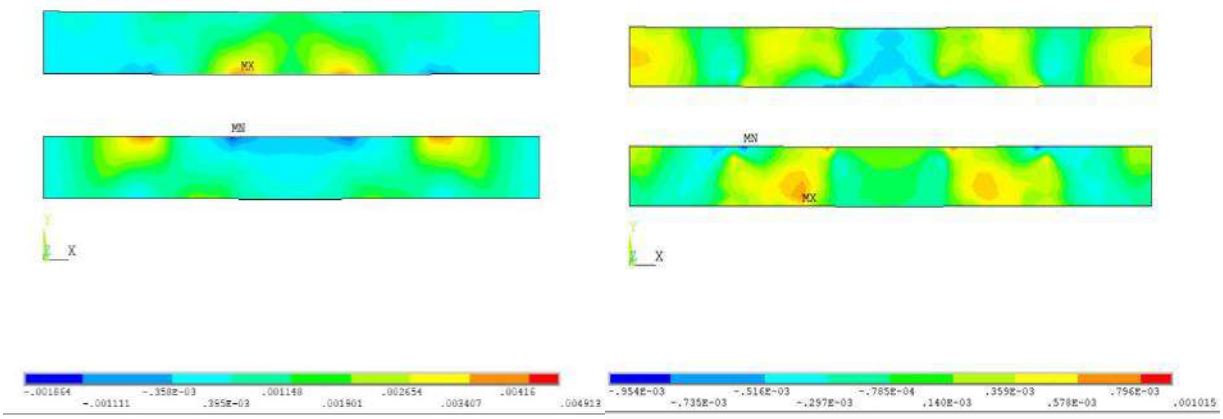

(a): strain in x- x-direction (b): strain in y- direction

Figure (6-66): Strain in basalt fiber strips at failure for beam B7

6.7.6 Strain in BFRP Strips of B8

Figure (6-67) show the strain distribution at failure of deep beam B8 at x-direction and y-direction, by studying this figure it can see that distribution of strain is similar to the distribution of stress in the basalt fiber strips with a maximum value of 0.001in x- direction and a maximum value of 0.0024 in y-direction that means that the basalt sheet reaches to its full capacity in y-direction where the elongation at failure is 0.025.strain at y- direction is bigger than the strain at x- direction by 2.4

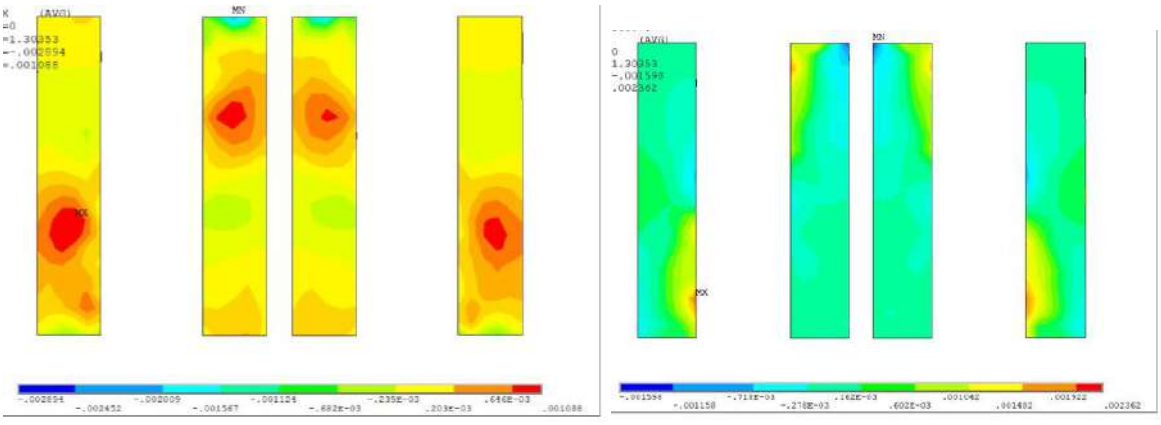

(a): strain in x- direction (b): strain in y- direction

Figure (6-67): Strain in basalt fiber strips at failure for beam B8

6.7.7 Strain in BFRP Strips of B9

Figure (6-68) shows the strain distribution at failure of deep beam B9 at x-direction and y-direction, by studying this figure it can see that distribution of strain is similar to the distribution of stress in the basalt fiber strips with a maximum value of 0.0033 in x- direction and a maximum value of 0.0008 in y-direction that means that the basalt sheet reaches to its full capacity in y-direction where the elongation at failure is 0.025.strain at x- direction is bigger than the strain at y- direction by 4.12.

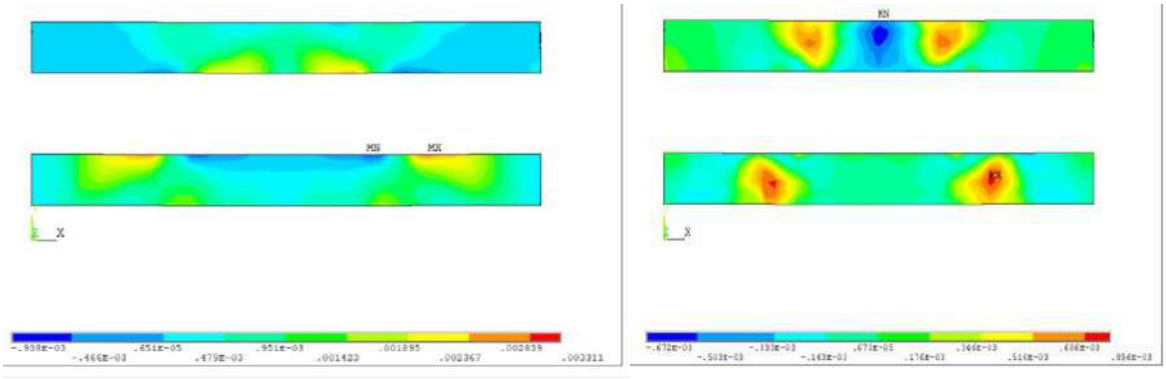

(a): strain in x- direction (b): strain in y- direction

Figure (6-68): Strain in basalt fiber strips at failure for beam B9

6.7.8 Strain in BFRP Strips of B10

Figure (6-69) show the strain distribution at failure of deep beam B8 at x-direction and y-direction, by studying this figure it can see that distribution of strain is similar to the distribution of stress in the basalt fiber strips with a maximum value of 0.001in x- direction and a maximum value of 0.003 in y-direction that means that the basalt sheet reaches to its full capacity in y-direction where the elongation at failure is 0.025.strain at y- direction is bigger than the strain at x- direction by 3 times.

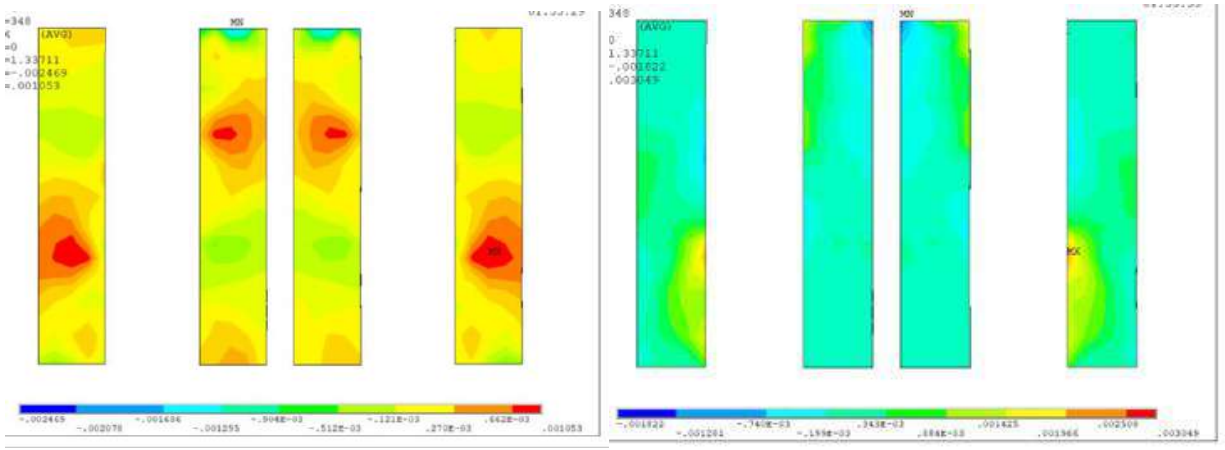

(a): strain in x- direction (b): strain in y- direction

Figure (6-69): Strain in basalt fiber strips at failure for beam B10

6.7.9 Strain in BFRP Strips of B11

Figure (6-70) show the strain distribution at failure of deep beam B9 at x-direction and y-direction, by studying this figure it can see that distribution of strain is similar to the distribution of stress in the basalt fiber strips with a maximum value of 0.0039 in x- direction and a maximum value of 0.001 in y-direction that means that the basalt sheet didnot reaches to its full capacity, Strain at x- direction is bigger than the strain at y- direction by 3.9 times.

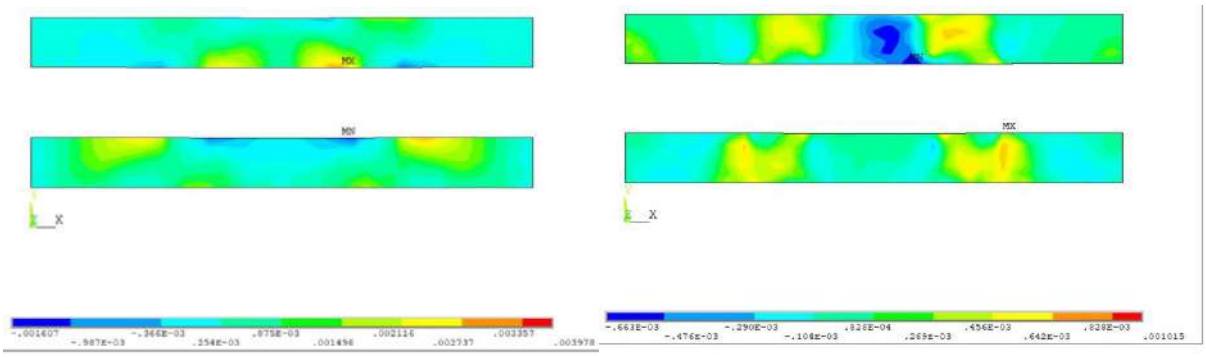

(a): strain in x- direction (b): strain in y- direction

Figure (6-70): Strain in basalt fiber strips at failure for beam B11

6.8 Analytical Model for Shear Strength Prediction

A technique for analysis that predicts the shear strength and accordingly the ultimate load of RC deep has been developed in this chapter

6.8.1 Prediction of Maximum Load in Solid Deep Beams

Equations used to predict the ultimate load in solid deep beams according to ACI-318 [5] are as follows:

$$P_u = 2 * vn \quad (6.2)$$

$$vn = fce * \sin\theta s * bw * ws + A_h * F_{yh} * \tan\theta s + A_v * F_{yv} \quad (6.3)$$

p_u is the ultimate load expected in solid deep beams.

vn: is the shear strength of deep beams.

$$\text{where } fce = 0.85\beta s \ fc' \quad (6.4)$$

fc: concrete compressive strength, *θs:* angle of strut according to x-axis, *wt* : twice concrete cover as illustrated in figure (6-71), *bw*: width of the beam section

$$ws = min\,[(wt\cos\theta s + wb\sin\theta s), (hc\cos\theta s + wb\sin\theta s)] \quad (6.5)$$

wb: width of bearing plate, A_h and A_v are the horizontal and vertical web reinforcement areas embedded within the effective width respectively. F_{yh} and F_{yv} are the yield stress of the horizontal and vertical web reinforcement respectively.βs for bottle-shaped struts with reinforcement satisfying Section A.3.3 of ACI 318-08 as shown in Table (6-2)

Table (6-2): values of ***βs***

1.00	For prismatic struts in uncracked compression zones
0.40	For struts in tension members
0.75	Struts may be bottle shaped and crack control reinforcement is included
0.60	Struts may be bottle shaped and crack control reinforcement is not included
0.60	For all other cases

Notes:
Crack control reinforcement requirement is $\sum \rho vi \sin \gamma i \leq 0.003$, where

ρvi = steel ratio of the *i*-th layer of reinforcement crossing the strut under review, and γi = angle between the axis of the strut and the bars.

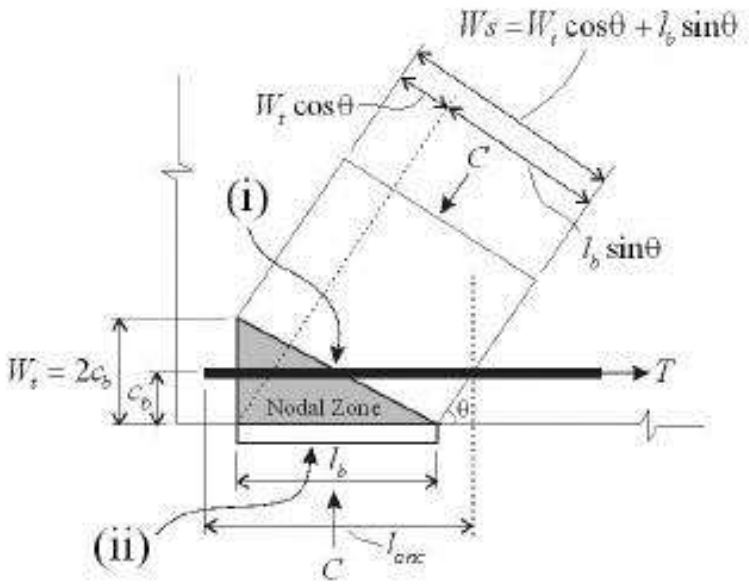

Figure (6-71): Illustration of terms in equation

6.8.2 Prediction of Maximum Loads in Deep Beams with Openings Strengthened with BFRP Strips

Pu expected = 2(Vf + Vc +Vsd+Vsw) (6.6)

Where Vf = contribution of BFRP strips to the shear strength. it has been applied using the properties of basalt fibers from testing three specimens of strips roughed with sand to simulate the contact of basalt and concrete, Vc = contribution of concrete to shear strength, Vsd = contribution of tension steel to shear strength, and Vsw is the contribution of web steel to shear strength Equations from (6.7) to (6.17) are listed in the **ACI-440 Code, 2014[83]**

$$vf = \frac{Avf * ffe * (\sin\alpha + cos\alpha) * dvf}{\text{sf}} \quad (6.7)$$

Where Avf is the area of FRP strip within spacing (sf) given by Eq. (6.8), ffe is the effective stress in FRP strip given by Eq. (6.9), α is the angle of FRP strip orientation about x- axis, dfv is the effective depth of FRP strip (distance from center of flexural reinforcement to the extreme fiber of strip, sf is the spacing center to center between strips in the direction perpendicular to BFRP strips.

$$Avf=2*n*tf*wf \quad (6.8)$$

Where n is number of layers,tf is the FRP strip thickness (mm), wf is the FRP strip width (mm)

$$ffe=\varepsilon fe*Ef \quad (6.9)$$

εfe is the effective strain in FRP strip given by Eq. (6.10), Ef is the modulus of elasticity of FRP strip (MPa)

$$\varepsilon fe=kv*\varepsilon fu\leq 0.004 \quad (6.10)$$

εfu is the rupture strain of FRP strip given by Eq. (6.11), kv is the bond dependent coefficient given by Eq. (6.12)

$$\varepsilon fu = \frac{ffu}{Ef} \quad (6.11)$$

ffu is the ultimate tensile strength of FRP strip (MPa)

$$Kv= \frac{K1*K2*Le}{11900\varepsilon fu} \quad (6.12)$$

K1 is the modified concrete factor given by Eq. (6.13),K2 is the modified FRP scheme factor given by Eq. (6.14), Le is the active bond length of FRP strip given by Eq. (6.15)

$$K1= \left(\frac{fc}{27}\right)^{2/3} \quad (6.13)$$

$$K_2=\frac{dfv-2le}{dfv} \quad \text{for two sides bonded} \quad (6.14\text{-a})$$

$$K_2=\frac{dfv-le}{dfv} \quad \text{for U-wrapped bonded} \quad (6.14\text{-b})$$

$$L_e=\frac{23300}{(nf*tf*Ef)0.58} \quad (6.15)$$

n_f is the modular ratio of elasticity given by Eq. (6.16)

$$n_f=\frac{Ef}{EC} \quad (6.16)$$

E_c is the modulus of elasticity of concrete given by Eq. (6.17)

$$E_c=4700\sqrt{f'c}(\text{MPa}) \quad (6.17)$$

6.8.2.1 Determination of Terms Vc, Vsd, and Vsw for Deep Beams with Opening by ASCE-ACI Practice [71], [72]

the simplified design expression for the strength of the beam with web openings can be written as

$$Vc=0.1\ f'c(\lambda 1)(\lambda 2)(\lambda 3)*b*D \quad (6.18)$$

where fc' = cylinder compressive strength of the concrete, which is assumed equal to 0.8 fcu, where fcu is the cube strength of concrete,

$$Vsd=\psi s\ As\ fsy\ \left(\frac{\tan\beta\ tan\varphi-1}{\tan\beta+\tan\varphi}\right) \quad (6.19)$$

β= angle of inclination of critical load path with horizontal

$$tan\varphi=\frac{f'c-\text{fct}}{2\sqrt{f'c}*fct} \quad (6.20)$$

$$Vsw=\psi w\ Kw\ \Sigma Aw\ fwy$$

Kw = 0.85 (for a horizontal web bar); cot ß (for a vertical web bar); and 1.15 (for inclined web bar)

The equations of the coefficients λ1, λ2, λ3, ψ_s and ψ_w are as follows

$$\lambda 1=\left(1-\frac{1}{3}\left(\frac{K1XN}{K2D}\right)\right) \text{ for } \left(\frac{K1XN}{K2D}\right)\leq 1 \quad (6.21)$$

$=\frac{2}{3}$ for $\left(\frac{K1XN}{K2D}\right)\geq 1$, where K_1X_N and K_2D are illustrated in Figure (6-72)

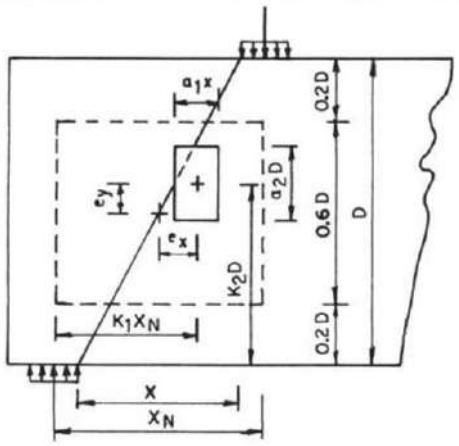

Figure (6-72): Typical position of an opening intercepting natural load path, **Ray S.P.)[24]**

$$\lambda 2=(1-\frac{\mathrm{ax}}{2X})(1-\frac{ay}{1.2h}) \quad (6.22)$$

where ax an ay are the dimensions of opening in x-direction and y-direction respectively,X is distance shear span

$$\lambda_3= (0.85\pm0.3(\frac{\mathrm{ex}}{Xnet}))(0.85\pm0.3(\frac{\mathrm{ey}}{ynet})) \quad (6.23)$$

where $e_x \leq X_N /4$, $e_y \leq 0.6D /4$, and $X_{net} =(X_N-a_1x)$, $Y_{net} =(0.6D-a_2D)$

Table (6-3) has presented a comparison between the analytical and experimental results. It can be concluded that the analytical model is nearly the same as the experimental result in reference deep beam(B1) which isn't strengthened with BFRP,Also B3 has been analyzed and the model give nearly the same of experimental result so we could expect the ultimate load for other types of openings (horizontal, circular, and square).In the beam (B4) ,the ultimate load could not reach its full shear strength predicted by the analytical model. This is because this beam failed untimely by rotation of three distinct segments in the shear span. deep beams strengthened vertically by BFRP (B4,B6,B8 and B10) For these specimens, the ratio of the experimental to analytical shear strength was in the range of 0.75–0.97. This suggests that a strength reduction factor of 0.8 should be adopted for strengthen RC deep beams with vertical BFRP to account for a possible change in the mode of failure. The ratio of the experimental to analytical strength of all horizontally strengthened specimens varied between 0.7 and 0.88. This suggests that a strength reduction factor of 0.8 should be adopted for strengthening RC deep beams with horizontal BFRP to account for a possible change in the mode of failure. it can be stated that the analytical procedure can give reasonable shear strength prediction for RC deep beams with openings strengthened with BFRP strips.

Table (6-3): Comparison between experimental and expected loads

Beam specimen	Experimental ultimate load Pu (kN)	Pu expected for non-strengthened beam (KN)(1)	Vf (kN)	Increase in ultimate load [2]	Total load expected. 1+2	exp. /expected.
B1	451.7	455.3	-	-	455.3	0.99
B2	636.3	455.3	107.4	214.7	670	0.95
B3	298.5	304.3	-	-	304.3	0.99
B4	298.5	304.3	48.3	96.6	400.9	0.74
B5	360	304.3	71.58	143.168	447.5	0.8
B6	353.9	304.3	32.2	64.4	368.7	0.96
B7	456.82	304.2	107.3	214.75	518.95	0.88
B8	307.4	301.5	37.17	74.34	375.8	0.82
B9	322.53	301.5	82.59	165.18	466.7	0.7
B10	312.5	309.5	40.3	80.6	390.1	0.81
B11	356.42	309.5	89.48	178.96	488.4	0.73
				Average		0.85
				Standard deviation		0.1
				Coefficient of variations		0.12

6.9 Parametric study

In this section, we will describe two parametric studies obtained from Ansys as follows, firstly the effect of increasing concrete compressive strength from 25 to 30 MPa and 35 MPa and comparing results with the analytical model for shear strength prediction, the comparison of the results are shown in table (6-5), also studying the effect of increasing concrete compressive strength is discussed by drawing stress-strain curves for different concrete compressive strength from ANSYS and the curve from experimental results. the second parameter is the effect of increasing the number of layers of BFRP sheets from two layers to four and six layers with constant concrete compressive strength 25MPa and comparing the results with the analytical model prediction as shown in table (6-6).

6.9.1 Effect of Increasing Concrete Compressive Strength

Figures from (6-73) to (6-84) show the load-deflection relationships of all deep beams from B1 to B11.from these figures it can concluded that increasing the concrete compressive strength affects slightly the failure capacity of solid deep beams and deep beams with openings, in solid deep beams failure load increased by 9.1 and 2.2 when the concrete compressive strength increased from 25 to 30, and from 30 to 35 respectively. In deep beams with vertical openings, the failure load increases by 21% and 22% when the concrete compressive strength increases from 25 to 30 and from 30 to 35 respectively. In the case of vertical strength of openings, when the concrete compressive strength increased from 25 to 30 N/mm^2, the failure loads increased by 19.1,14,19 and 21% for vertical, horizontal, circular and square openings respectively. In the case of vertical strength of openings, when the concrete compressive strength increased from 30 to 35 N/mm^2, the failure loads increased by 12,28.6,16.4 and 15% for vertical, horizontal, circular and square openings respectively. In the case of horizontal strength of openings, when the

concrete compressive strength increased from 25 to 30 N/mm^2, the failure loads increased by 11.3,14.6,22.3 and 14.6% for vertical, horizontal, circular and square openings respectively. In the case of horizontal strength of openings, when the concrete compressive strength increased from 30 to 35 N/mm^2, the failure loads increased by 20.1,18.4,15.5 and 18.5% for vertical, horizontal, circular and square openings respectively.

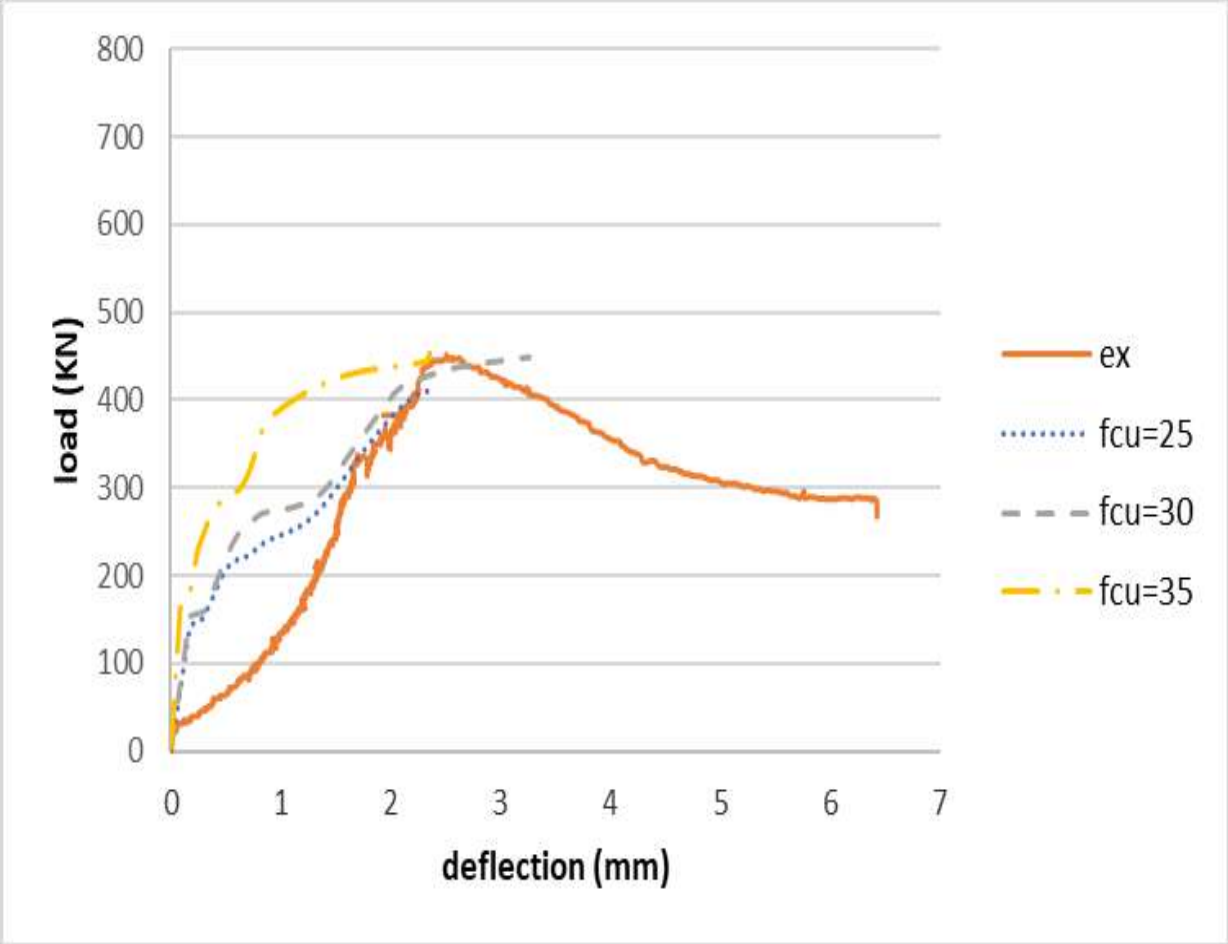

Figure (6-73): Load deflection curves for different values of concrete compressive strength for B1

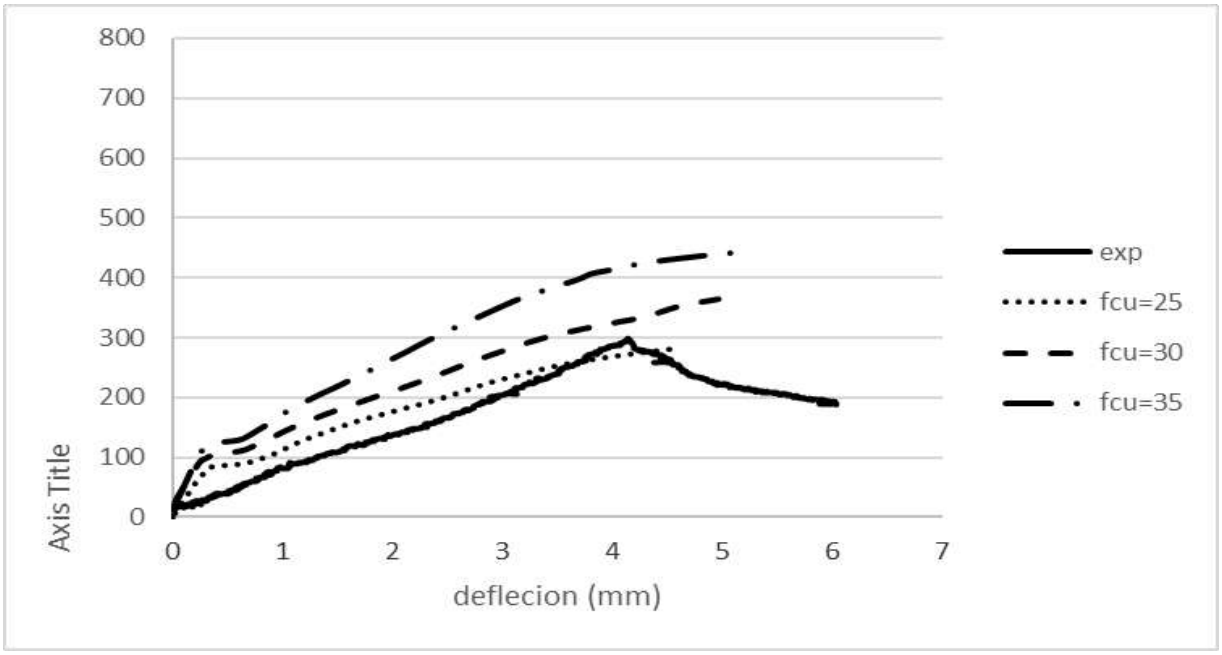

Figure (6-74): Load deflection curves for different values of concrete compressive strength for B3

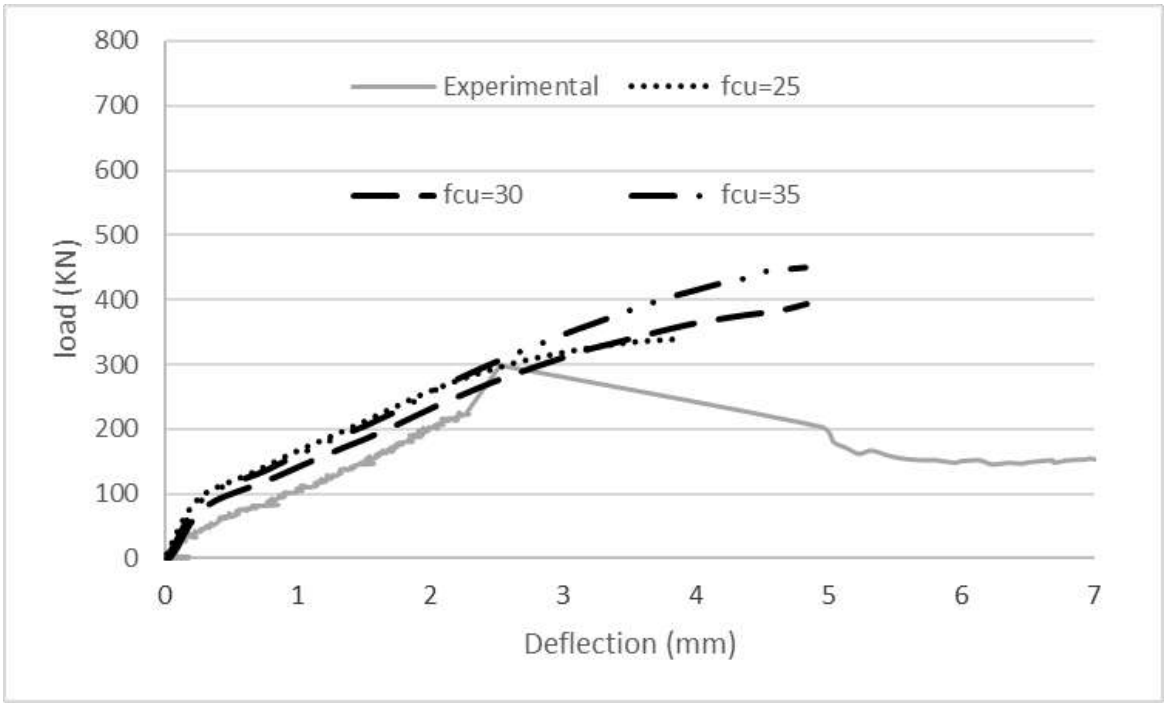

Figure (6-75): Load deflection curves for different values of concrete compressive strength for B4

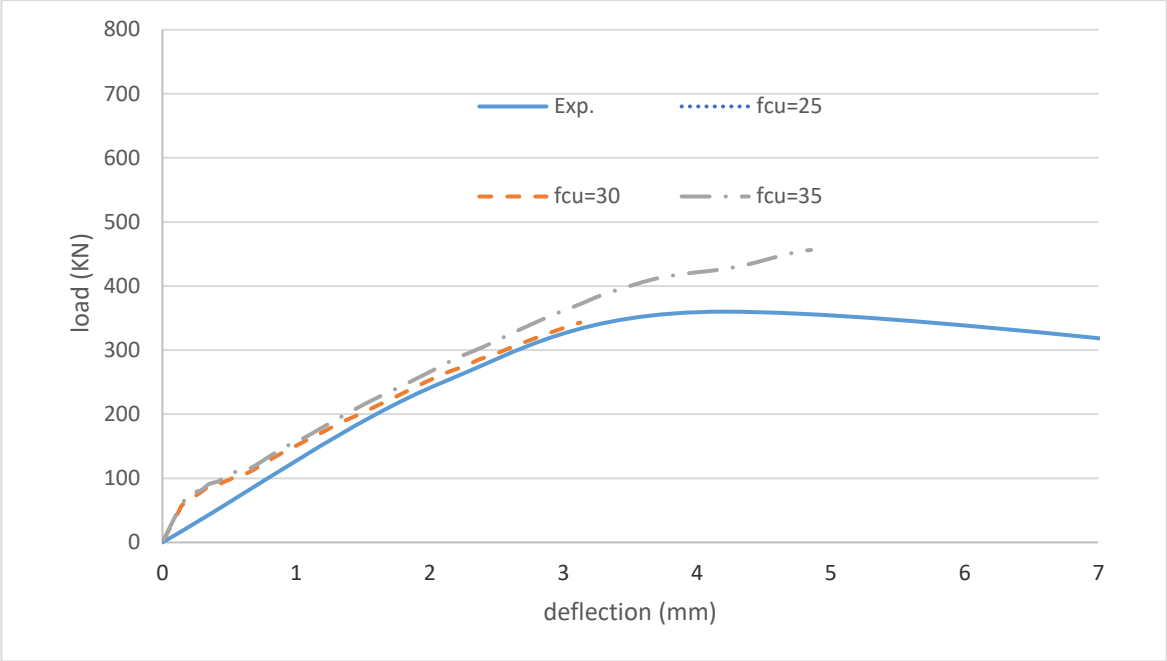

Figure (6-76): Load deflection curves for different values of concrete compressive strength for B5

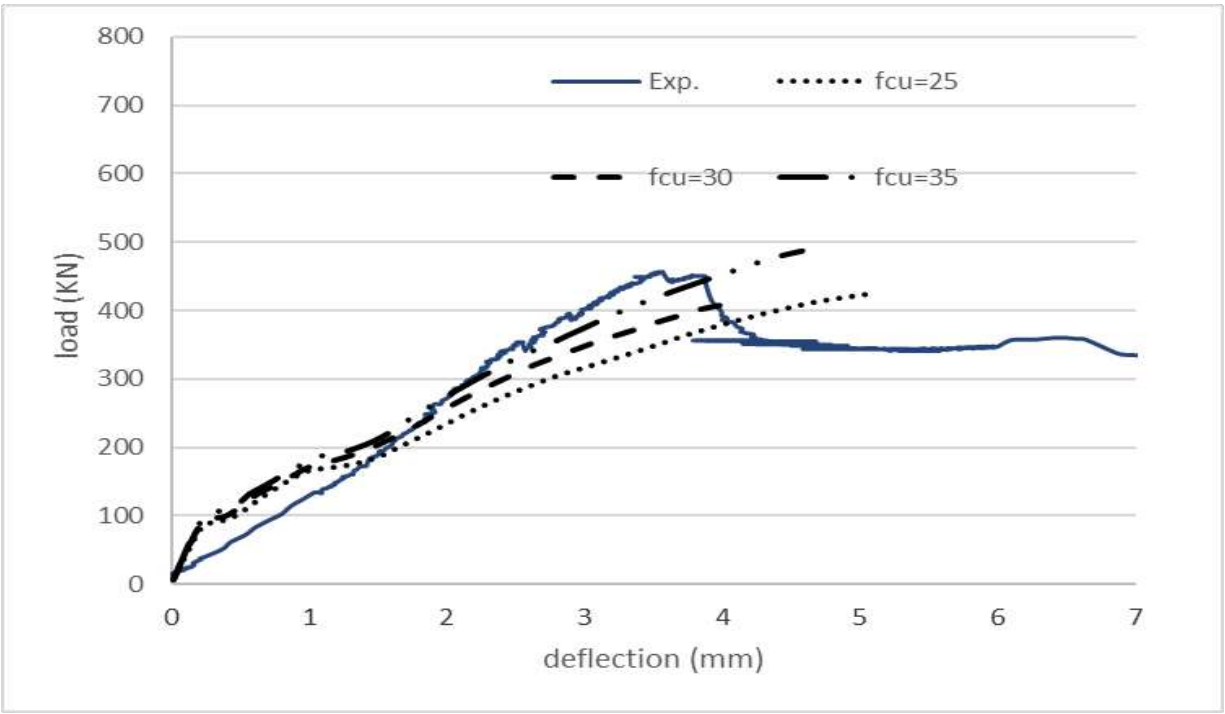

Figure (6-77): Load deflection curves for different values of concrete compressive strength for B7

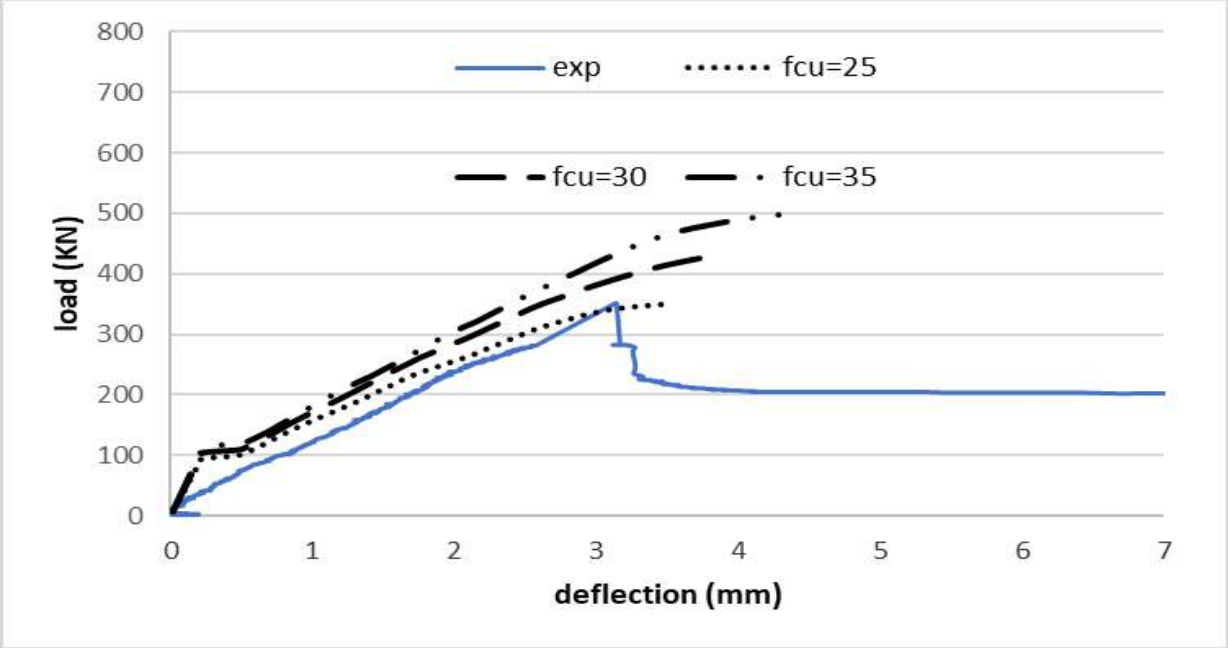

Figure (6-78): Load deflection curves for different values of concrete compressive strength for B8

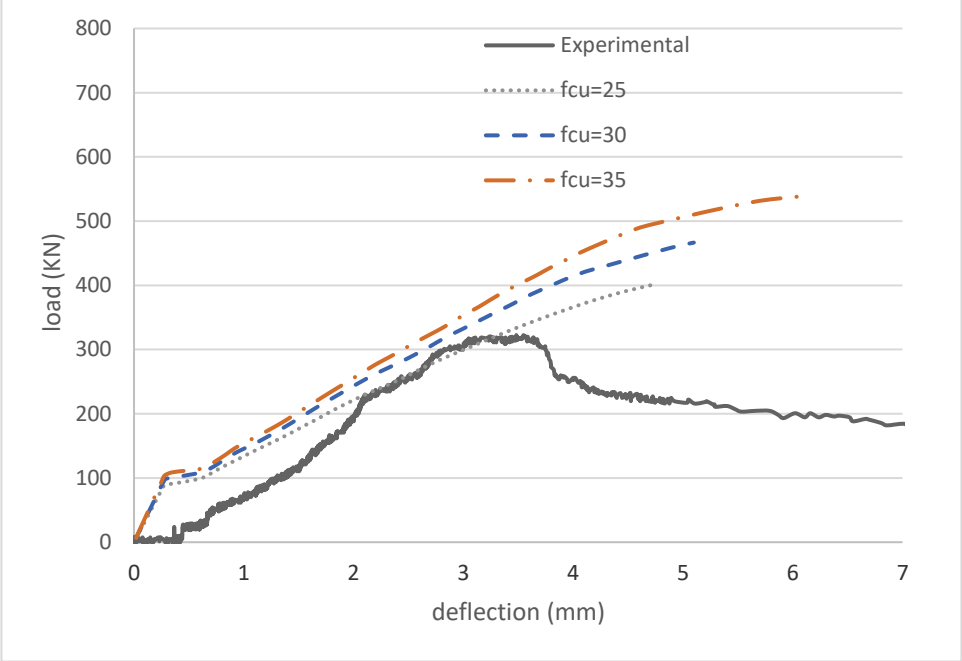

Figure (6-79): Load deflection curves for different values of concrete compressive strength for B9

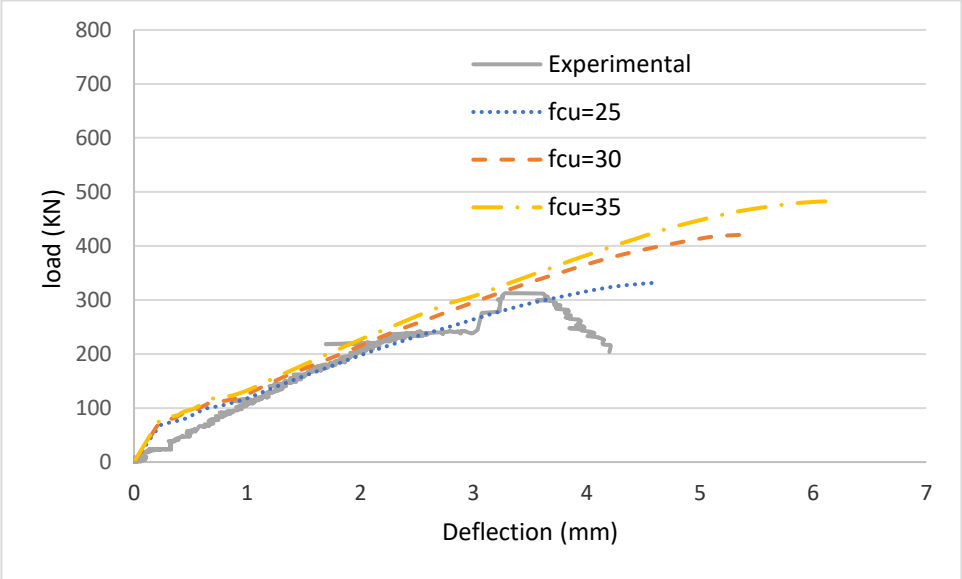

Figure (6-80): Load deflection curves for different values of concrete compressive strength for B10

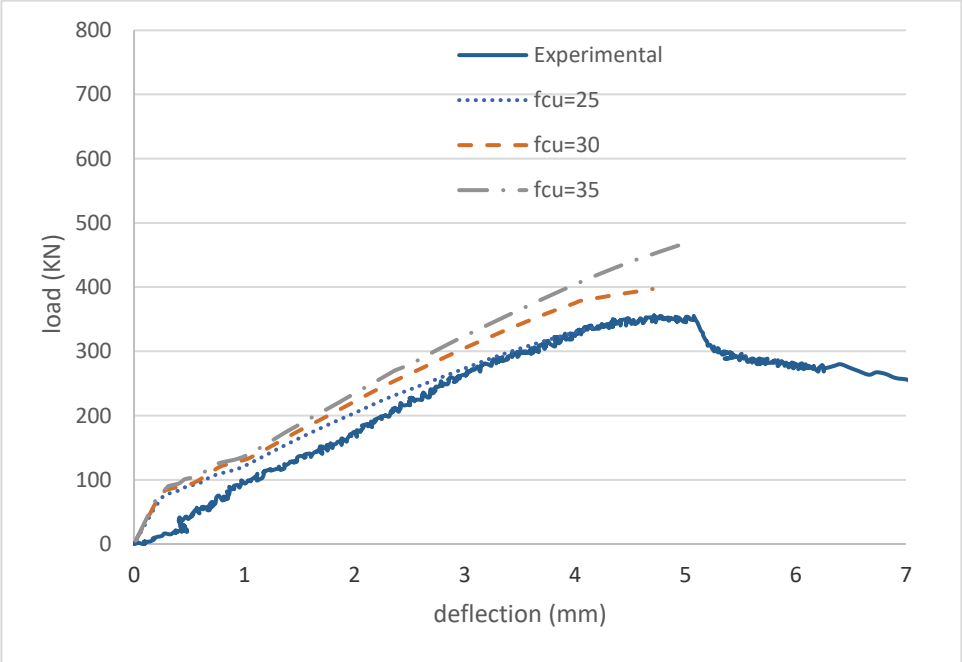

Figure (6-81): Load deflection curves for different values of concrete compressive strength for B11

Figure (6-82) show the values of failure loads for all specimens with different values of concrete compressive strength 25,30 and 35 MPa. from that figure it can see that the increasing concrete compressive strength has high influence on the

capacities of deep beams with opening (B3) whereas the compressive strength increases from 25 MPa to 30MPa, the failure load increases nearly by 21% while the compressive strength increases from 30 MPa to 35MPa, the failure load increases nearly by 22%. while it had less effect on solid deep beam (B1) whereas the compressive strength increases from 25 MPa to 30MPa, the failure load increases by 9.1% while the compressive strength increases from 30 MPa to 35MPa, the failure load increases only by 2.2%. in the case of deep beam with openings strengthened with vertical BFRP, when the compressive strength increases from 25 MPa to 30MPa, the failure load increases by 19.1% while the compressive strength increases from 30 MPa to 35MPa, the failure load increases only by12%. the effect of increasing the compressive strength of concrete in the case of a deep beam with vertical openings strengthened with horizontal BFRP sheets, when the compressive strength increases from 25 MPa to 30MPa, the failure load increases by 11.3% while the compressive strength increases from 30 MPa to 35MPa, the failure load increases by 20%. in the case of a deep beam with horizontal openings strengthened with vertical BFRP sheets, when the compressive strength increases from 25 MPa to 30MPa, the failure load increases by 14% while the compressive strength increases from 30 MPa to 35MPa, the failure load increases by 29%. In B7 when the compressive strength increases from 25 MPa to 30MPa, the failure load increases by 14.6% while the compressive strength increases from 30 MPa to 35MPa, the failure load increases only by 18.4%.By studying B8 it was founded that when the compressive strength increases from 25 MPa to 30MPa, the failure load increases by 19% while the compressive strength increases from 30 MPa to 35MPa, the failure load increases only by 16.4%. In B9 when the compressive strength increases from 25 MPa to 30MPa, the failure load increases by 22.3% while the compressive strength increases from 30 MPa to 35MPa, the failure load increases only by 15.5%. B10 show large effect whereas

the compressive strength increases from 25 MPa to 30MPa, the failure load increases by 21% while the compressive strength increases from 30 MPa to 35MPa, the failure load increases only by 15%. In B11 when the compressive strength increases from 25 MPa to 30MPa, the failure load increases by 14.6% while the compressive strength increases from 30 MPa to 35MPa, the failure load increases only by 18.5%.

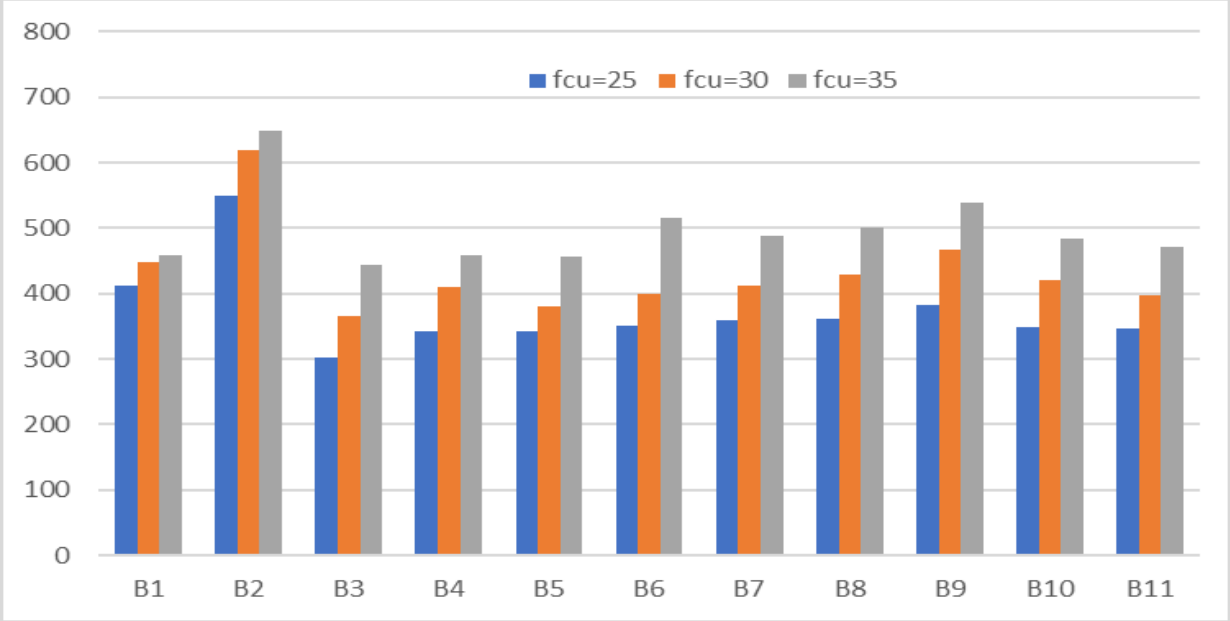

Figure (6-82): Failure loads for all beams with different values of Fcu

Table (6-4) shows a comparison between Ansys results and expected results from equation listed previously. Accuracy for the analytical models is gaged in terms of a load ratio that is defined as the ratio of the measured to the computed loads. The ratio has an average of 0.9, standard deviation of 0.13 and coefficient of variation = 0.14. The statistical results of the predictions of Table (6-4) indicate that the analytical model is reliable

.

Table (6-4): Comparison between Ansys results and expected failure loads.

NO	Symbol	fcu	P ANS (KN)	Pu without strengthening (KN)	VF (KN)	Increasing failure load	Pu expected	$\frac{PA}{PE}$
1	B1	25	428.90	455.30	-	-	455.30	0.94
2	B2	25	618.00	455.30	107.4	214.75	670.05	0.92
3	B3	25	281.40	304.30	-	-	304.30	0.92
4	B4	25	339.00	304.30	48.30	96.60	400.90	0.84
5	B5	25	341.50	304.30	71.60	143.16	447.50	0.76
6	B6	25	341.00	304.20	32.20	64.40	363.70	0.90
7	B7	25	363.60	304.20	107.60	214.75	514.00	0.80
8	B8	25	355.00	301.50	37.20	74.20	376.10	0.90
9	B9	25	401.00	301.50	82.60	165.18	467.10	0.80
10	B10	25	320.25	309.50	40.30	80.60	385.95	0.80
11	B11	25	339.00	309.50	89.50	178.96	484.30	0.70
12	B1	30	448.90	524.00	-	-	-	0.86
13	B2	30	618.00	524.00	127.10	254.20	778.20	0.79
14	B3	30	364.50	337.00	-	-	337.00	1.08
15	B4	30	408.90	337.00	57.20	114.40	448.40	0.91
16	B5	30	380.00	337.00	84.70	169.51	506.50	0.75
17	B6	30	400.00	337.00	38.10	76.30	413.30	0.97
18	B7	30	423.00	337.00	127.10	254.20	591.20	0.71
19	B8	30	429.50	333.60	44.00	88.00	421.60	1.02
20	B9	30	466.50	333.60	97.80	195.50	529.10	0.88
21	B10	30	420.50	343.10	47.70	95.40	438.50	0.96
22	B11	30	397.00	343.10	105.90	211.90	555.00	0.71
23	B1	35	458.90	592.69	-	-	592.70	0.77
24	B2	35	647.85	592.69	146.50	293.10	885.50	0.73
25	B3	35	444.50	367.10	-	-	367.10	1.21
26	B4	35	457.50	367.10	65.90	131.90	499.00	0.92
27	B5	35	456.25	367.10	97.70	195.40	562.50	0.81
28	B6	35	514.50	367.10	44.00	88.00	455.10	1.13
29	B7	35	487.30	367.10	146.50	293.10	660.20	0.74
30	B8	35	500.00	363.20	50.70	101.51	464.70	1.07
31	B9	35	539.00	363.20	112.70	225.50	588.70	0.91
32	B10	35	483.00	374.30	54.90	109.90	483.80	1.00
33	B11	35	470.50	374.30	122.13	244.30	618.60	0.76
						Average		0.9
						Standard deviation		0.13
						Coefficient of variation		0.14

6.9.2 Effect of increasing number of layers

6.9.2.1 Effect of Increasing Number of Layers for B2

Increasing the number of layers in solid deep beams strengthened with horizontal BFRP from two layers to three layers increases the failure loads by 9% while increasing number of layers from three layers to four layers decreases the failure load by 34%. This is because the failure was strut crushing and the beam become over reinforced, that is the beam need to increase the compressive strength from 25MPa to 30 or 35MPa. Figure (5-83) shows the values of failure loads for different number of layers.

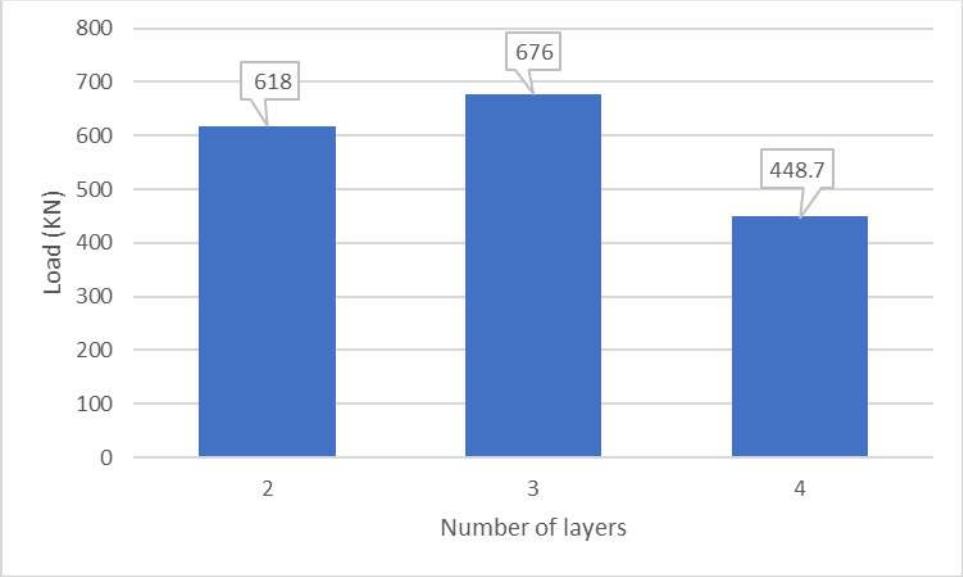

Figure (6-83): The values of failure loads for different numbers of layers for B2

6.9.2.2 Effect of Increasing the Number of Layers for B4

Increasing the number of layers in deep beams with vertical openings strengthened with vertical BFRP from two layers to four layers increases the failure loads only by 7% while increasing the layers from four layers to six layers increases the failure load by 3%. These results show that increasing number of layers did not affect on the failure capacity of the deep beam with vertical opening. that is the beam need

to increase the compressive strength from 25MPa to 30 or 35MPa. Figure (5-84) shows the values of failure loads for different number of layers for B4.

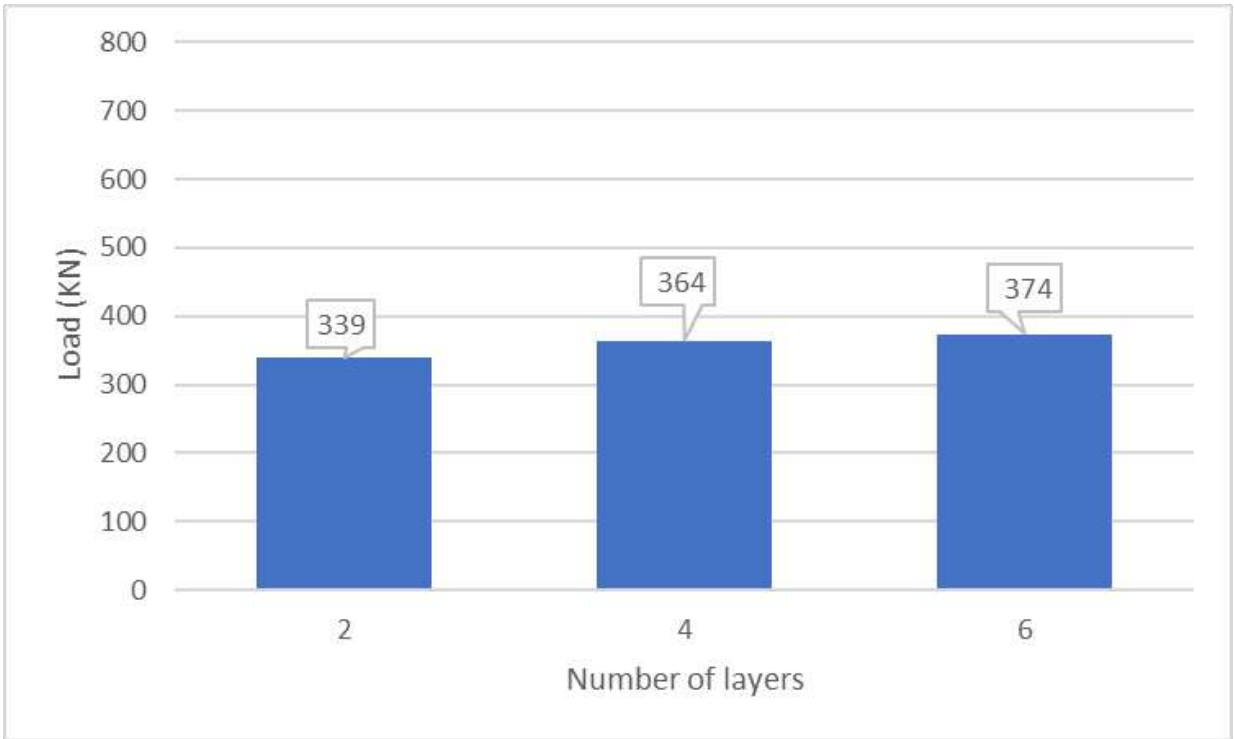

Figure (6-84): The values of failure loads for different number of layers for B4

6.9.2.3 Effect of Increasing the Number of Layers for B5

In this specimen ANSYS couldn't complete the run using a compressive strength of 25 MPa, so we use a compressive strength of 35 MPa to show the effect of increasing the number of layers. Increasing the number of layers in deep beams with vertical openings strengthened with horizontal BFRP from two layers to four layers increases the failure loads only by 3.4% while increasing the failure layers from three layers to four layers decreases the failure load by 34%. This is because the failure was strut crushing and the beam become over reinforced, that is the beam need to increase the compressive strength from 35MPa to 40 or 45MPa or trying using high strength concrete. Figure (6-85) shows the values of failure loads for different number of layers for B5.

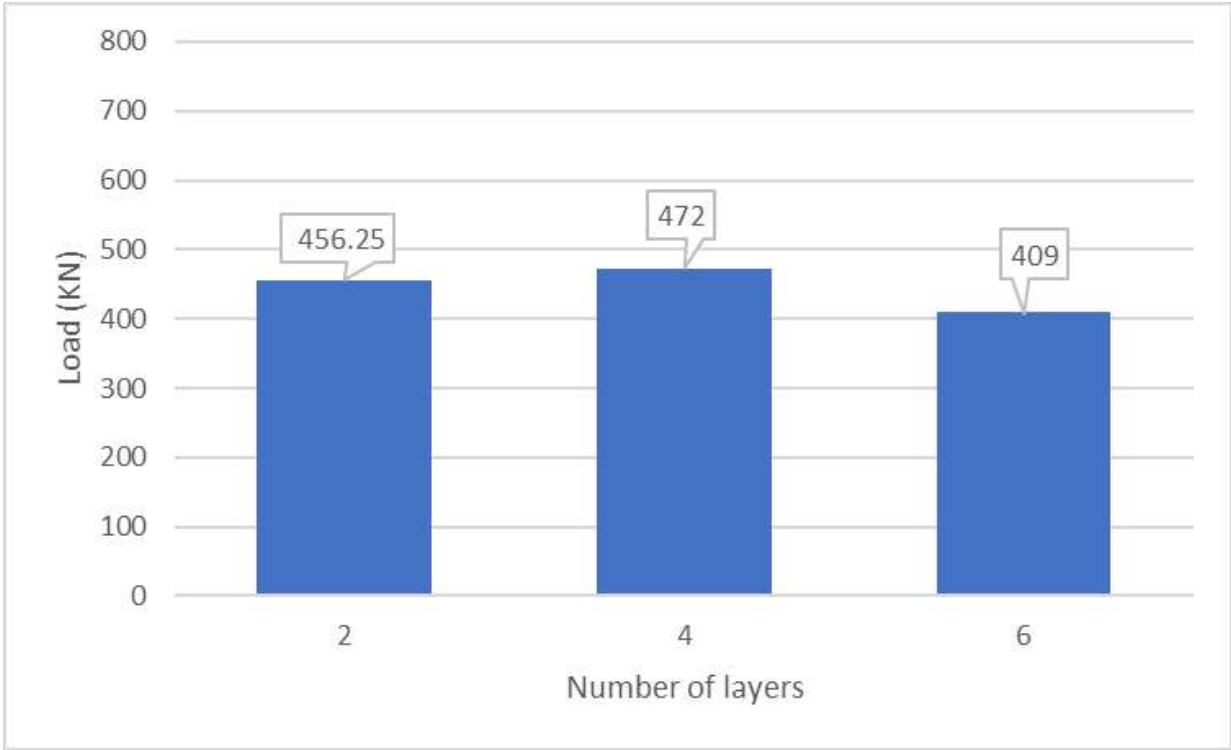

Figure (6-85): The values of failure loads for different number of layers for B5

6.9.2.4 Effect of Increasing the Number of Layers for B6

Increasing the number of layers in deep beams with horizontal openings strengthened with vertical BFRP from two layers to four layers increases the failure loads only by 1% while increasing the layers from four layers to six layers increases the failure load by 4%. These results show that increasing number of layers did not affect on the failure capacity of the deep beam with vertical opening. that is the beam need to increase the compressive strength from 25MPa to 30 or 35MPa. Figure (6-86) shows the values of failure loads for different number of layers for B6.

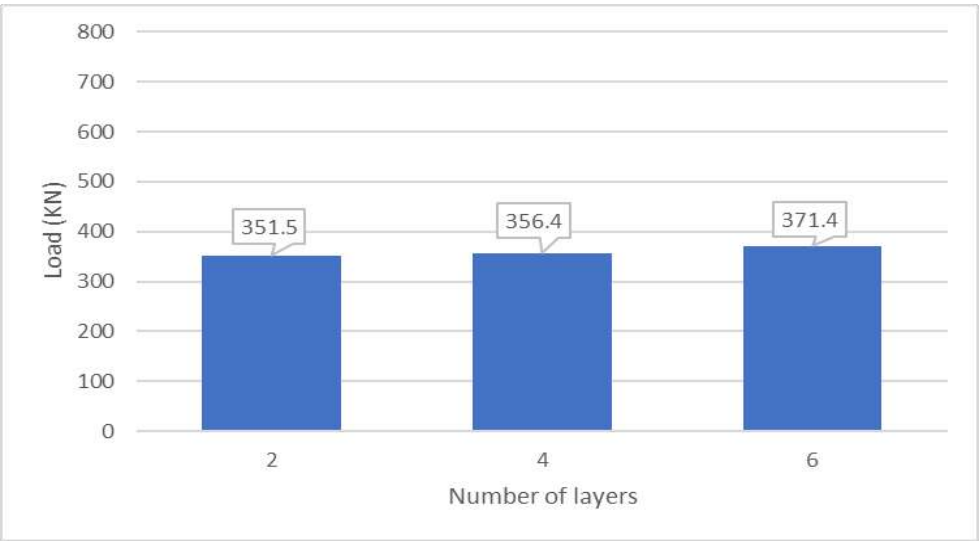

Figure (6-87): The values of failure loads for different number of layers for B6

6.9.2.5 Effect of Increasing the Number of Layers for B7

Increasing the number of layers in deep beams with horizontal openings strengthened with horizontal BFRP from two layers to four layers increases the failure loads by 20.7% while increasing the layers from four layers to six layers decreases the failure load by 7.4%. this is because the failure was strut crushing and the beam became over-reinforced, that is the beam needs to increase the compressive strength from 25MPa to 30 or 35MPa. Or using H.S.C. Figure (6-87) shows the values of failure loads for different number of layers for B7.

6.9.2.6 Effect of Increasing the Number of Layers for B8

Increasing the number of layers in deep beams with circular openings strengthened with vertical BFRP from two layers to four layers decreases the failure loads by 1% while increasing the layers from four layers to six layers increases the failure load by 1%. These results show that increasing number of layers did not affect on the failure capacity of the deep beam with vertical opening. That is the beam need

to increase the compressive strength from 25MPa to 30 or 35MPa. Figure (6-88) shows the values of failure loads for different number of layers for B8.

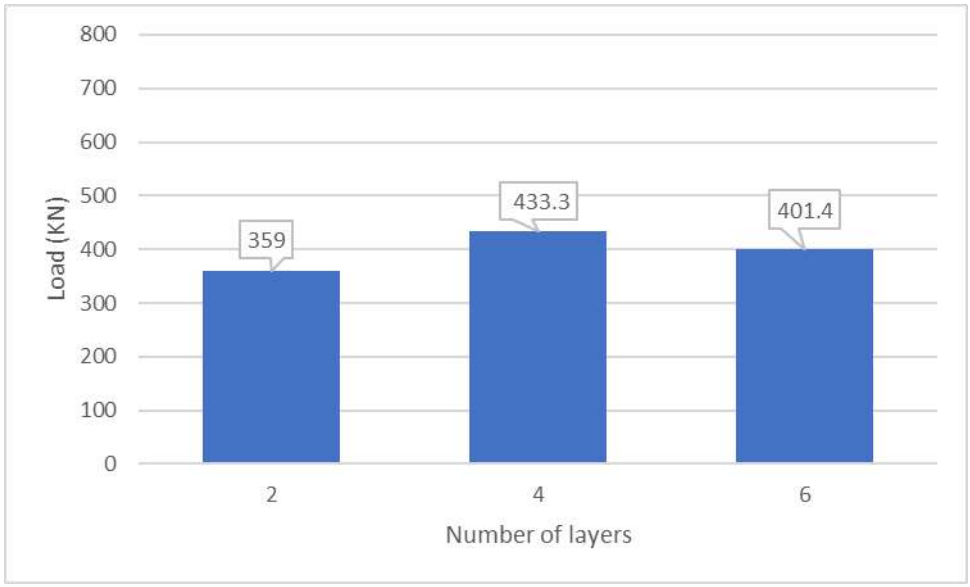

Figure (6-87): The values of failure loads for different number of layers for B7

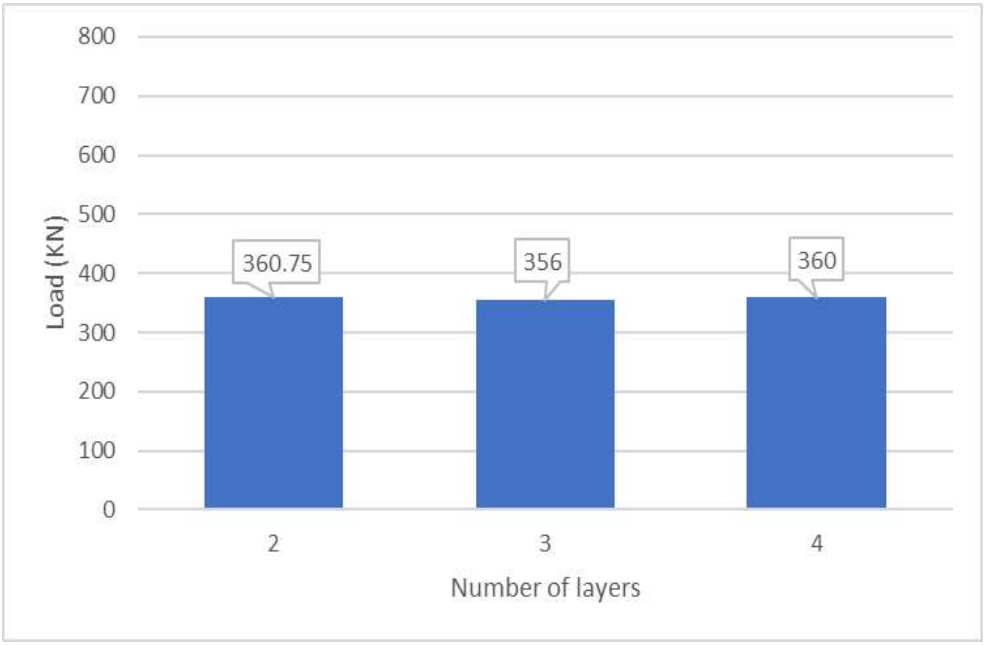

Figure (6-88): The values of failure loads for different number of layers for B8

6.9.2.7 Effect of Increasing the Number of Layers for B9

Increasing the number of layers in deep beams with circular openings strengthened with horizontal BFRP from two layers to four layers increases the failure loads only by 2.6% while increasing the layers from four layers to six layers increases the failure load by 3%. These results show that increasing number of layers did not effect on the failure capacity of the deep beam with circular opening. that is the beam needs to increase the compressive strength from 25MPa to 30 or 35MPa. Figure (6-89) shows the values of failure loads for different number of layers for B9.

6.9.2.8 Effect of Increasing the Number of Layers for B10

Increasing the number of layers in deep beams with square openings strengthened with vertical BFRP from two layers to four layers increases the failure loads only by 2% while increasing the layers from four layers to six layers increases the failure load by 5%. These results show that increasing number of layers did not effect on the failure capacity of the deep beam with circular opening. that is the beam needs to increase the compressive strength from 25MPa to 30 or 35MPa. Figure (6-91) shows the values of failure loads for different number of layers for B10.

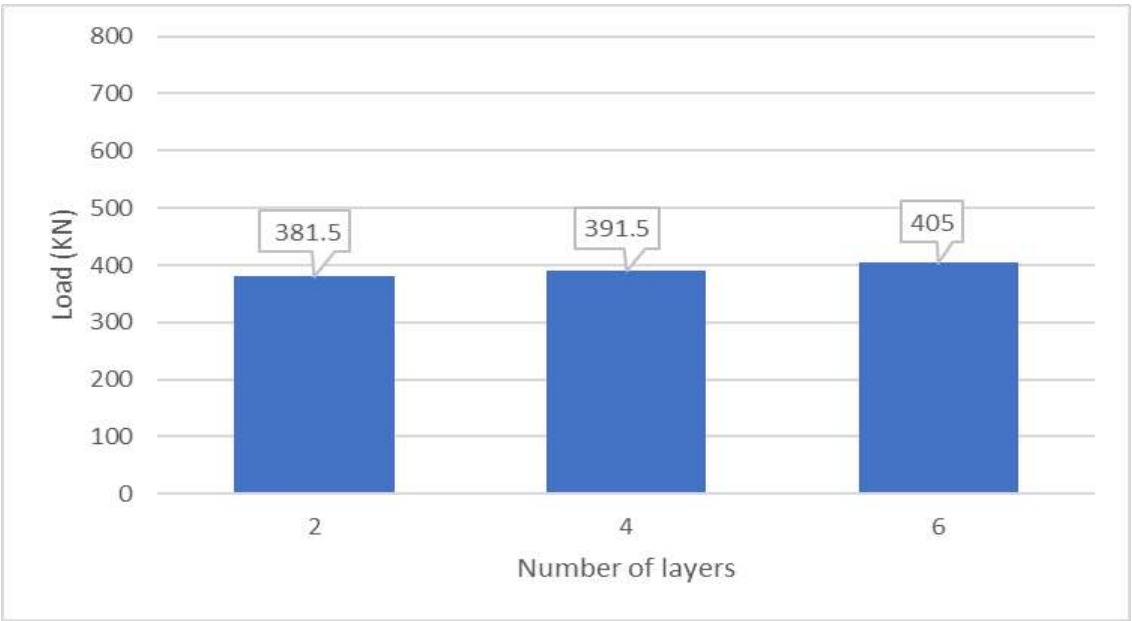

Figure (6-90): The values of failure loads for different number of layers for B9

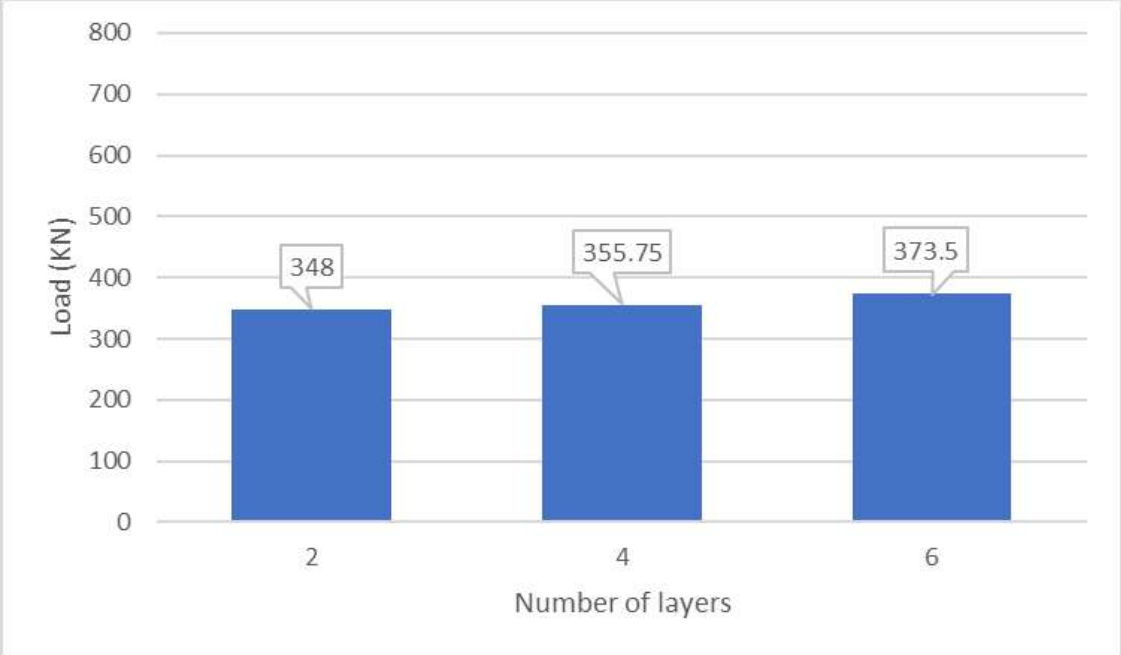

Figure (6-91): The values of failure loads for different numbers of layers for B10

6.9.2.9 Effect of Increasing the Number of Layers for B11

Increasing the number of layers in deep beams with circular openings strengthened with horizontal BFRP from two layers to four layers increases the failure loads

only by 1.9 % while increasing the layers from four layers to six layers increases the failure load by 0.6%. These results show that the increasing number of layers did not effect on the failure capacity of the deep beam with circular opening. that is the beam needs to increase the compressive strength from 25MPa to 30 or 35MPa. Figure (6-92) shows the values of failure loads for different number of layers for B11.

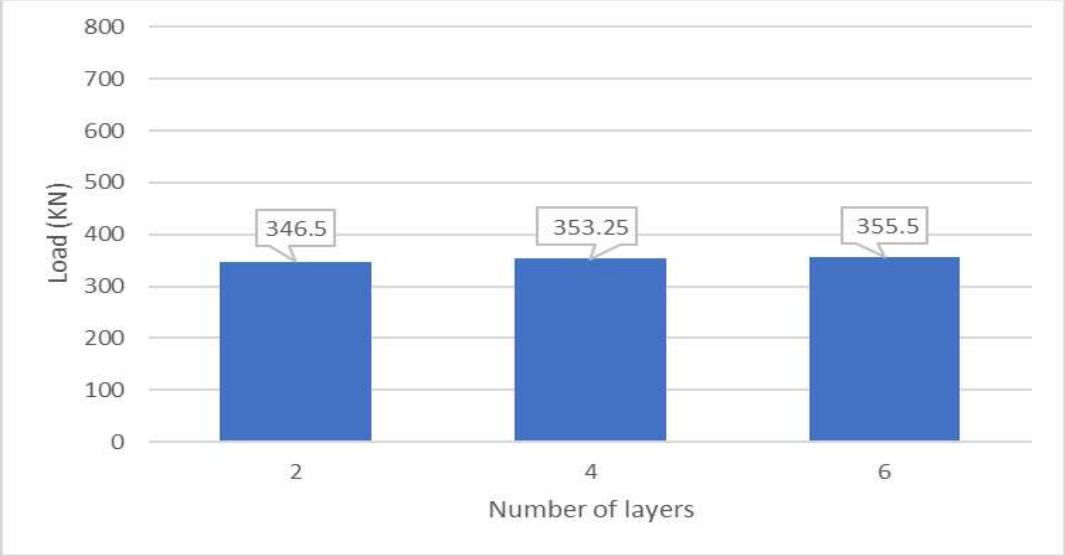

Figure (6-92): The values of failure loads for different number of layers for B11

Table (6-5) shows the values of failure loads for all specimens resulted from ANSYS for different numbers of layers and the results expected from the analytical model illustrated previously. A comparison between Ansys results and expected results from equations listed previously. Accuracy for the analytical models is gaged in terms of a load ratio that is defined as the ratio of the measured to the computed loads. The ratio has an average of 0.73, standard deviation of 0.15 and a coefficient of variation = 0.2. The statistical results of the predictions of Table (6-5) indicate that the analytical model is reliable.

Table (6-5): Comparison between Ansys results and expected failure loads for different number of layers.

No	Symbol	N	P ANS (KN)	Pu without strengthening (KN)	VF (KN)	Increasing failure load	Pu expected	$\frac{PANS}{Pexp}$
1	B1	-	428.90	455.30	-	-	455.30	0.93
2	B2	2	618.00	455.30	107.40	214.75	670.05	0.92
3	B3	-	281.40	304.30	-	-	300.60	0.93
4	B4	1	306.00	304.30	24.150	48.30	352.60	0.87
5	B4	2	339.00	304.30	48.30	96.60	400.90	0.84
6	B5	2	341.50	304.30	71.60	143.20	447.50	0.76
7	B6	2	341.00	304.20	32.20	64.40	368.60	0.92
8	B7	2	363.60	304.20	107.60	214.75	518.95	0.70
9	B8	2	355.00	301.50	37.17	74.20	375.70	0.94
10	B9	2	401.00	301.50	82.59	165.18	466.68	0.86
11	B10	2	320.25	309.50	40.30	80.60	390.10	0.82
12	B11	2	339.00	309.50	89.48	178.96	488.46	0.70
13	B2	3	676.00	455.30	161.00	322.00	777.30	0.87
14	B4	4	364.00	304.30	96.60	193.20	497.50	0.73
15	B5	4	472.00	367.10	195.40	390.80	757.80	0.62
16	B6	4	356.40	304.20	64.40	128.80	433.00	0.82
17	B7	4	433.30	304.20	215.20	430.40	734.60	0.60
18	B8	3	356.00	301.50	55.65	111.30	412.80	0.86
19	B9	4	391.50	301.50	165.00	330.00	631.90	0.62
20	B10	4	355.75	309.50	80.50	161.00	470.50	0.76
21	B11	4	353.25	309.50	178.70	357.60	667.10	0.53
22	B2	4	448.70	455.30	214.70	429.50	884.80	0.51
23	B4	6	374.00	304.30	144.90	289.80	594.10	0.63
24	B5	6	409.00	367.10	293.10	586.20	953.30	0.43
25	B6	6	371.40	304.20	96.60	193.20	497.50	0.75
26	B7	6	401.40	304.20	322.80	645.60	949.80	0.42
27	B8	4	360.00	301.50	74.20	148.40	449.90	0.80
28	B9	6	405.00	301.50	247.50	495.00	796.50	0.51
29	B10	6	373.50	309.50	120.75	241.50	551.00	0.68
30	B11	6	355.50	309.50	268.00	536.00	845.50	0.42
						Average		0.72
						Standard deviation		0.16
						Coefficient of variation		0.22

CHAPTER SEVEN
CONCLUSIONS AND RECOMMENDATIONS

7.1 Introduction

This study studied the effect of strengthening deep beams without openings and strengthening openings in them horizontally and vertically using basalt fiber strips. A practical and analytical program has been developed to study the behavior of deep beams strengthened with basalt fiber-reinforced polymer (BFRP) strips. The practical program consists of eleven deep beams designed as American code, with various types of openings strengthened vertically and horizontally using BFRP strips. The results of deflection, cracking load, crack propagation, ultimate load, and failure character are recorded, the same specimens are analyzed using mathematical equations and analysis from ANSYS 19 R2, and the results are compared. Also, additional parameters have been added to the study by using ANSYS, this parameters are the concrete compressive strength and the increasing number of layers. This chapter describes the main conclusions of the experimental and finite element analysis results of the reinforced beams and is followed by recommendations for future work at the same field.

7.2 Conclusions

Based on the experimental and F.E results and its discussion in this study the following conclusions can be achieved:

1. Use of basalt fiber strips instead of other fibers such as carbon is saving the environment from pollution because it doesn’t produce any toxic reactions with air or with water and it also saves natural resources which it can be recycled and reuse in building so, it is an advantage to use it as

a strengthening material to enhance the behavior of the structure elements.

2. The number of cracks became less due to the use of BFRP strips. Also, the cracking loads in the strengthened beams appeared at a higher load when compared with the un-strengthened beams.
3. The ultimate load of the strengthened beams generally is greater than that in the un-strengthened beams, so the externally bonded BFRP enhances the load capacity.
4. the beam without opening strengthened by horizontal Basalt fiber-reinforced polymer (BFRP) strips gives a higher ultimate load than the control deep beam by about 41%.
5. Openings in deep beams degrade the strength of the deep beams by (34, 33.7, 33.2, and 32.4) while strengthening these openings by vertical BFRP strips enhances the strength of the deep beams with opening by (0, 12.1, 11.7, and 3.2) for vertical, horizontal, circular and square openings respectively. while in the previous studies using CFRP in strengthening deep beams with openings, the ultimate load was increased by (10-40) %.
6. The shape of the opening does not greatly affect the capacity of the deep beam, but what may affect is the ratio of the height of the opening to the thickness of the beam(a/h), that is, the ratio of the cut part of the beam height. In horizontal reinforcement, we find that the greater this ratio, the lower the capacity of the deep beams. Therefore, the horizontal rectangular opening is the best among the types of openings. Despite the constant area, therefore, with the same area, we can obtain the least effect of the opening by making a horizontal rectangular opening.
7. Strengthen the beams with horizontal BFRP strips enhances the strength of the beam with opening by (8%-53%) according to the type of opening.

8. Strengthen the beams with vertical BFRP strips enhances the strength of the beam with opening by (4.6%-18.5%) according to the type of opening.
9. The horizontal rectangular strengthen openings with vertical BFRP strips are the best type of opening in the group of deep beams strengthened vertically which it could reach 78% of the beam's original structural capacity when compared to a solid beam.
10. The horizontal rectangular strengthen openings with horizontal BFRP strips are the best type of opening which could reach 101% of the beam's original structural capacity Contrary to what was usual previously that circular opening is the best type of opening, that may be because of the shear behavior of deep beams in the horizontal direction.
11. BFRP changes the mode of failure for solid deep beams from shear to shear-flexure failure while BFRP strips don't affect the modes of failure for deep beams with different types of opening, only it decreases the number of cracks
12. Strengthening the deep beam with BFRP increases the stiffness of the deep beam in case of a rectangular vertical opening in the ultimate stage than cracking stage unlike other deep beams with openings, the stiffness at ultimate load is less than the stiffness at the cracking load.
13. The stiffness increased at the ultimate stage than that in the cracking stage in beams strengthened with BFRP strips.
14. The energy absorption capacity is increased when the beam is strengthened with basalt fiber strips of about 19 to 58.6 % for different types of openings.
15. Horizontal strength of a solid deep beam increases the energy absorption by 156%, which is more than one and half the energy absorption of the beam without strengthening .

16. Horizontal strength for deep beam with openings increase the energy absorbtion capacity by 156.6%, which is more than one and half of the energy for the deep beam without strenghting.
17. Horizontal strength of openings has a greater effect than vertical strength. The capacity of the deep beams increased by 20.6, 29.1, 5, and 14% in the case of horizontal, vertical, circular, and square openings, respectively. Also, the crack load appeared later in the case of horizontal reinforcement than vertical reinforcement.
18. The analytical investigation used by this study using ACI-440 code provisions and ASCE-ACI practice is to give good agreement results when compared with experimental results, so we can consider this method of equations to predict the ultimate load for deep beams strengthened with BFRP.
19. The FE models developed in the current study were capable of predicting the nonlinear shear behavior of the tested deep beams with good accuracy. The ratio of the load capacity predicted numerically by the adopted models to that obtained from the tests was on average 1 with a standard deviation of 0.09.
20. Increasing the concrete compressive strength affects slightly the ultimate capacity of solid deep beams and deep beams with openings, in solid deep beams ultimate load increased by 9.1 and 2.2 when the concrete compressive strength increased from 25 to 30, and from 30 to 35 respectively.
21. In deep beams with vertical openings, the ultimate load increases by 21% and 22% when the concrete compressive strength increases from 25 to 30 and from 30 to 35 respectively.
22. In the case of vertical strength of openings, when the concrete compressive strength increased from 25 to 30 N/mm^2, the ultimate loads

increased by 19.1,14,19 and 21% for vertical, horizontal, circular and square openings respectively.

23. In the case of vertical strength of openings, when the concrete compressive strength increased from 30 to 35 N/mm^2, the ultimate loads increased by 12,28.6,16.4 and 15% for vertical, horizontal, circular and square openings respectively.
24. In the case of horizontal strength of openings, when the concrete compressive strength increased from 25 to 30 N/mm^2, the ultimate loads increased by 11.3,14.6,22.3 and 14.6% for vertical, horizontal, circular and square openings respectively.
25. In the case of horizontal strength of openings, when the concrete compressive strength increased from 30 to 35 N/mm^2, the ultimate loads increased by 20.1,18.4,15.5 and 18.5% for vertical, horizontal, circular and square openings respectively.
26. Increasing the number of BFRP layers did not result in a proportional increase in the strength gain in the case of concrete compressive strength equal to 25N/mm^2 that is because the failure occurred due to concrete crushing.
27. The influence of increasing concrete compressive strength is more than increasing the number of layers on the behavior of deep beams with and without openings.

7.3 Recommendations for Future Work:

(1) use another type of resin.
(2) change the dimension of openings.
(3) use a combined system horizontal and vertical around the opening.
(4) Use diagonal basalt fibers around the openings perpendicular to cracks.
(5) Use high strength concrete.

REFERENCES

1- de Paiva, HA Rawdon, and Chester P. Siess. "Strength and behavior of deep beams in shear." *Journal of the Structural Division* 91.5 (1965): 19-41.https://doi.org/10.1061/JSDEAG.0001329

2- ACI Committee. "Building code requirements for structural concrete (ACI 318-19) and commentary." American Concrete Institute, 2019.

3- Campione, Giuseppe, and Giovanni Minafò. "Behaviour of concrete deep beams with openings and low shear span-to-depth ratio." *Engineering Structures* 41 (2012): 294-306.

4- Ramakrishnan, V., and R. K. Panchalan. "A new construction Material—Non-corrosive basalt bar reinforced concrete." *Special Publication* 229 (2005): 253-270.

5- Shetty, M. S., and A. K. Jain. Concrete Technology (Theory and Practice), 8e. S. Chand Publishing, 2019.

6- Czigány, Tibor, János Vad, and Kornél Pölöskei. "Basalt fiber as a reinforcement of polymer composites." Periodica Polytechnica Mechanical Engineering 49.1 (2005): 3-14.

7- Branston, John-Sebastian. *Properties and applications of basalt fibre reinforced concrete*. Diss. University of Windsor (Canada), 2015.

8- Ralph, Calvin, et al. "Relationships among the chemical, mechanical and geometrical properties of basalt fibers." *Textile Research Journal* 89.15 (2019): 3056-3066.

9- Jamshaid H, Mishra R. A green material from rock: basalt fiber–a review. The Journal of The Textile Institute. 2015:1-15.

10- Singha K. A short review on basalt fiber. International Journal of Textile Science. 2012;1(4):19-28

11- Fiore V, Scalici T, Di Bella G, Valenza A. A review on basalt fibre and its composites. Composites Part B: Engineering. 2015;74:74-94.

12- Kamenny Vek. http://www.basfiber.com/2. (accessed October 1, 2015).

13- Lee JJ, Song J, Kim H. Chemical stability of basalt fiber in alkaline solution. Fibers and Polymers. 2014;15(11):2329-34.

14- Rabinovich F, Zueva V, Makeeva L. Stability of basalt fibers in a medium of hydrating cement. Glass and Ceramics. 2001;58(11-12):431-4

15- Fibers, Basalt. "Alternative to Glass." *Composites Technology* (2006).

16- Kumbhar, Vishal Pandurang. "An overview: basalt rock fibers-new construction material." *Acta Engineering International* 2.1 (2014): 11-18. (www.laseroptronix.se/exoma/ basaltinformation.pdf).

17- http://www.npo-vulkan.com/index_en.php

18- Ólafsson, Hannibal, and Eyþór Þórhallsson. "Basalt fibre bar Reinforcement of concrete structures." *Reykjavík University* (2009): 5-12.

19- Européen, C. "Eurocode 2: Design of concrete structures—part 1-1: General rules and rules for buildings." *London: British Standard Institution* (2004).

20- Mohamed, Emad Ibrahim Ahmed. *Analysis & Design Of Deep Reinforced Concrete Beams Using Strut-Tie Method*. Diss. University of Khartoum, 2015.

21- Erlin, Bernard. "Portland cement and concrete." *Rev. Eng. Geol* 2 (1969): 81-103.

22- Uhlmann, H. L. B. "The theory of girder walls with special reference to reinforced concrete design." *The Structural Engineer* 30.8 (1952): 172-181.

23- Kong FK, Sharp GR, Appleton SC, Beaumont CJ, Kubik LA. “Structural idealization for deep beams with web openings: Further evidence.”. Magazine Concr Res 1978;30(103):89–95

24- Ray, S. P. "Deep beams with web openings." *Reinforced concrete deep beams* (1990): 288.

25- Tan KH, Tong K, Tang CY. Consistent strut-and-tie modelling of deep beams with web openings. Magazine Concr Res 2003;55(1):65–75.

26- Tseng CC, Hwang SJ, Lu WY. “Shear strength prediction of reinforced concrete deep beams with web openings.”. ACI Struct J 2017;114(6):1569–79.

27- Liu J, Shear Mihaylov B. strength of RC deep beams with web openings based on two-parameter kinematic theory. Struct Concr 2020;21:349–61. https://doi.org/10. 1002/suco.201800356.

28- Mihaylov BI, Bentz EC, Collins MP. Two-parameter kinematic theory for shear behaviour of deep beams. ACI Struct J 2013;110(3):447–56

29- Vecchio FJ, Collins MP. The modified compression – Field theory for reinforced concrete elements subjected to shear. ACI J Proc 1986;83(2):219–31.

30- Wong PS, Vecchio FJ. VecTor 2 and formworks user's manuals, 213. Toronto: Dept. of Civil Engineering, Univ. of Toronto; 2002.

31- CSA A23.3. "Design of Concrete Structures Standard.". Mississauga, Ontario, Canada: Canadian Standards Association; 2014. p. 295.

32- Kuchma, Daniel A., and Tjen N. Tjhin. "Cast (computer aided strut-and-tie) design tool." *Structures 2001: A Structural Engineering Odyssey*. 2001. 1-7.

33- High, Cory, et al. "Use of basalt fibers for concrete structures." *Construction and Building materials* 96 (2015): 37-46.

34- Ahmed, Mohamed M., et al. "FLEXURAL BEHAVIOR OF BASALT FRPRC BEAMS UNDER REPEATED LOAD." *JES. Journal of Engineering Sciences* 42.5 (2014): 1179-1192.

35- El-Kom, S. Dynamic Analysis of Concrete Structures Reinforced with Basalt Fiber.21017

36- Thorhallsson, Eythor Rafn, and Jónas Thór Snaebjornsson. "Basalt fibers as new material for reinforcement and confinement of concrete." *Solid State Phenomena* 249 (2016): 79-84.

37- Irine, Fathima. "Strength aspects of basalt fiber reinforced concrete." *Int. J. Innov. Res. Adv. Eng* 1.8 (2014): 192-198.

38- Surya Sunder, S., Nisha Babu, and Dinu Paulose. "Experimental Study on Strengthening of Openings in RC Beams using BFRP Fabric." *International Journal of Innovative Research in Science, Engineering and Technology* 5.8 (2016).

39- Chin, Siew Choo, Nasir Shafiq, and Muhd Fadhil Nuruddin. "FRP as strengthening material for Reinforced Concrete beams with openings—A review." *KSCE Journal of Civil Engineering* 19 (2015): 213-219.

40- Hamdy, K. S., et al. "Finite Element Analysis on the behavior of Strengthened RC Shallow T-Beams with Large Openings at Shear Zone Using CFRP and BFRP sheets." (2017).

41- WY Lu, HW Yu, CL Chen, SL Liu. High-strength concrete deep beams with web openings strengthened by carbon fiber reinforced plastics." *Computers and Concrete* (2015)

42- SHENG, TONG FOO. "Shear Strengthening of RC Deep Beams with Large Openings Using Carbon Fiber Reinforced Polymers (CFRP)." (2015).

43- Shakir, Qasim, Yahya Mo Yahya, and Ali Jasim. "Strengthening of reinforced self-compacting concrete T-deep beam with large opening by carbon fiber sheets." *Kufa Journal of Engineering* 10.2 (2019): 76-89.

44- El Maaddawy, Tamer, and Sayed Sherif. "FRP composites for shear strengthening of reinforced concrete deep beams with openings." *Composite Structures* 89.1 (2009): 60-69.

45- Hawileh, Rami A., Tamer A. El-Maaddawy, and Mohannad Z. Naser. "Nonlinear finite element modeling of concrete deep beams with openings strengthened with externally-bonded composites." *Materials & Design* 42 (2012): 378-387.

46- Lam, Lalin, et al. "Behavior of RC deep beams strengthened in shear using glass fiber reinforced polymer with mechanical anchors." *Proceedings of the International Conference on Environment and Civil Engineering (ICEACE'2015), Pattaya, Thailand*. Vol. 24. 2015.

47- Hussain, Qudeer, and Amorn Pimanmas. "Shear strengthening of RC deep beams with sprayed fiber-reinforced polymer composites (SFRP): Part 2 Finite element analysis." *Latin American Journal of Solids and Structures* 12 (2015): 1266-1295.

48- Hussain, Qudeer, and Amorn Pimanma. "Shear strengthening of RC deep beams with circular openings using externally bonded SFRP composites." *Proceedings of the IABSE-JSCE Joint Conference on Advances in Bridge Engineering*. 2015.

49- Al-Ghanem, Hana, Aya Al-Asi, and Maha Alqam. "Shear and flexural behavior of reinforced concrete deep beams strengthened with CFRP composites." *Modern Applied Science* 11.10 (2017): 110-110.

50- Kumar, G. H. "Experimental and numerical studies on behaviour of FRP strengthened deep beams with openings." *Department of Civil Engineering National Institute of Technology, Rourkela* (2012).

51- Abdel-Kareem, Ahmed H. "Shear strengthening of reinforced concrete beams with rectangular web openings by FRP Composites." *Advances in concrete construction* 2.4 (2014): 281.
52- El-Kareim, Ata, et al. "Behavior and strength of reinforced concrete flanged deep beams with web openings." *Structures*. Vol. 27. Elsevier, 2020.
53- Ghali, Mona K., et al. "Behaviour of T-shaped RC deep beams with openings under different loading conditions." *Structures*. Vol. 31. Elsevier, 2021.
54- Hassan, Nasr Z., and Omnia F. Youseef. "Behavior of high strength reinforced concrete Deep beams with openings."2018
55- Nasr Z. Hassan, Fouad I. Khairallah, Waleed A. Abd Elfatah and Mahmoud B. Saad. " Experimental study of self-compacting reinforced concrete deep beams with openings. ". 2017
56- Knight M, Thomson N Underground infrastructure research. CRC Press, Boca Raton. (2001)
57- Al-Gasham, Thaar S., Jasim M. Mhalhal, and Hussain A. Jabir. "Influence of post-heating on the behavior of reinforced self-compacting concrete hollow columns." *Structures*. Vol. 22. Elsevier, 2019.
58- Al-Gasham, Thaar S., Jasim M. Mhalhal, and Hussain A. Jabir. "Improving punching behavior of interior voided slab-column connections using steel sheets." *Engineering Structures* 199 (2019): 109614.
59- Oukaili, Nazar K., and Thaar S. Al-Gasham. "Shear strengthening with CFRP sheets applied in reinforced concrete flat plates with openings." *FRPRCS-12/APFIS-2015-Joint Conference of the 12th International Symposium on Fiber Reinforced Polymers for Reinforced Concrete Structures, FRPRCS 2015 and the 5th Asia-Pacific Conference on Fiber Reinforced Polymers in Structures, APFIS 2015*. 2015.
60- Al-Gasham, Thaar S., Ali N. Hilo, and Manal A. Alawsi. "Structural behavior of reinforced concrete one-way slabs voided by polystyrene balls." *Case Studies in Construction Materials* 11 (2019): e00292.
61- Abbass, Ahmmad, Sallal Abid, and Mustafa Özakça. "Experimental investigation on the effect of steel fibers on the flexural behavior and ductility of high-strength concrete hollow beams." *Advances in Civil Engineering* 2019 (2019).

62- Abbass, Ahmmad A., et al. "Flexural response of hollow high strength concrete beams considering different size reductions." *Structures*. Vol. 23. Elsevier, 2020.
63- Abid, Sallal R., et al. "Low-velocity impact tests on self-compacting concrete prisms." *IOP Conference Series: Materials Science and Engineering*. Vol. 888. No. 1. IOP Publishing, 2020.
64- Haridharan, M. K., et al. "Impact response of two-layered grouted aggregate fibrous concrete composite under falling mass impact." *Construction and Building Materials* 263 (2020): 120628.
65- Salaimanimagudam, Meivazhisalai Parasuraman, et al. "Impact response of hammerhead pier fibrous concrete beams designed with topology optimization." *Periodica Polytechnica Civil Engineering* 64.4 (2020): 1244-1258.https://doi.org/10.3311/PPci.16664.
66- Abid, Sallal R., et al. "Repeated drop-weight impact tests on self-compacting concrete reinforced with micro-steel fiber." *Heliyon* 6.1 (2020).
67- Abid, Sallal R., et al. "Suggested modified testing techniques to the ACI 544-R repeated drop-weight impact test." *Construction and Building Materials* 244 (2020): 118321.
68- Jabir, Hussain A., et al. "Repeated drop-weight impact tests on RPC containing hybrid fibers." *Applied Mechanics and Materials* 897 (2020): 49-55.
69- Spadea G, Bencardino F and Swamy R N. Strengthening and upgrading structures with bonded CFRP sheets design aspects for structural integrity Proceedings of 3rd International Symposium on Non-Metallic (FRP) Reinforcement for Concrete Structures,1997. 629–636.
70- Tan, Kiang Hwee, and Haidong Zhao. "Strengthening of openings in one-way reinforced-concrete slabs using carbon fiber-reinforced polymer systems." *Journal of Composites for Construction* 8.5 (2004): 393-402.
71- Jabir, Hussain A., Thaar S. Al-Gasham, and Jasim M. Mhalhal. "Structural performance of reinforced concrete corbels exposed to high fire flame." *UEMK 2018 BİLDİRİ ÖZETLERİ KİTABI 18-19 Ekim 2018 Hukuk Fakültesi* 544 (2018).
72- Thompson, Mary Kathryn, and John Martin Thompson. *ANSYS mechanical APDL for finite element analysis*. Butterworth-Heinemann, 2017..

73- Jayajothi, P., R. Kumutha, and K. Vijai. "Finite element analysis of FRP strengthened RC beams using ANSYS." (2013): 631-642.
74- Fathelbab, F. A., M. S. Ramadan, and A. Al-Tantawy. "Finite element modelling of strengthened simple beams using FRP techniques: a parametric study." *Concrete Research Letters* 2.2 (2011): 228-240.
75- Abbas, S. M., Nazim Belhocine, Asmaa A. ElGanainy, and Mark Horton. "A historical public debt database." (2010).
76- Lovász, László, and Michael D. Plummer. *Matching theory*. Vol. 367. American Mathematical Soc., 2009.
77- Santhakumar, R., E. Chandrasekaran, and R. Dhanaraj. "Analysis of retrofitted reinforced concrete shear beams using carbon fiber composites." *Electronic journal of structural engineering* 4 (2004): 66-74.
78- Supaviriyakit, Teeraphot, Phuwanat Pornpongsaroj, and Amorn Pimanmas. "Finite element analysis of FRP-strengthened RC beams." *Songklanakarin Journal of science and technology* 26.4 (2004): 497-507.
79- Ali, Osama, et al. "Probabilistic calibration of the strength reduction factor for the design of rectangular short concrete columns reinforced with FRP bars under eccentric axial loading–Update of ACI 440 rules." *Journal of Building Engineering* 43 (2021): 103096.
80- Shah, Surendra P., Stuart E. Swartz, and Chengsheng Ouyang. *Fracture mechanics of concrete: applications of fracture mechanics to concrete, rock and other quasi-brittle materials*. John Wiley & Sons, 1995.
81- Bangash, M. YH. "Concrete and concrete structures: Numerical modelling and applications." (1989).
82- ASCE-ACI Committee 445. "Closure to “recent approaches to shear design of structural concrete” by ASCE-ACI committee 445 on shear and torsion." *Journal of Structural Engineering* 126.7 (2000): 856-856.
83- Mansur MA, Alwis WA.Reinforced fibre concrete deep beams with web openings.Int J Cem Compos Lightweight Concr 1984;6(4):263 - 71
84- Chapelle, Dominique, and Klaus-Jürgen Bathe. "Fundamental considerations for the finite element analysis of shell structures." *Computers & Structures* 66.1 (1998): 19-36.

85- Aiello, Maria Antonietta, et al. "Guide for the design and construction of externally bonded FRP systems for strengthening existing structures." (2014): 1-154.

ملخص الرسالة

سلوك الكمرات العميقة ذات فتحات مدعمة بأستخدام شرائح ألياف البازلت

المقدمة:

ان ألياف البازلت هى ألياف صديقة للبيئة ولا تشكل خطورة عليها حيث يتم انتاجها من صخور البازلت عن طريق تشكيلها بالانصهار ايضا الياف البازلت لها مقاومة كيميائية عالية ,بالاضافة الى تحملها العالى لدرجات الحرارة الى جانب ان سطح الياف البازلت الخشن يعطى تماسك جيد مع المادة اللاحمة كما ان له مقاومة عالية للزحف لذا فان هذا البحث يهدف الى استخدام هذه الالياف فى تدعيم الفتحات الموجوده فى الكمرات العميقه ودراسه سلوك هذه الكمرات العميقة عند تدعيمها بالياف البازلت فى حالة عدم وجود فتحات.

الهدف من البحث:

دراسة عملية ونظرية لسلوك الكمرات العميقة المدعمة بالياف البازلت عن طريق دراسة :

1- تدعيم الكمرات العميقة ذات الفتحات

2- تدعيم الكمرات العميقه فى حاله عدم وجود فتحات

3- تغيير اتجاه شرائح التدعيم

أهمية البحث:

يوجد العديد من الأبحاث التى تتحدث عن العناصر الانشائية المصنوعة من الخرسانة المسلحة والمدعمة باستخدام الياف الكربون والزجاج والحديد ولكن الأبحاث التى تتناول دراسه الكمرات العميقة التى بها فتحات مدعمة بالياف البازلت غير متاحة ولذلك فان هذا البحث يتناول دراسة سلوك الكمرات العميقة المدعمة بألياف البازلت فى حالتى وجود فتحات وعدم وجود فتحات

محتوى الرسالة:

تحتوى الرسالة على سبعه أبواب بخلاف المراجع والملحقات والأبواب كالاتى:

الباب الاول :مقدمة

هذا الباب يشمل المقدمة والهدف من الرسالة ومحتوياتها

الباب الثانى :الدراسات السابقة

يشمل هذا الباب على نبذة تاريخية للمواد المركبة وانواعها المختلفة وطرق تصنيعها والتطبيقات المختلفة لاستخدام الاسياخ المصنعة من الياف البوليمرات المركبة فى الهندسة

الانشـائية وايضـا يحتـوى هـذا البـاب علـى خـواص المـواد اللاحمـة للبـويمرات واخيـرا الأبحاث السابقة فى هذا المجال

الباب الثالث:البرنامج العملى

يشـتمل هـذا البـاب علـى خـواص المـواد المسـتخدمة ,طريقـة تجهيـز العينـات ,طريقـة الاختبـار والبرنـامج العملـى للكمـرات العميقـة ذات الفتحـات المدعمـة باسـتخدام اليـاف البازلـت وايضـا الكمـرات العميقـة المدعمـة مـن غيـر وجـود فتحـات وهـذا البرنـامج العملـى يشـتمل علـى خمسـة مجموعات :

المجموعة الأولى :

تتكون من كمرتين عميقتين واحدة مدعمة أفقيا بطبقتين من اليـاف البازلـت والاخـرى كمـرة عميقـة غير مدعمة , تلك الكمرتين تم تسليحهم بالحديد العادى بأبعاد (150×500×1000مم).وتستخدم تلك الكمرات فى المقارنة ما بينها وبين باقى المجموعات .

المجموعة الثانية :

تتكـون مـن ثلاثـة كمـرات عميقـة بابعـاد (150×500×1000مـم) الأولـى بهـا فتحتـين مسـتطيلتين بابعـاد (100×200 مـم) ولـيس بهـا تـدعيم والثانيـه بـنفس ابعـاد الفتحـات ولكـن مدعمـة بطبقتـين مـن اليـاف البازلـت تـدعيما رأسـيا والثالثـة بهـا نفـس ابعـاد الفتحـات ولكـن مدعمة بالياف البازلت تدعيما افقيا

المجموعة الثالثة:

تتكـون مـن كمـرتين عميقتـين بأبعـاد (150×500×1000مـم) الأولـى بهـا فتحتـين بابعـاد (100×200 مـم) اى انهـا فتحـة أفقيـة ومدعمـة رأسـيا بطبقتـين مـن أليـاف البازلـت والكمـرة الثانية لها نفس الفتحات ولكن مدعمة افقيا باستخدام طبقتين من الياف البازلت

المجموعة الرابعة:

تتكون من كمرتين بابعاد (150×500×1000مم) الأولى ذات فتحتين دائرتين بقطر 160 مم مدعمة رأسيا بطبقتين من البازلت والثانية بنفس الفتحات ولكن مدعمة أفقيا بطبقتين من ألياف البازلت

المجموعة الخامسة :

تتكون من كمرتين بابعاد (150×500×1000مم) الأولى ذات فتحتين مربعين بطول 140 مم ومدعمة رأسيا باستخدام طبقتين من ألياف البازلت والثانية لها نفس الفتحات ولكن مدعمة أفقيا باستخدام طبقتين من ألياف البازلت

الباب الرابع: النتائج العملية

يشتمل هذا الباب على عرض النتائج المعملية وتحليلها للكمرات التى تم اختبارها

الباب الخامس :تحليل ومناقشة النتائج المعملية

يشتمل هذا الباب على مناقشة النتائج المعملية بعد تحليلها

الباب السادس : التحليل النظرى باستخدام العناصر المحددة

يشتمل هذا الباب على عمل مماثلة للعينات العملية ومقارنة نتائجها مع نتائج العملى.

الباب السابع :النتائج والتوصيات للابحاث المستقبلية

يحتوى هذا الباب على اهم النتائج المستخلصة من البحث والتى يمكن ايجازها فى التالى :

1. استخدام صفائح الألياف البازلتية بدلا من الألياف الأخرى مثل الكربون ينقذ البيئة من التلوث لأنها لا تنتج أي تفاعلات سامة مع الهواء أو مع الماء كما أنها توفر الموارد الطبيعية التي يمكن إعادة تدويرها وإعادة استخدامها في البناء ومن مميزات استخدامه كمادة تقوية لتعزيز سلوك العناصر الهيكلية.

2. أصبح عدد الشروخ أقل بسبب استخدام الياف البازلت. كما أن أحمال التشريخ في الكمرات المقواة ظهرت عند حمل أعلى مقارنة مع العتبات غير المقواة

3. بشكل عام حمل الانهيار للكمرات المدعمه أكبر من الحمل في الكمرات غير المدعمه، وبالتالي فإن الياف البازلت تعزز سعة الحمولة.

4. الكمرة العميقه بدون فتحة معززة بصفائح البوليمر المقوى بالألياف البازلتية الأفقية (BFRP) تعطي حمل نهائي أعلى من الكمرة العميقة المتحكم بها بحوالي 41%.

5. الفتحات في الكمرات العميقة تقلل من قوة الكمرات العميقة بمقدار (34، 33.7، 33.2، 32.4) بينما تقوية هذه الفتحات بألياف البازلت العمودية تعزز قوة الكمرات العميقة مع الفتح بمقدار (0، 12.1، 11.7، 3.2).) للعمودي والأفقي والدائري والفتحات المربعة على التوالي. بينما في الدراسات السابقة التي استخدمت مادة الكربون في تقوية الكمرات العميقة ذات الفتحات فقد تم زيادة الحمل الأقصى بنسبة (10-40)%.

6. لا يؤثر شكل الفتحة بشكل كبير على قدرة الشعاع العميق، ولكن ما قد يؤثر هو نسبة ارتفاع الفتحة إلى سمك الكمره (a/h)، أي نسبة الجزء المقطوع من ارتفاع الكمره. وفي التسليح الأفقي نجد أنه كلما زادت هذه النسبة قلت سعة الكمرات العميقة. ولذلك فإن الفتحة المستطيلة الأفقية هي الأفضل بين أنواع الفتحات. على الرغم من أن المساحة ثابتة، إلا أنه مع نفس المساحة، يمكننا الحصول على أقل تأثير للفتحة عن طريق عمل فتحة مستطيلة أفقية.

7. تدعيم الكمرات بألياف البازلت الأفقية تعزز قوة العتبة مع الفتح بنسبة (8%-53%) حسب نوع الفتحة.

8. تدعيم الكمرات بألياف البازلت العمودية تعزز قوة الكمرة مع الفتح بنسبة (4.6%-18.5%) حسب نوع الفتح.

9. تعتبر الفتحات الأفقية المستطيلة المدعمه بألياف البازلت الرأسية أفضل نوع من الفتحات ضمن مجموعة الكمرات العميقة المقوية رأسياً والتي يمكن أن تصل إلى 78% من القدرة الهيكلية الأصلية للكمرة بالمقارنة مع الكمرات الصلبة.

10. تعتبر الفتحات المستطيلة الأفقية المعززة بألياف البازلت الأفقية أفضل أنواع الفتحات حيث يمكن أن تصل إلى 101% من القدرة الهيكلية الأصلية للكمرة على عكس ما كان معتاداً سابقاً أن الفتح الدائري هو أفضل أنواع الفتحات، وقد يكون ذلك بسبب سلوك القص للعتبات العميقة في الاتجاه الأفقي.

11. تغير الياف البازلت نمط الفشل للكمرات العميقة الصلبة من فشل القص إلى ثني القص بينما لا تؤثر الياف البازلت على أوضاع الفشل للكمرات العميقة ذات أنواع الفتحات المختلفة، فقط تقلل من عدد الشروخ

12. تقوية الكمرات العميقة بـألياف البازلت تزيد من صلابة الكمره العميقة في حالة الفتح الرأسي المستطيل في المرحلة النهائية عن مرحلة التتشريخ بعكس الكمرات العميقة الأخرى ذات الفتحات فإن الصلابة عند الحمل النهائي تكون أقل من الصلابة عند حمل التشريخ .

جامعة حلوان

كلية الهندسة بالمطرية

قسم الهندسة المدنية

سلوك الكمرات العميقة ذات فتحات مدعمة باستخدام شرائح الياف البازلت

رسالة
مقدمة للحصول على
درجه دكتوراة الفلسفة فى العلوم الهندسية
قسم الهندسة المدنية
كلية الهندسة بالمطرية –جامعة حلوان - مصر

مقدمه من

م/ هدى عوض عبد الظاهر

ماجستير العلوم الهندسية قسم الهندسة المدنية , جامعة حلوان , نوفمبر 2016

يعتمد من لجنه الممتحنين:

ا.د / محمد عبد الرازق ابراهيم

استاذ المنشات الخرسانية – كلية الهندسة – جامعه الازهر

ا.م.د / نصر زينهم حسن

استاذ مساعد بقسم الهندسة المدنية- كلية الهندسة بالمطرية – جامعه حلوان

ا.د / مصطفى عبد المجيد عثمان

استاذ المنشات الخرسانية –قسم الهندسة المدنية – كلية الهندسة بالمطرية –جامعه حلوان

أ.م.د. هاله ممدوح اسماعيل

استاذ مساعد بقسم الهندسة المدنية- كلية الهندسة بالمطرية –جامعه حلوان

المشرفون:

ا.د / مصطفى عبد المجيد عثمان

استاذ المنشات الخرسانية –قسم الهندسة المدنية – كليه الهندسة بالمطرية –جامعه حلوان

أ.م.د. هاله ممدوح اسماعيل

استاذ مساعد بقسم الهندسة المدنية - كلية الهندسة بالمطرية –جامعه حلوان

جامعة حلوان

كلية الهندسة بالمطرية

قسم الهندسة المدنية

سلوك الكمرات العميقة ذات فتحات مدعمة باستخدام شرائح الياف البازلت

رسالة
مقدمة للحصول على
درجة دكتوراة الفلسفة فى العلوم الهندسية
قسم الهندسة المدنية
كلية الهندسة بالمطرية –جامعة حلوان - مصر

مقدمة من

م/ هدى عوض عبد الظاهر

ماجستيرالعلوم الهندسية قسم الهندسة المدنية

جامعة حلوان , نوفمبر 2016

المشرفون

أ.د. مصطفى عبد المجيد عثمان

استاذ المنشات الخرسانية

قسم الهندسة المدنية

كليه الهندسة بالمطرية - جامعة حلوان

أ.م.د.هاله ممدوح اسماعيل

استاذ مساعد

قسم الهندسة المدنية

كليه الهندسة بالمطرية - جامعة حلوان

القاهره
2024